F

4079

ADA034079

LASER RESONATOR STUDIES

University of Arkansas
Electrical Engineering Department
Fayettville, AR 72701

December 1976

Final Report

Approved for public release; distribution unlimited.

COPY AVAILABLE TO DDC DOES NOT
PERMIT FULLY LEGIBLE PRODUCTION

DDC

JAN 6 1977

A

AIR FORCE WEAPONS LABORATORY
Air Force Systems Command
Kirtland Air Force Base, NM 87117

This final report was prepared by University of Arkansas, Electrical Engineering Department, Fayettville, AR, under Contract F29601-74-C-0077, Job Order 317J1809, with the Air Force Weapons Laboratory, Kirtland AFB, NM. Dr. John A. Hanlon (ALO) was the Laboratory Project Officer-in-Charge.

When US Government drawings, specifications, or other data are used for any purpose other than a definitely related Government procurement operation, the Government thereby incurs no responsibility nor any obligation whatsoever, and the fact that the Government may have formulated, furnished, or in any way supplied the said drawings, specifications, or other data is not to be regarded by implication or otherwise as in any manner licensing the holder or any other person or corporation or conveying any rights or permission to manufacture, use, or sell any patented invention that may in any way be related thereto.

This technical report has been reviewed and is approved for publication.

This report has been reviewed by the Information Office (OI) and is releasable to the National Technical Information Service (NTIS). At NTIS, it will be available to the general public, including foreign nations.

DR. JOHN A. HANLON
Project Officer

FOR THE COMMANDER

J. D. DILLOW
Maj, USAF
Chief, Advanced Beam Control Branch

ARMAND D. MAIO
Lt Colonel, USAF
Chief, Advanced Laser Technology
Division

REPORT DOCUMENTATION PAGE

READ INSTRUCTIONS BEFORE COMPLETING FORM

1. REPORT NUMBER	2. GOVT ACCESSION NO.	3. RECIPIENT'S CATALOG NUMBER
AFWL-TR-75-333		

4. TITLE (and Subtitle)

LASER RESONATOR STUDIES

5. TYPE OF REPORT & PERIOD COVERED

Final Report

6. PERFORMING ORG. REPORT NUMBER

7. AUTHOR(s)

M. M. Johnson
L. G. Collier
G. E. Smith

8. CONTRACT OR GRANT NUMBER(s)

F29601-74-C-0077

9. PERFORMING ORGANIZATION NAME AND ADDRESS

University of Arkansas
Electrical Engineering Department
Fayettville, AR 72701

10. PROGRAM ELEMENT, PROJECT, TASK AREA & WORK UNIT NUMBERS

317J1809

11. CONTROLLING OFFICE NAME AND ADDRESS

Air Force Weapons Laboratory (ALO)
Kirtland Air Force Base, NM 87117

12. REPORT DATE

December 1976

13. NUMBER OF PAGES

184

14. MONITORING AGENCY NAME & ADDRESS(if different from Controlling Office)

15. SECURITY CLASS. (of this report)

Unclassified

15a. DECLASSIFICATION/DOWNGRADING SCHEDULE

16. DISTRIBUTION STATEMENT (of this Report)

Approved for public release; distribution unlimited.

17. DISTRIBUTION STATEMENT (of the abstract entered in Block 20, if different from Report)

18. SUPPLEMENTARY NOTES

19. KEY WORDS (Continue on reverse side if necessary and identify by block number)

Masers
Lasers
Optics
Unstable Resonators

(+ or − jℓ times phi)
(where ℓ is an integer)

20. ABSTRACT (Continue on reverse side if necessary and identify by block number)

The goal of the study was to find a hole-coupled resonator with good azimuthal mode discrimination for potential uses in high power laser applications. Two computer programs were developed to aid in the analysis of hole-coupled resonators. The first program calculates the scalar eigenmodes, of circular cylindrical resonators with exp $(\pm j\ell\phi)$ (ℓ integer) azimuthal variation and arbitrary radical mirror figure. Graphs of the radial mode eigenvalues (versus Fresnel number) for the four lowest order azimuthal modes revealed that (over)

DD FORM 1473 1 JAN 73   EDITION OF 1 NOV 65 IS OBSOLETE

409489

typically, the larger the hole becomes in a hole-coupled resonator, the higher the azimuthal index of the dominant (lowest loss) mode (media gain saturation not included). The lowest order azimuthal mode losses were almost identical in one negative branch toroidal hole-coupled resonator and in a positive branch resonator where both mirrors had on-axis holes. The second computer program calculates the radial mirror profiles by a non-linear multiple regression technique such that the eigenmode magnitude and/or phase profiles are best, least squares, fits to use specified radial mode profiles. Tests showed, for example, that a field, uniform magnitude and phase, could be achieved in the hole for $\ell = 0$ of a hole-coupled resonator. In most instances however the $\ell = 0$ mode was not the dominant arbitrary azimuthal field variation so that best fits to desired azimuthal is designed for the lowest loss mode.

CONTENTS

ILLUSTRATIONS

iii

ABBREVIATIONS AND SYMBOLS

A	Outer radius of mirror
B	Mirror separation
D	Radius of mirror focal ring
H	Radius of hole in mirror
M	Geometric field magnification factor
N	Fresnel number
R	Mirror radius of curvature
ℓ	Azimuthal mode index
m	Radial mode index
γ	eigenvalue
λ	wavelength
HUR	Resonator 1 of Figure 1
HUR CC	Resonator 2 of Figure 1
HUR NB	Resonator 3 of Figure 1
HUR NB CC	Resonator 4 of Figure 1

SECTION I
INTRODUCTION

The objective of this study was to investigate large mode volume hole-coupled optical resonators for high power laser applications. The work program was divided into six tasks with the following primary objectives.

Task 1 - To determine the usefulness of hole coupled resonators a computer program was to be developed to calculate and plot the eigenvalues, the internal resonator fields, the far-field pattern of the output beam, and the sensitivity of length misadjustment. Two specified hole-coupled resonators were to be analyzed.

Task 2 - A computer program was to be created to optimize the figure of laser resonator mirrors such that the dominant resonator mode would be the best fit, in a least squares sense to a desired, user specified, mode. The test case would be a uniform amplitude and uniform phase distribution over a circular aperture at the output plane of the resonator. Once the mirror figures were found, the resonator was to be analyzed using the tools developed in Task 1.

Task 3 - A study was to be made to determine the ratio of annular to hole output coupling required to achieve good azimuthal mode discrimination in a designated resonator configuration.

Task 4 - A study similar to that of Task 3 was to be conducted for a resonator with holes in both mirrors.

Task 5 - An investigation was to be made of the possibility of using conformal mapping techniques to transform circular geometries to rectangular geometries where the resonator eigenmode calculations could be expedited using the fast Fourier transform.

1

Task 6 - The field fitting program of Task 2 was to be improved and applied to various "desired" mode shapes while noting the effects on the azimuthal mode discrimination properties of the associated resonators.

The results of Tasks 1 through 5 are presented in Sections II through VI, respectively. Since the results of Task 6 primarily yielded improvements in the results of Task 2, they are included in Section III.

The capabilities of two computer programs developed during the contract period are described in Sections II and III. Details related to the calculation methods used in the programs are contained in appendixes A and B.

SECTION II

TASK 1 - RESULTS

A. General Information

A computer program has been developed and used to analyze the eigen-
modes of several hole-coupled resonators. The program can compute and
plot: 1) the eigenvalues versus the outer resonator Fresnel number, 2)
the internal resonator fields (magnitude and phase), and 3) the far-field
patterns of circular cylinderical resonators having mirrors of arbitrary
radial figure in the Fresnel approximation.

The method of calculation used in the program is similar to that
described by Siegman and Miller in their article on the Prony method [1]*,
but with appropriate modifications to accommodate arbitrary radial mirror
figures. To dispense with the problem of the "spurious" eigenvalues
which they described, the Prony calculation itself is iterated to insure
converged (or non-converged) solutions. The initial vector for each
Prony calculation after the first one is taken as the sum of the nor-
malized eigenvectors computed during the previous calculation. In cases
where convergence is not achieved after a specified number of iterations,
those eigenvalues and eigenfunctions are discarded. More specific details
concerning the method of calculation and computer programming are contained
in Appendix A.

Two hole-coupled resonators were identified by the Air Force project
officer [2] as test cases for analysis using the computer program. The
mirror profiles of these two resonators, designated HUR and HUR CC are
depicted in Figure 1. The other two resonators shown in the same figure
are considered "negative branch" versions of the first two. These four
resonators are confocal versions of a more general class of resonators

---

*Numbers in brackets indicate references.

3
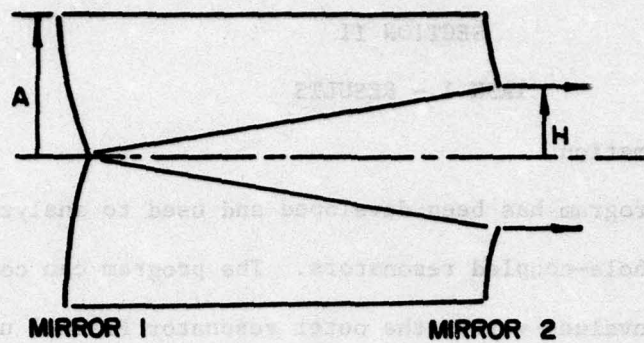
RESONATOR 1
HUR

$H = \dfrac{M-1}{M} A$

$M \geq 1$

$D_1 = A$

$D_2 = D_1$

MIRROR 1   MIRROR 2
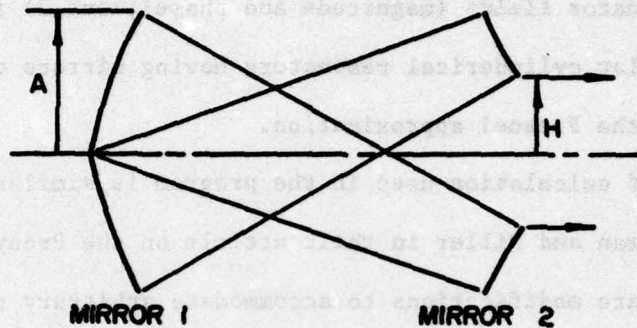
RESONATOR 2
HUR CC

$H = \dfrac{M-1}{M} A$

$D_1 = \dfrac{M}{1-M} A$

$M \geq 1$

$D_2 = -D_1$

MIRROR 1   MIRROR 2
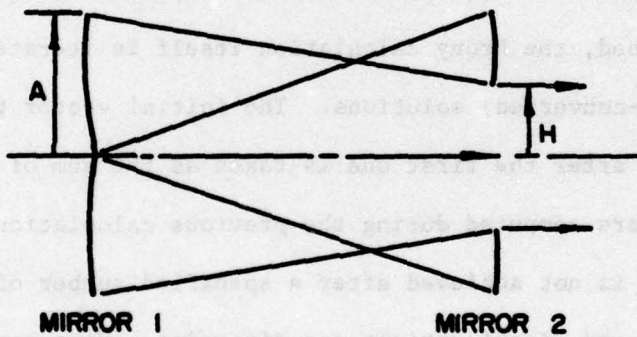
RESONATOR 3
HUR NB

$H = \dfrac{M+1}{M} A$

$D_1 = \dfrac{M}{M-1} A$

$M \leq -1$

$D_2 = D_1$

MIRROR 1   MIRROR 2
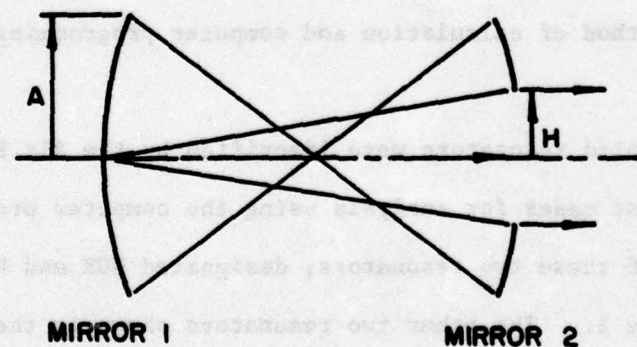
RESONATOR 4
HUR NB CC

$H = \dfrac{M+1}{M} A$

$D_1 = \dfrac{1+M}{1-M} A$

$M \leq -1$

$D_2 = -D_1$

MIRROR 1   MIRROR 2

Figure 1 - Four Confocal Hole-Coupled Resonator Configurations
(M - Magnification, D_1 and D_2 are the radii of the
focal rings of Mirrors 1 and 2, respectively.)

4

in which the mirrors are conic sections with arbitrary off-axis spherical curvature. These are "confocal" but not in the usual sense because the mirrors have focal rings rather than focal points. The radii of the focal rings are designated D_1 and D_2 for mirrors 1 and 2, respectively. Both mirrors have an outer radius of A. Mirror 2 has a central output aperture, or hole, of radius H. A magnification $M = A/(A-H)$ is associated with the first two resonators, and a negative magnification $M = A/(H-A)$ is associated with the "negative branch" configurations.

The computer program was used to plot the radial mode eigenvalues versus the outer resonator Fresnel number $N = A^2/(B\lambda)$ (B-mirror separation, λ-wavelength) for various magnifications and azimuthal mode indices ℓ (where azimuthal variation of the form exp $(\pm j\ell\phi)$ has been assumed). The program was also used to plot the internal resonator fields and the far-field patterns for various Fresnel numbers. Representative plots are shown and discussed in the following subsections.

B. Analysis of Resonator 1 - HUR

Figures 2 through 6 show the eigenvalue plots for resonator 1 of Figure 1 for magnifications $M = \sqrt{2}$, 5/3, 2, 3, and 8, respectively. The eigenvalues intertwine in a slightly more complicated fashion than those of the conventional unstable resonator (e.g., see reference 1). An even more significant difference between the mode of this resonator and a conventional unstable resonator is that only for very small Fresnel numbers ($N \approx 1$) is the $\ell=0$ mode dominant. (The dominant mode at a given Fresnel number is the mode with the largest eigenvalue magnitude $|\gamma|$ or lowest losses $1 - |\gamma|^2$.) For example, in comparing parts a, b, c, and d of Figure 2 for $M = \sqrt{2}$, the $\ell=0$, 1, 2, and 3 azimuthal modes are dominant within the approximate Fresnel number ranges 0-1.5, 1.5-5.5, 5.5-9.5, and 9.5-?, respectively.

5
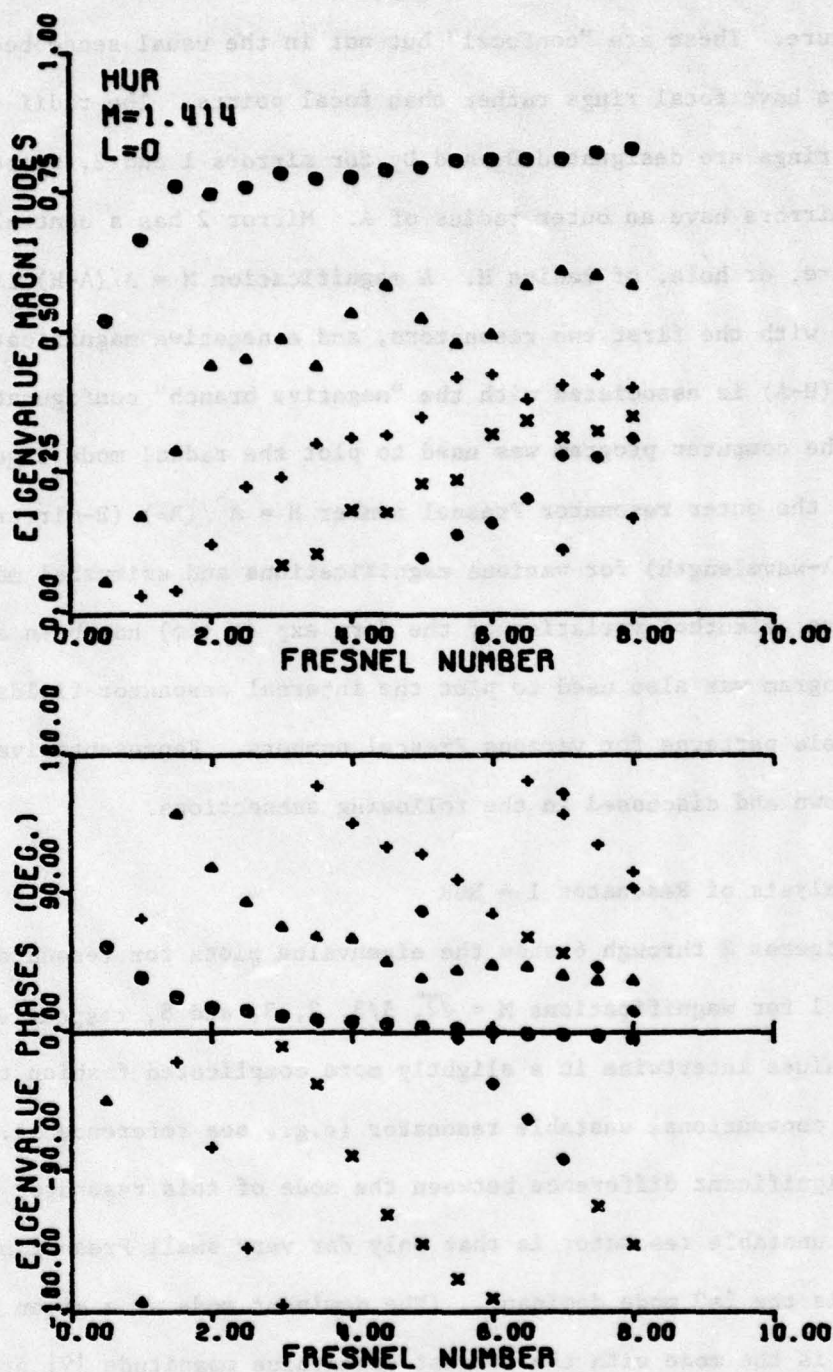
Figure 2a Eigenvalues of HUR for M = $\sqrt{2}$, ℓ =0

6

Figure 2b $\ell = 1$

Figure 2c $\ell = 2$

EIGENVALUE MAGNITUDES

HUR
M=1.414
L=3

FRESNEL NUMBER

EIGENVALUE PHASES (DEG.)

FRESNEL NUMBER

Figure 2d ℓ = 3

9
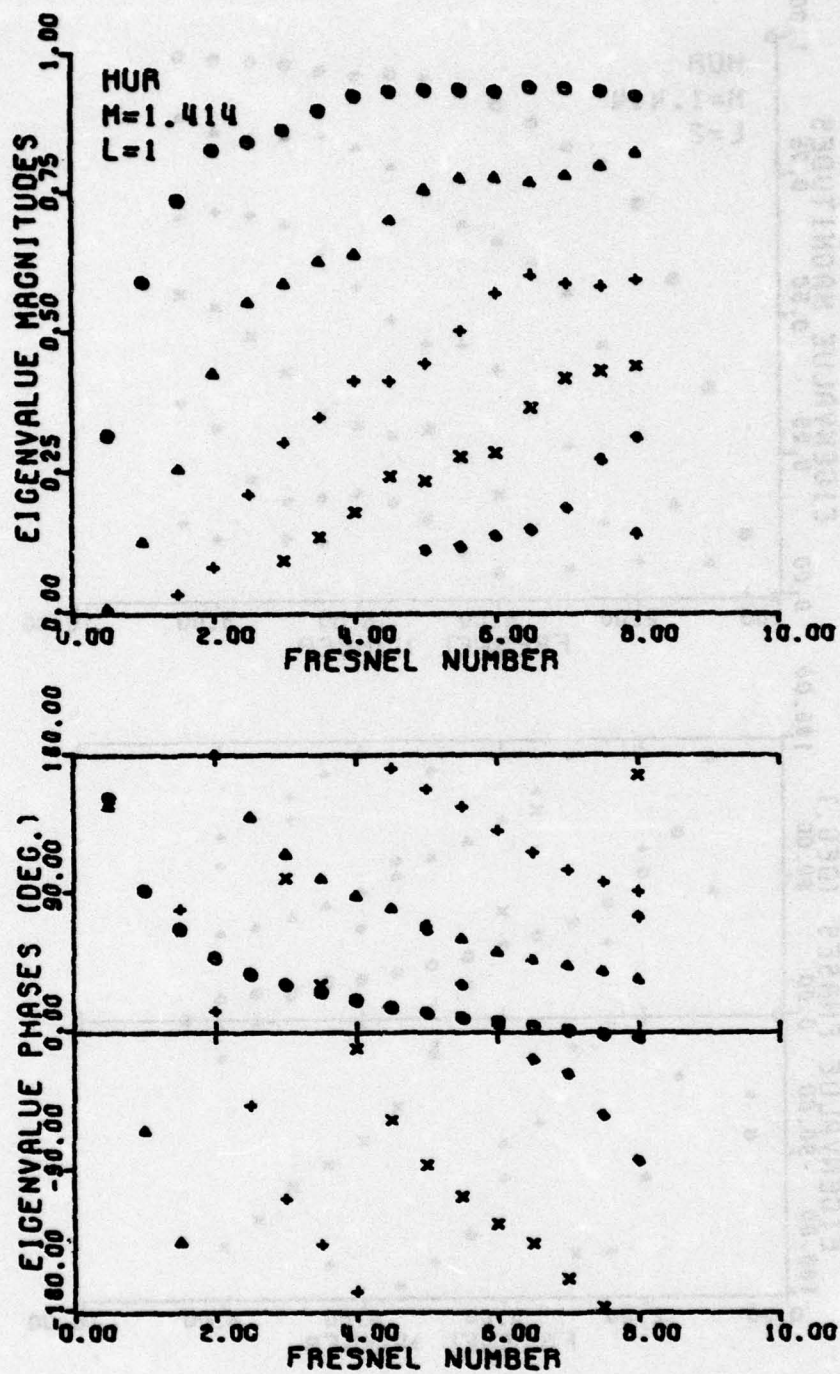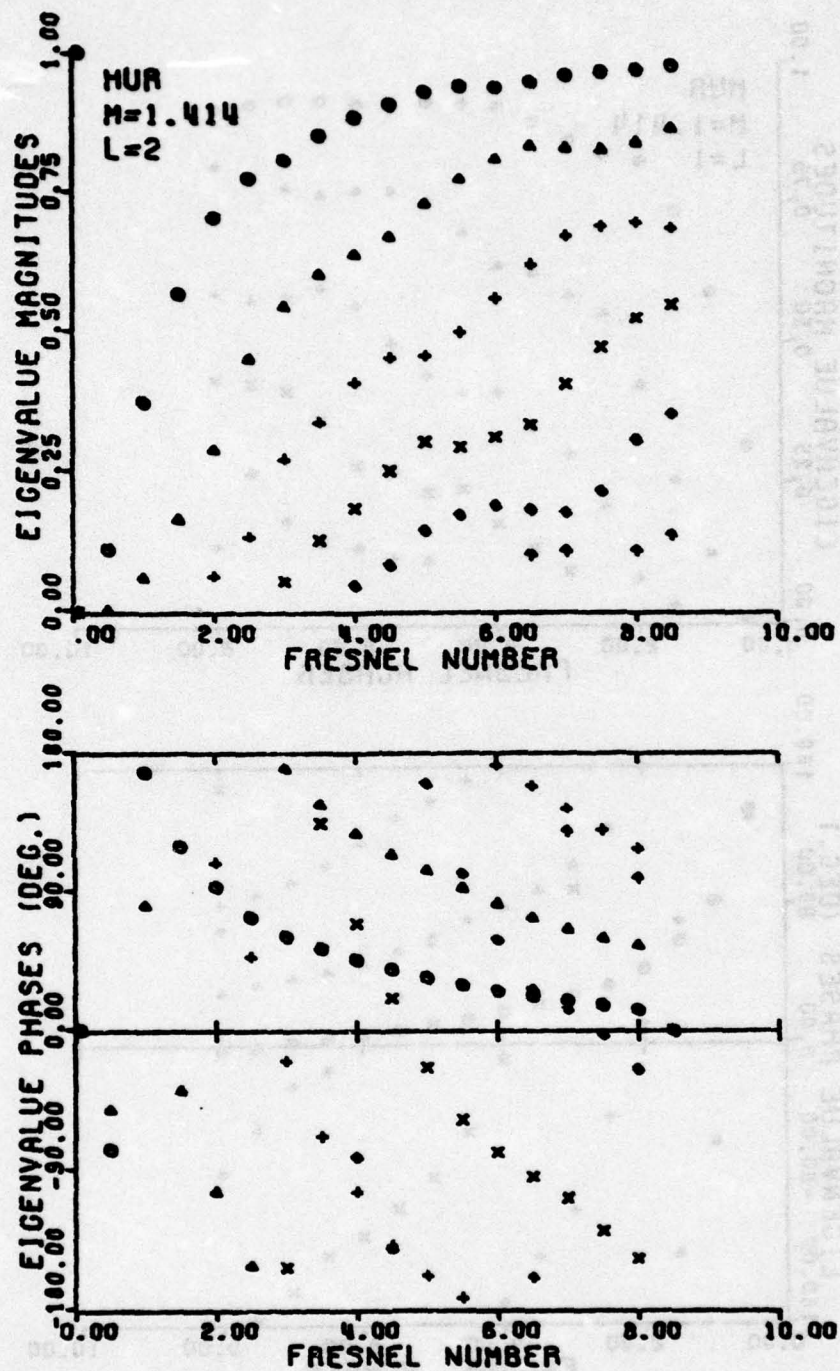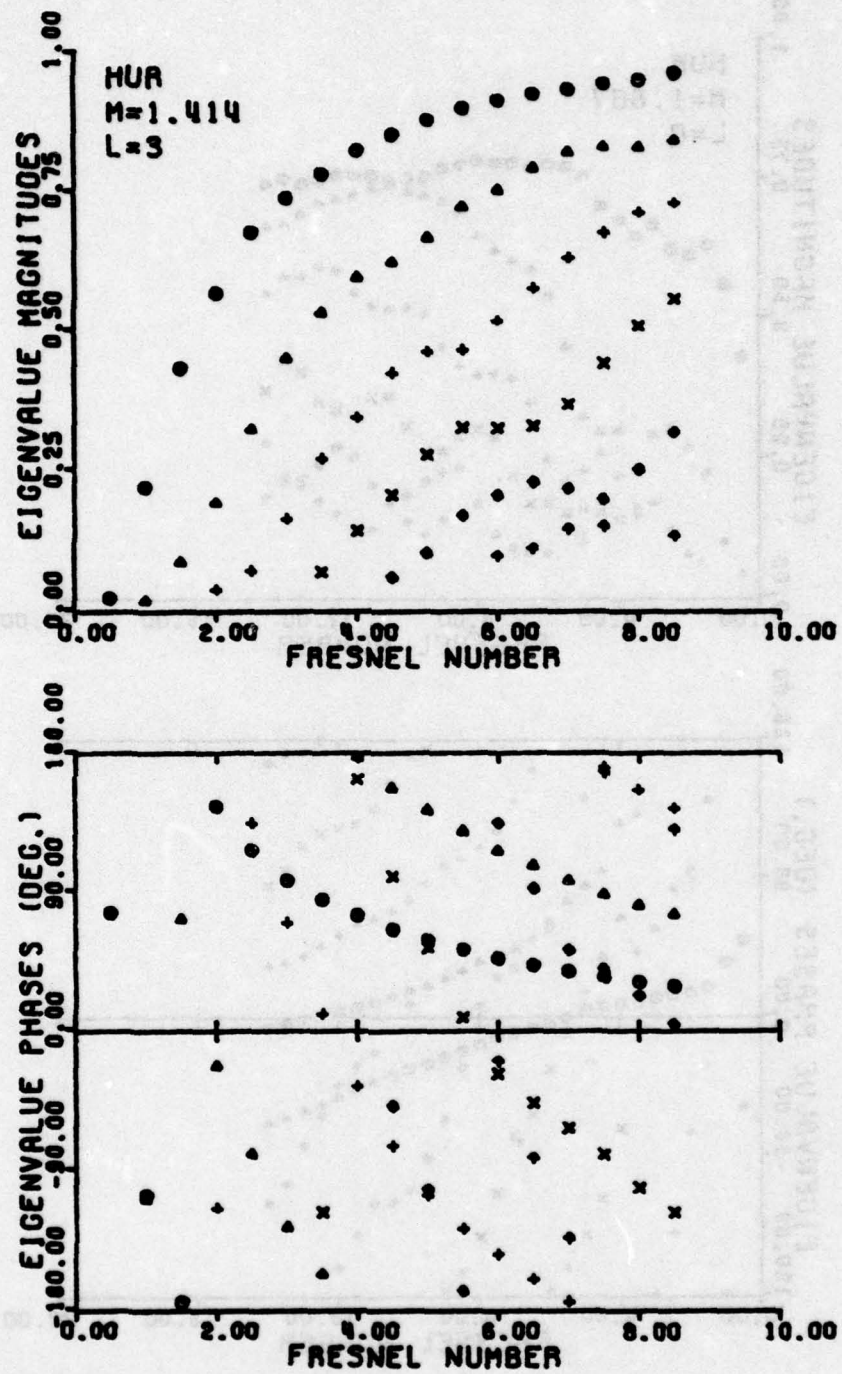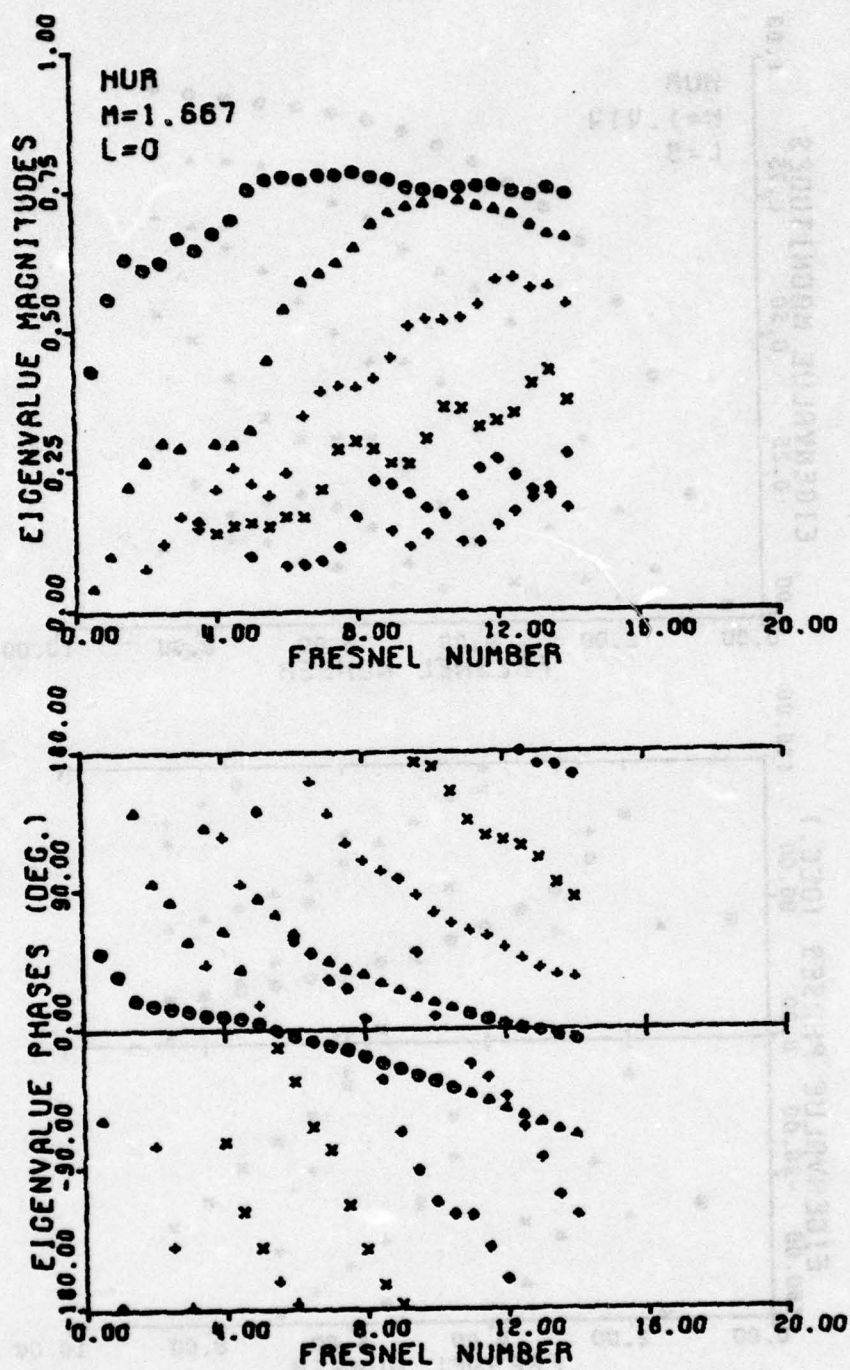
Figure 3a Eigenvalues of HUR for M = 5/3, ℓ = 0

10

Figure 3b ℓ = 1

11
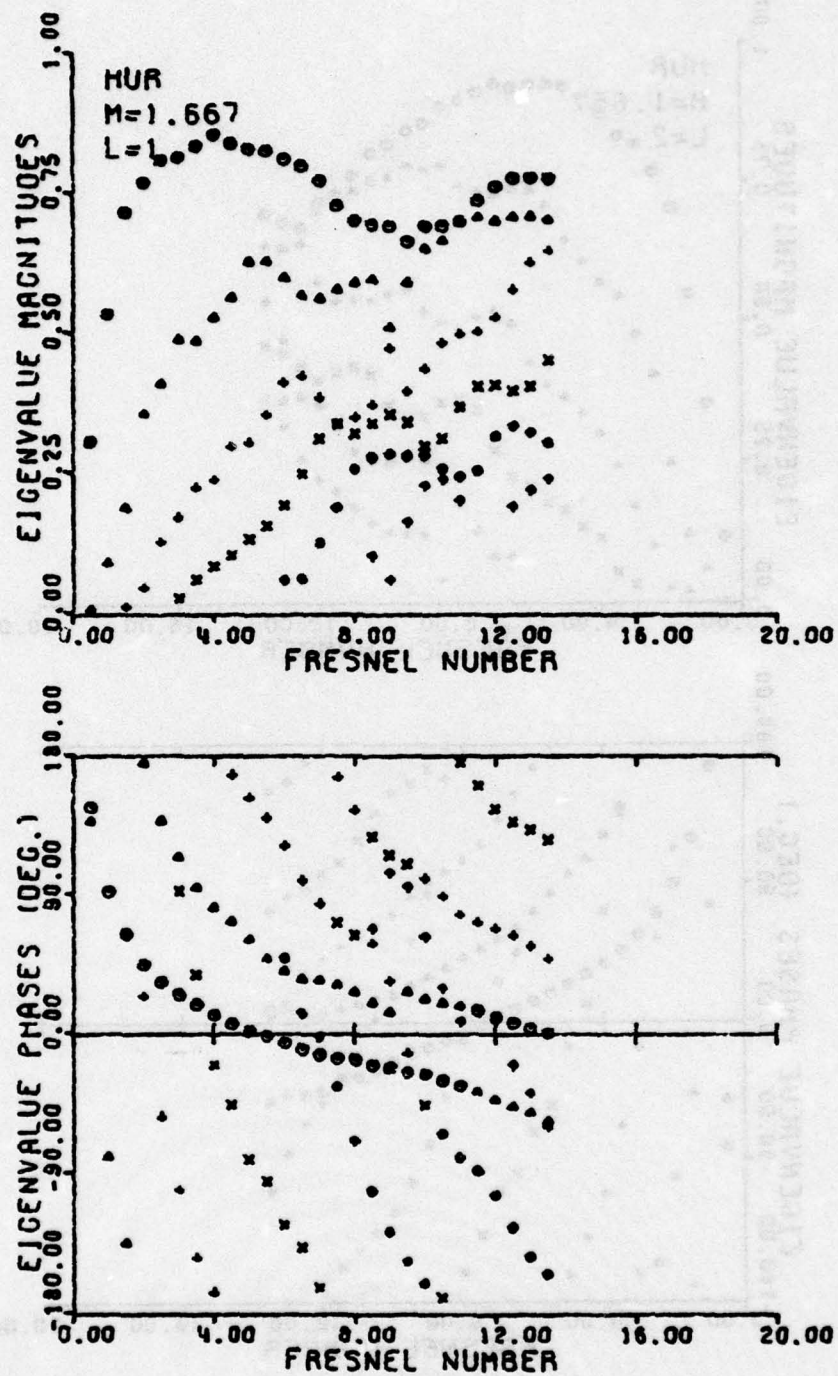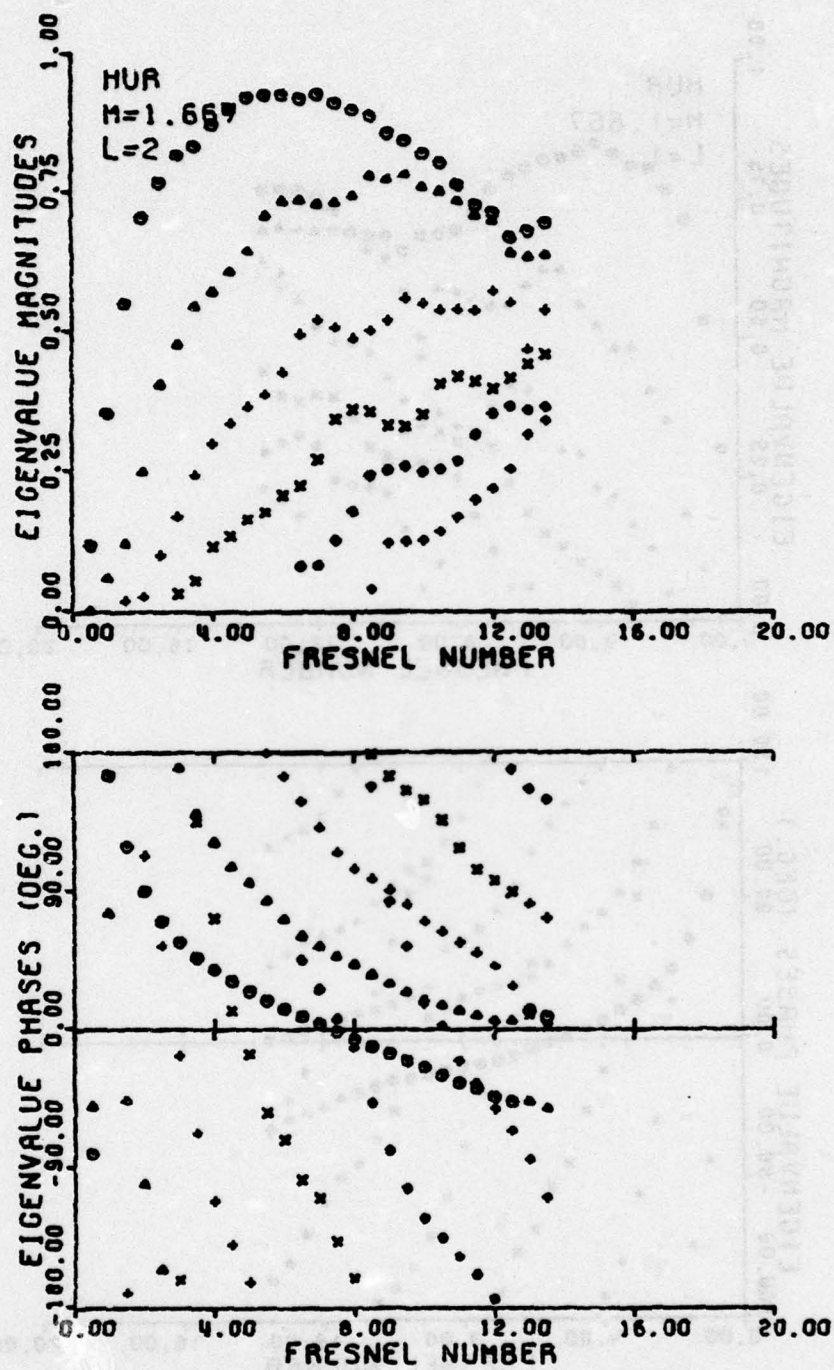
Figure 3c $\ell = 2$

12
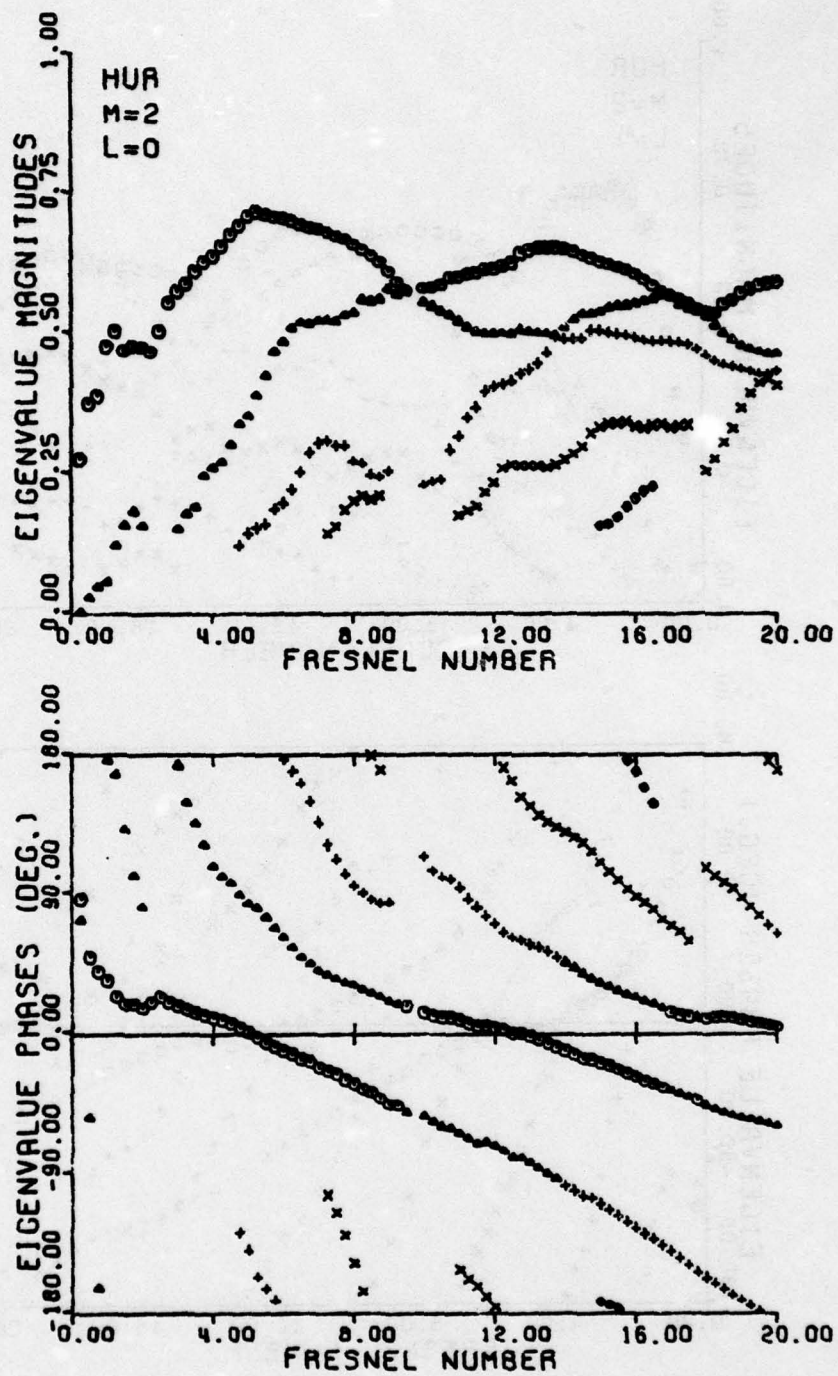
Figure 4a   Eigenvalues of HUR for M = 2, ℓ = 0

13

Figure 4b ℓ = 1

14

Figure 4c $l = 2$

15

Figure 4d $\ell = 3$

16
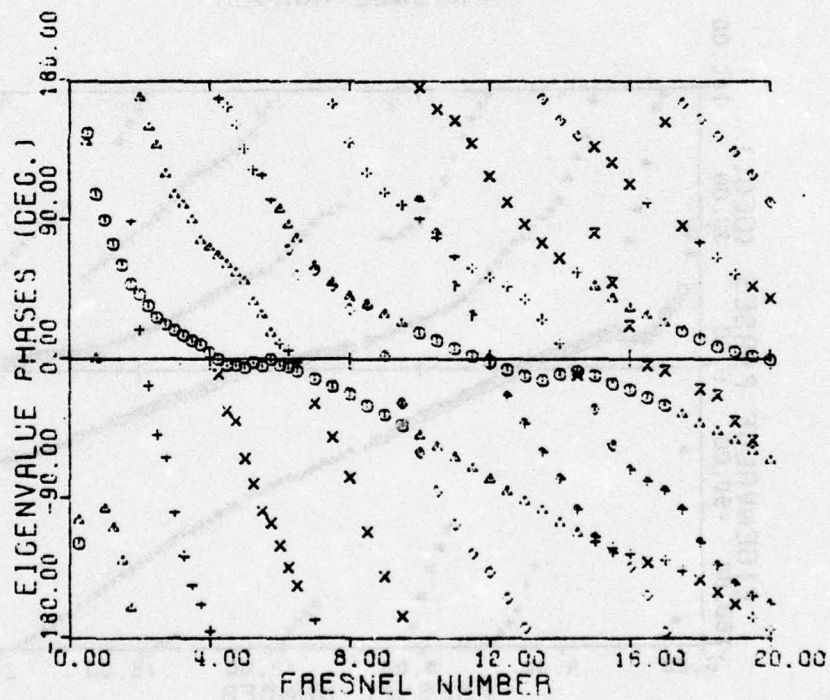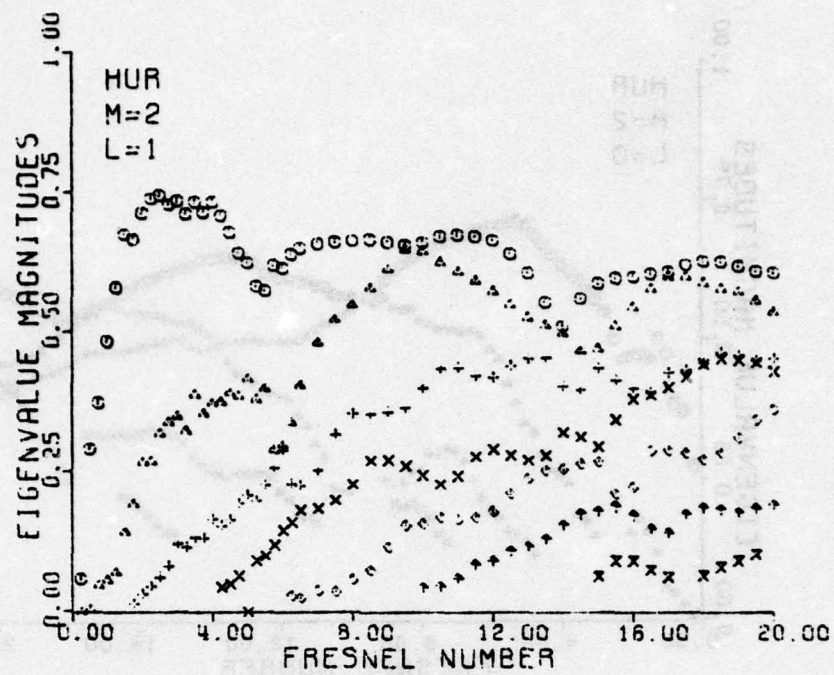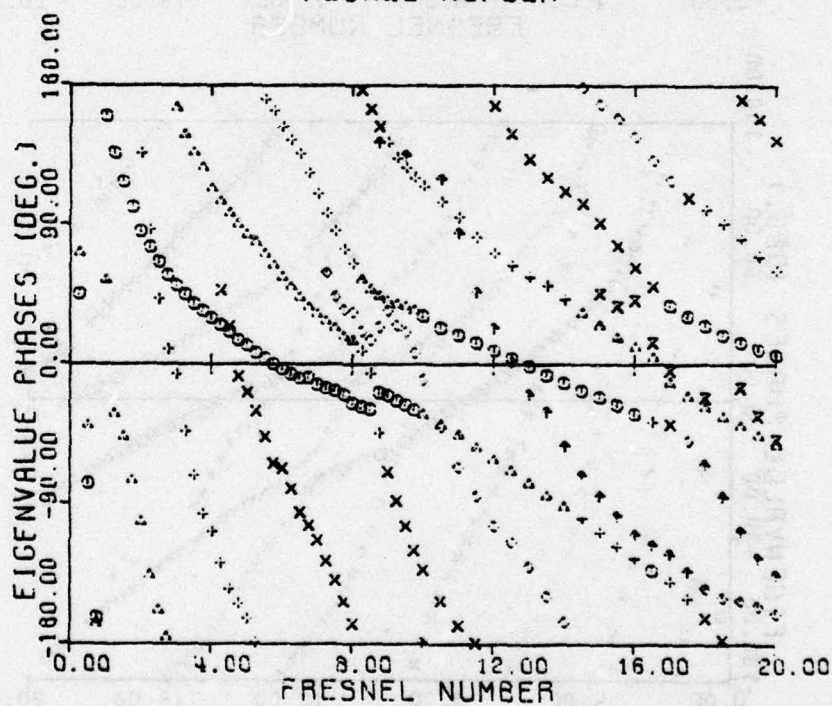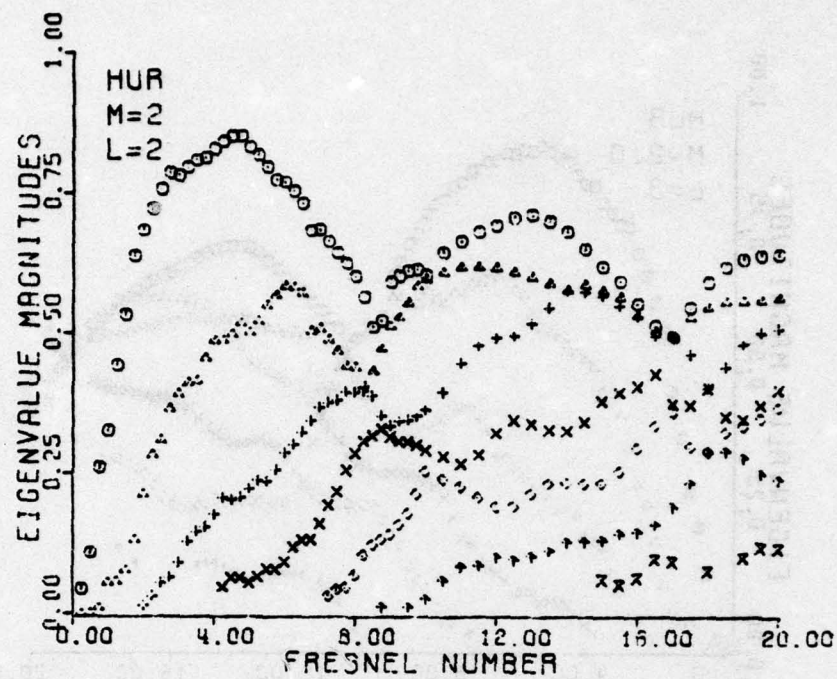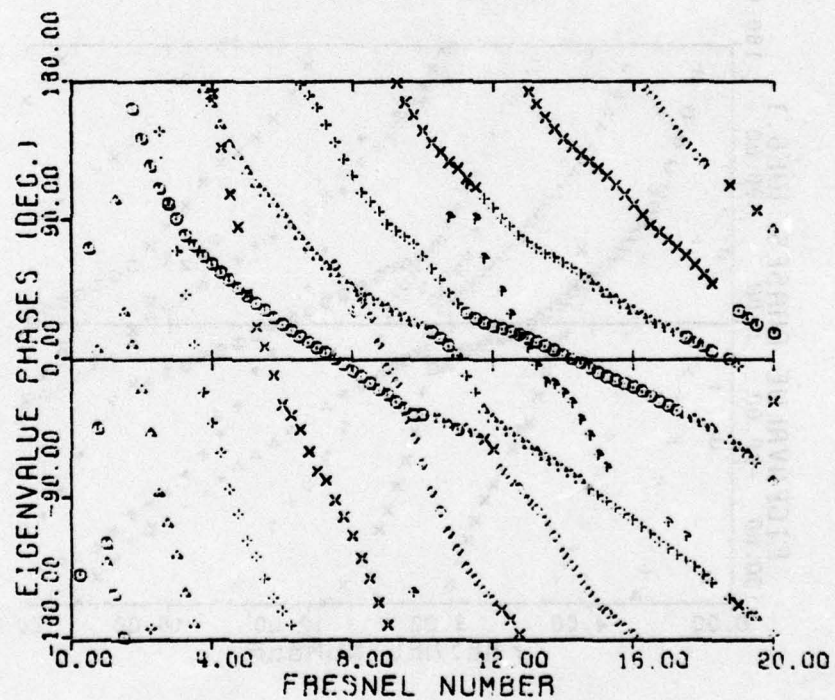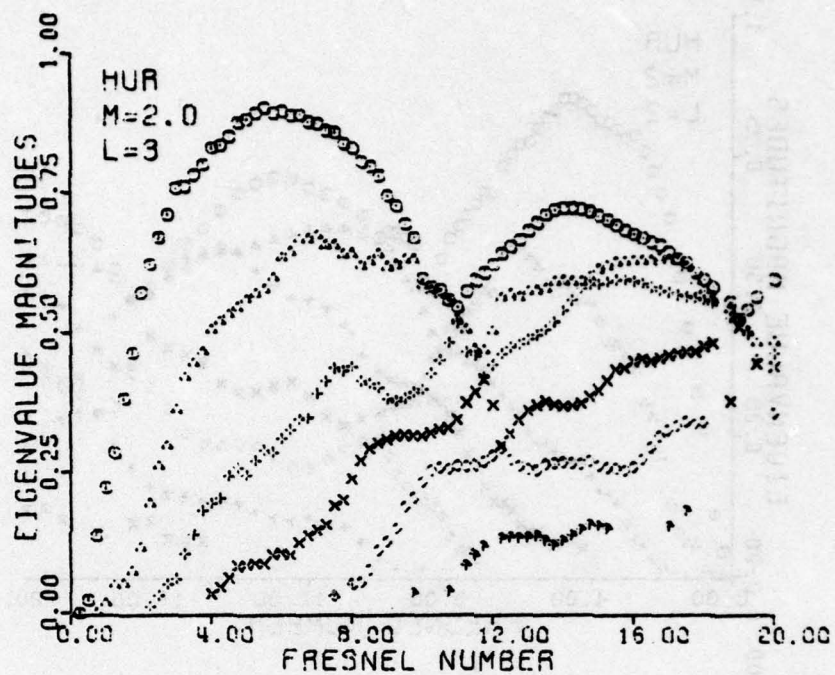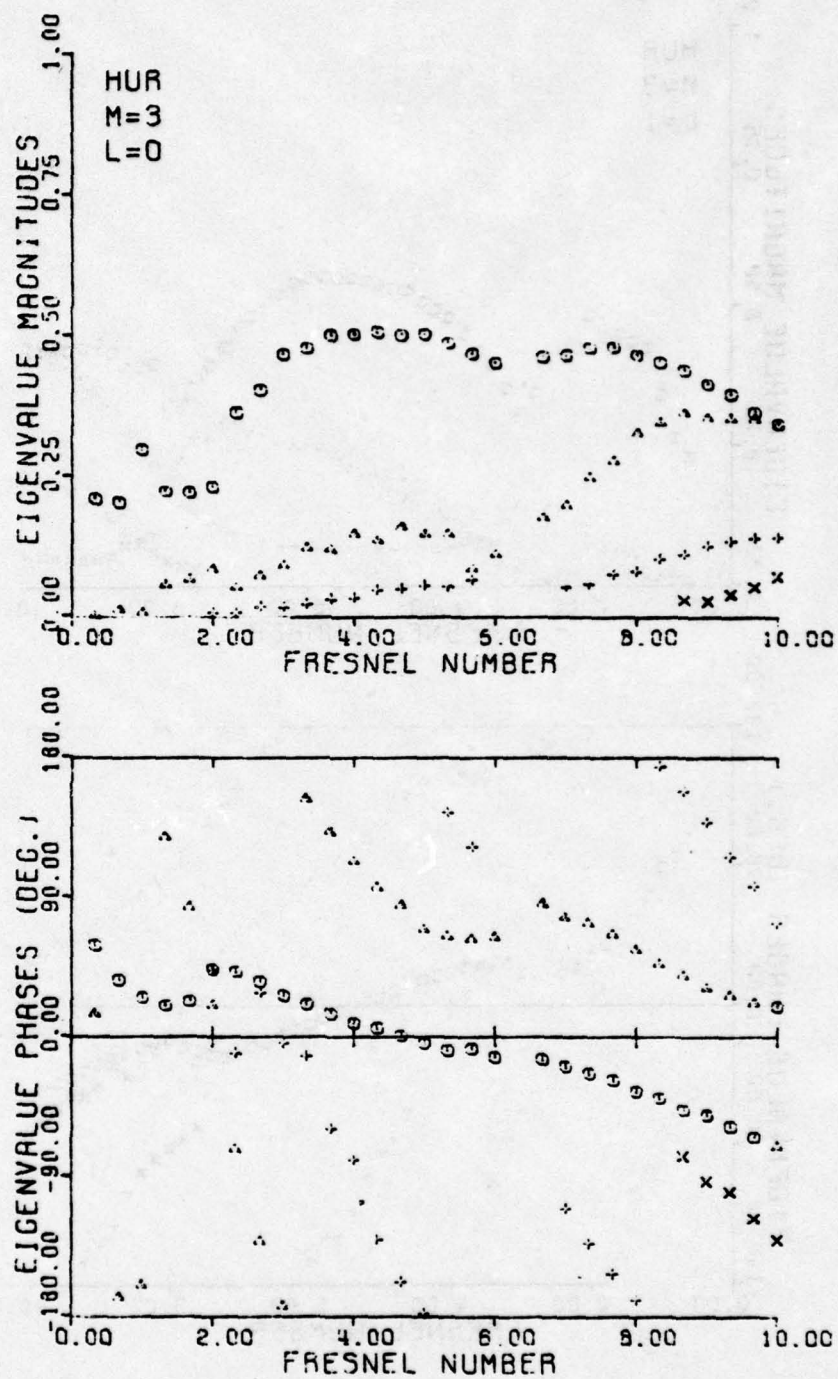
Figure 5a   Eigenvalues of HUR for M = 3, ℓ = 0

17

Figure 5b ℓ = 1

18

Figure 5c $\ell = 2$

19

Figure 5d $\ell = 3$

20
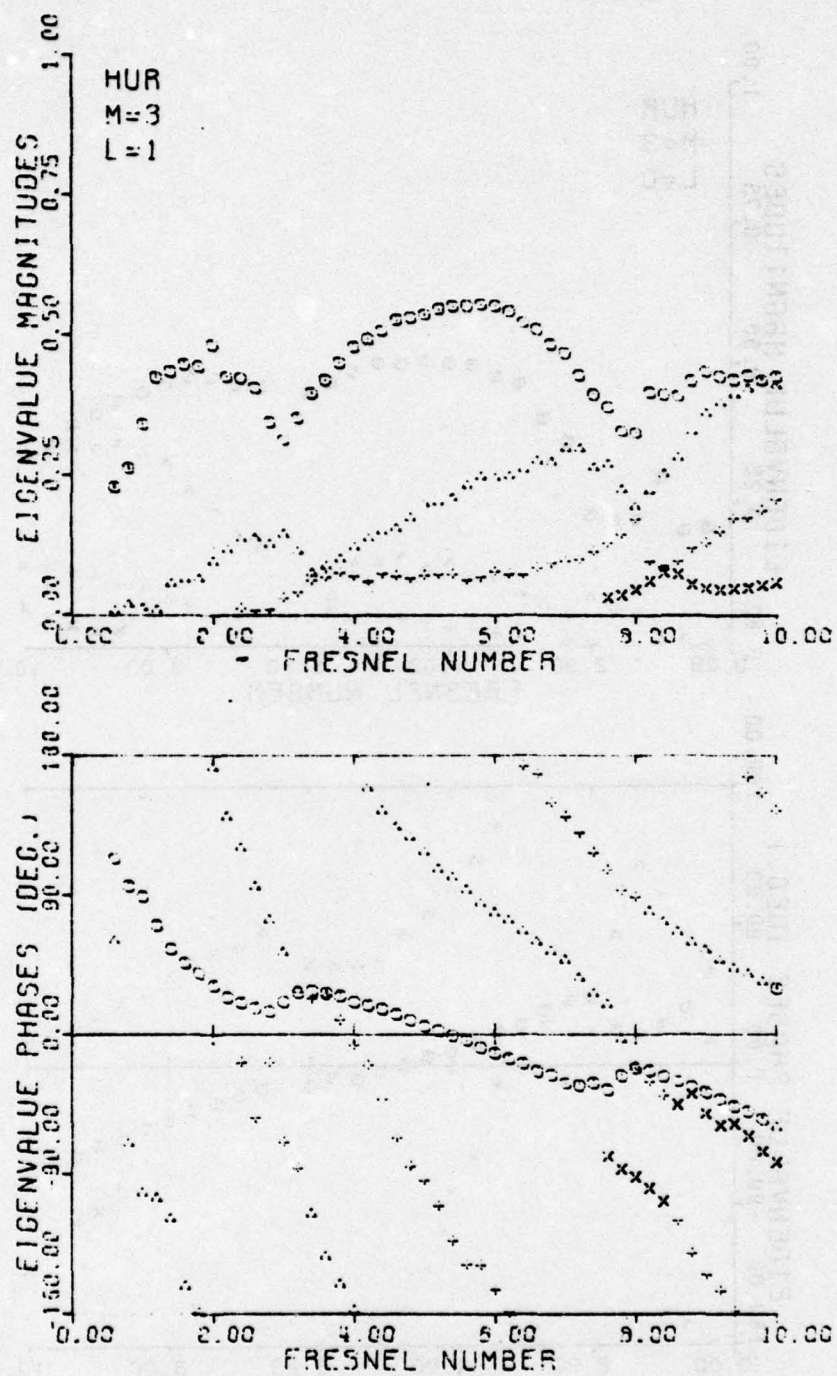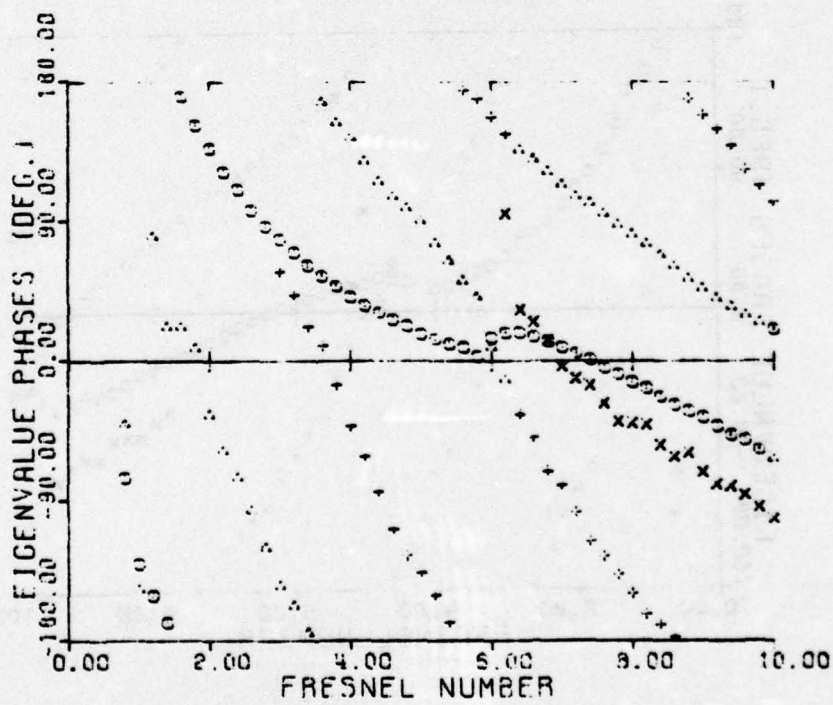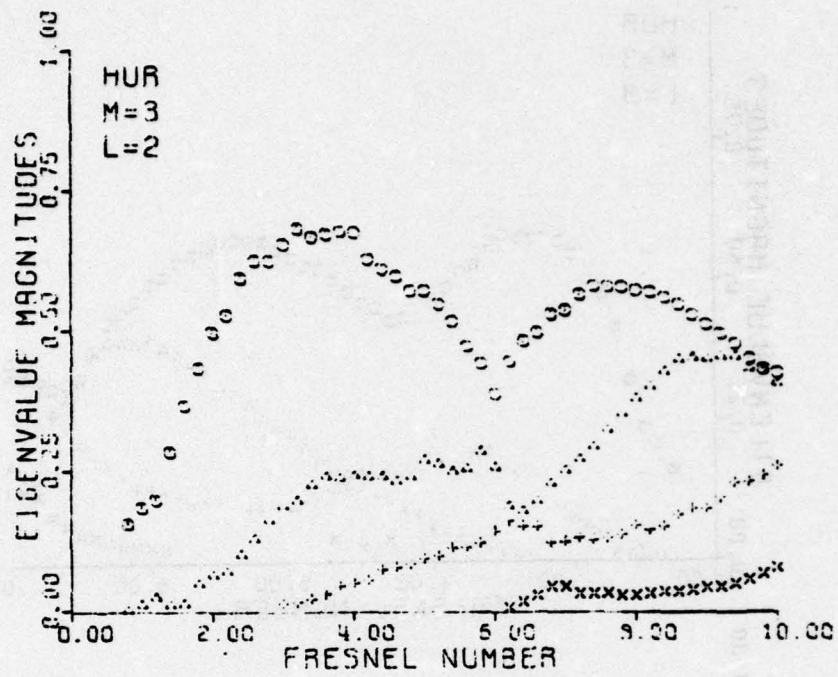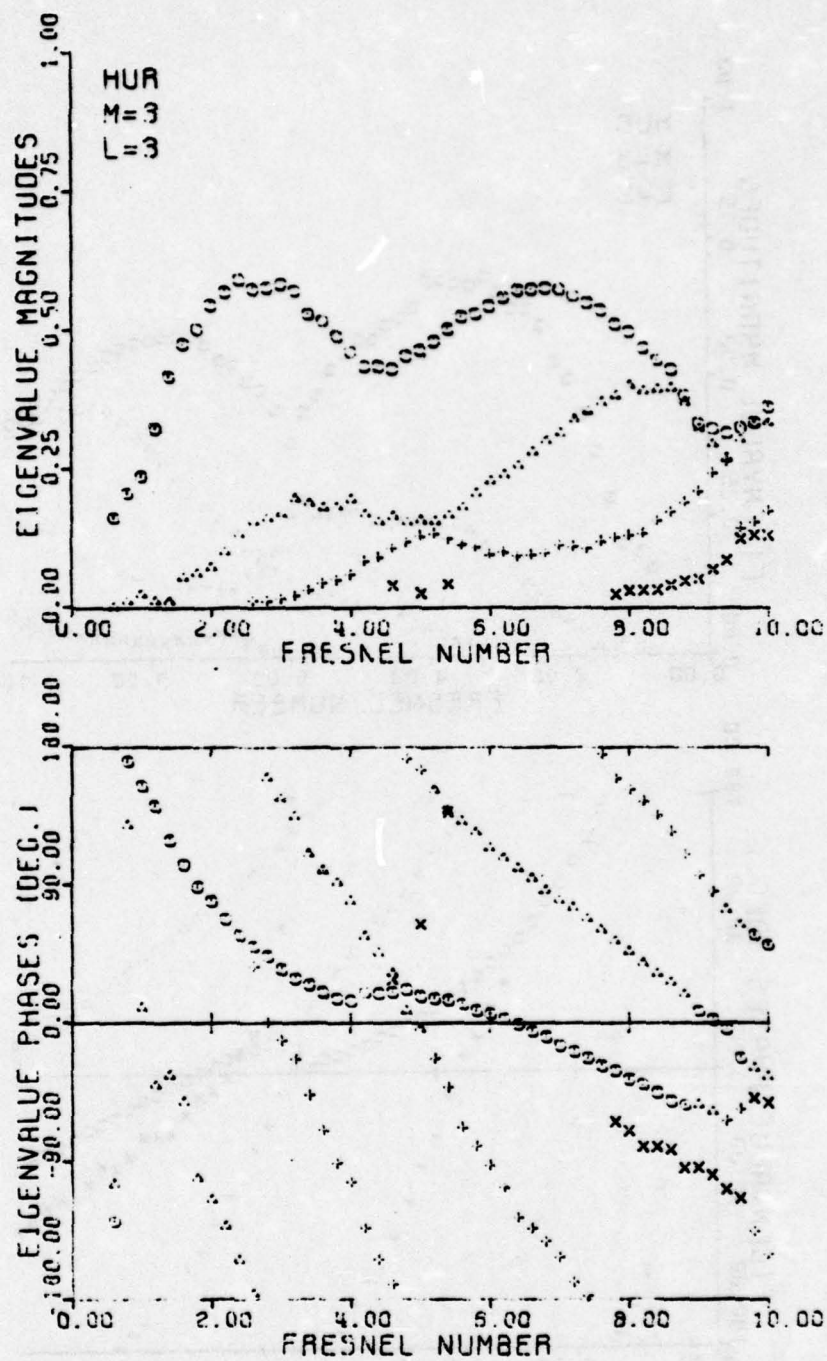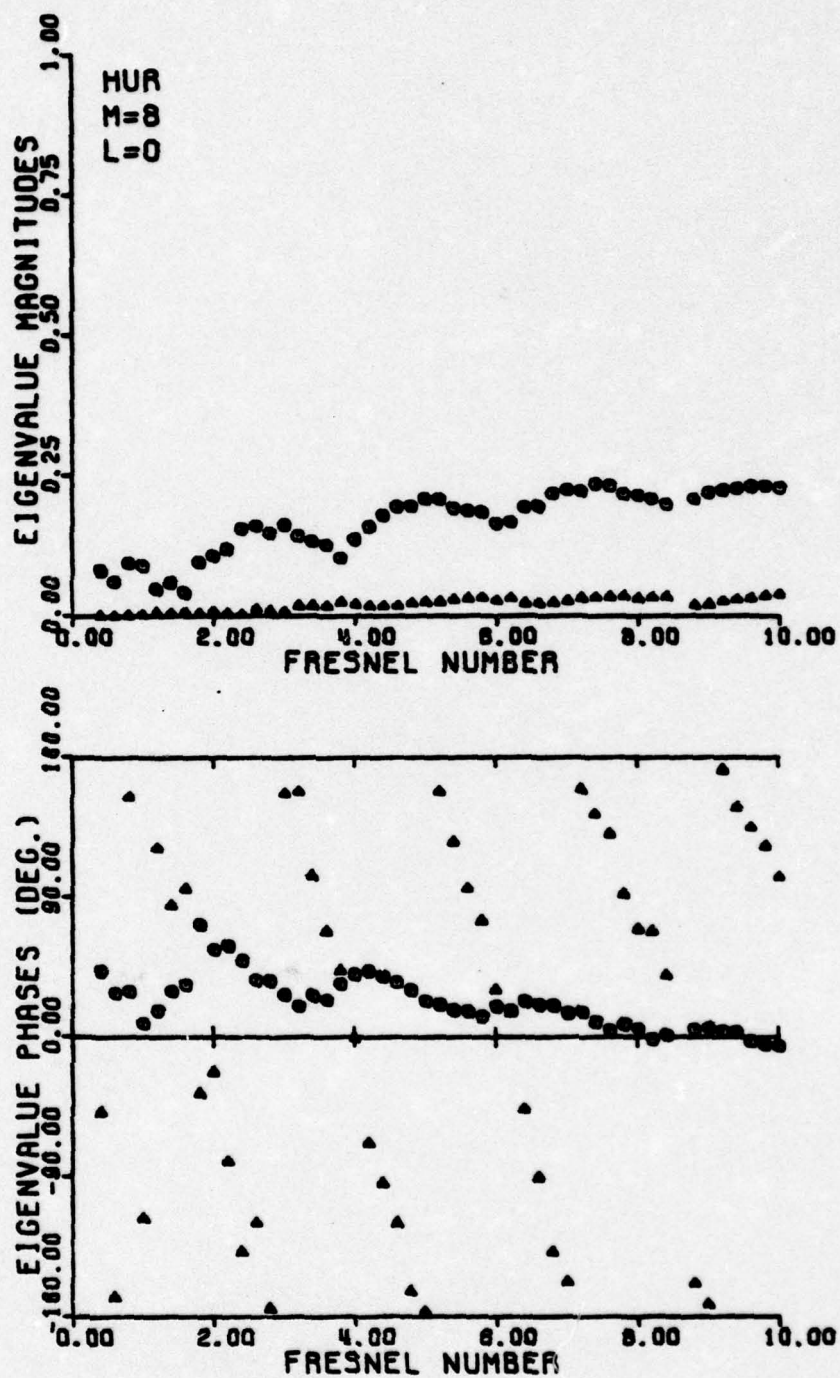
Figure 6a   Eigenvalues of HUR for M = 8, ℓ = 0

HUR
M=8
L=0
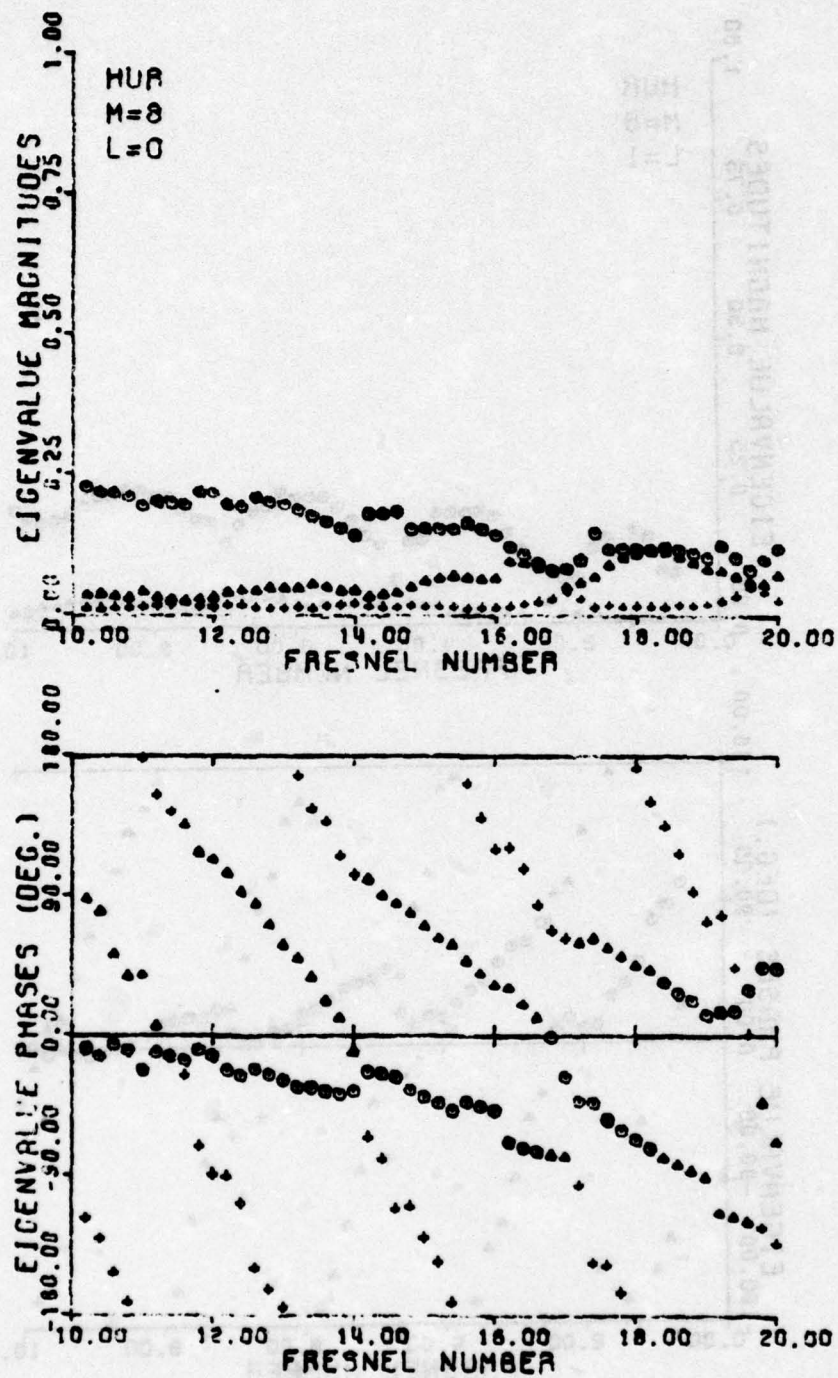
Figure 6a   Continued

21.1

HUR
M=8
L=1

Figure 6b ℓ = 1

22
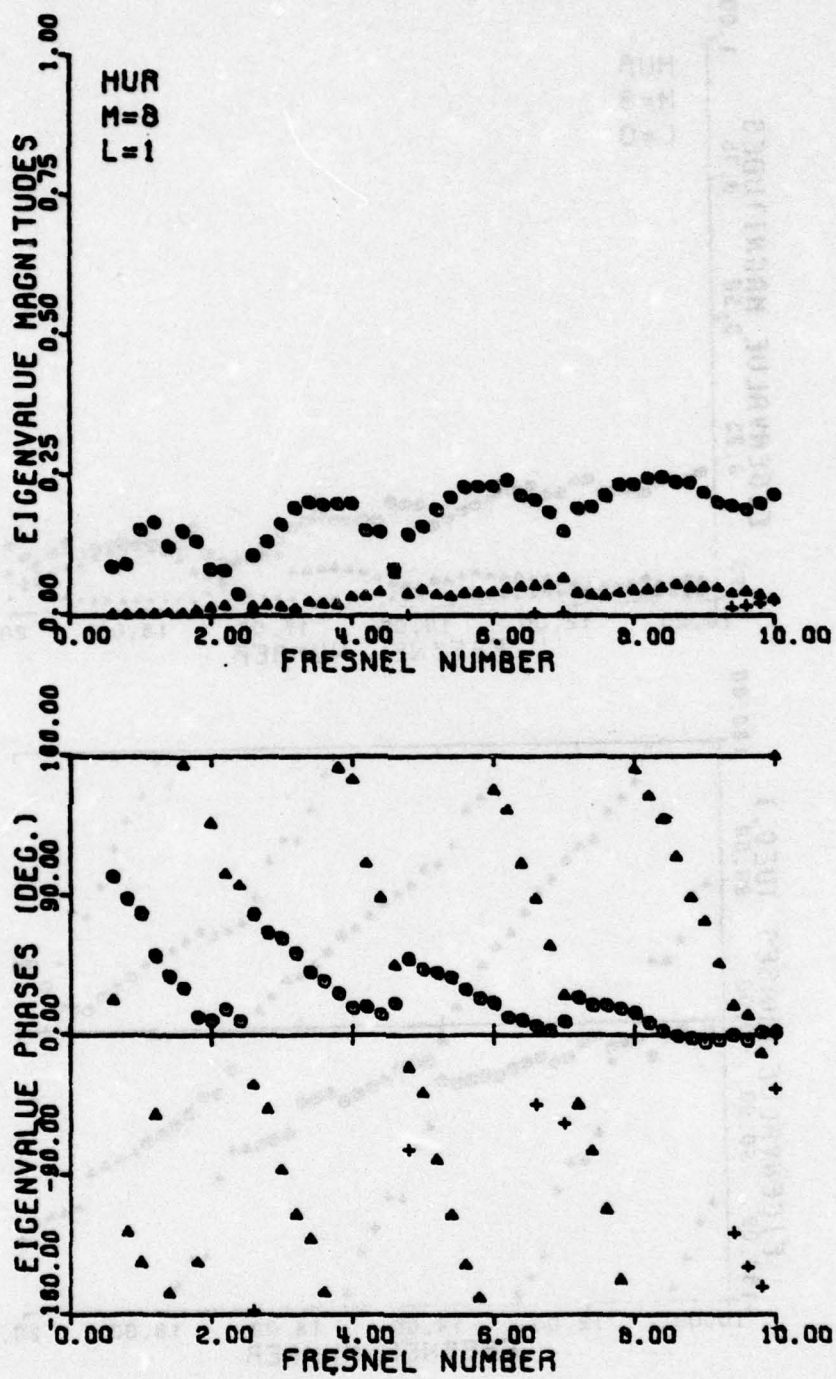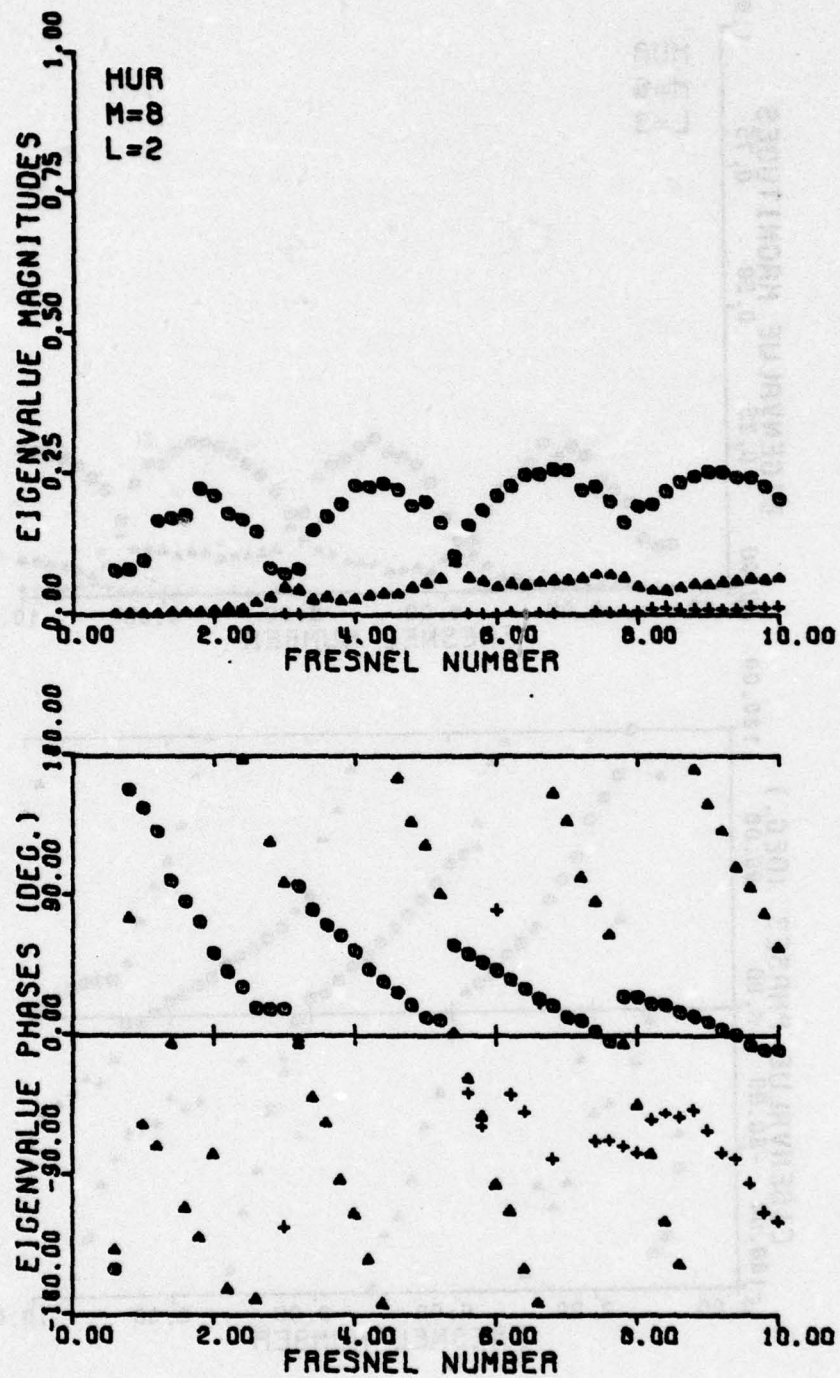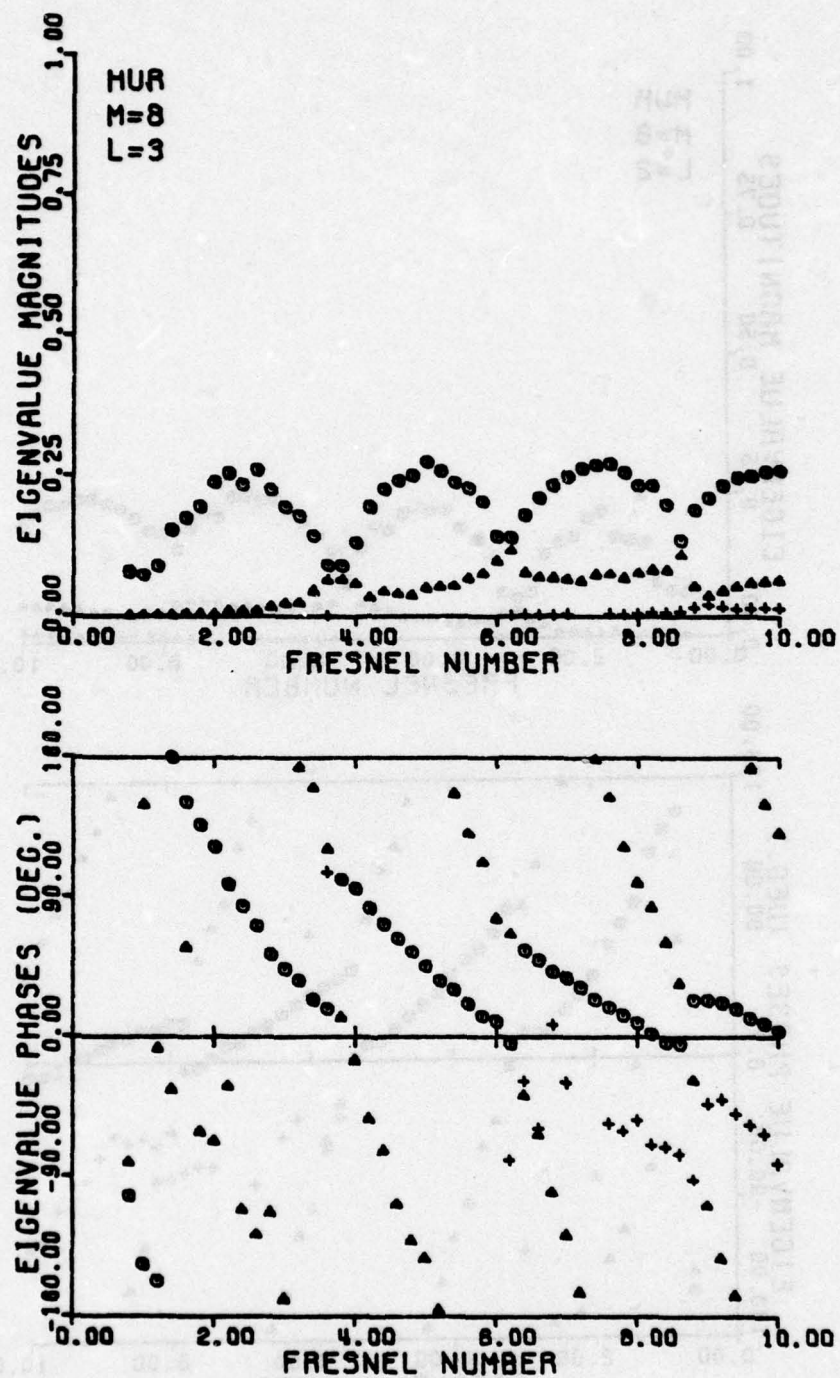
Figure 6c $\ell = 2$

Figure 6d $l = 3$

Figure 7 shows the radial eigenmode of field plots for the lowest order azimuthal mode $\ell=0$, for M=2 and N=6. The eigenvalues for the three radial modes can be found in Figure 4a at N=6. Figure 7a shows the amplitude and phase of the three lowest loss radial modes in a plane just after being reflected from mirror 1. Probably the most striking feature is the rather sharp magnitude peak at the center of the mirror (relative radial coordinate equal to zero). The phase of the lowest loss radial mode decreases approximately 90° from the center of the mirror to the outer edge (relative radial coordinate equal unity). The phase of the next lowest loss mode on the other hand increases to approximately 90° near the outer edge but then decreases to near zero at the edge. The phase profile of the third lowest loss mode has even more variation.

Figure 7b shows the same fields except plotted in a plane just incident on mirror 2. At this magnification the radius of the hole in mirror 2 is one half the outer mirror radius. Since the fraction of the field in the hole relative to that on the mirror increases for the higher order radial modes it is easy to understand that the higher order modes have more losses. Both the magnitude and the phase of the lowest loss radial mode are fairly uniform in the output hole which results in the near "ideal" far-field beam profile shown in Figure 7c. For comparison, the far-field pattern corresponding to uniform illumination of the hole with the same power as in the lowest order radial mode for $\ell=0$ is also shown. Finally the integrated far-field intensity associated with the two far-field plots of Figure 7c are shown in Figure 7d. Out to the half-power beam width, the two plots are virtually identical. The fact that there is slightly more power within a given beam angle larger

25
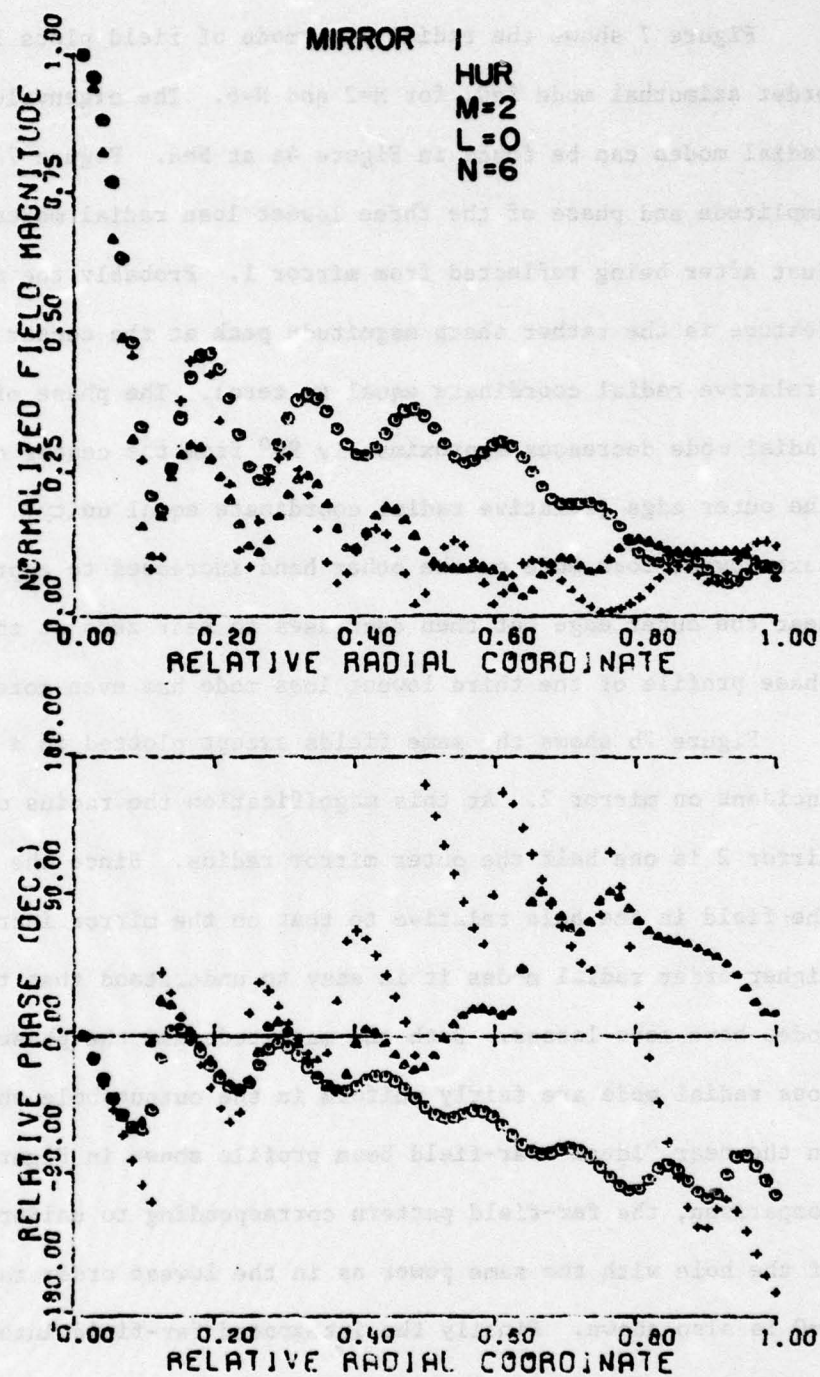
Figure 7a Radial mode profiles reflected from mirror 1 of HUR for M = 2, ℓ = 0, N = 6
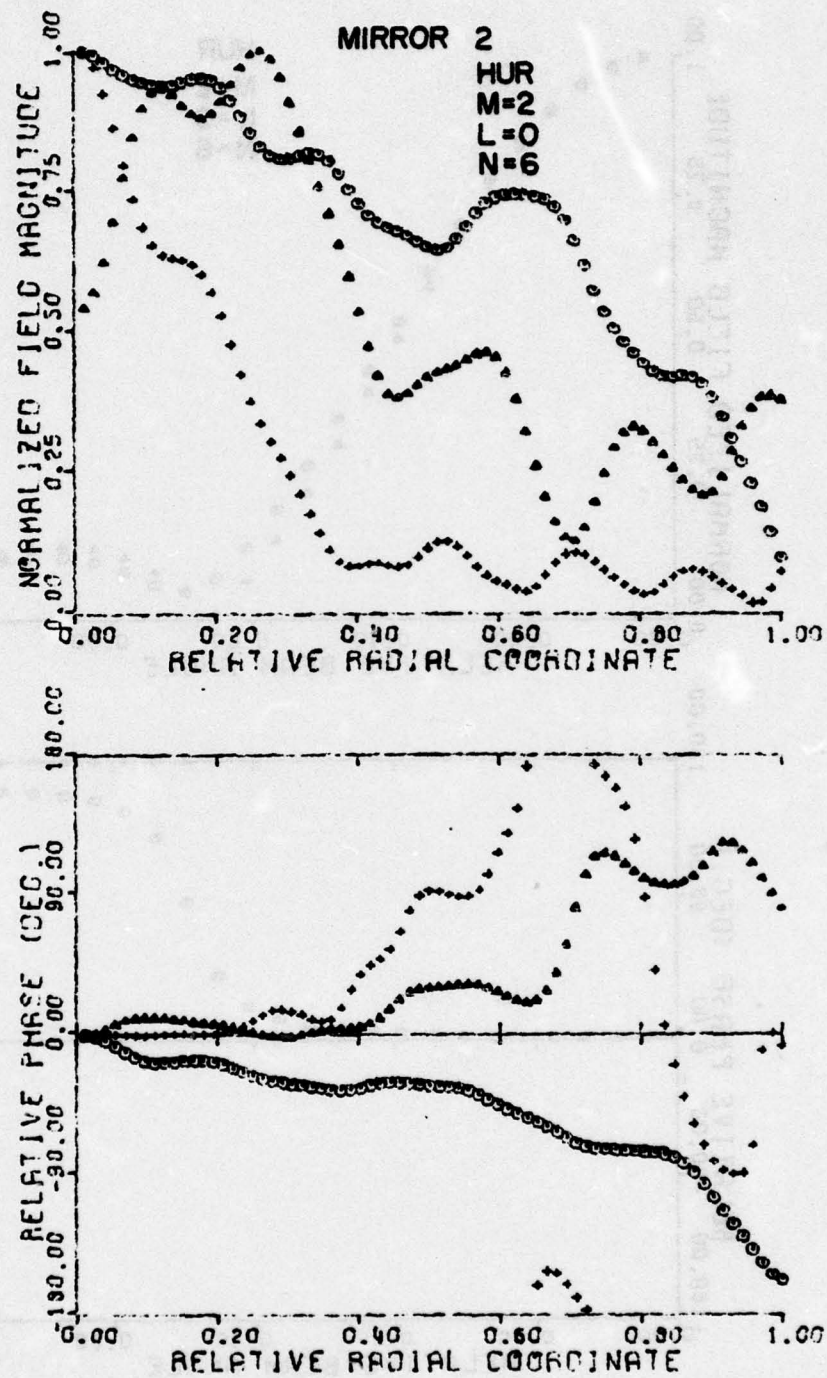
Figure 7b Radial mode profiles in a plane incident at
mirror 2

27
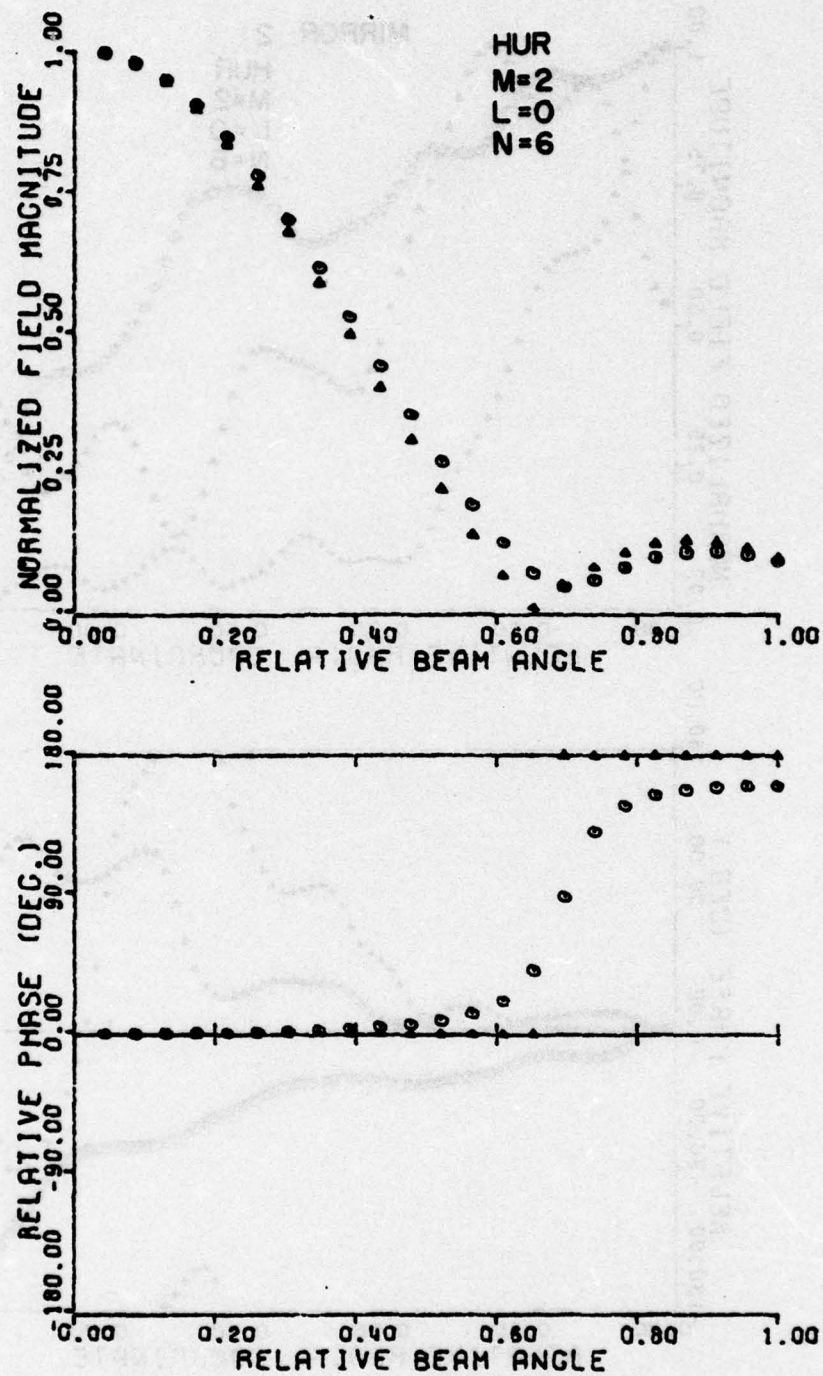
Figure 7c   Far-field pattern of lowest loss radial mode and
reference field (uniformly illuminated aperture)

28
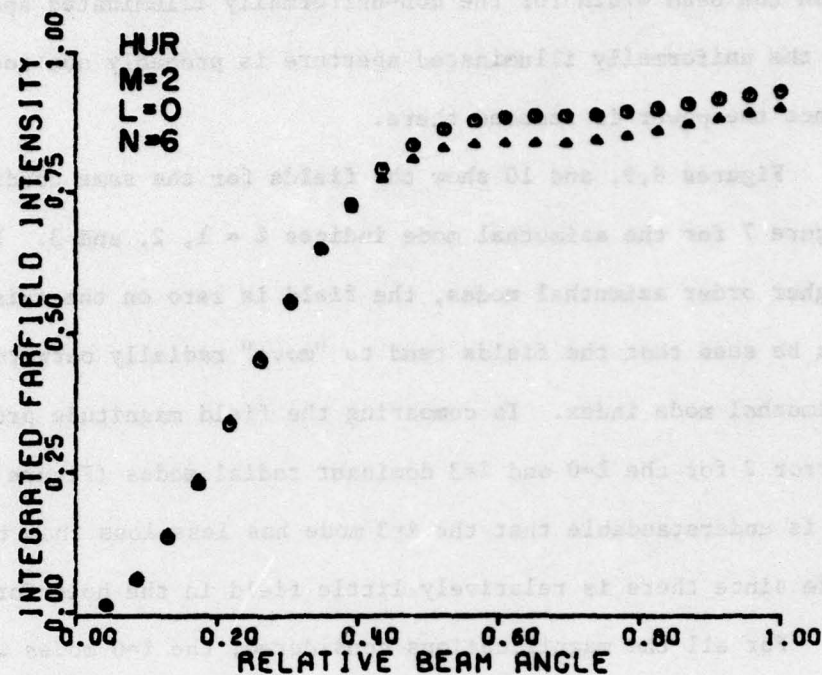
Figure 7d Integrated far-field intensity

than the beam width for the non-uniformly illuminated aperture relative to the uniformly illuminated aperture is probably not too significant, since the power is reduced there.

Figures 8,9, and 10 show the fields for the same conditions as Figure 7 for the azimuthal mode indices ℓ = 1, 2, and 3. For these higher order azimuthal modes, the field is zero on the axis. Also, it can be seen that the fields tend to "move" radially outward for increasing azimuthal mode index. In comparing the field magnitude profiles at mirror 2 for the ℓ=0 and ℓ=3 dominant radial modes (Figure 7b and 10b), it is understandable that the ℓ=3 mode has less loss than the ℓ=0 mode since there is relatively little field in the hole for the ℓ=3 mode.

For all the magnifications considered, the ℓ=0 modes were dominant only at very small Fresnel numbers. Increasing the size of the hole from zero apparently increases the losses more rapidly for the ℓ=0 mode than the higher order azimuthal modes. Thus, to obtain any significant power output from this type resonator in the ℓ=0 mode will require that some method be devised which would discriminate against the higher order azimuthal modes.

C. Analysis of Resonator 2 - HUR CC

Figure 11 shows the eigenvalues for the four lowest order azimuthal modes for resonator 2 of Figure 1 with M=2. Only for Fresnel numbers less than 0.5 is the ℓ=0 mode dominant. The computer program has considerable difficulties in achieving converged solutions for Fresnel numbers greater than N=6. A clue to the difficulty can be obtained by examining the complex field structure for the ℓ=0 and ℓ=1 modes in Figures 12 and 13 at N=4. The large number of grid points required to delineate these

30
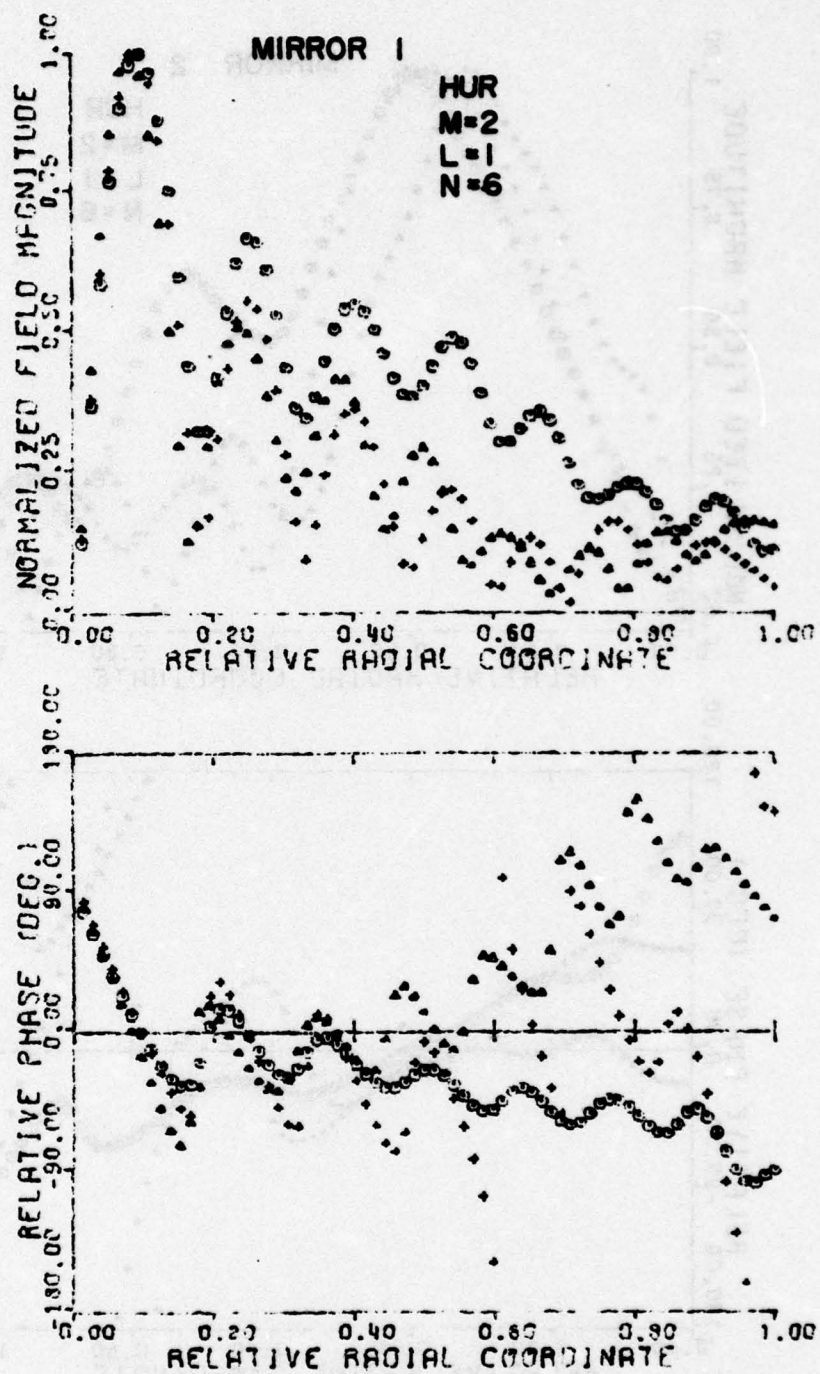
Figure 8a   Radial mode profiles reflected from mirror 1 of HUR
for M = 2, ℓ = 1, N = 6
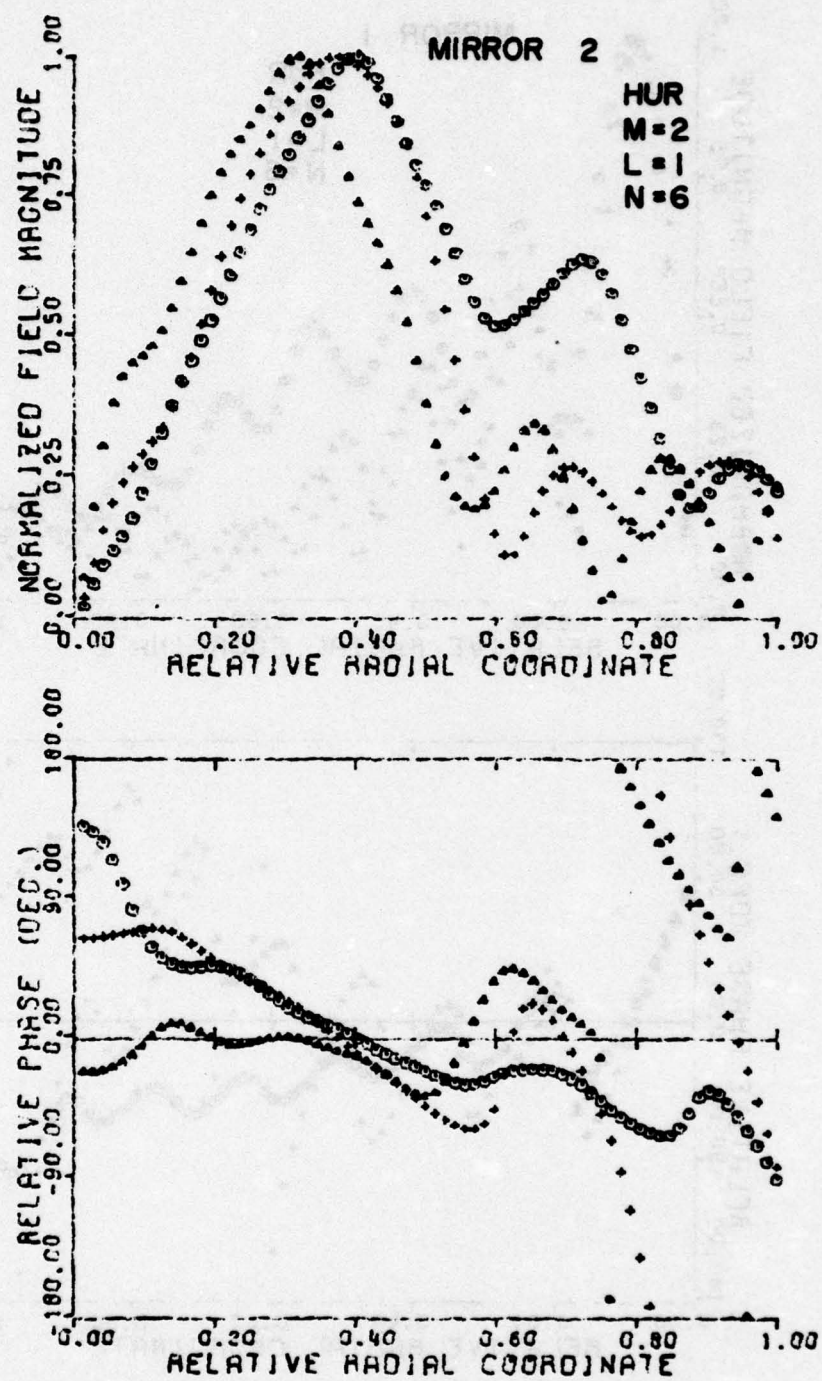
Figure 8b Radial mode profiles in a plane incident at mirror 2

32
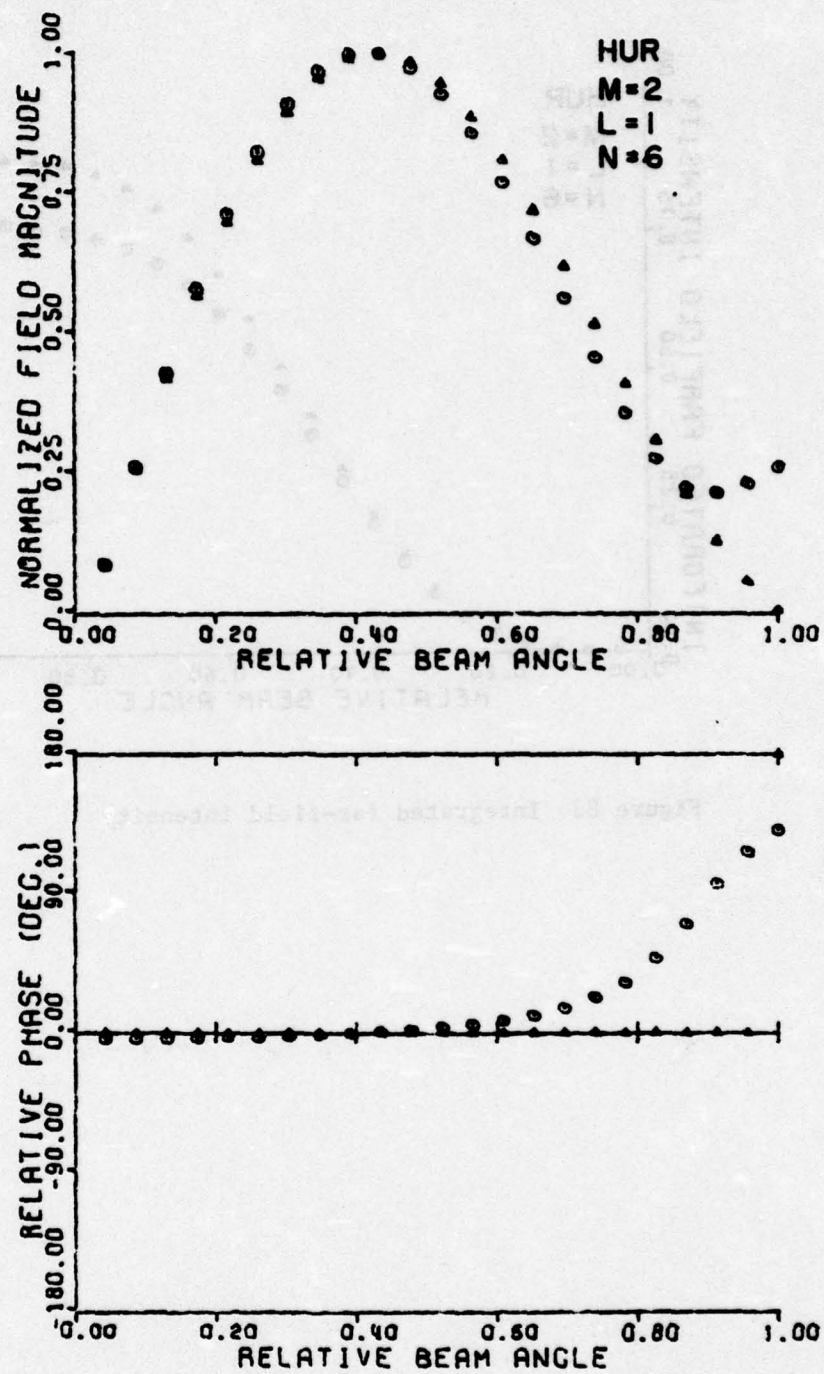
Figure 8c   Far-field pattern of lowest loss radial mode and
reference field

33
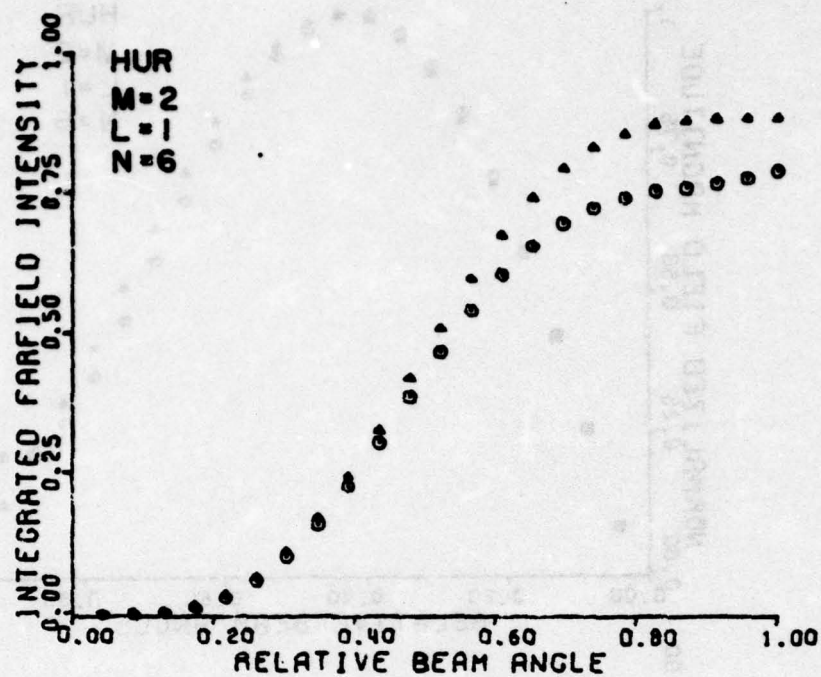
Figure 8d   Integrated far-field intensity
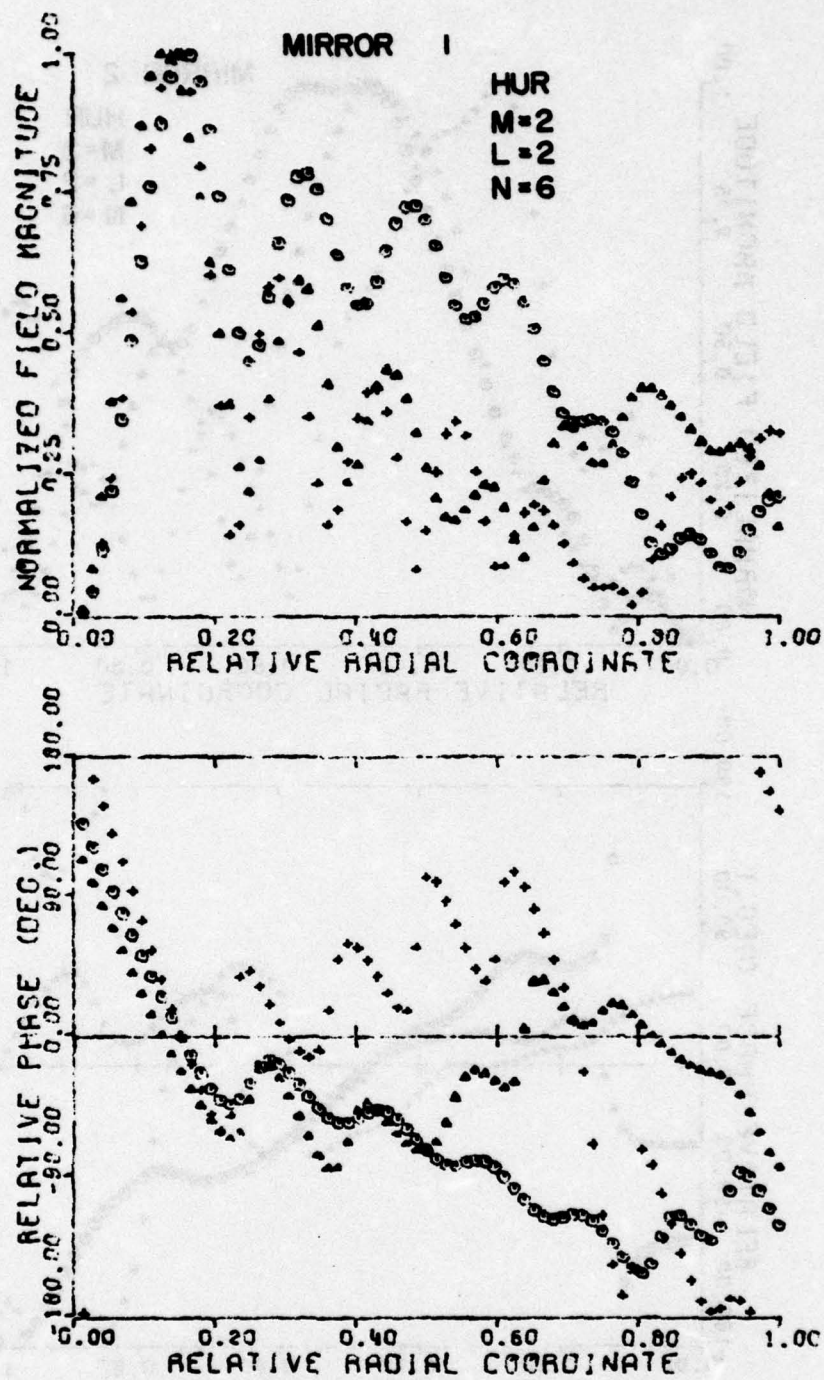
Figure 9a   Radial mode profiles reflected from mirror 1 of
HUR for M = 2, ℓ = 2, N = 6
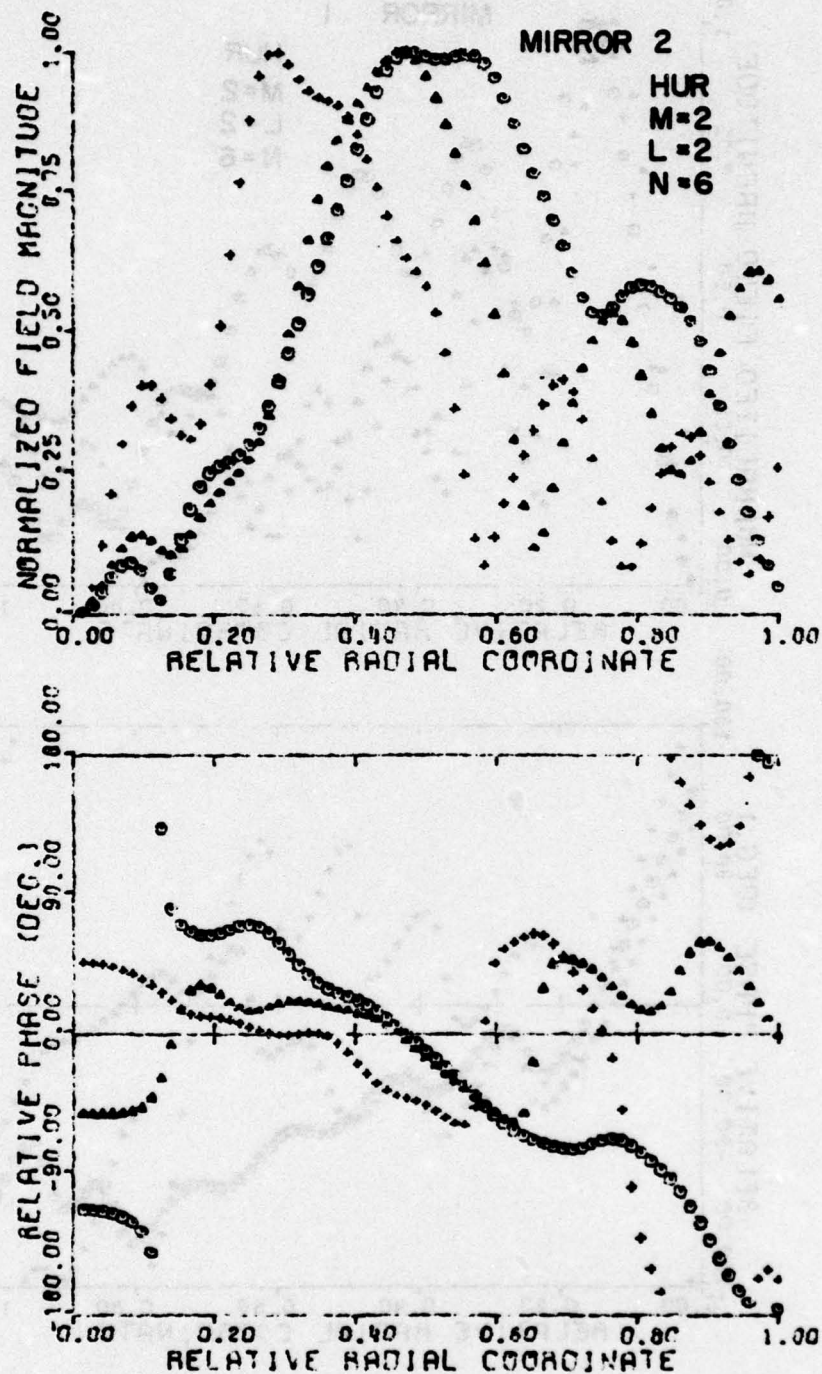
Figure 9b   Radial mode profiles in a plane incident at mirror 2
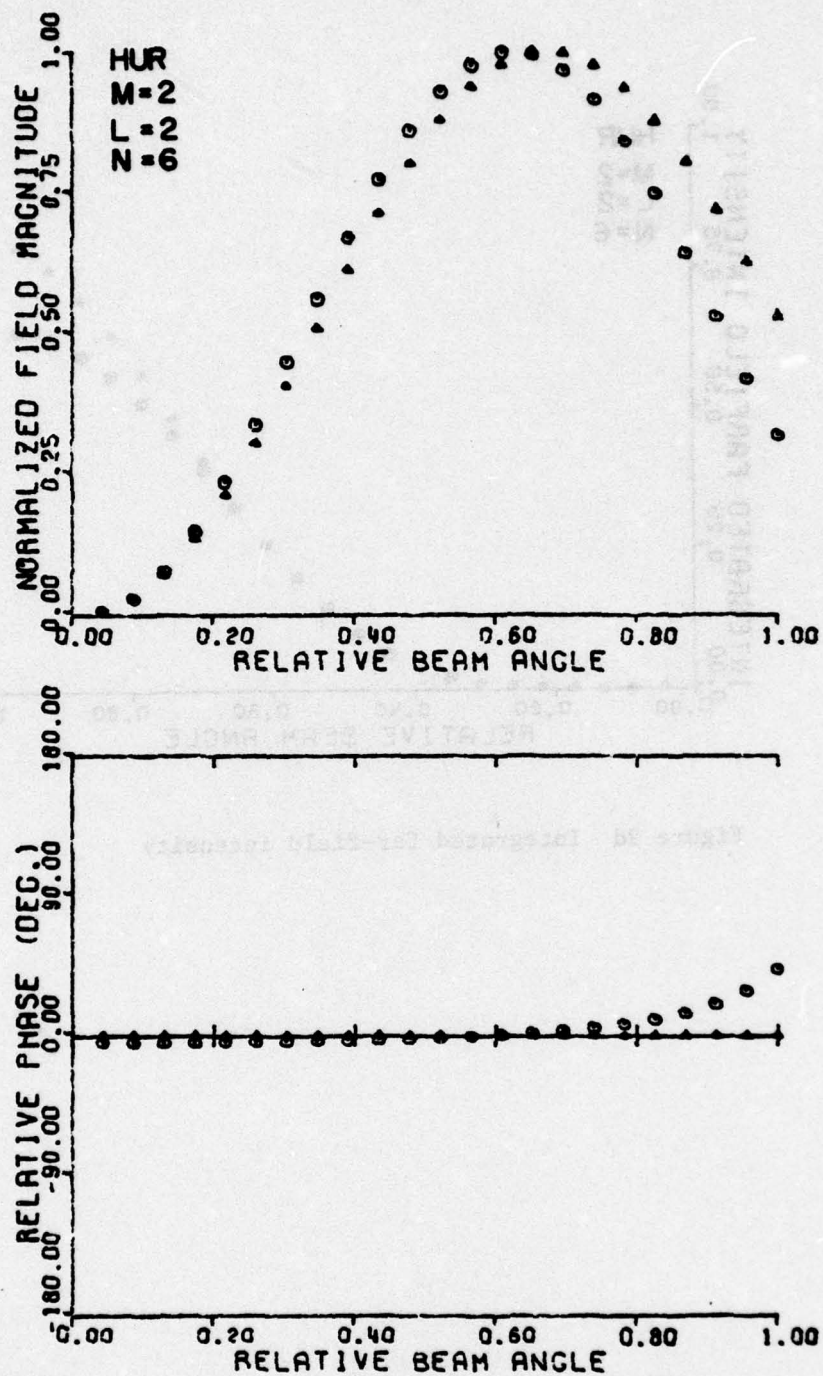
Figure 9c Far-field pattern of lowest loss radial mode and reference field (uniformly illuminated aperture)

37
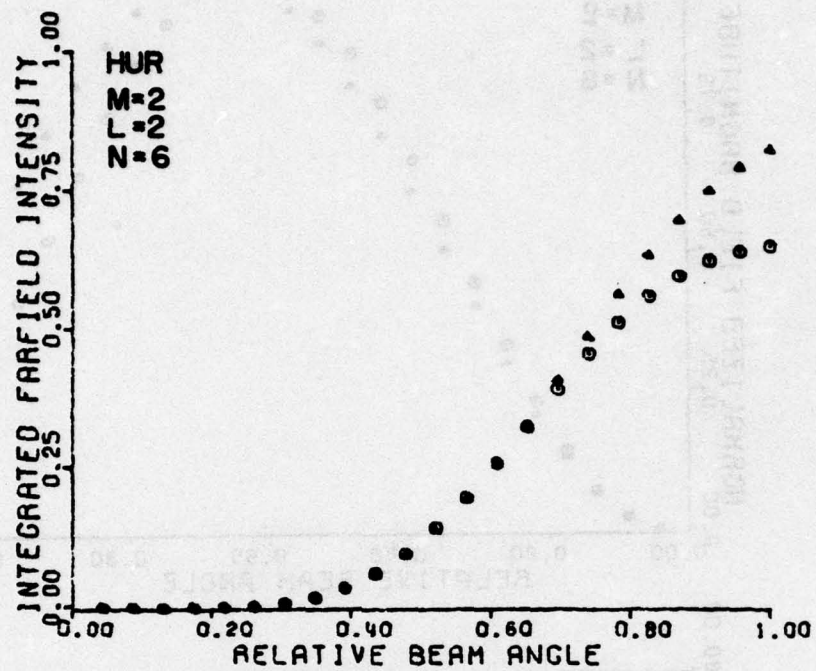
Figure 9d Integrated far-field intensity
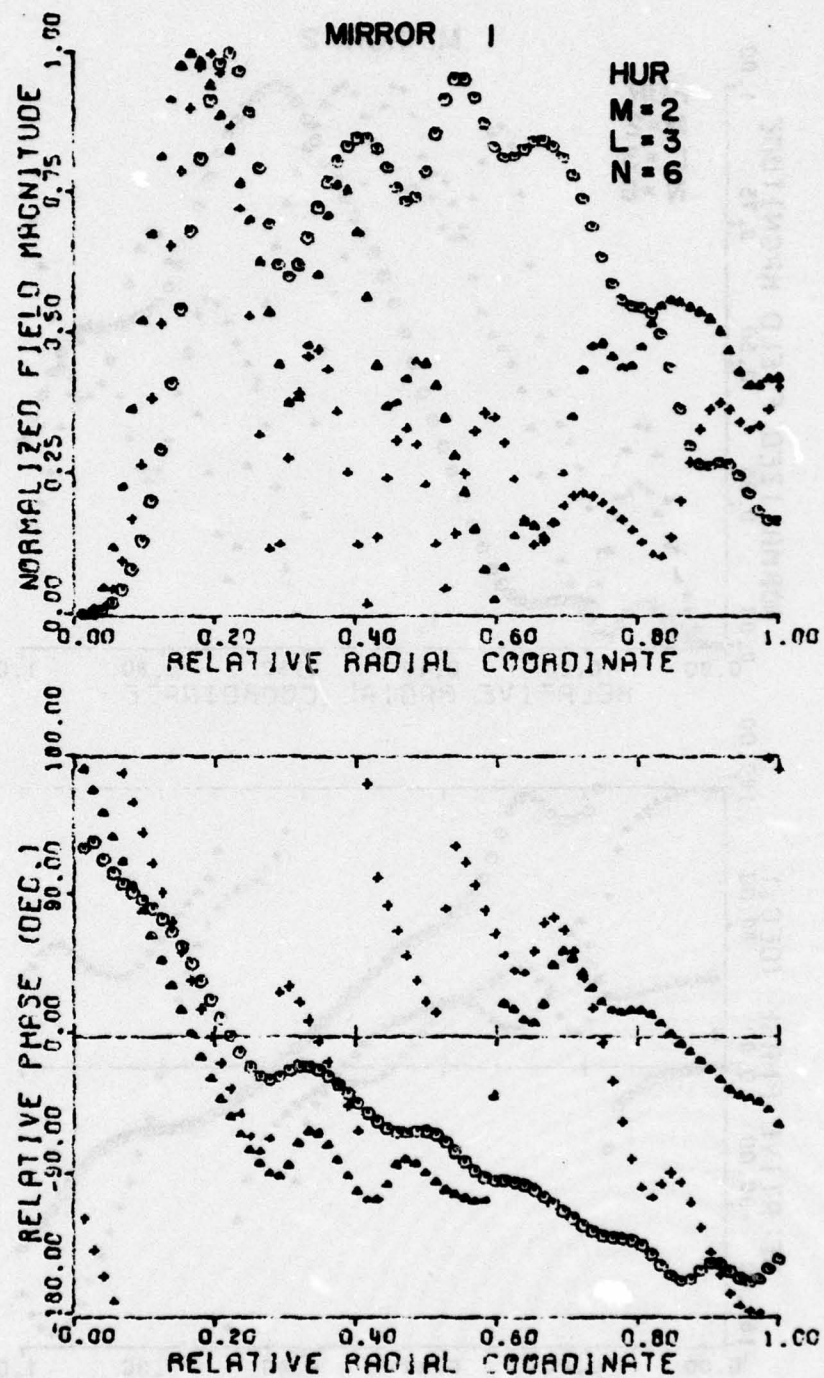
Figure 10a Radial mode profiles reflected from mirror 1 of
HUR for M = 2, ℓ =3, N = 6
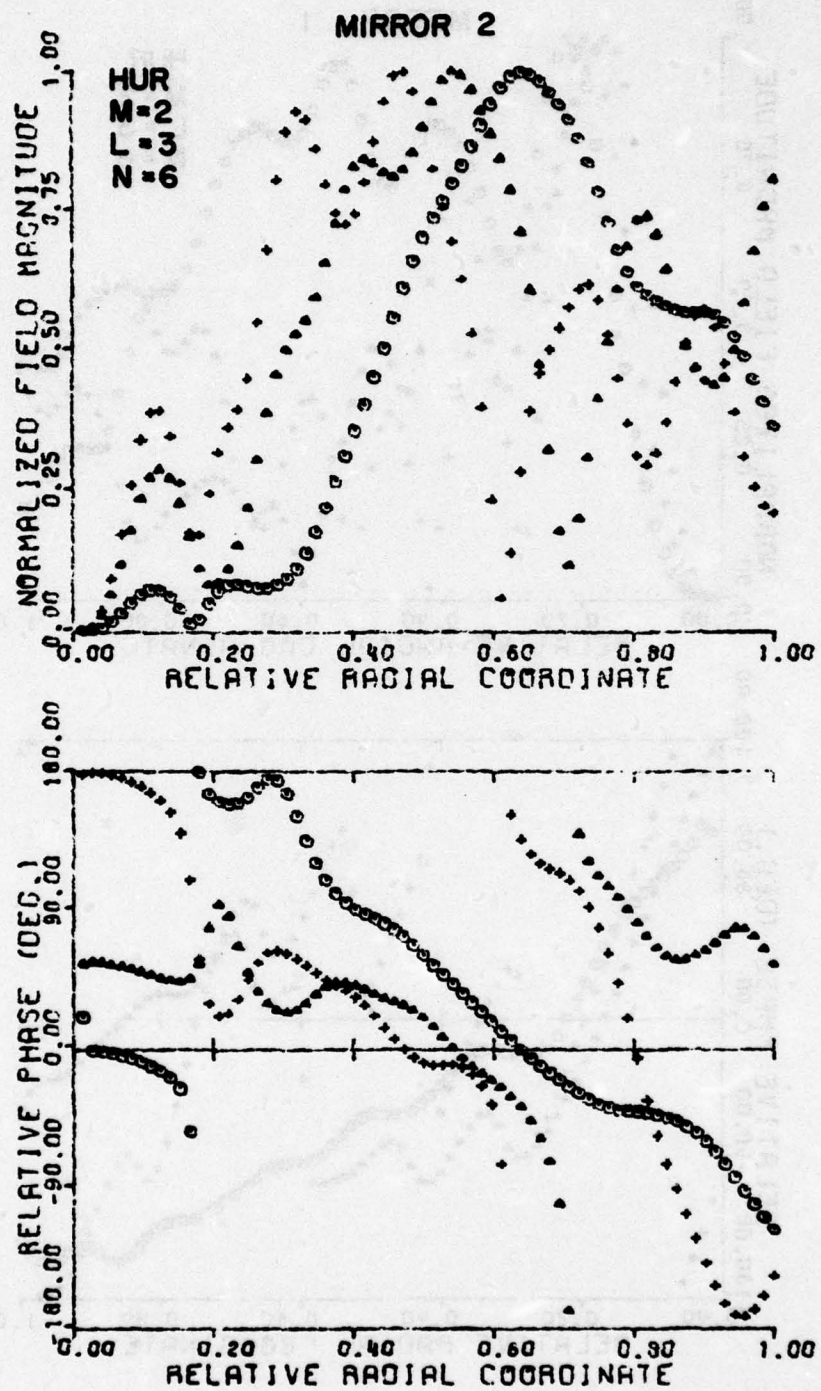
Figure 10b Radial mode profiles in a plane incident at
mirror 2.

40
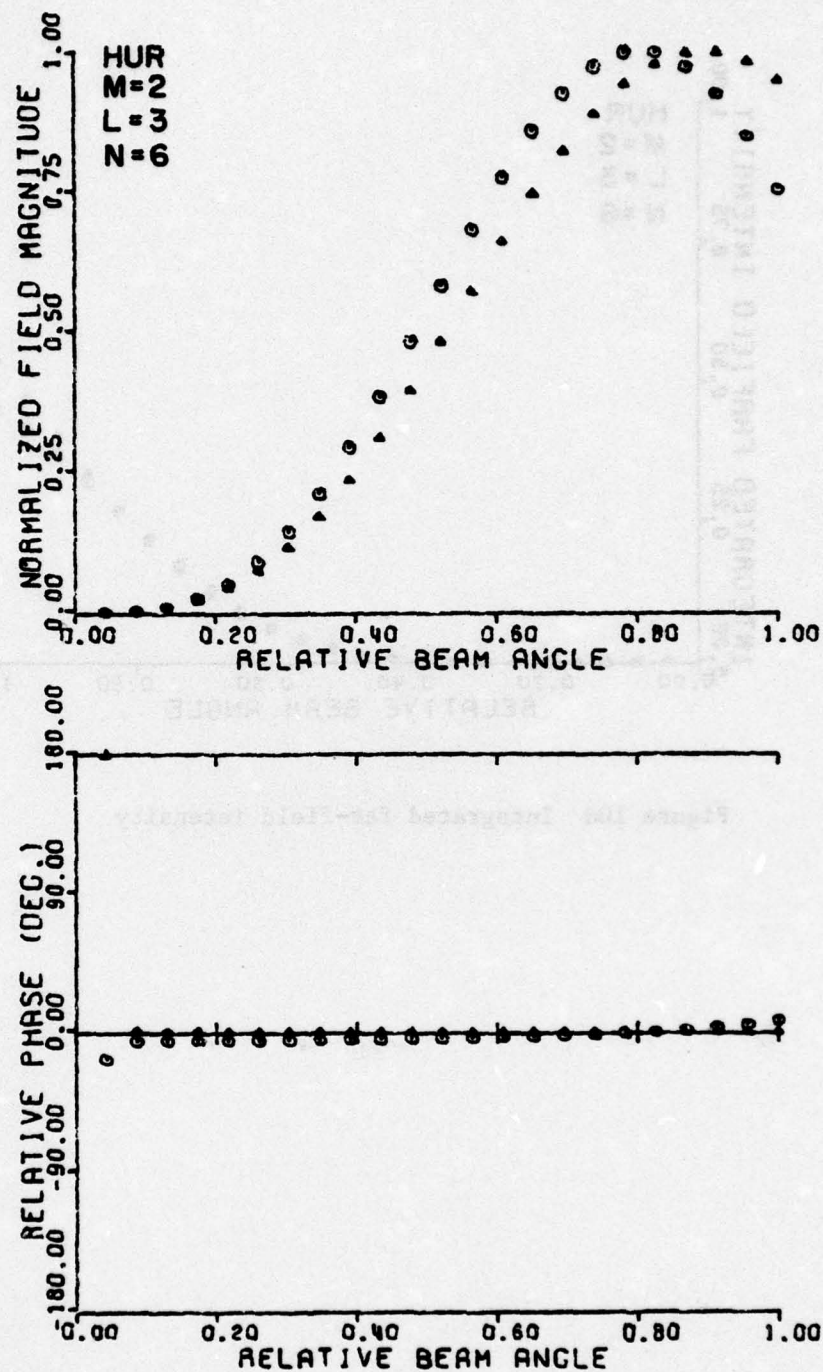
Figure 10c   Far-field pattern of lowest loss radial mode
and reference field (uniformly illuminated
aperture)

41
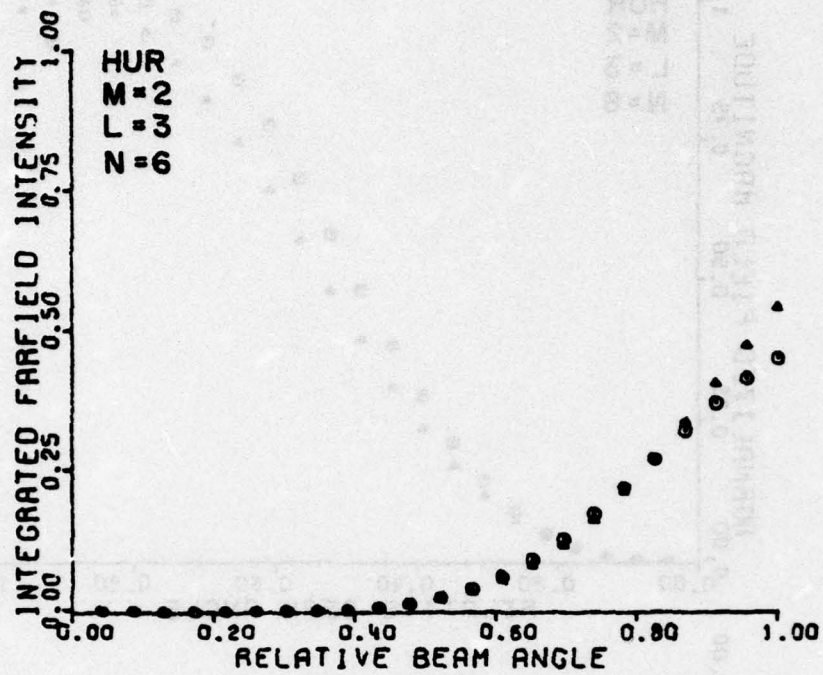
Figure 10d   Integrated far-field intensity

42
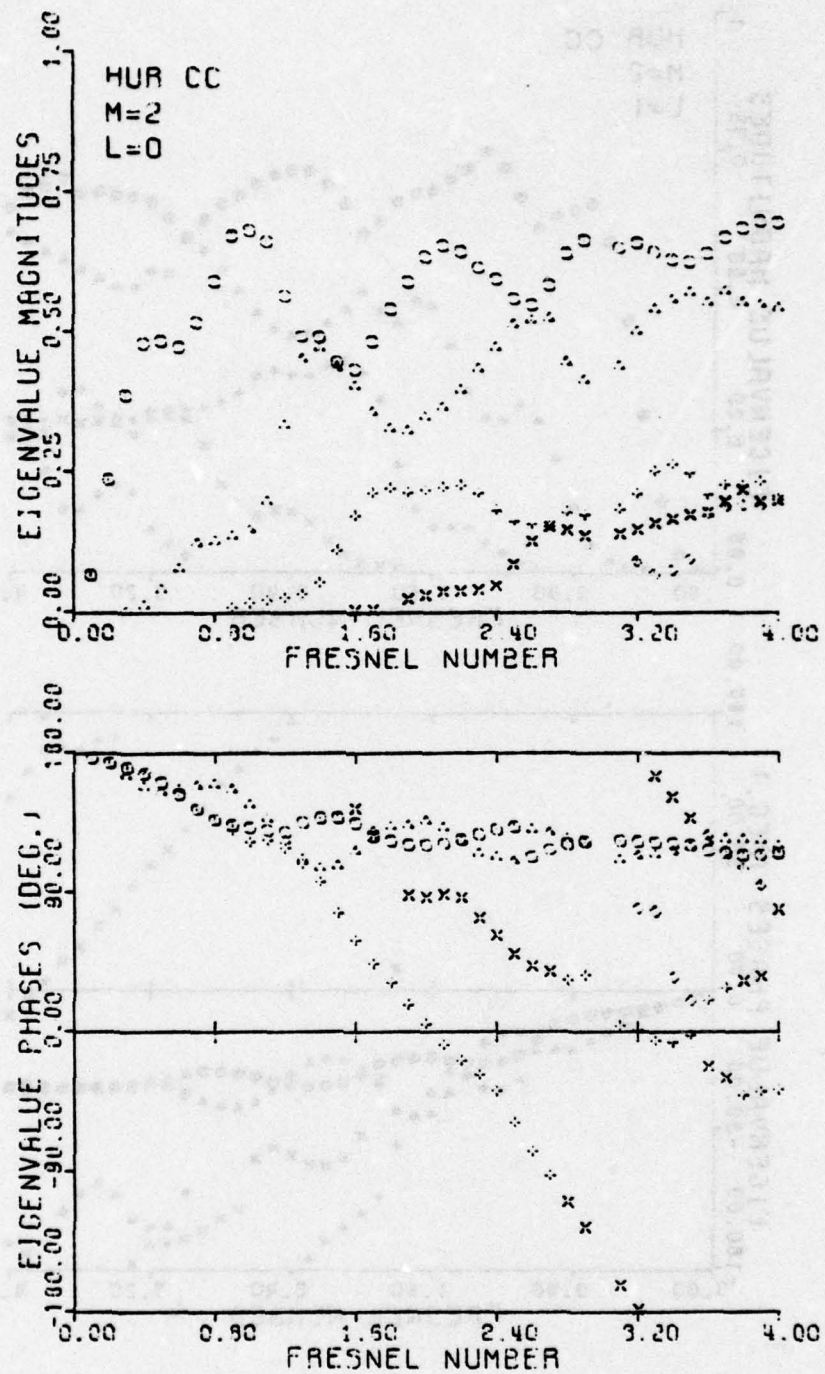
Figure 11a   Eigenvalues of HUR CC for M = 2, ℓ = 0

43

Figure 11b $\ell = 1$

HUR CC
M=2
L=2

EIGENVALUE MAGNITUDES

FRESNEL NUMBER

EIGENVALUE PHASES (DEG.)

FRESNEL NUMBER

Figure 11c $\ell = 2$

45

Figure 11d ℓ = 3

46
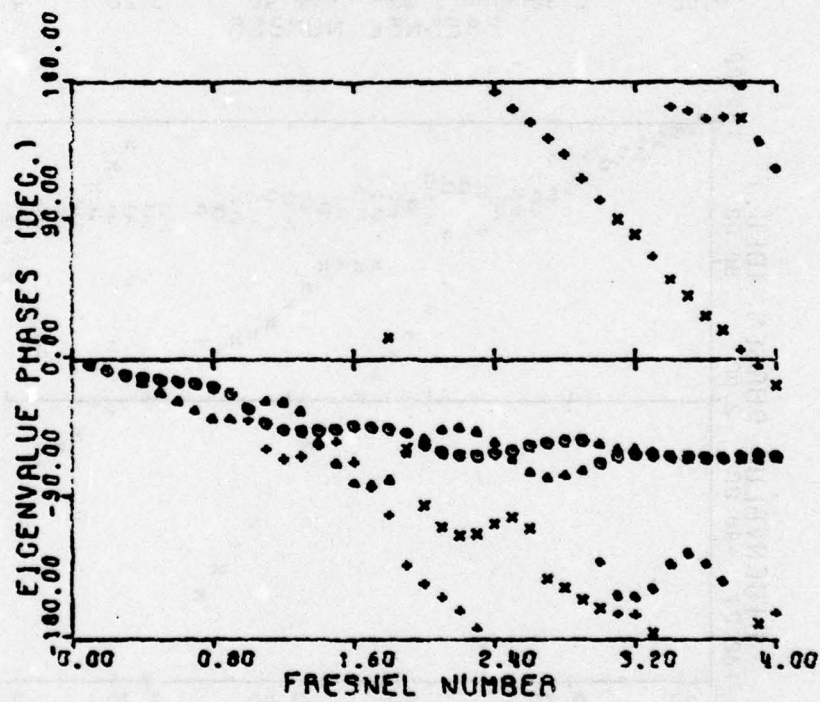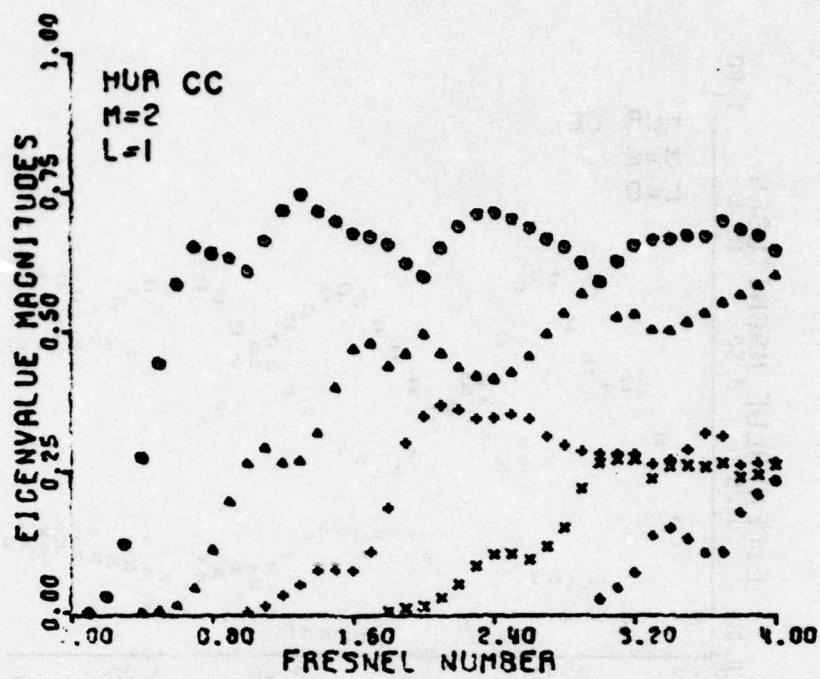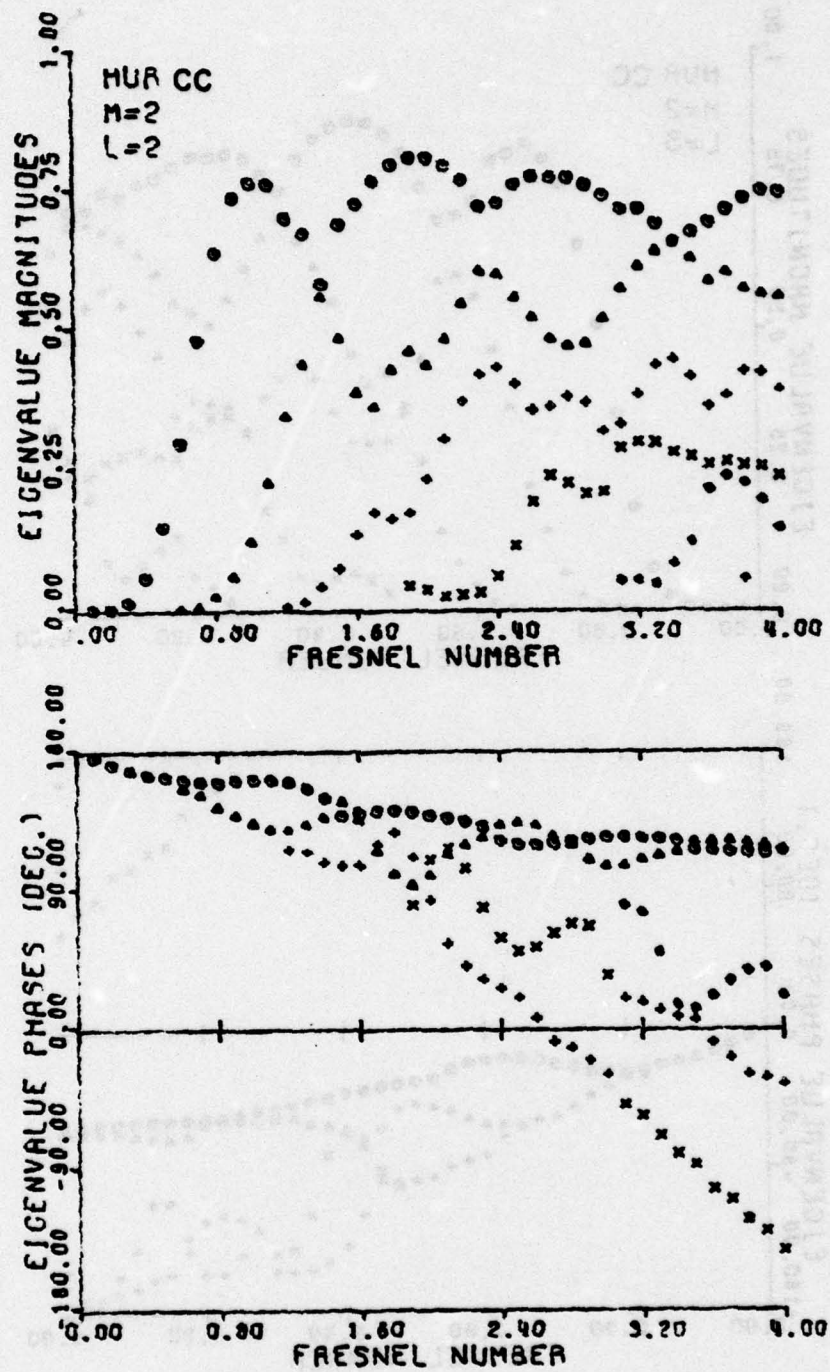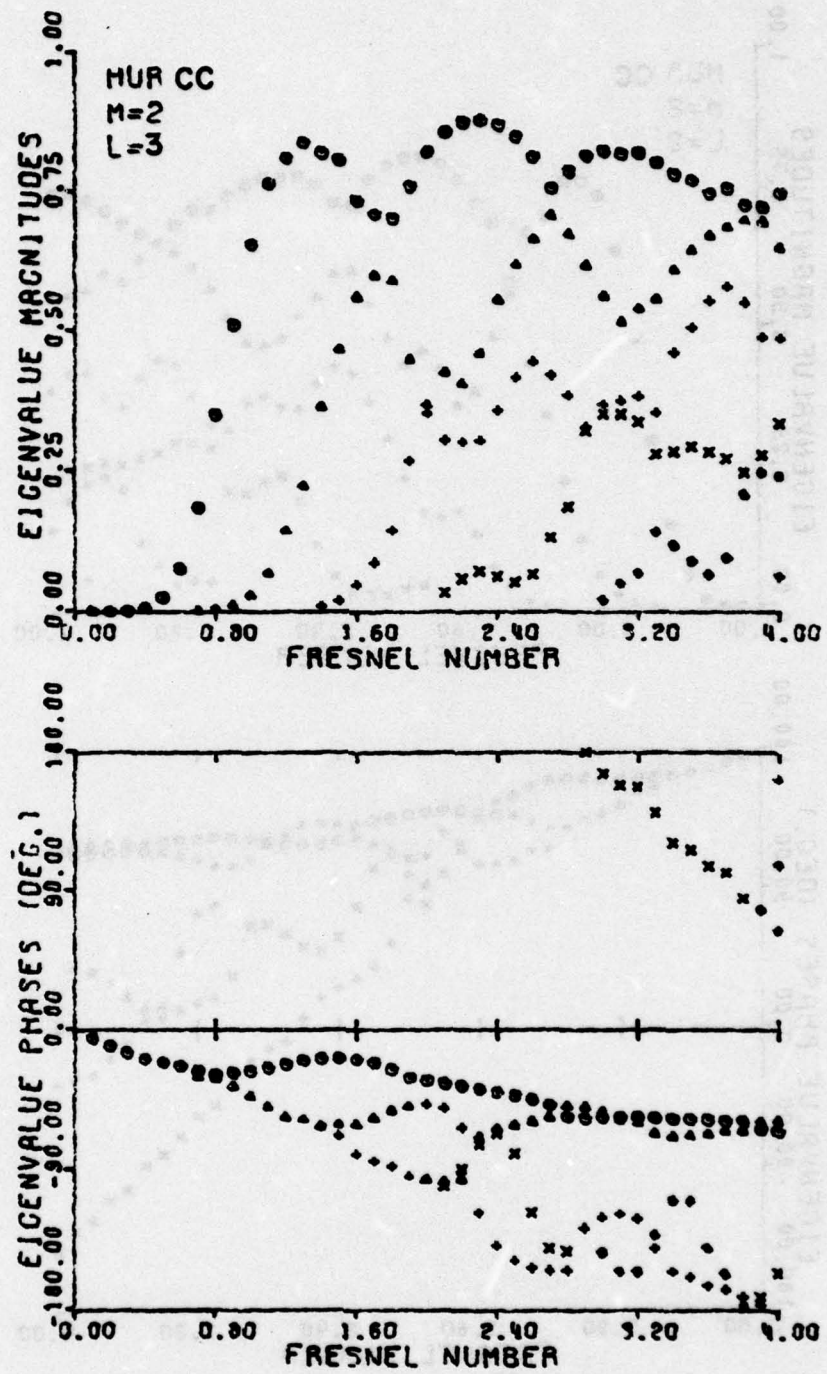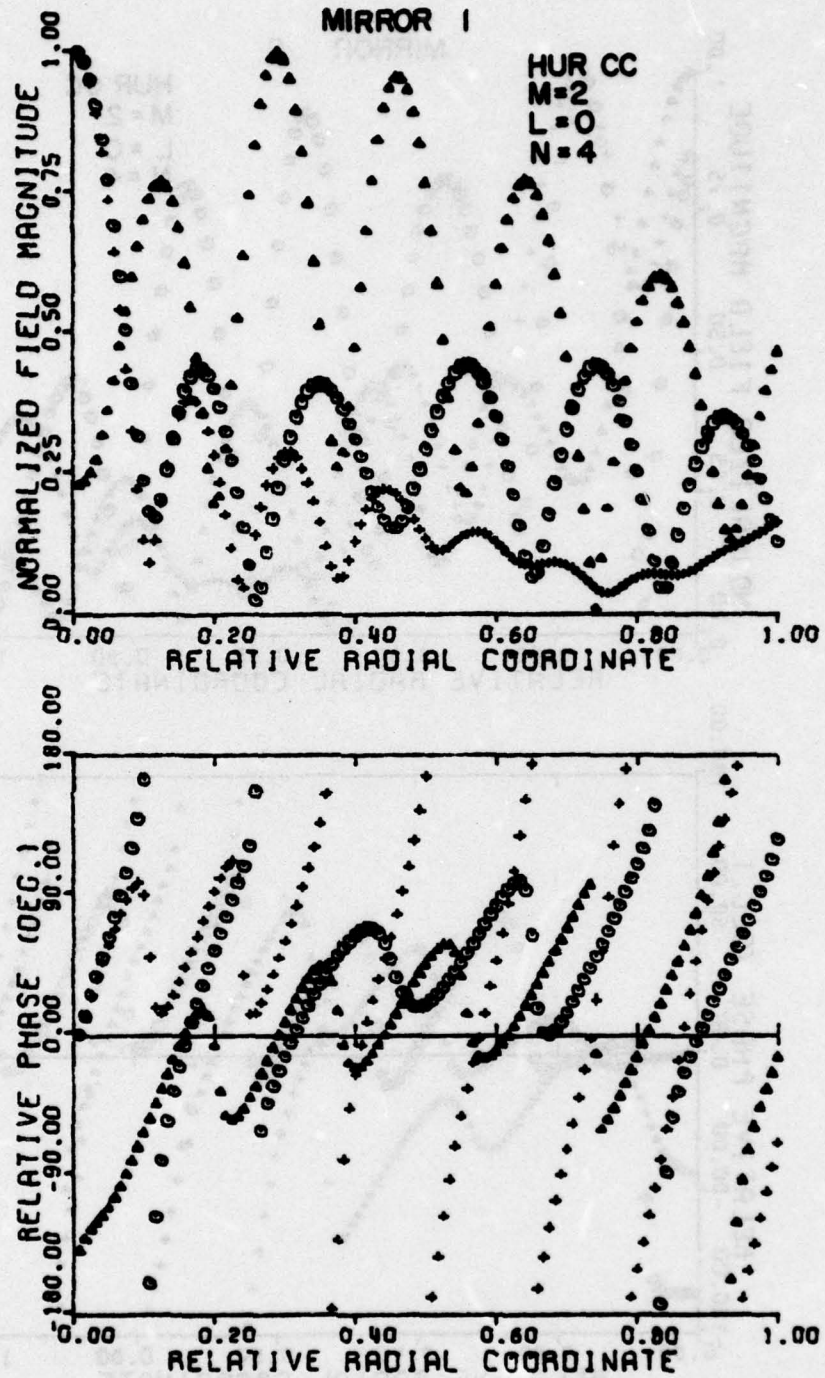
Figure 12a Radial mode profiles in a plane reflected from
mirror 1 of HUR CC for M = 2, ℓ = 0, N = 4
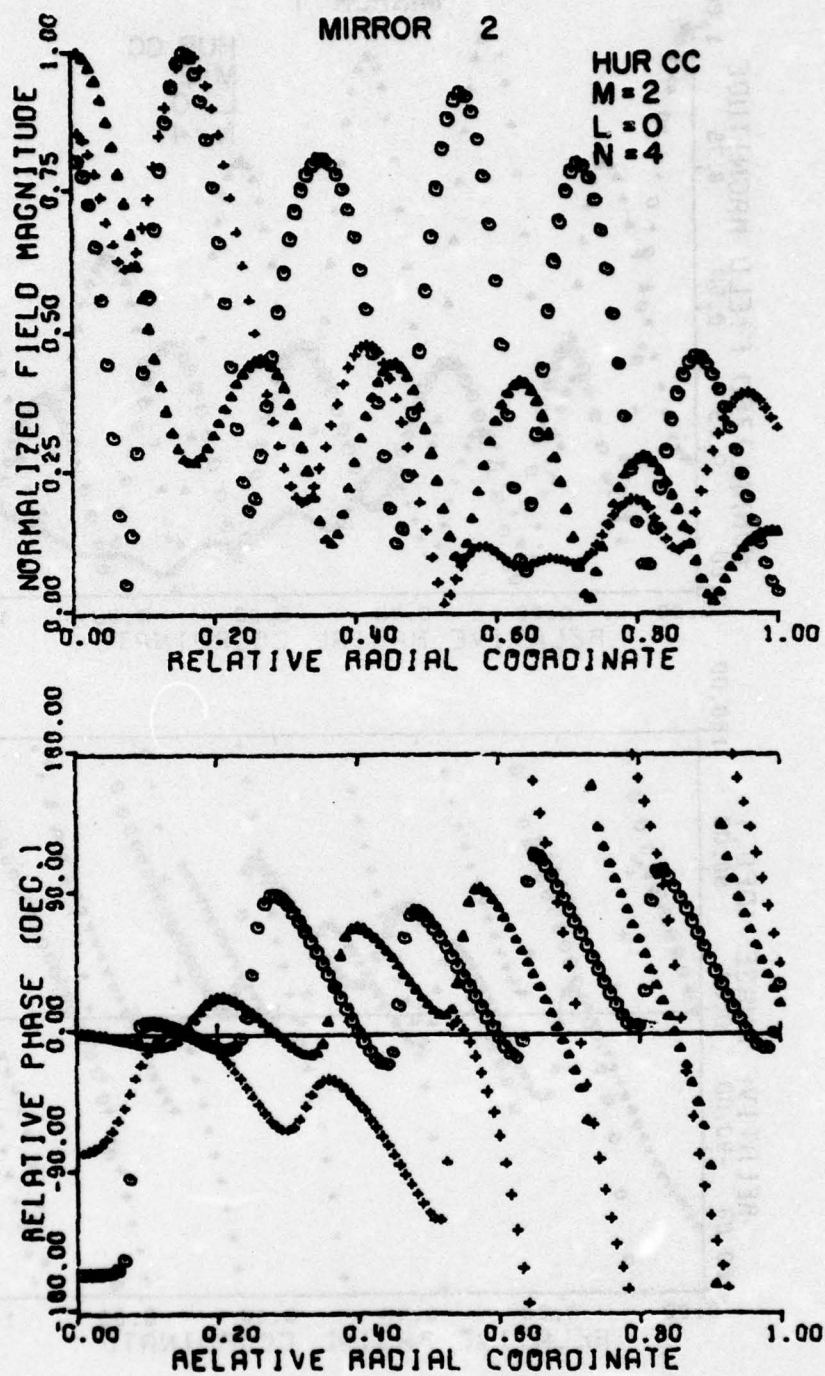
Figure 12b Radial mode profiles incident on a plane at mirror 2

48
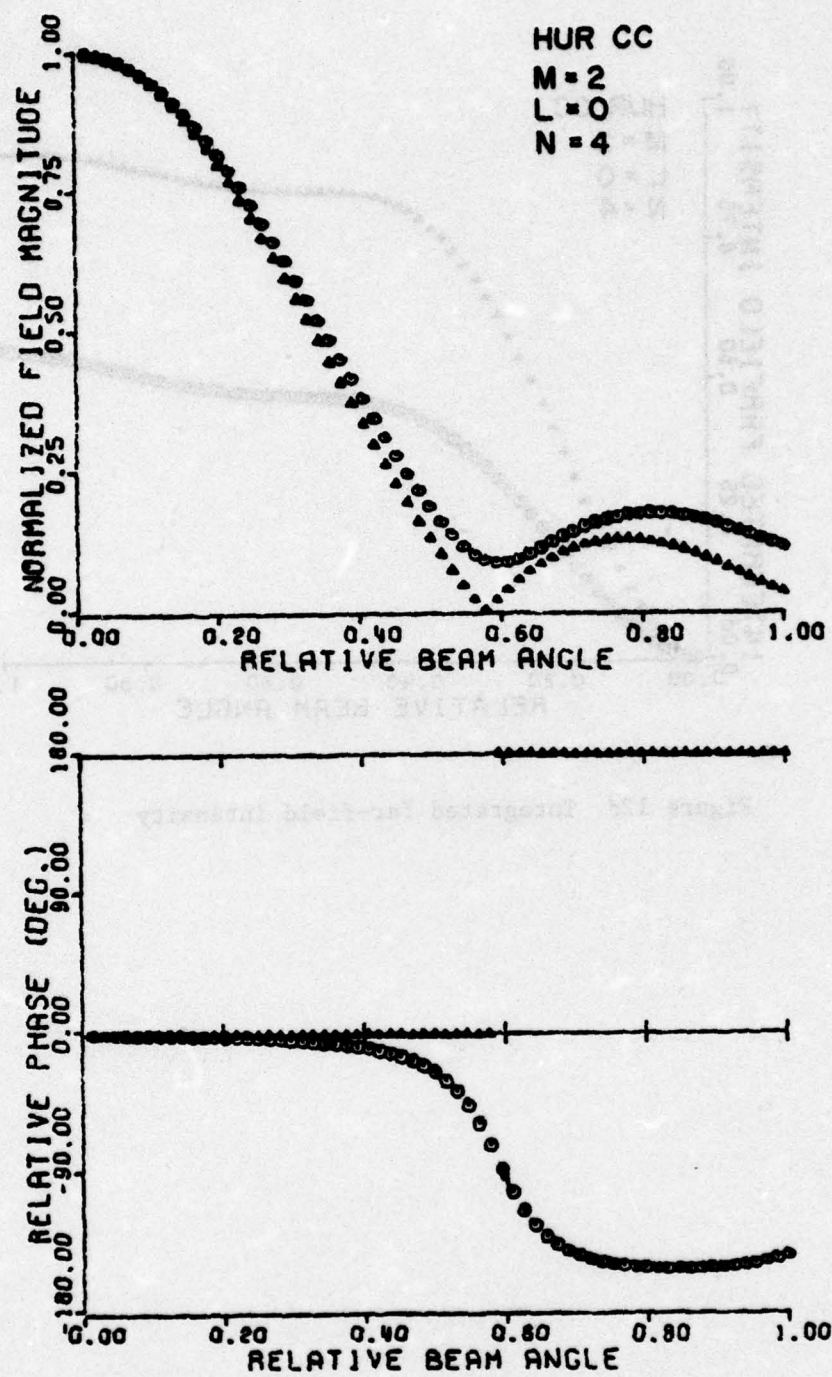
Figure 12c   Far-field patterns

49
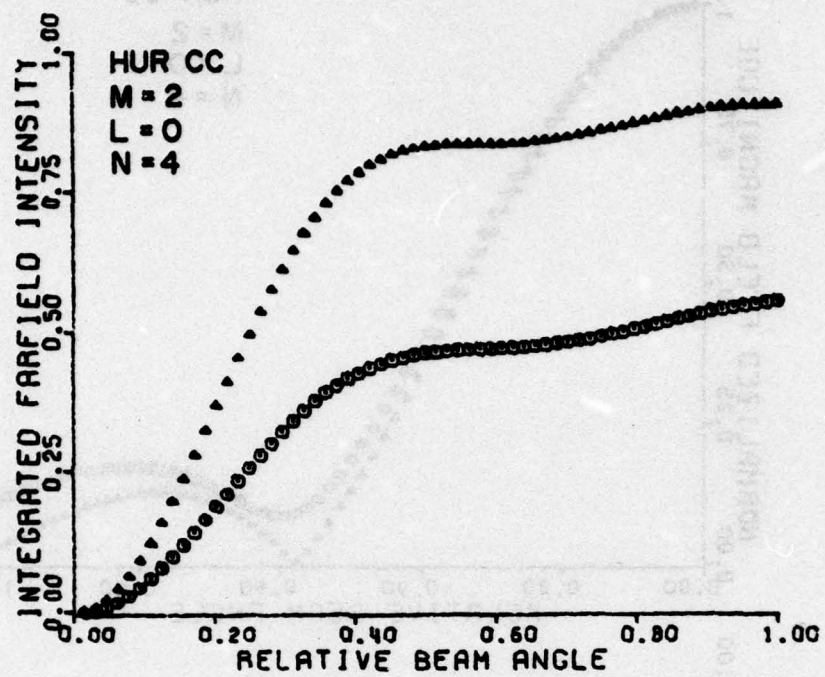
Figure 12d   Integrated far-field intensity

50
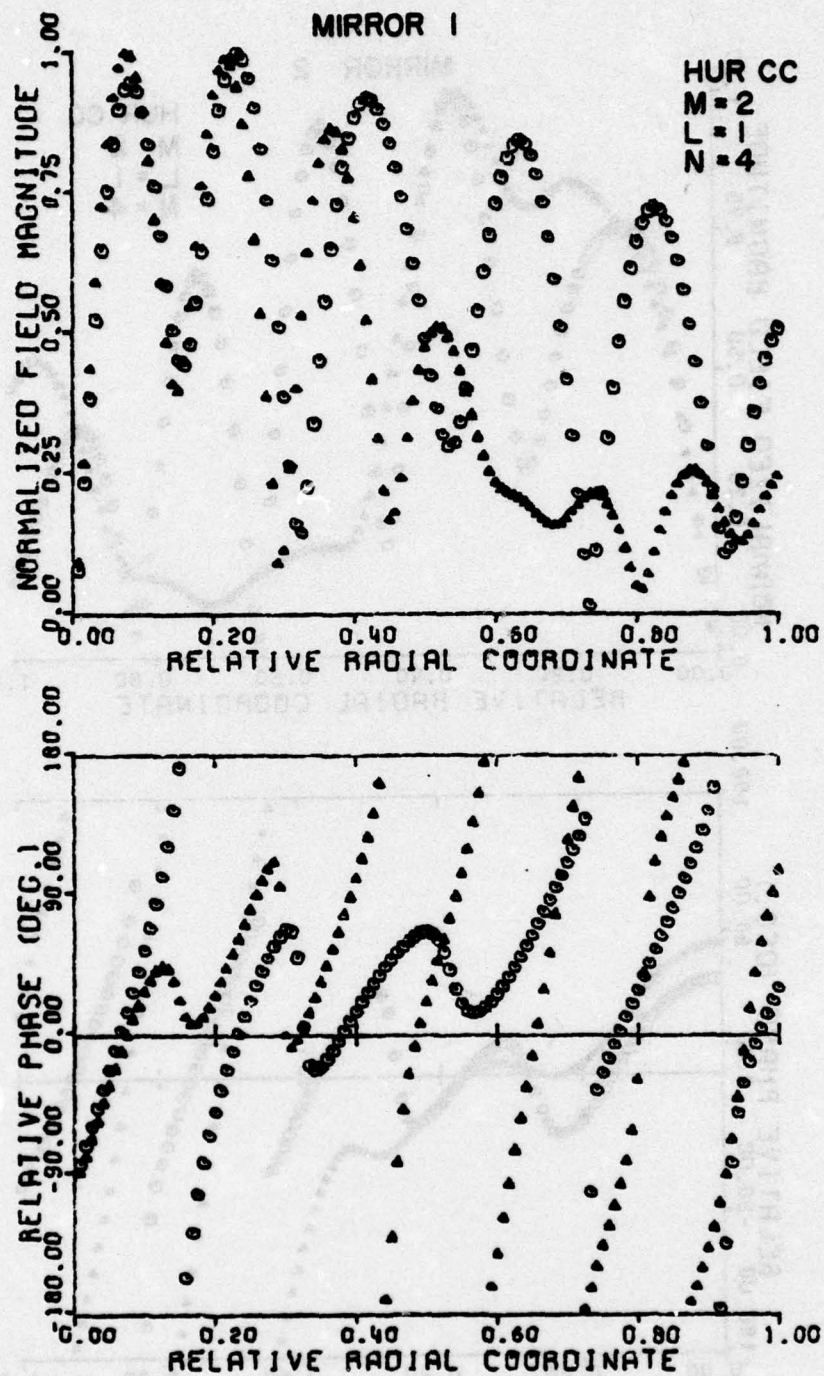
MIRROR 1

Figure 13a   Radial mode profiles in a plane reflected from
mirror 1 of HUR CC for M = 2, ℓ = 1, N = 4

51
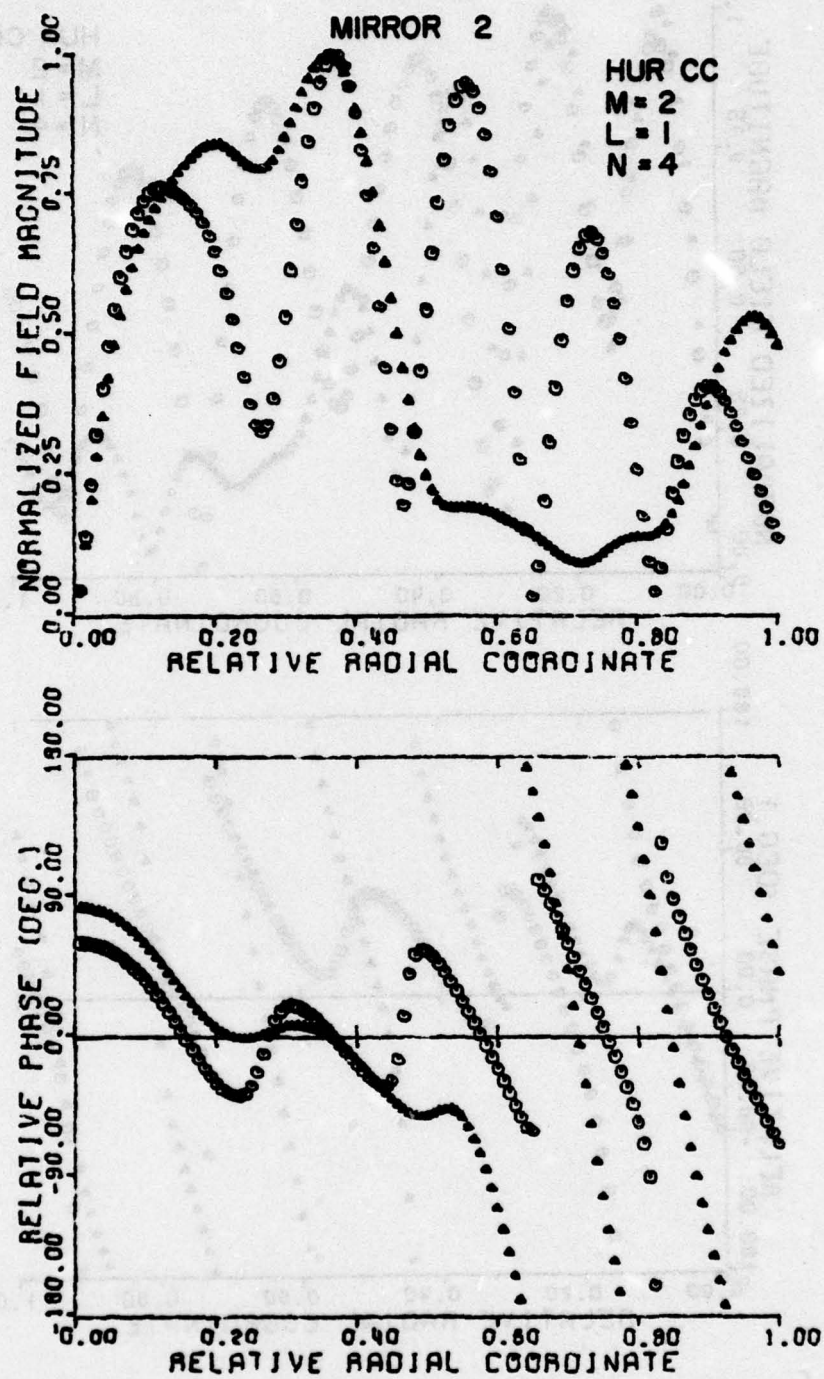
Figure 13b Radial mode profiles incident on a plane at mirror 2
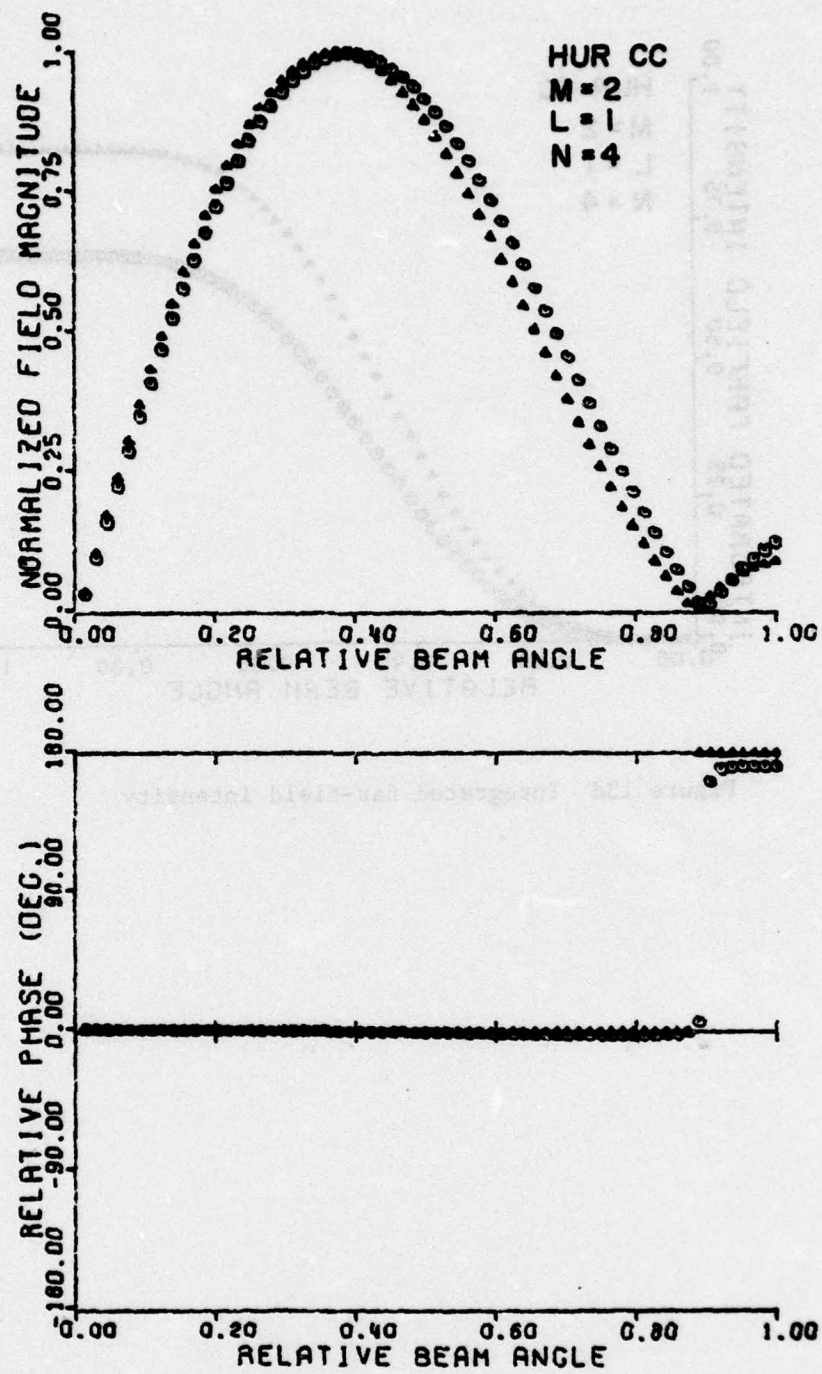
Figure 13c   Far-field patterns

53
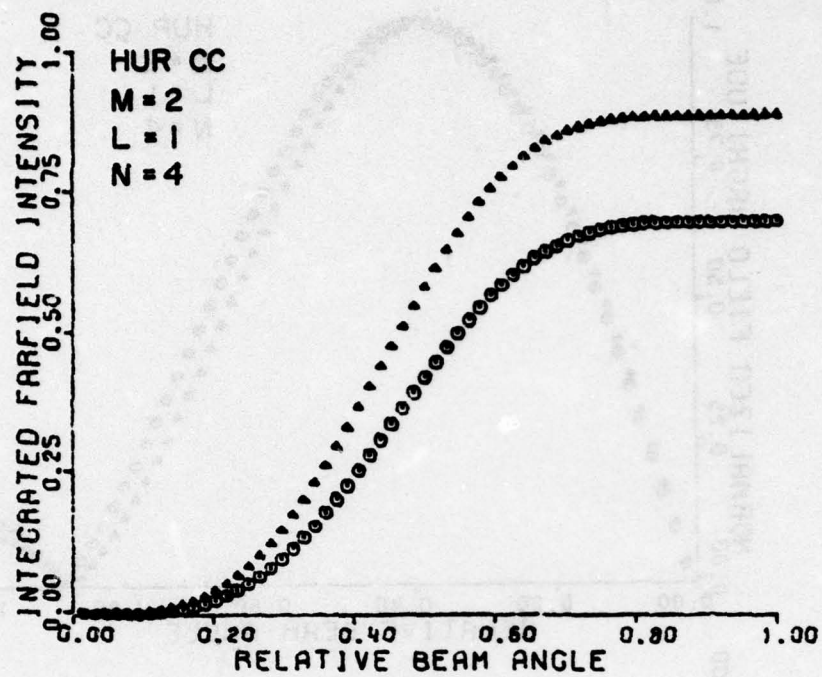
Figure 13d Integrated far-field intensity

"interference" patterns makes the calculations at Fresnel numbers larger than about N=6 prohibitively expensive. Even if the $\ell=0$ were dominant at reasonably large Fresnel numbers, this resonator would be objectionable because of the poor far-field performance as seen in Figure 12d. From these and other calculations it has been concluded that this resonator configuration would not provide a high quality output beam.

D. Analysis of Resonators 3 and 4

Even though resonators 3 and 4 were not specifically designated for analysis, some preliminary calculations were made to determine their potential for use as hole-coupled resonators. Figures 14, 15, and 16 show the eigenvalues calculated for resonator 3 of Figure 1 for magnifications M= -1, -2, and -3. These plots are interesting in that the radial mode eigenvalues do not cross as has been the case for all previously examined stable and unstable resonators. Another interesting and potentially more important aspect of these graphs is that the azimuthal mode eigenvalues tend to become degenerate as the Fresnel number increases. Thus only minimal azimuthal mode discrimination should be required to achieve $\ell=0$ mode operation. Hence if the theory of reference [3] about the role of mode volume with regard to mode discrimination by an active medium is correct, then the $\ell=0$ mode could be the dominant mode when the resonator contains a saturable gain medium since the $\ell=0$ mode is the only mode that does not have zero amplitude on axis.

The excellent radial mode discrimination and the possibility that $\ell=0$ mode may be favored because of its mode volume make resonator 3 the most promising hole-coupled resonator investigated to date. In addition to continued theoretical analysis, an experimental study of this type of resonator should be conducted.

55
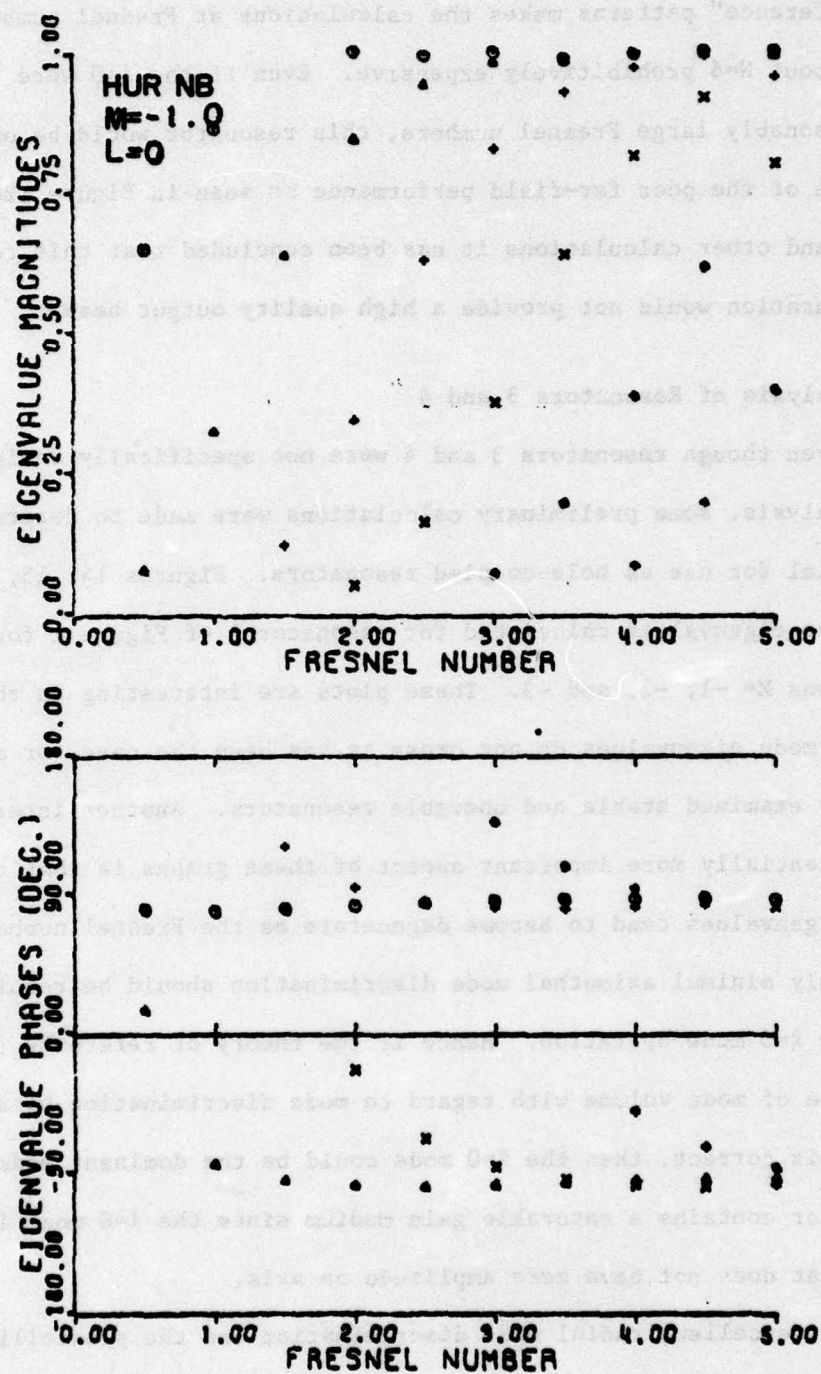
Figure 14a Eigenvalues of HUR NB for M = -1, ℓ =0

Figure 14b ℓ = 2

57
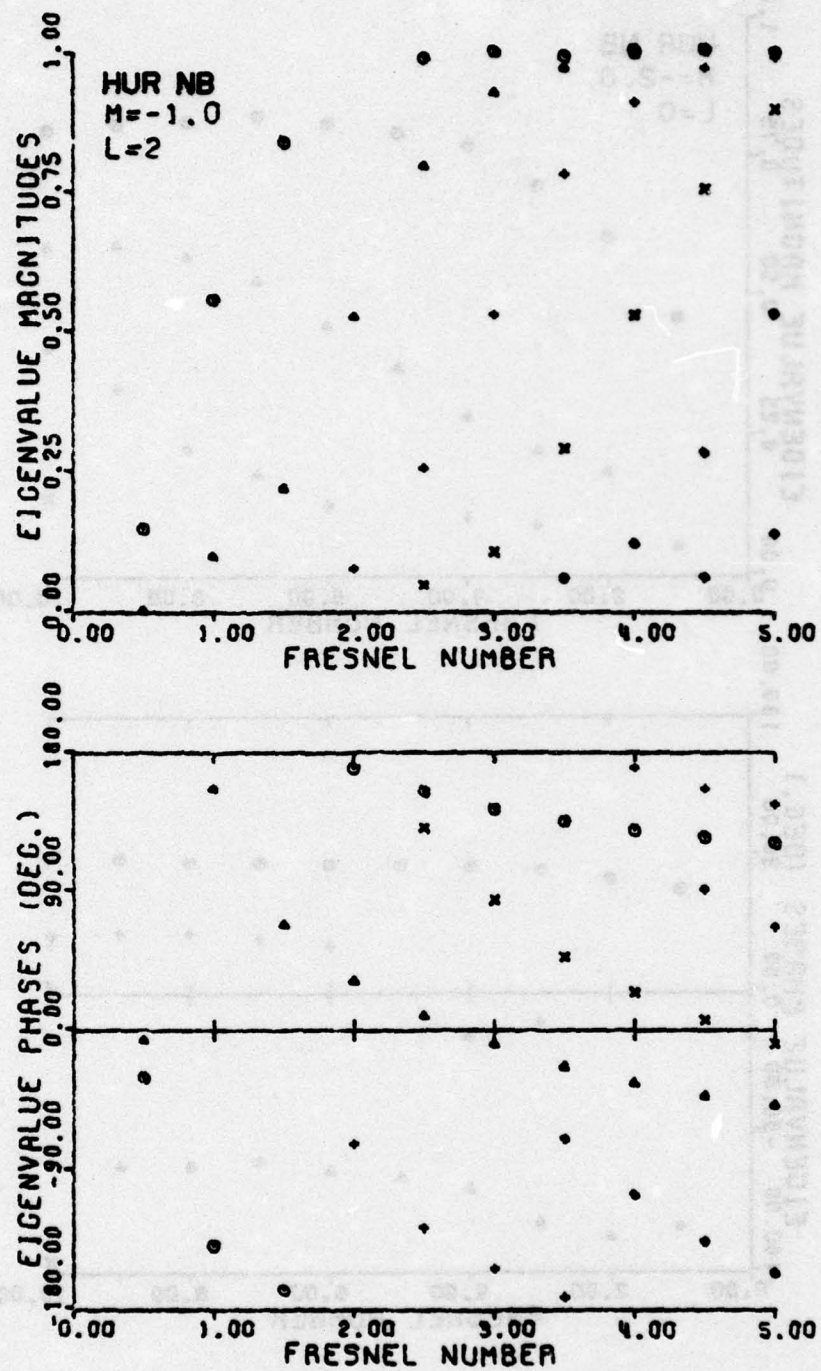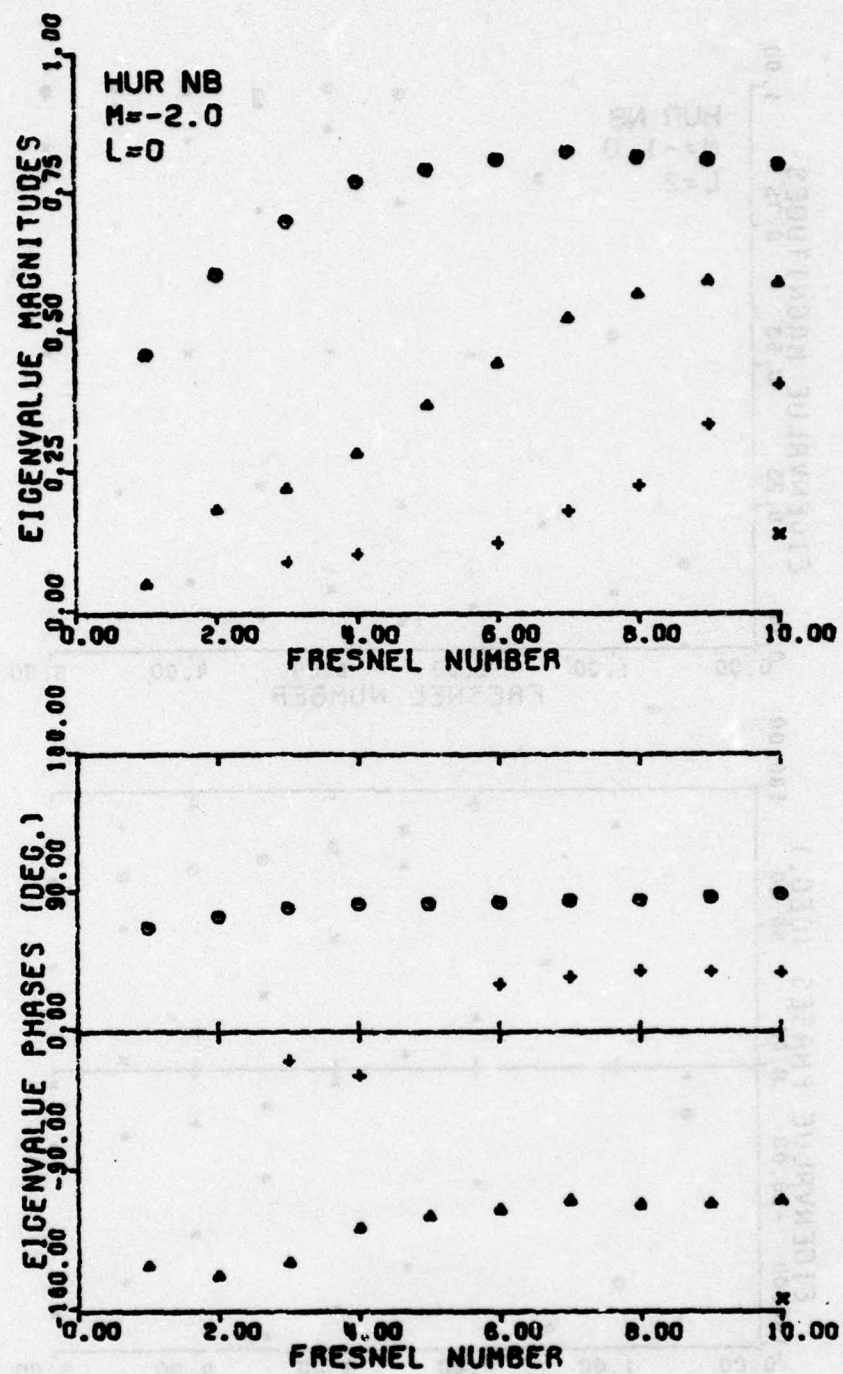
Figure 15a Eigenvalues of HUR NB for M = -2, ℓ = 0

58
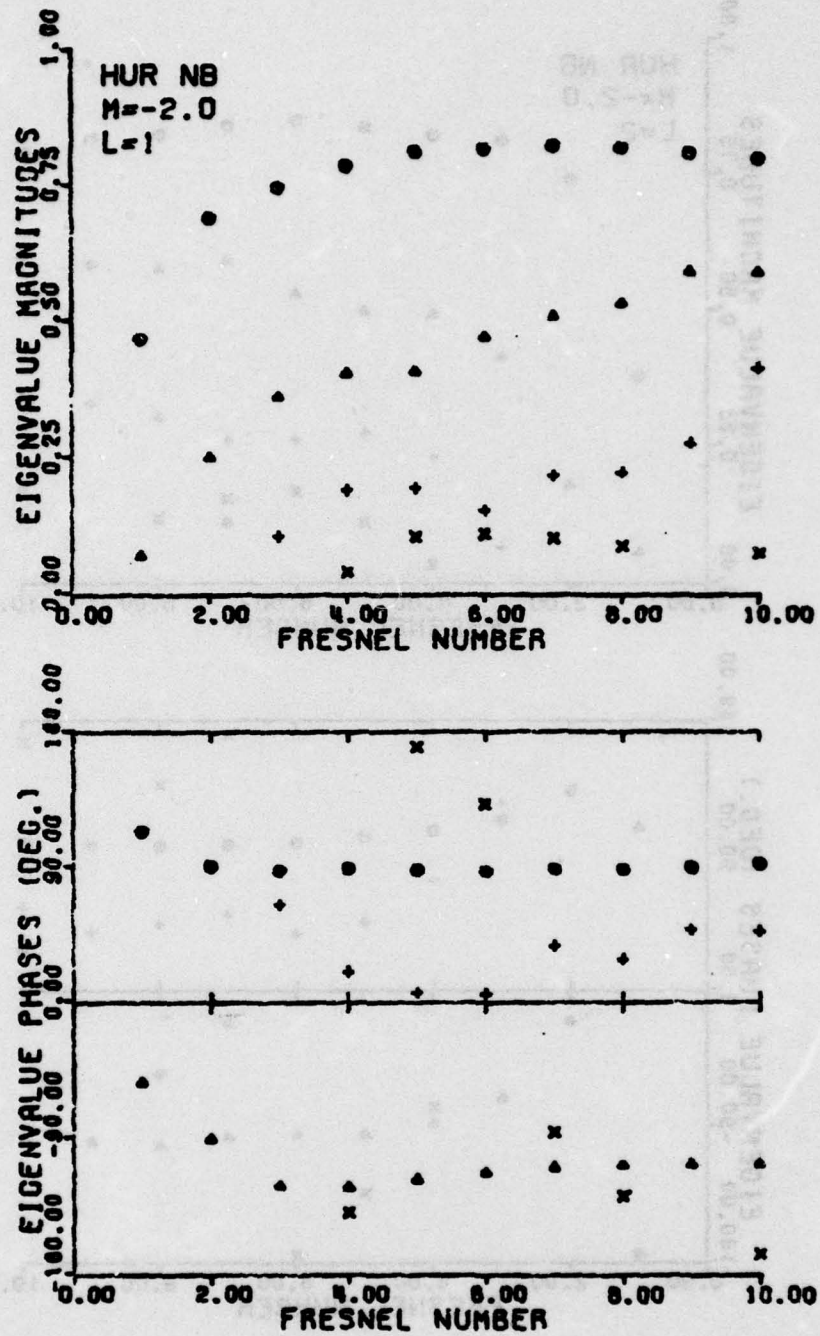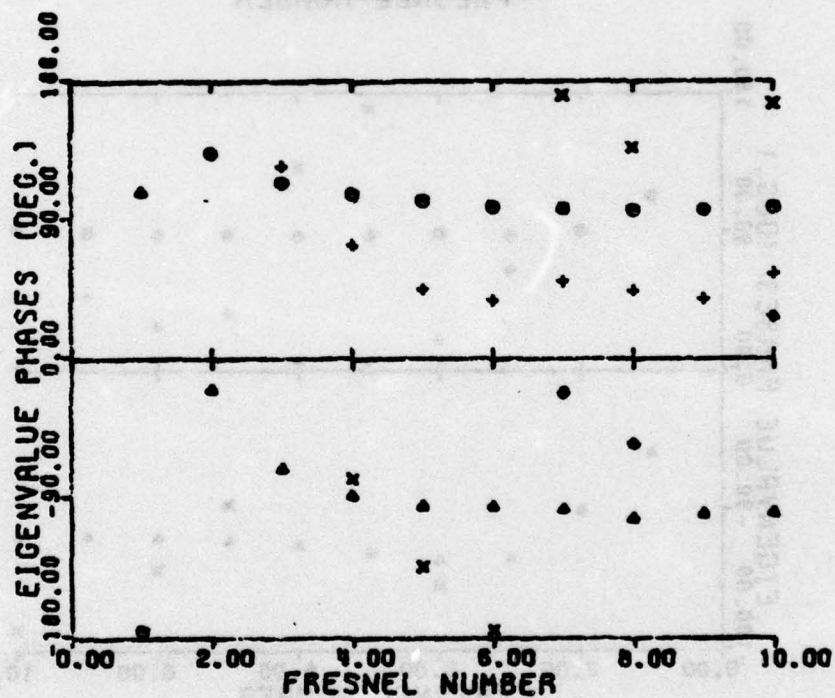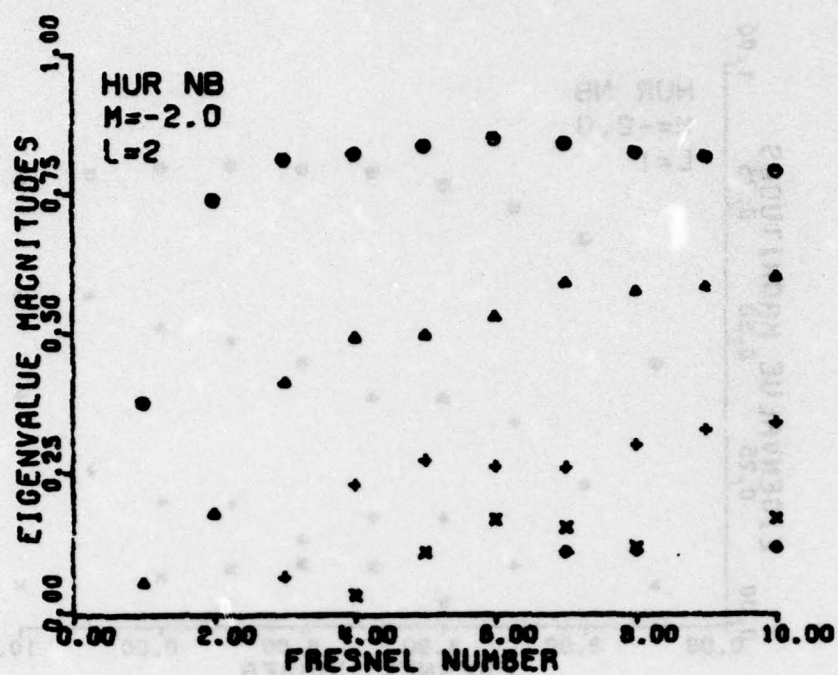
Figure 15b $\ell = 1$

Figure 15c $\ell = 2$
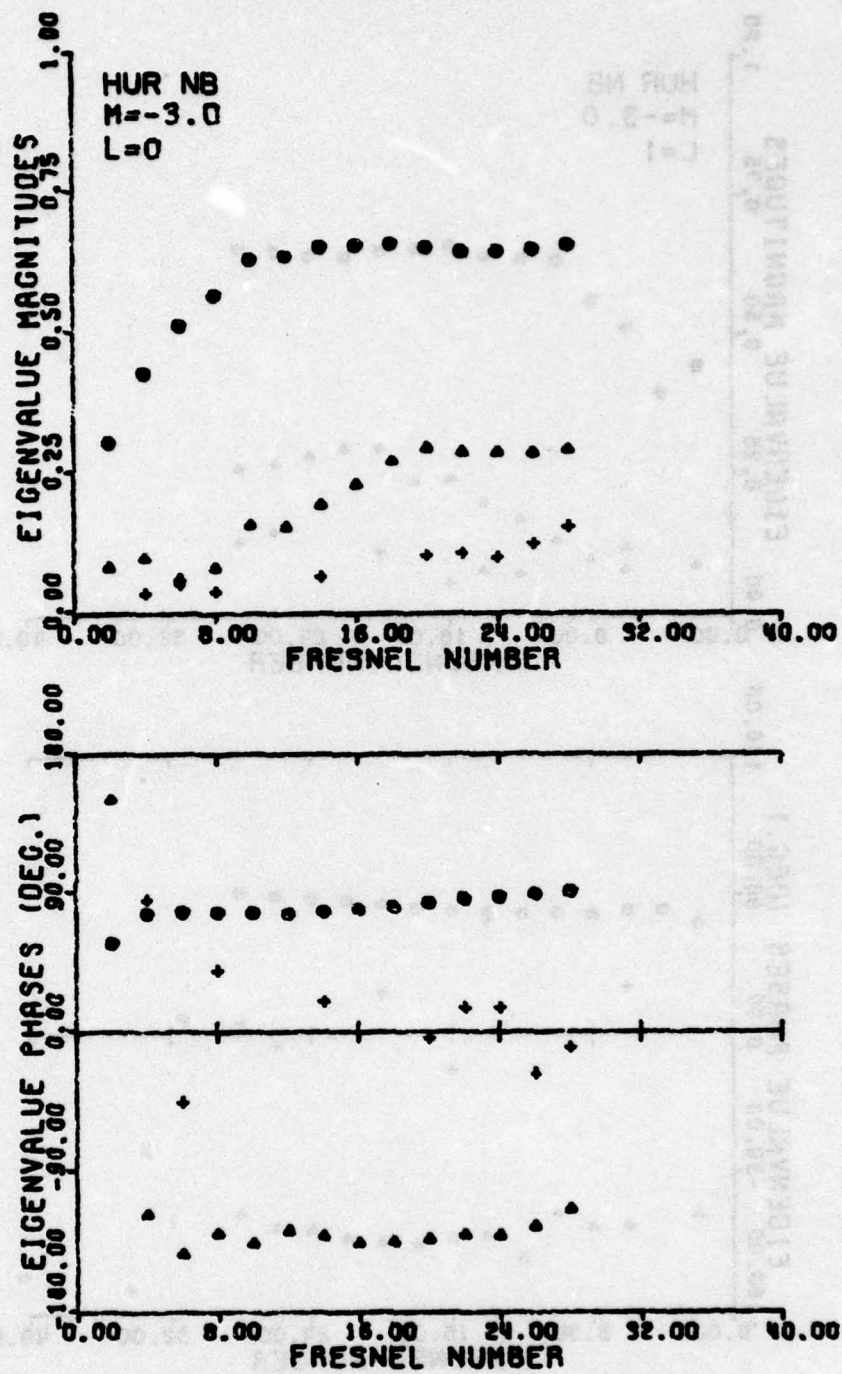
Figure 16a   Eigenvalues of HUR NB for M = -3, ℓ = 0

HUR NB
M=-3.0
L=1

Figure 16b ℓ = 1

62

HUR NB
M=-3.0
L=2

EIGENVALUE MAGNITUDES

1.00
0.75
0.50
0.25
0.00

0.00   8.00   16.00   24.00   32.00   40.00
FRESNEL NUMBER

EIGENVALUE PHASES (DEG.)

180.00
90.00
0.00
-90.00
-180.00

0.00   8.00   16.00   24.00   32.00   40.00
FRESNEL NUMBER
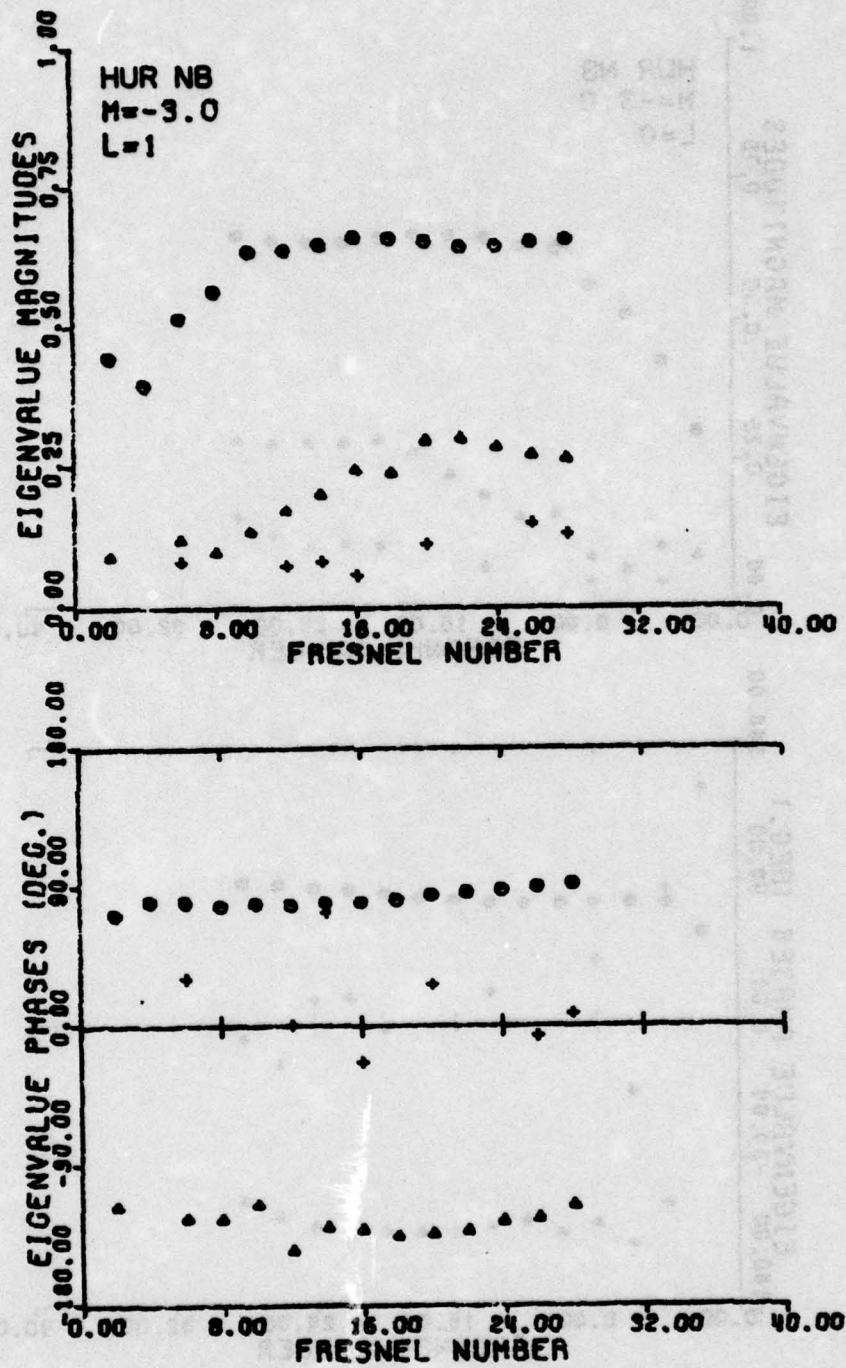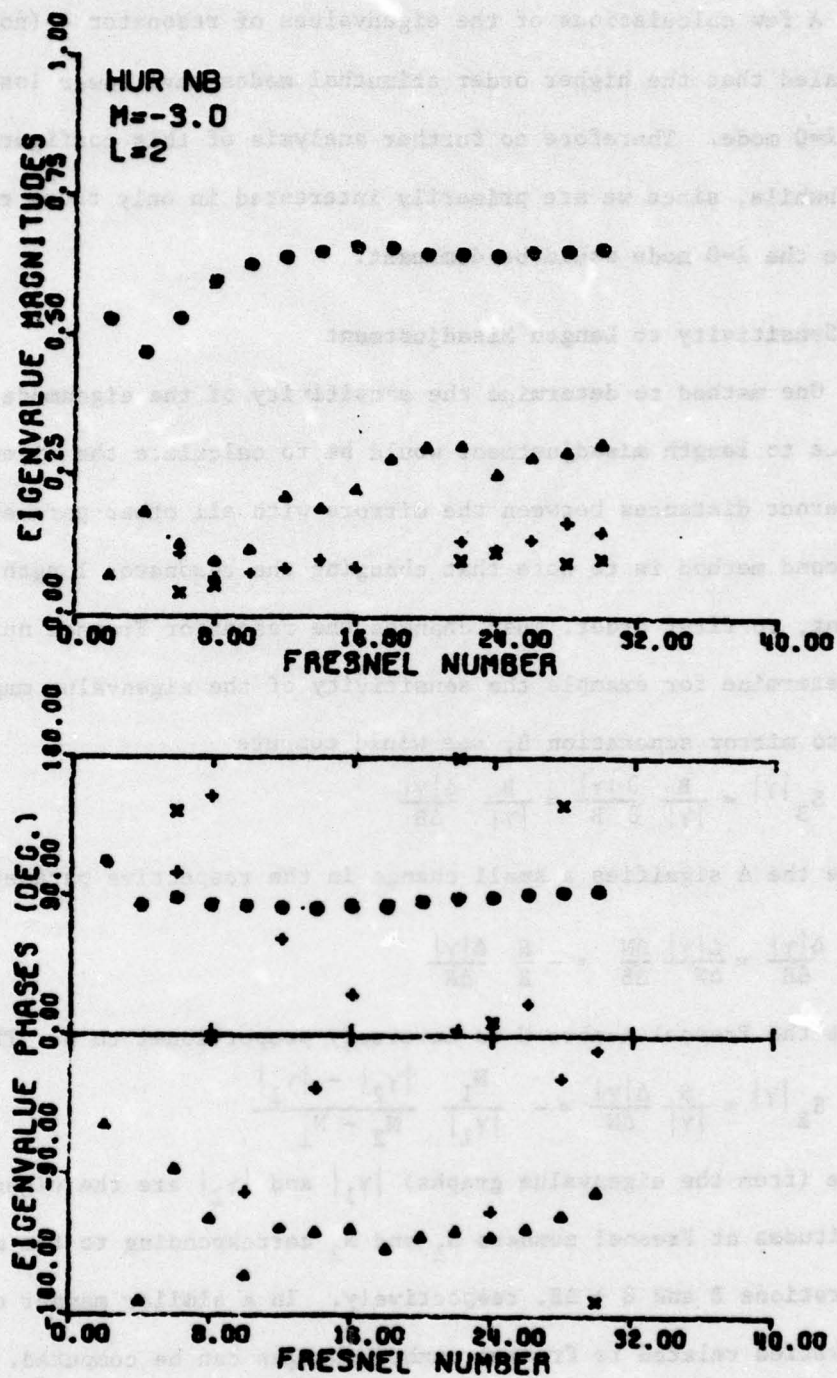
Figure 16c $\ell = 2$

A few calculations of the eigenvalues of resonator 4 (not shown) revealed that the higher order azimuthal modes have lower losses than the $\ell=0$ mode. Therefore no further analysis of this configuration seems worthwhile, since we are primarily interested in only those resonators where the $\ell=0$ mode would be dominant.

E. Sensitivity to Length Misadjustment

One method to determine the sensitivity of the eigenmode characteristics to length misadjustment would be to calculate the eigenmodes for different distances between the mirrors with all other parameters fixed. A second method is to note that changing the resonator length a small amount, to first order, just changes the resonator Fresnel number. Hence, to determine for example the sensitivity of the eigenvalue magnitude $|\gamma|$ to mirror separation B, one would compute

$$S_B^{|\gamma|} = \frac{B}{|\gamma|} \frac{\partial |\gamma|}{\partial B} \simeq \frac{B}{|\gamma|} \frac{\Delta |\gamma|}{\Delta B}$$

where the Δ signifies a small change in the respective parameter. Note

$$\frac{\Delta |\gamma|}{\Delta B} \simeq \frac{\Delta |\gamma|}{\Delta N} \frac{\Delta N}{\Delta B} = -\frac{N}{B} \frac{\Delta |\gamma|}{\Delta N}$$

since the Fresnel number N is inversely proportional to B. Thus

$$S_B^{|\gamma|} \simeq \frac{N}{|\gamma|} \frac{\Delta |\gamma|}{\Delta N} = -\frac{N_1}{|\gamma_1|} \frac{|\gamma_2| - |\gamma_1|}{N_2 - N_1}$$

where (from the eigenvalue graphs) $|\gamma_1|$ and $|\gamma_2|$ are the eigenvalue magnitudes at Fresnel numbers N_1 and N_2 corresponding to the mirror separations B and $B + \Delta B$, respectively. In a similar manner other sensitivities related to Fresnel number changes can be computed.

64

SECTION III

RESULTS OF TASKS 2 AND 6

A. Introduction

A computer program has been developed which calculates the resonator mirror figures to obtain an optimum fit in a least squares sense to a specified, or desired, radial eigenmode amplitude and phase profile. A description of the calculation technique used in the computer program is given in Appendix B. The program was to be tested by noting how well it performed in trying to achieve: 1) a maximum mode volume, 2) uniform amplitude and phase in the output of a hole-coupled resonator, and 3) maximum far-field on-axis intensity. Tests conducted during work on Task 2 indicated that the program performed satisfactorily except when the resonator had little mode discrimination. Later while working on Task 6, the Prony method of calculating the fields, which was used in Task 1, was incorporated into the program, and the program's performance improved significantly. The test cases were repeated, and better fits to the desired fields were obtained. These latter tests results are described in the following subsections, along with some additional test results obtained during Task 6.

Before results are described, the main limitation of this approach to designing resonators should be mentioned. The program calculates the mirror curvatures, or figure, for an optimum fit of the lowest loss radial mode of a particular azimuthal mode index to the desired mode profile. In all the test cases, the $\ell=0$ mode index was used. After the "optimum" resonator had been found, it was analyzed using the tools of Task 1. In almost all cases, a higher order azimuthal mode was found to have fewer losses than the $\ell=0$ mode for which the resonator was designed. To assure that the resonator is designed for the lowest loss radial and

65

azimuthal mode, the one dimensional radial field propagator would have to be replaced with a full mirror propagator. Neither time nor sufficient computer funds were available to make this important modification.

B. Maximum Mode Volume

In an attempt to achieve a maximum mode volume, the program was given the task of trying to achieve a uniform field magnitude over the entire output plane of the hole-coupled resonator shown in Figure 17. Maximizing the field in one "plane" does not guarantee a maximum mode "volume", but the program is currently structured to fit fields in only one plane. Since the least squares minimization procedure finds a local minimum for the mean square error, it is best that the initial resonator configuration be one in which the fields are already close to the desired fields.

The beginning and ending resonator configurations along with the eigenvalues for the two lowest order radial and four lowest order azimuthal modes indices ($m=0,1$ and $\ell=0,1,2,3$) are shown in Figure 17a. Figure 17b shows the desired, beginning, and ending field on the output mirror

(2) for $\ell = 0$. Note that the ending field magnitude is a very good fit to the desired field but that the eigenvalue for this mode ($|\gamma_{00}|=0.656$) is not the largest eigenvalue. For reference purposes the associated fields on the other mirror (1) are shown in Figure 17c.

It appears that the ending field on mirror 1 has less mode "volume" than the beginning field, but the situation is somewhat distorted by the central peak since the fields are normalized by peak amplitudes rather than average intensity as would be required for a fair mode volume comparison. Apparently the uniform fill on mirror 2 was obtained somewhat
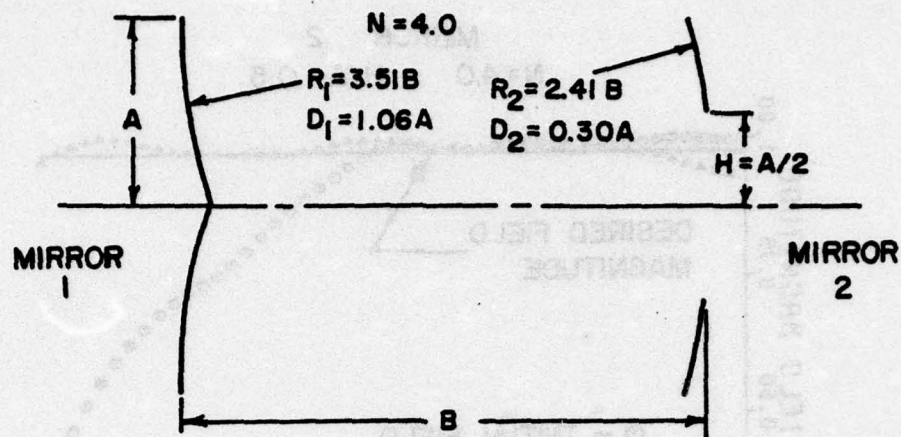
66

N = 4.0

$R_1 = 3.51B$ $R_2 = 2.41B$
$D_1 = 1.06A$ $D_2 = 0.30A$

MIRROR 1   MIRROR 2

H = A/2

A   B

The Initial Cavity Eigenvalues, $\gamma_{\ell m}$

m \ ℓ	0	1	2	3
0	0.728 63°	0.758 68°	0.834 88°	0.869 120°
1	0.310 −170°	0.398 148°	0.573 −168°	0.607 −114°

N = 4.0

$R_1 = 6.97B$ $R_2 = 0.84B$
$D_1 = 2.99A$ $D = 0.49A$

MIRROR 1   MIRROR 2

H = A/2

A   B
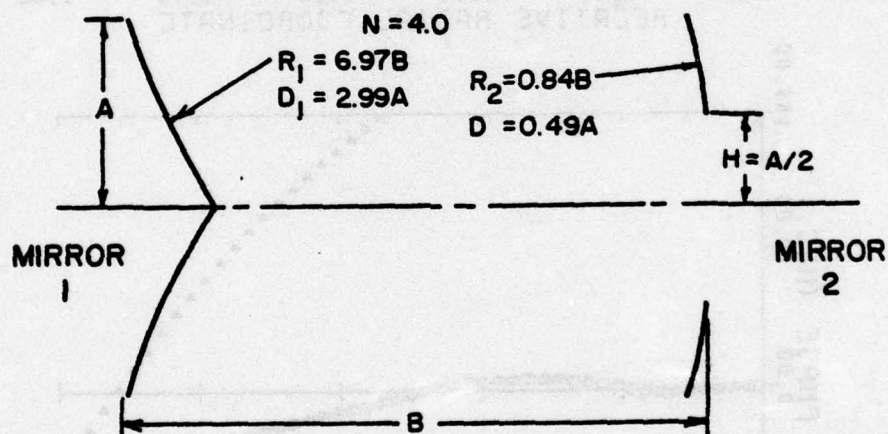
The Final Cavity Eigenvalues, $\gamma_{\ell m}$

m \ ℓ	0	1	2	3
0	0.656 −140°	0.654 −134°	0.663 −111°	0.624 −72°
1	0.253 −26°	0.280 15°	0.216 67°	0.136 130°

Figure 17a   Schematic and eigenvalues of resonator to achieve
a uniform field magnitude on mirror 2, N = 4, ℓ = 0
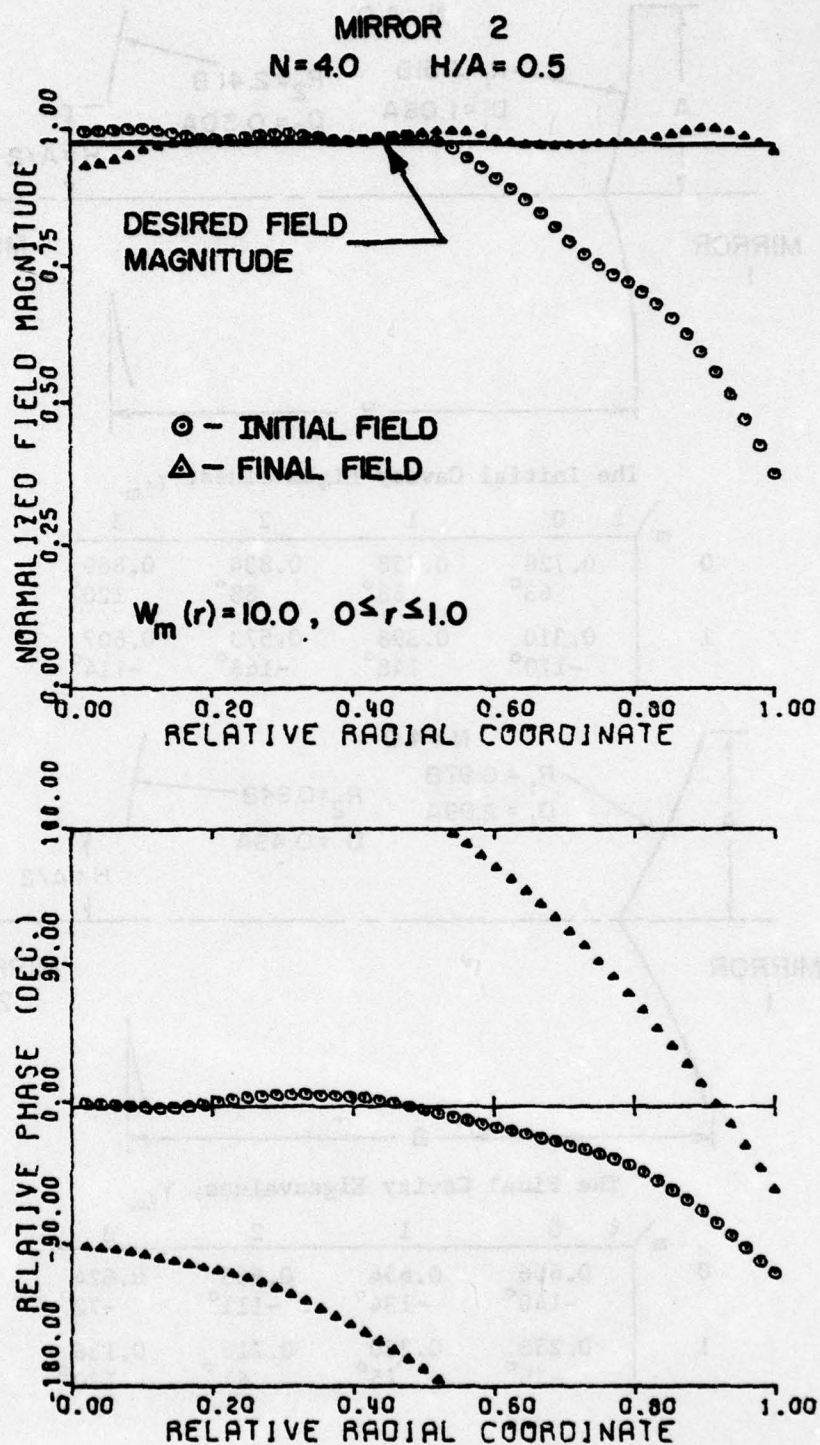
Figure 17b Fields in a plane incident on mirror 2

MIRROR   1

⊙ – INITIAL FIELD
△ – FINAL FIELD

NORMALIZED FIELD MAGNITUDE

1.00
0.75
0.50
0.25
0.00

0.00   0.20   0.40   0.60   0.80   1.00
RELATIVE RADIAL COORDINATE

RELATIVE PHASE (DEG.)

180.00
90.00
0.00
-90.00
-180.00

0.00   0.20   0.40   0.60   0.80   1.00
RELATIVE RADIAL COORDINATE
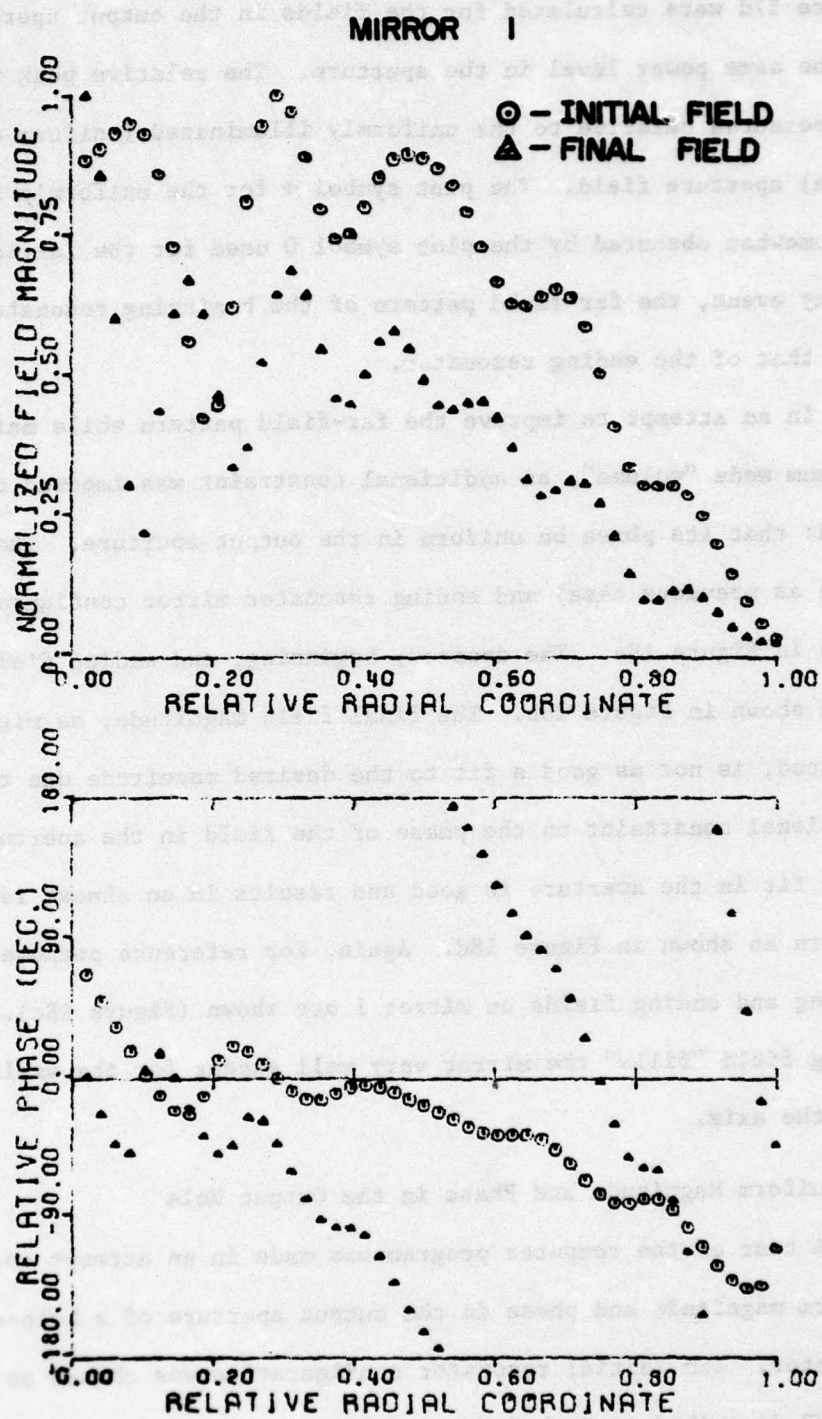
Figure 17c   Fields in a plane reflected from mirror 1

at the expense of the fill on mirror 1. The far-field beam patterns of
Figure 17d were calculated for the fields in the output aperture normalized
to the same power level in the aperture. The relative peak values given
are measured relative to the uniformly illuminated (uniform amplitude and
phase) aperture field. The plot symbol + for the uniformly illuminated case
is somewhat obscured by the plot symbol 0 used for the initial field.
In any event, the far-field pattern of the beginning resonator is better
than that of the ending resonator.

In an attempt to improve the far-field pattern while maintaining a
maximum mode "volume", an additional constraint was imposed on the desired
field: that its phase be uniform in the output aperture. The beginning
(same as previous case) and ending resonator mirror configurations are
shown in Figure 18a. The desired, beginning, and ending fields on mirror
2 are shown in Figure 18b. The final field magnitude, as might be
expected, is not as good a fit to the desired magnitude due to the
additional constraint on the phase of the field in the aperture. The
phase fit in the aperture is good and results in an almost ideal far-field
pattern as shown in Figure 18d. Again, for reference purposes the be-
ginning and ending fields on mirror 1 are shown (Figure 18c). The
ending field "fills" the mirror very well except for the small region
near the axis.

C. Uniform Magnitude and Phase in the Output Hole

A test of the computer program was made in an attempt to achieve
uniform magnitude and phase in the output aperture of a hole-coupled
resonator. The initial resonator configuration was chosen as that of
the HUR described in Task 1 (resonator 1 of Figure 1). The beginning

70

FAR – FIELD

RELATIVE PEAK VALUES

⊙ – 0.99
△ – 0.92
+ – 1.00

⊙ – INITIAL FIELD
△ – FINAL FIELD
+ – REFERENCE
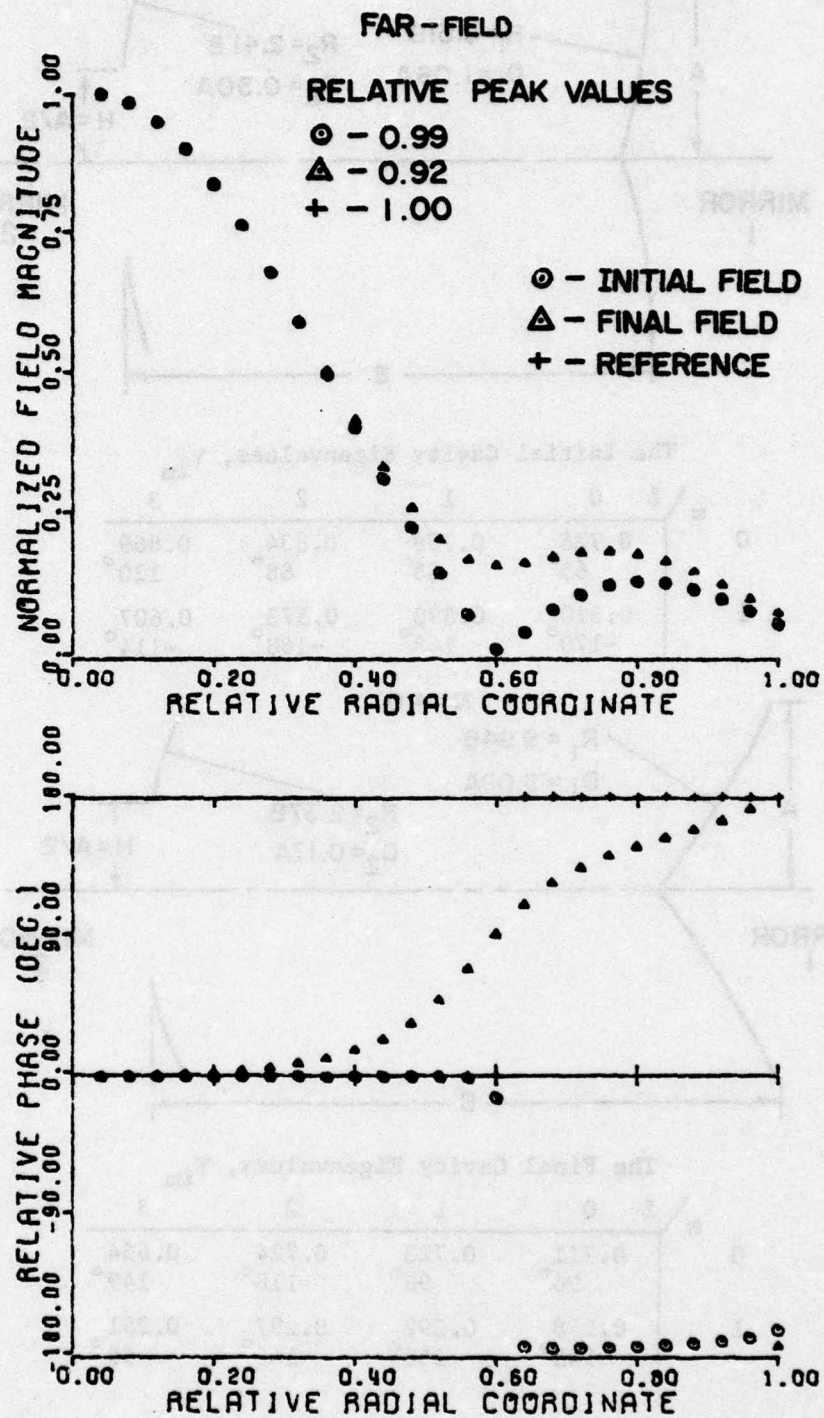
Figure 17d   Far-field patterns

N = 4.0

$R_1 = 3.51B$
$D_1 = 1.06A$

$R_2 = 2.41B$
$D_2 = 0.30A$

A

$H = A/2$

MIRROR 1

MIRROR 2

B

The Initial Cavity Eigenvalues, $\gamma_{\ell m}$

m \\ ℓ	0	1	2	3
0	0.728 63°	0.758 68°	0.834 88°	0.869 120°
1	0.310 −170°	0.398 148°	0.573 −168°	0.607 −114°

N = 4.0

$R_1 = 9.94B$
$D_1 = 3.09A$

$R_2 = 2.37B$
$D_2 = 0.17A$

A

$H = A/2$

MIRROR 1

MIRROR 2

B
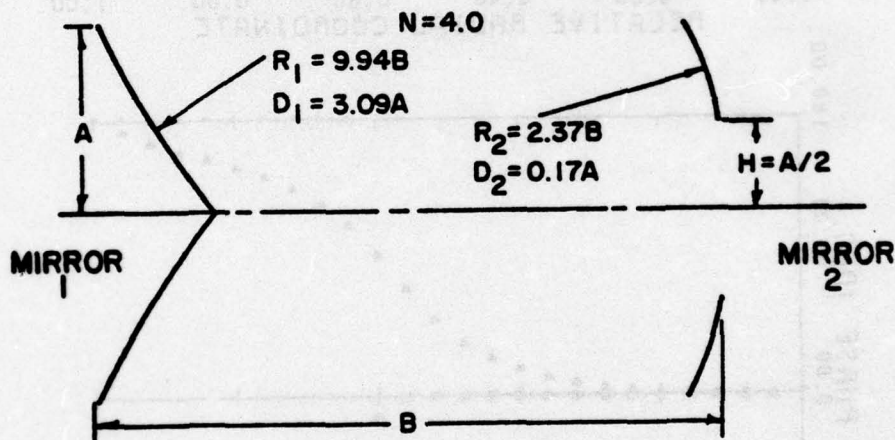
The Final Cavity Eigenvalues, $\gamma_{\ell m}$

m \\ ℓ	0	1	2	3
0	0.711 90°	0.723 96°	0.724 118°	0.654 149°
1	0.178 −145°	0.292 156°	0.297 −146°	0.251 −99°

Figure 18a   Schematic and eigenvalues of resonator to achieve
a uniform field magnitude and uniform phase in
hole at mirror 2, N = 4, ℓ = 0
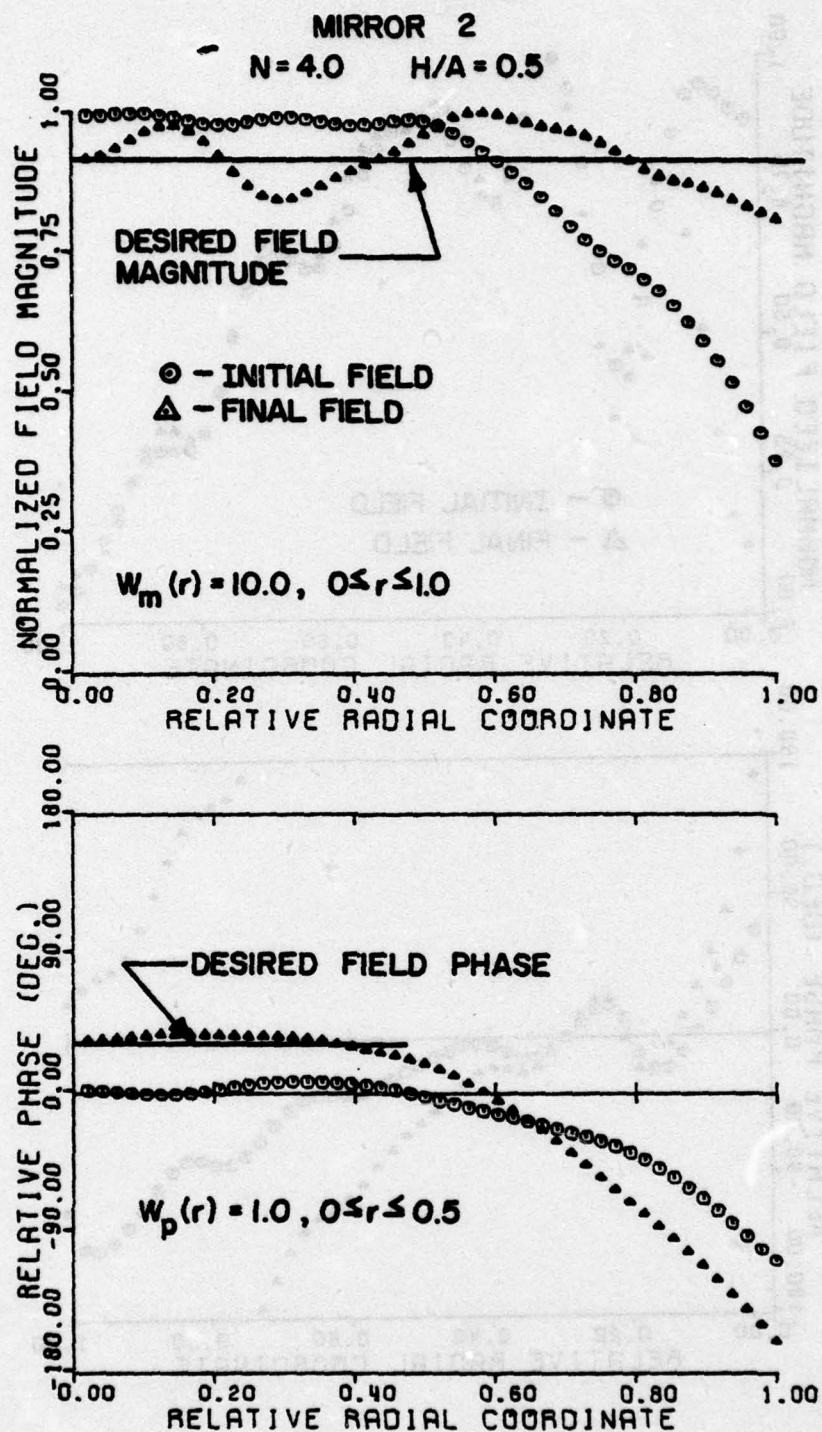
Figure 18b Fields in a plane incident of mirror 2

73

MIRROR 1

○ — INITIAL FIELD
△ — FINAL FIELD
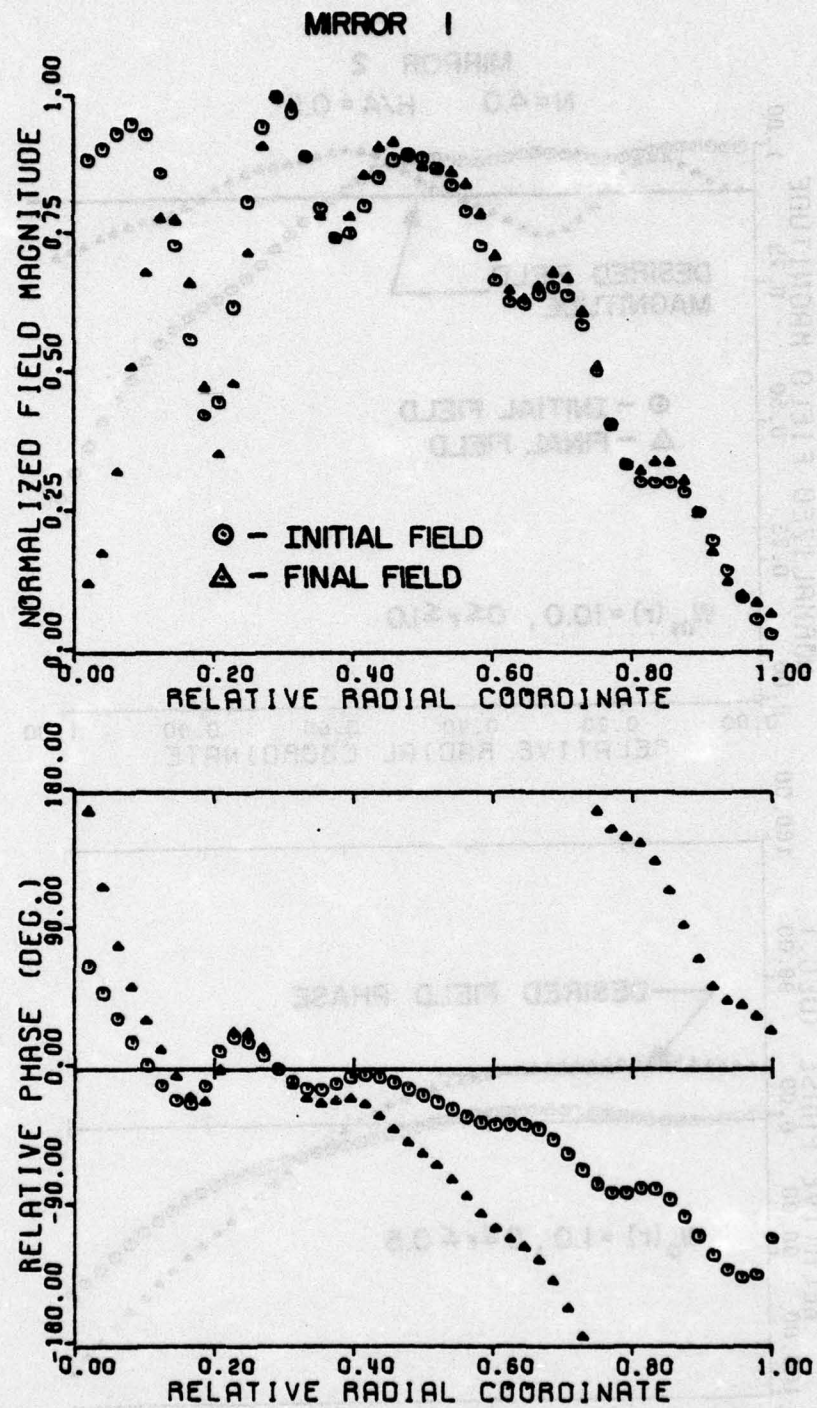
Figure 18c   Field in a plane reflected from mirror 1

74

FAR-FIELD

RELATIVE PEAK VALUES

⊙ - 0.99
△ - 0.99
+ - 1.00

⊙ - INITIAL FIELD
△ - FINAL FIELD
+ - REFERENCE

NORMALIZED FIELD MAGNITUDE

1.00
0.75
0.50
0.25
0.00

0.00   0.20   0.40   0.60   0.80   1.00
RELATIVE RADIAL COORDINATE

RELATIVE PHASE (DEG.)

180.00
90.00
0.00
-90.00
-180.00

0.00   0.20   0.40   0.60   0.80   1.00
RELATIVE RADIAL COORDINATE
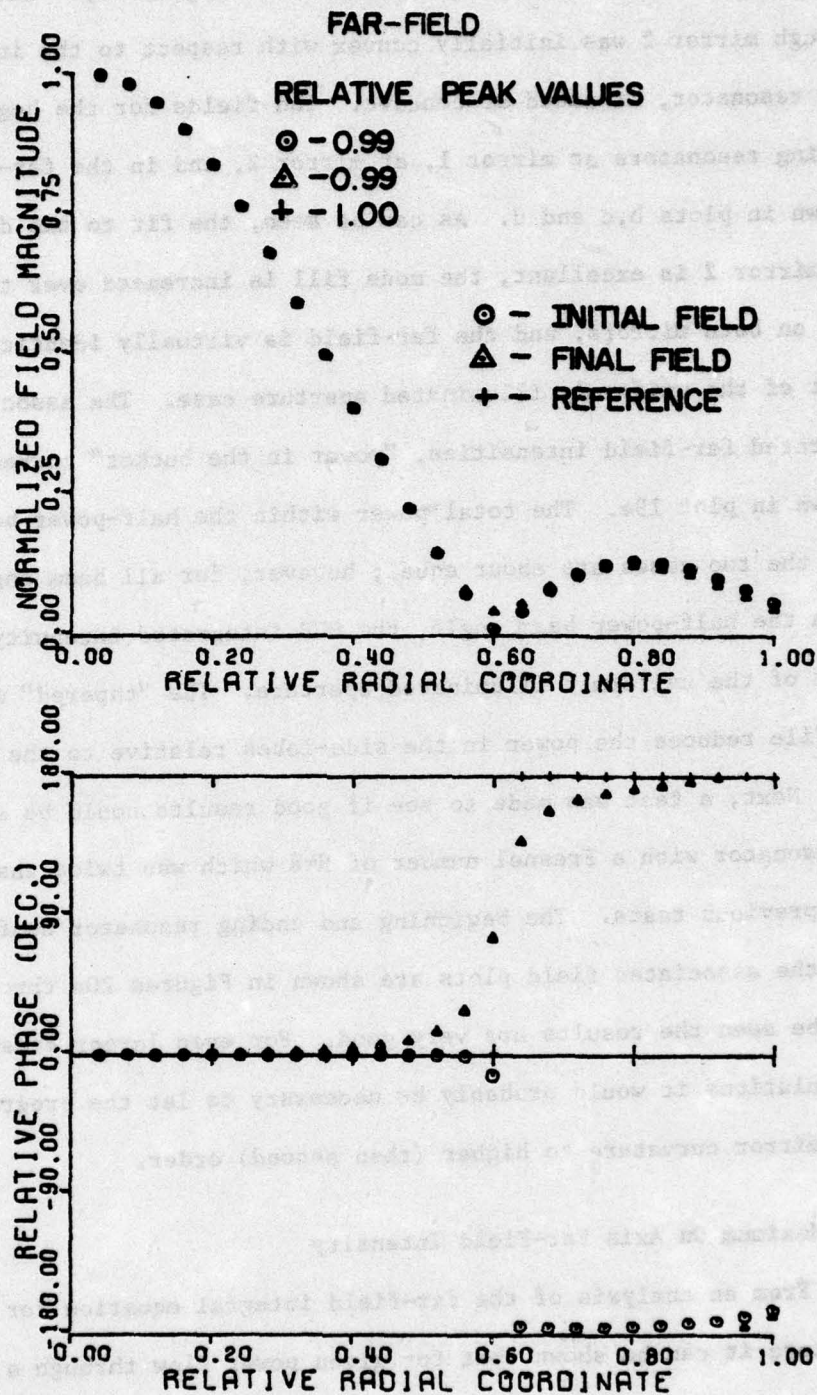
Figure 18d Far-field patterns

and ending mirror profiles are depicted in Figure 19a. Note that even though mirror 2 was initially convex with respect to the interior of the resonator, it ended as concave. The fields for the beginning and ending resonators at mirror 1, at mirror 2, and in the far-field are shown in plots b,c and d. As can be seen, the fit to the desired field on mirror 2 is excellent, the mode fill is increased over that of the HUR on both mirrors, and the far-field is virtually identical with that of the uniformly illuminated aperture case. The associated integrated far-field intensities, "power in the bucket" curves are shown in plot 19e. The total power within the half-power beam width for the two cases are about equal; however, for all beam angles greater than the half-power beam angle, the HUR integrated intensity exceeds that of the uniformly illuminated aperture. The "tapered" magnitude profile reduces the power in the side-lobes relative to the main lobe.

Next, a test was made to see if good results could be achieved for a resonator with a Fresnel number of N=8 which was twice that used for the previous tests. The beginning and ending resonator configurations and the associated field plots are shown in Figures 20a through 20e. As can be seen the results are very good. For even larger Fresnel number calculations it would probably be necessary to let the program calculate the mirror curvature to higher (than second) order.

D. Maximum On Axis Far-Field Intensity

From an analysis of the far-field integral equation for a circular aperture it can be shown that for given power flow through a fixed aperture the maximum on-axis far-field intensity is achieved when the field in the aperture is uniform. Therefore, it was decided to have the program attempt to maximize the power within a given beam angle, rather than to maximize the

76
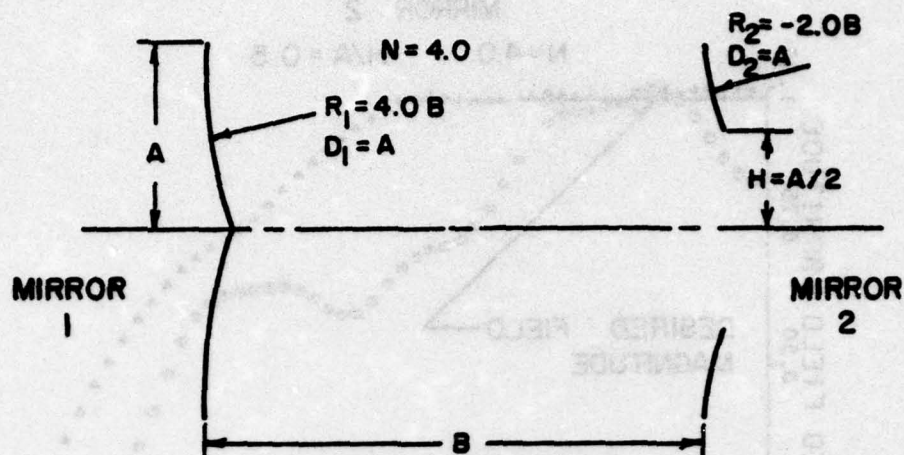
The Initial Cavity Eigenvalues, $\gamma_{\ell m}$

m	ℓ 0	1	2	3
0	0.637 11°	0.711 5°	0.823 30°	0.823 62°
1	0.258 107°	0.340 72°	0.470 114°	0.500 164°
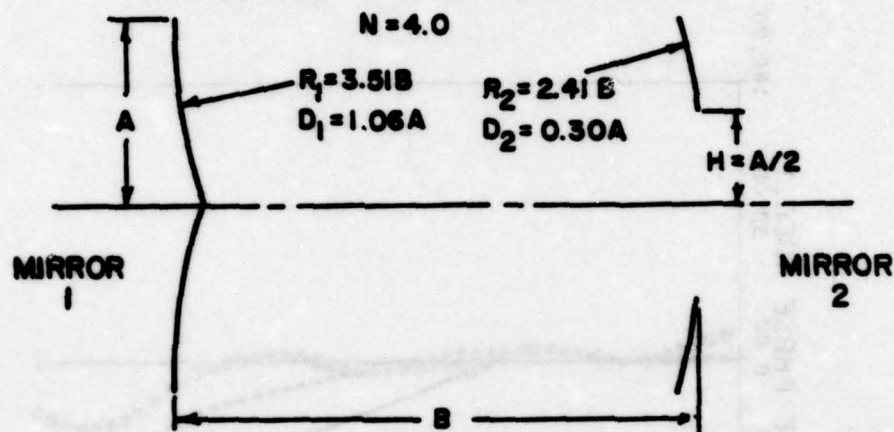
The Final Cavity Eigenvalues, $\gamma_{\ell m}$

m	ℓ 0	1	2	3
0	0.728 63°	0.758 68°	0.834 88°	0.869 120°
1	0.310 −170°	0.398 148°	0.573 −168°	0.607 −114°

Figure 19a Schematic and eigenvalues of a resonator to achieve uniform magnitude and phase in hole of mirror 2, N = 4, ℓ = 0
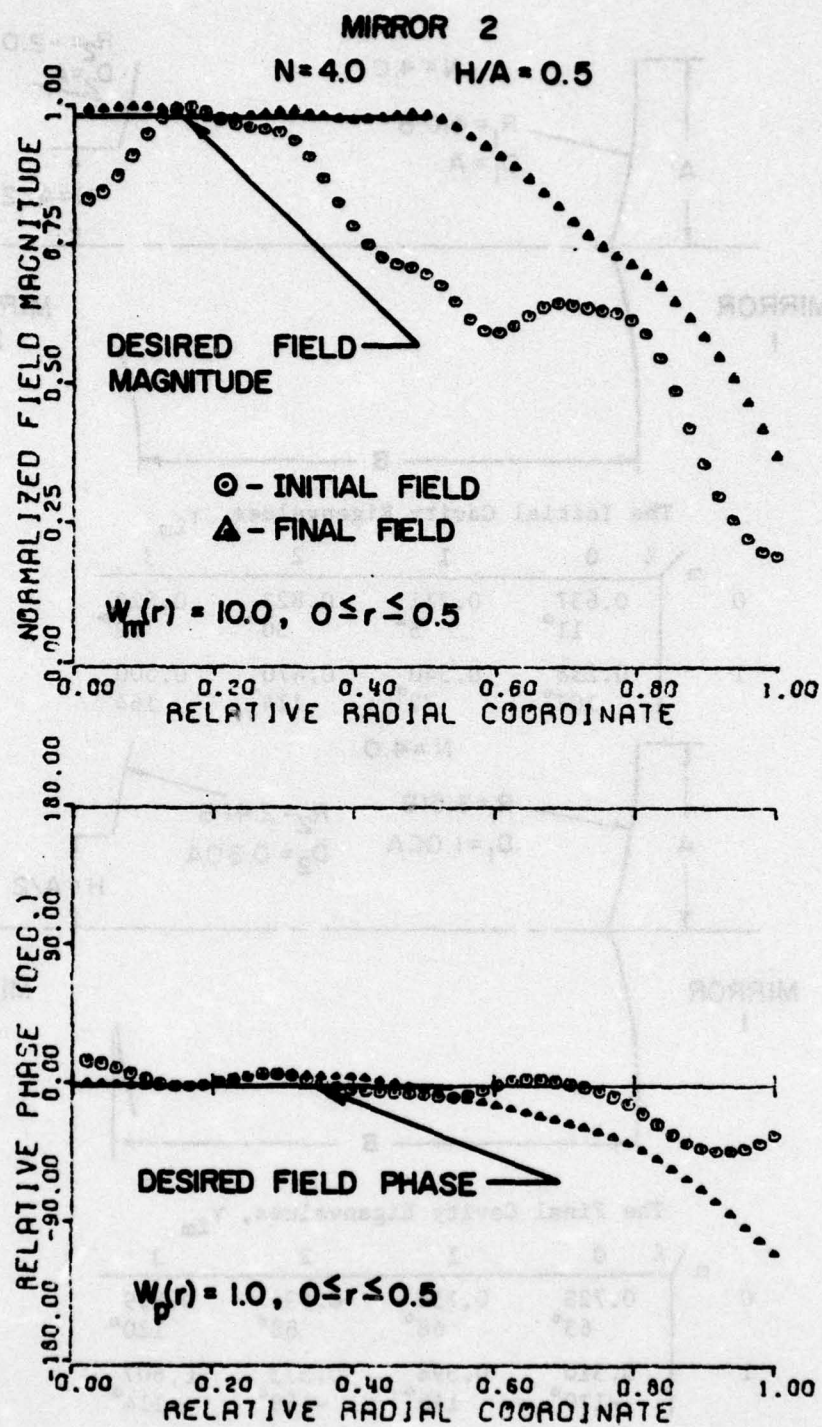
Figure 19b Fields in a plane incident on mirror 2
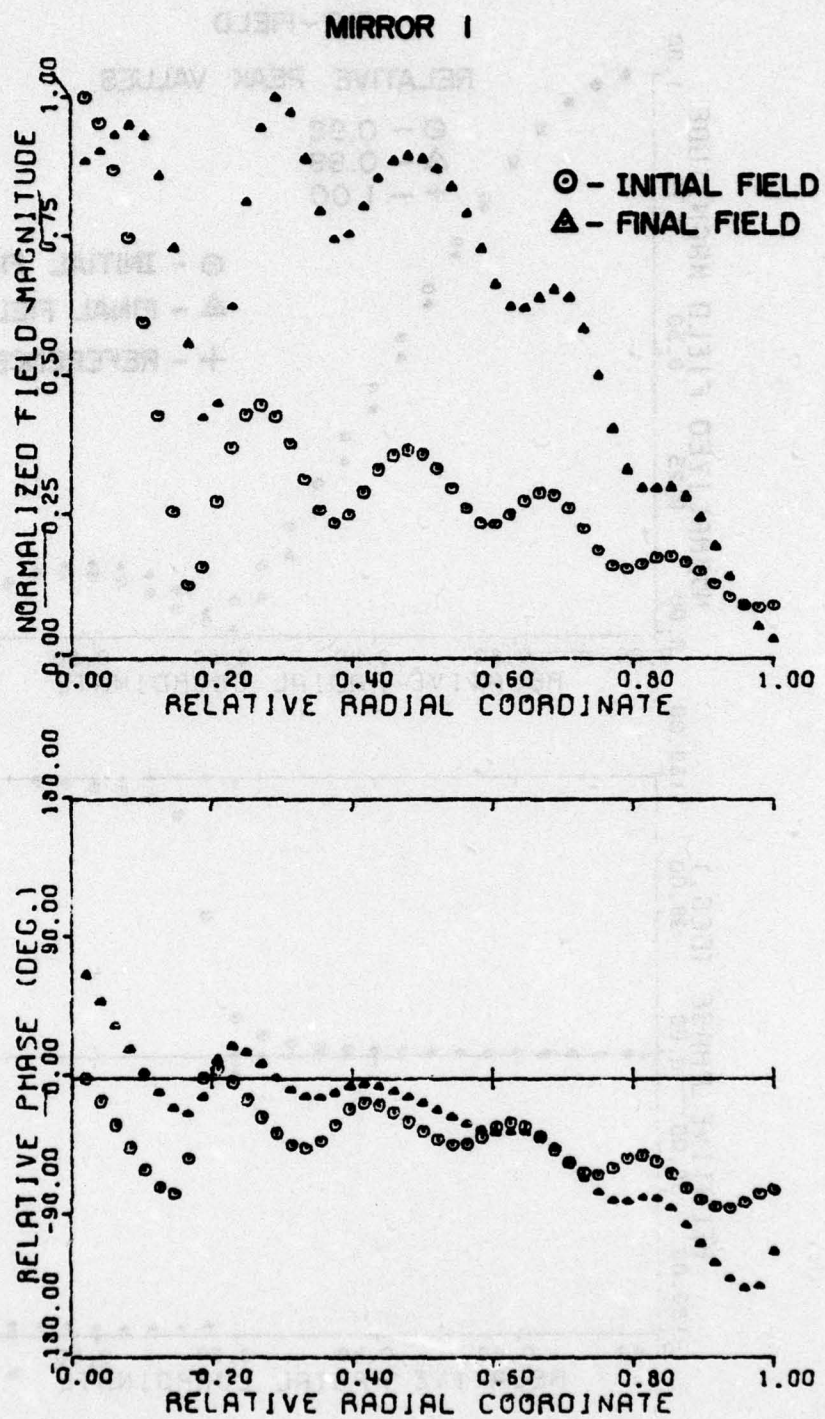
Figure 19c Fields in a plane reflected from mirror 1
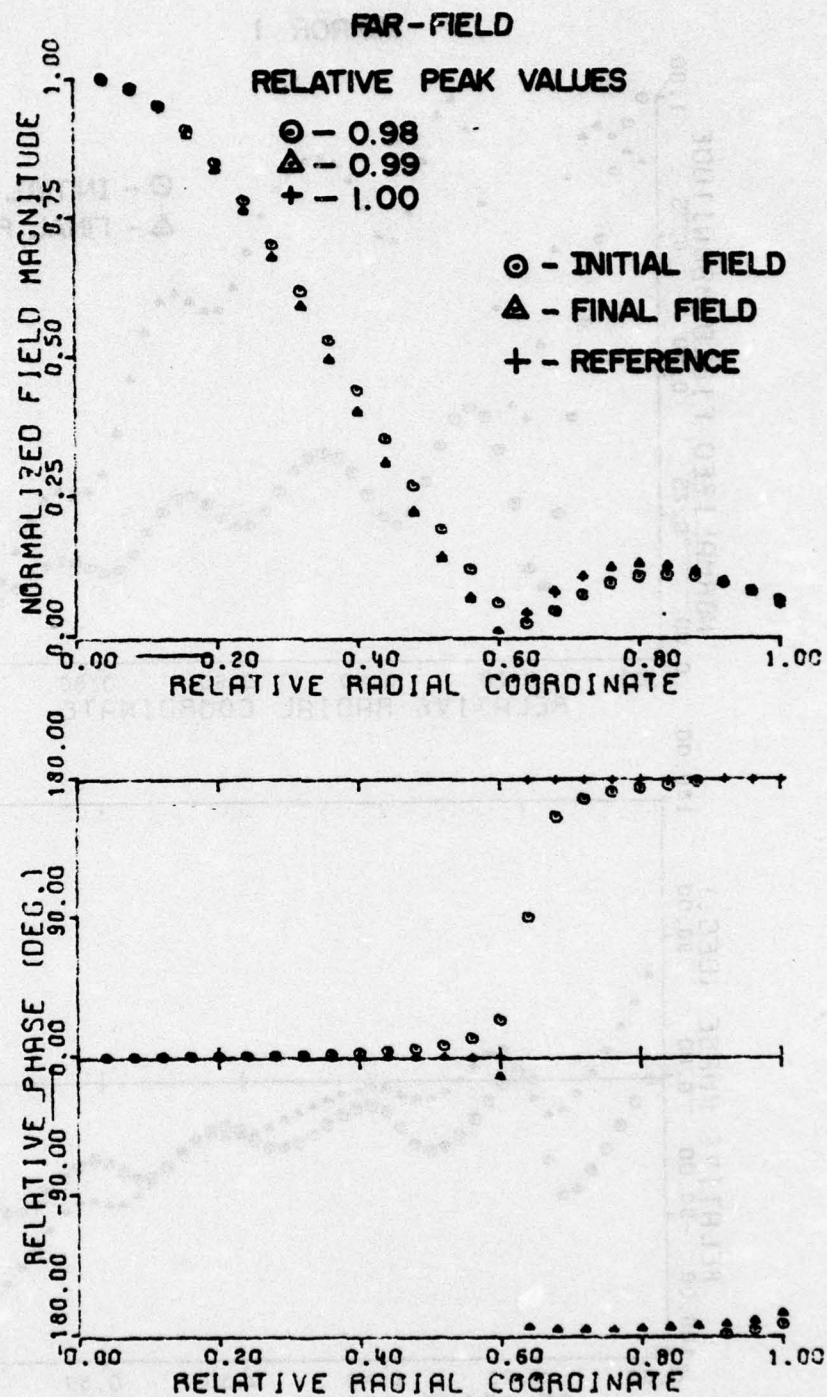
Figure 19d Far-field patterns
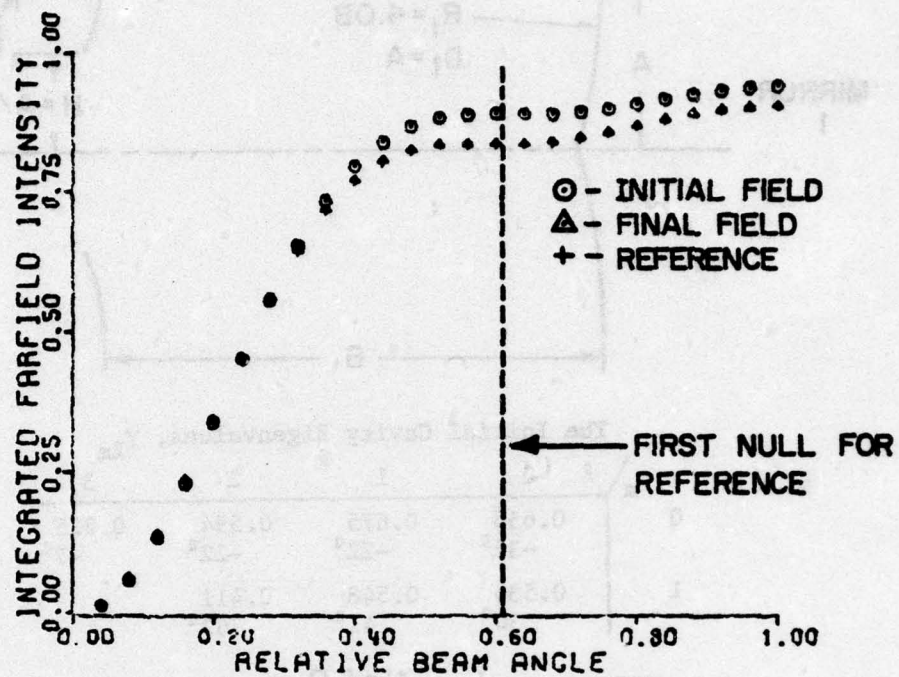
Figure 19e   Integrated far-field intensities

N = 8.0

$R_1 = 4.0B$
$D_1 = A$

$R_2 = -2.0B$
$D_2 = A$
$H = A/2$

MIRROR 1

MIRROR 2

A

B

The Initial Cavity Eigenvalues, $\gamma_{\ell m}$

m \ ℓ	0	1	2	3
0	0.656 -32°	0.675 -22°	0.594 -22°	0.825 -7°
1	0.536 30°	0.548 41°	0.411 63°	

N = 8.0

$R_1 = 3.70B$
$D_1 = 0.87A$

$R_2 = -3.42B$
$D_2 = 1.10A$
$H = A/2$

MIRROR 1

MIRROR 2

A

B
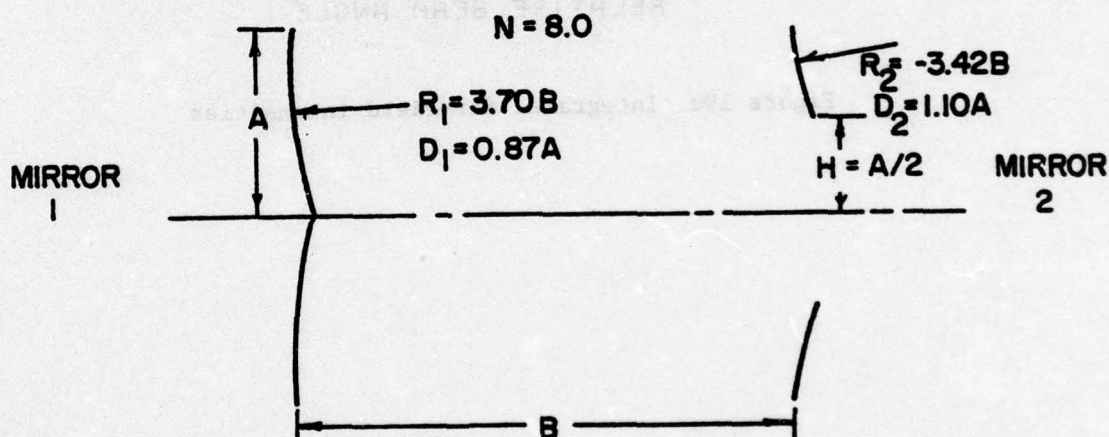
The Final Cavity Eigenvalues, $\gamma_{\ell m}$

m \ ℓ	0	1	2	3
0	0.687 -22°	0.717 -16°	0.688 -8°	0.792 2°
1	0.490 56°	0.560 63°	0.504 81°	

Figure 20a Schematic and eigenvalues of a resonator to achieve uniform magnitude and phase in hole of mirror 2, $N = 8$, $\ell = 0$

END

DATE
FILMED
2-77

Figure 20b Fields in a plane incident on mirror 2

Figure 20c   Fields in a plane reflected from mirror 1

84
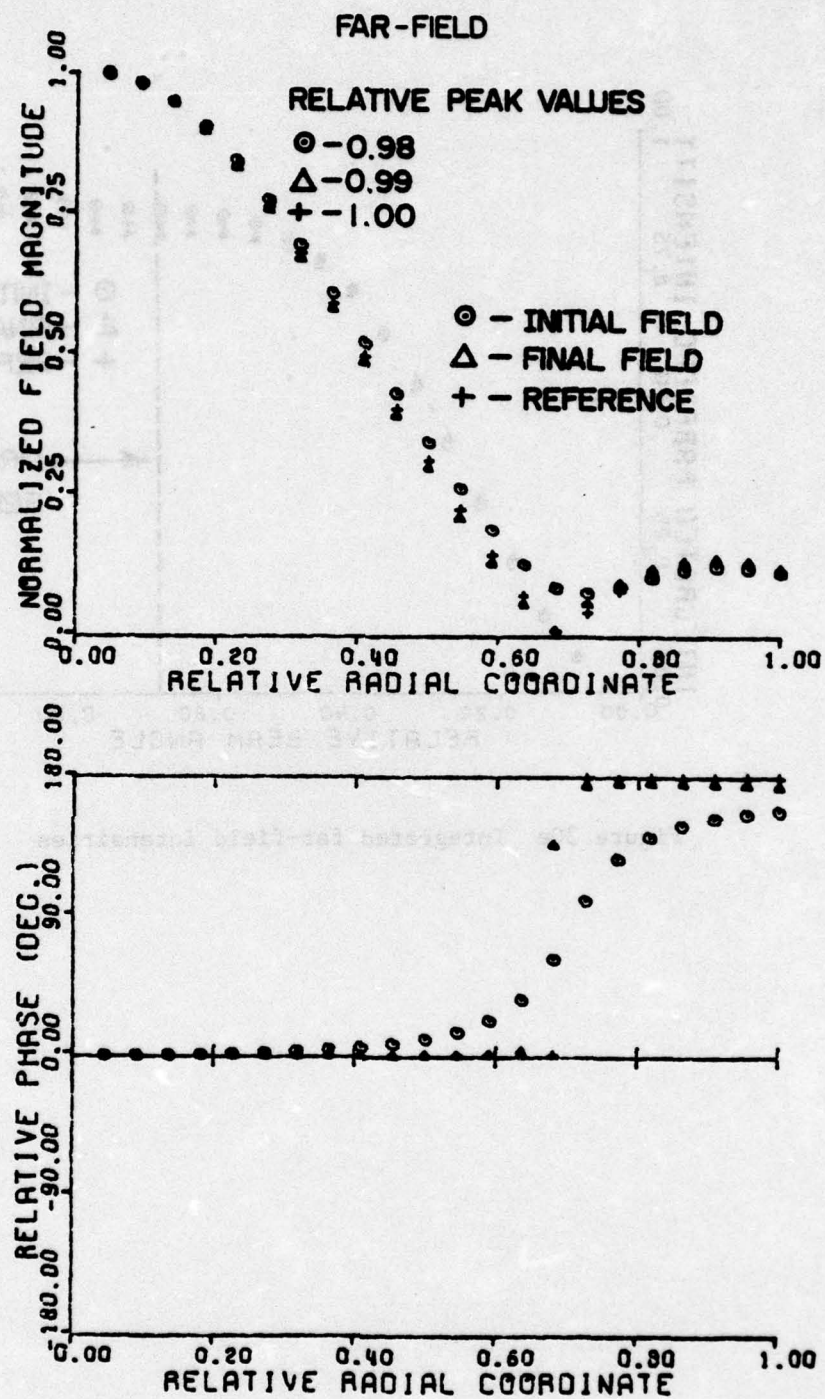
Figure 20d Far-field patterns
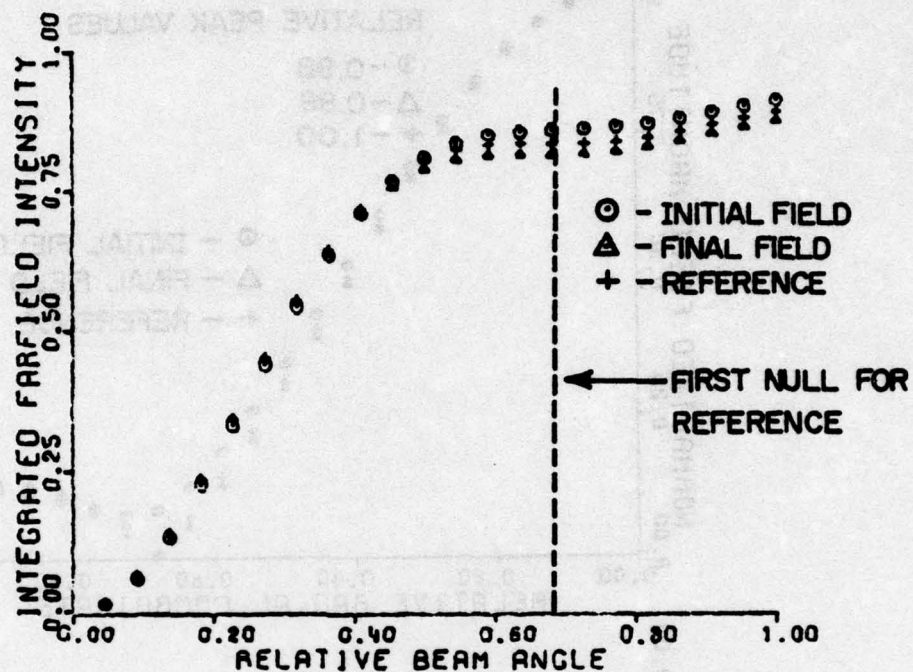
Figure 20e   Integrated far-field intensities

far-field on-axis intensity. The approach taken was to request that the program find a resonator whose integrated far-field intensity was equal to its maximum possible value over a specified beam angle. Of course the ideal far-field magnitude profile which would satisfy this condition would be an on-axis delta function. The beginning and ending resonator configurations are shown in Figure 21a. Figure 21b shows the resulting integrated far-field intensity, and it can be seen that the final intensity is a better fit to the desired intensity than that of the uniformly illuminated aperture. This results in a significant decrease in the first side lobe peak relative to the reference as shown in Figure 21c. In Figure 21d it can be seen that the field magnitude in the aperture of mirror 2 is tapered and the phase is uniform. The final field on mirror 1 in Figure 21e, although itself quite peaked on axis, is more slowly varying than the fields of the other hole-coupled configurations examined.

E. A "Hole-Coupled" Resonator with a Dominant $\ell=0$ Mode

Many additional tests have been made of the program's ability to fit desired fields, and in most tests the program was able to achieve a good fit. Once the resonator parameters were found, the eigenvalues for the higher order azimuthal modes were calculated using the program developed during Task 1. It was found that none of the hole-coupled resonators had good azimuthal mode discrimination. The only hole-coupled resonators found for which the $\ell=0$ mode was dominant had very high losses over the outer edges of the mirror(s).

One "hole-coupled" resonator in which the $\ell=0$ mode was dominant is shown is Figure 22. The mirror profiles are extremely exaggerated to show their general shape. No R and D values are given because the mirror figures were calculated to third order. The beginning configuration
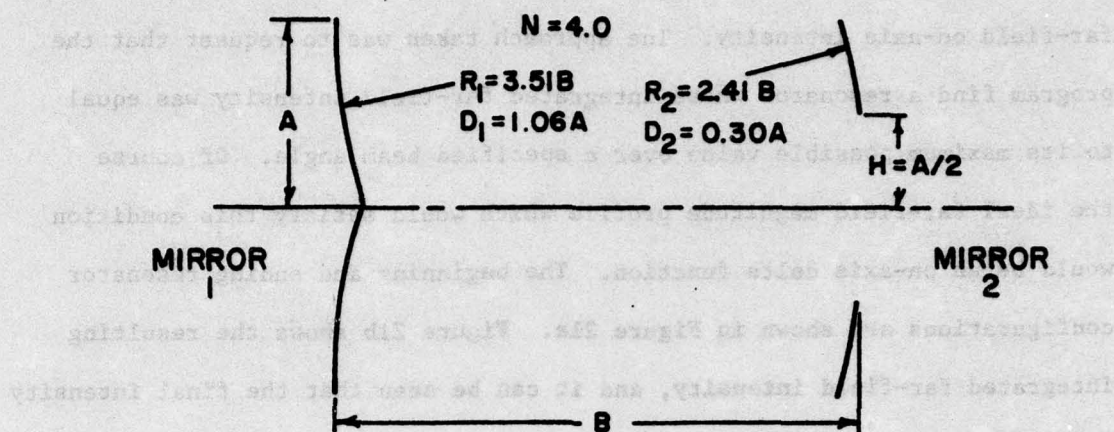
87

N = 4.0

R₁ = 3.51B
D₁ = 1.06A

R₂ = 2.41 B
D₂ = 0.30A

H = A/2

A

MIRROR 1

MIRROR 2

B

The Initial Cavity Eigenvalues, $\gamma_{\ell m}$

m	ℓ 0	1	2	3
0	0.728 63°	0.758 68°	0.834 88°	0.869 120°
1	0.310 −170°	0.398 148°	0.573 −168°	0.607 −114°

N = 4.0

R₁ = 2.83B
D₁ = 0.82A

R₂ = 2.32B
D₂ = 0.26A

H = A/2

A

MIRROR 1

MIRROR 2

B
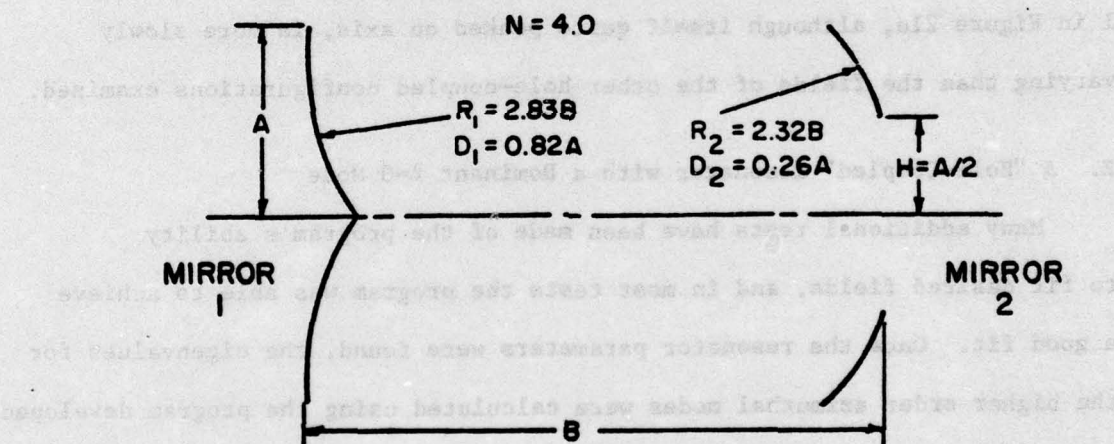
The Final Cavity Eigenvalues, $\gamma_{\ell m}$

m	ℓ 0	1	2	3
0	0.559 156°	0.582 153°	0.766 176°	0.892 −144°
1	0.370 −48°	0.380 −124°	0.589 −65°	0.677 −8°

Figure 21a Schematic and eigenvalues of resonator to achieve a maximum integrated far-field intensity, N = 4, ℓ = 0

88
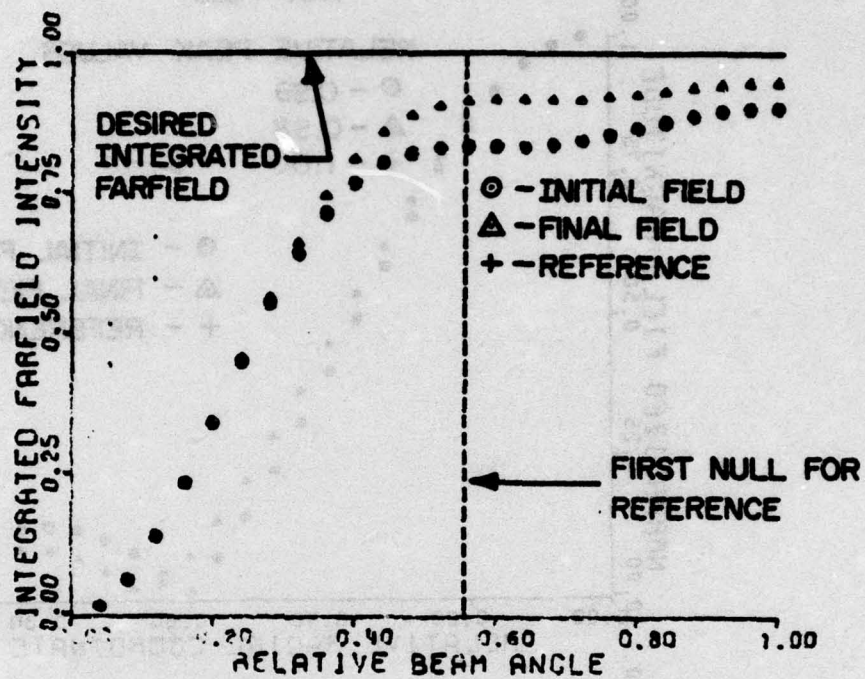
Figure 21b Integrated far-field intensities
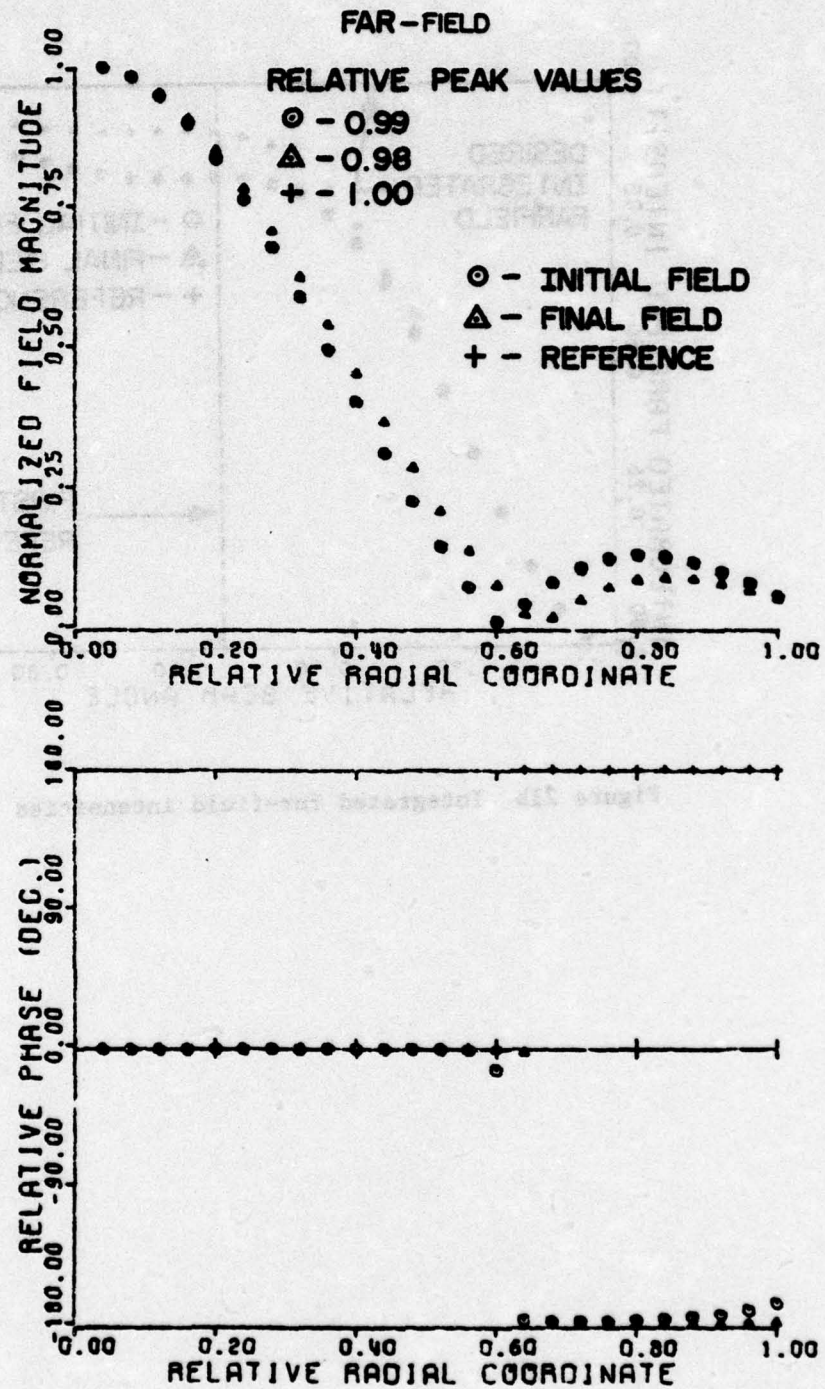
Figure 21c Far-field patterns
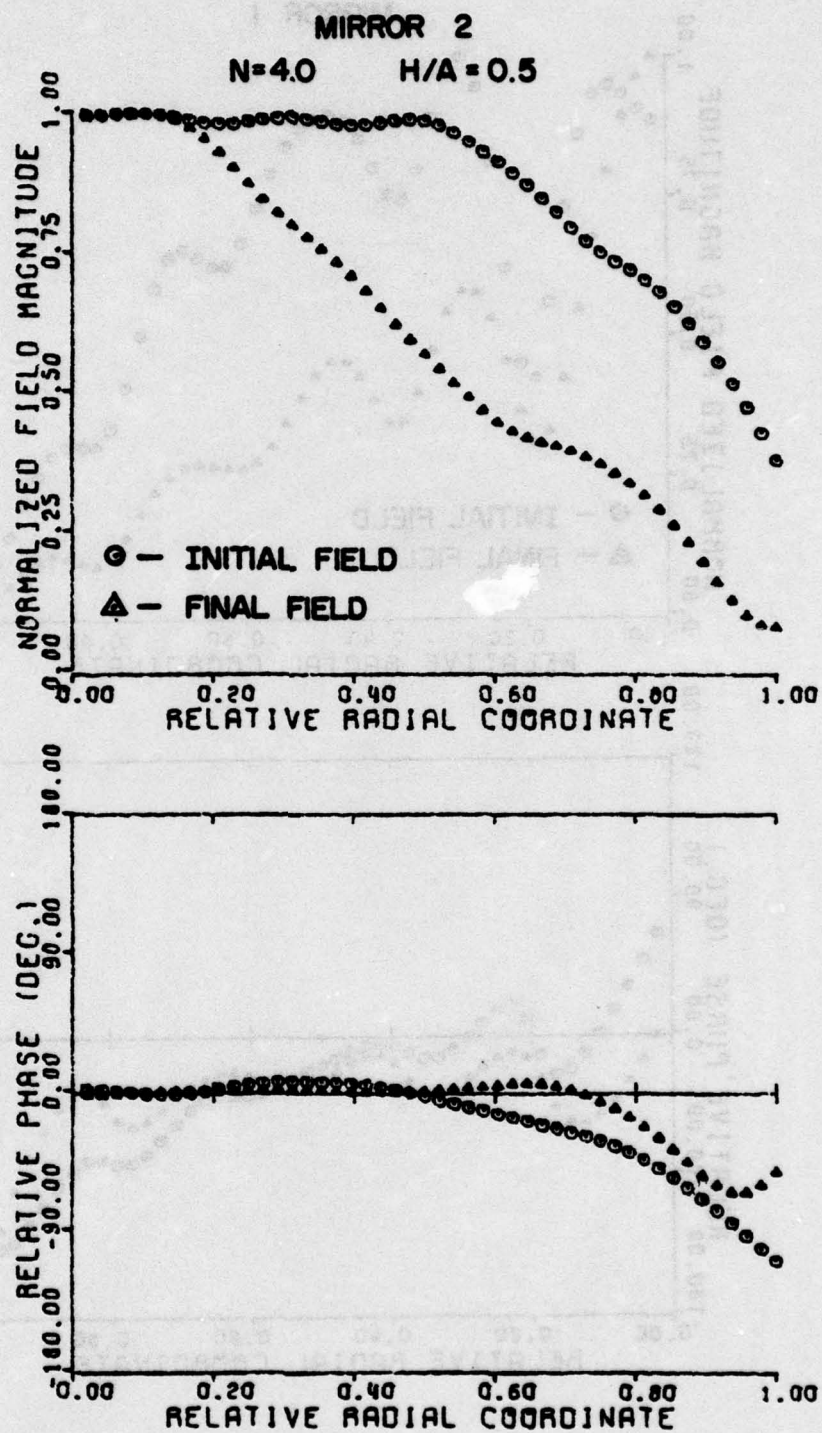
MIRROR 2
N=4.0   H/A = 0.5

Figure 21d   Field in a plane incident on mirror 2
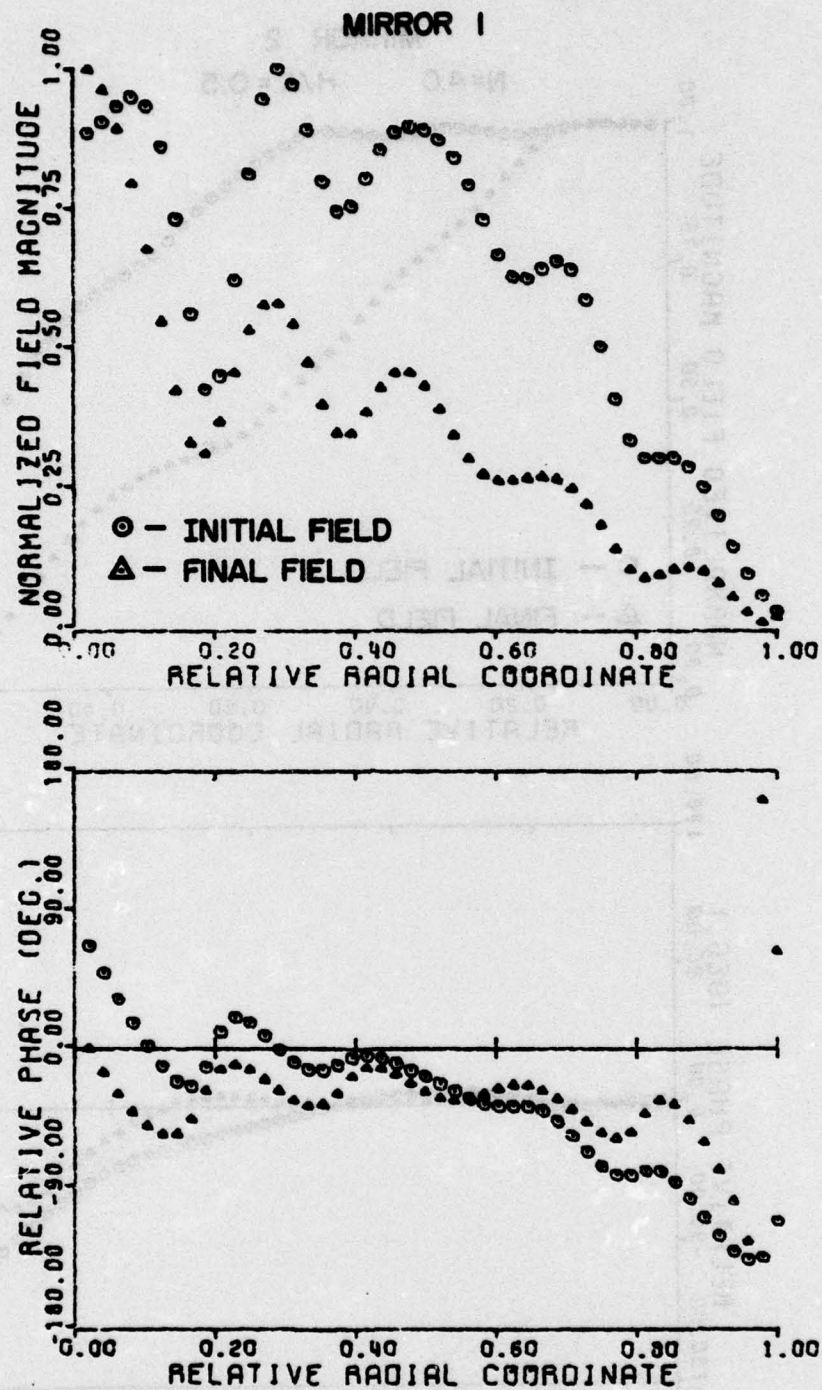
Figure 21e Field in a plane reflected from mirror 1

N = 9.0

A_1

$A_2 = 2A_1/3$

$H = A_1/3$

MIRROR 1

MIRROR 2

B
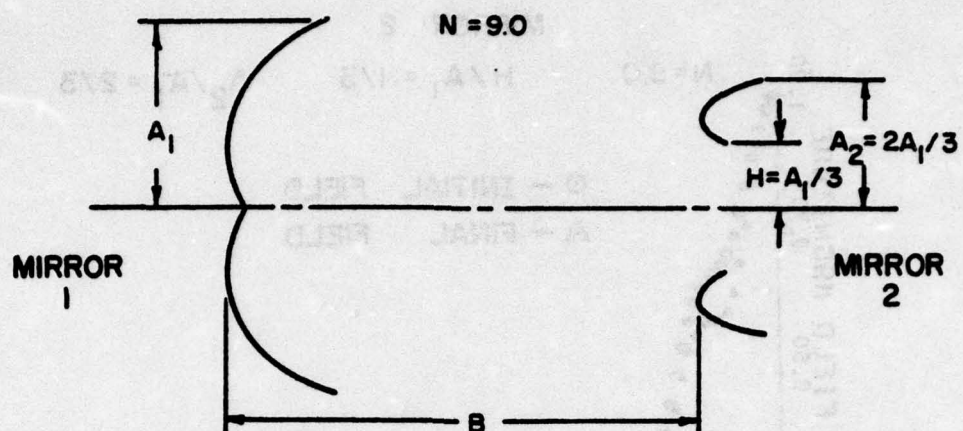
The Initial Cavity Eigenvalues, $\gamma_{\ell m}$

m \ ℓ	0	1	2	3
0	0.565 75°	0.514 75°	0.562 80°	0.518 115°
1	0.243 123°	0.157 −53°	0.307 125°	0.335 164°

N = 9.0

A_1

$A_2 = 2A_1/3$

$H = A/3$

MIRROR 1

MIRROR 2

B
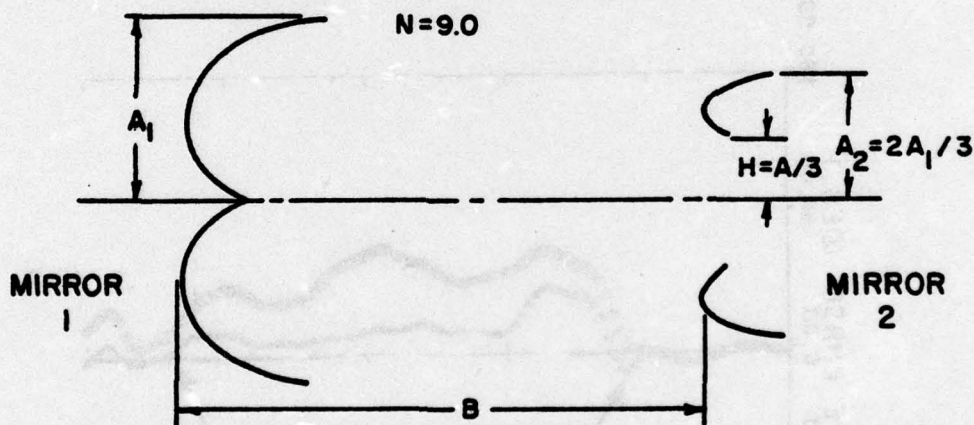
The Final Cavity Eigenvalues, $\gamma_{\ell m}$

m \ ℓ	0	1	2	3
0	0.515 −5°	0.436 −2°	0.478 14°	0.385 67°
1	0.228 9°	0.294 21°	0.284 63°	0.330 24°

Figure 22a   Schematic and eigenvalues of resonator to achieve uniform phase as indicated in Figure 22b, N = 9, $\ell = 0$

93
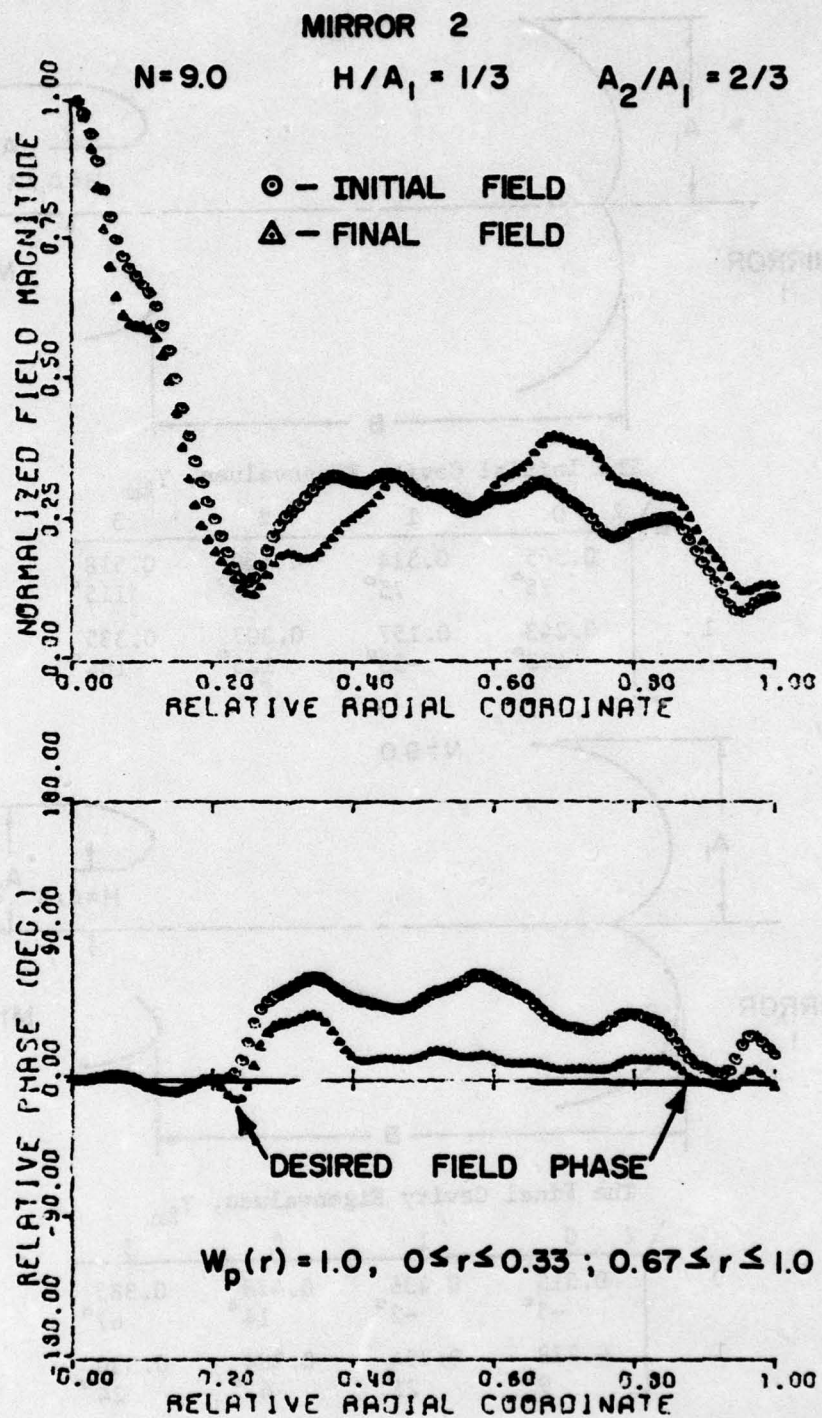
Figure 22b Field in a plane incident on mirror 2
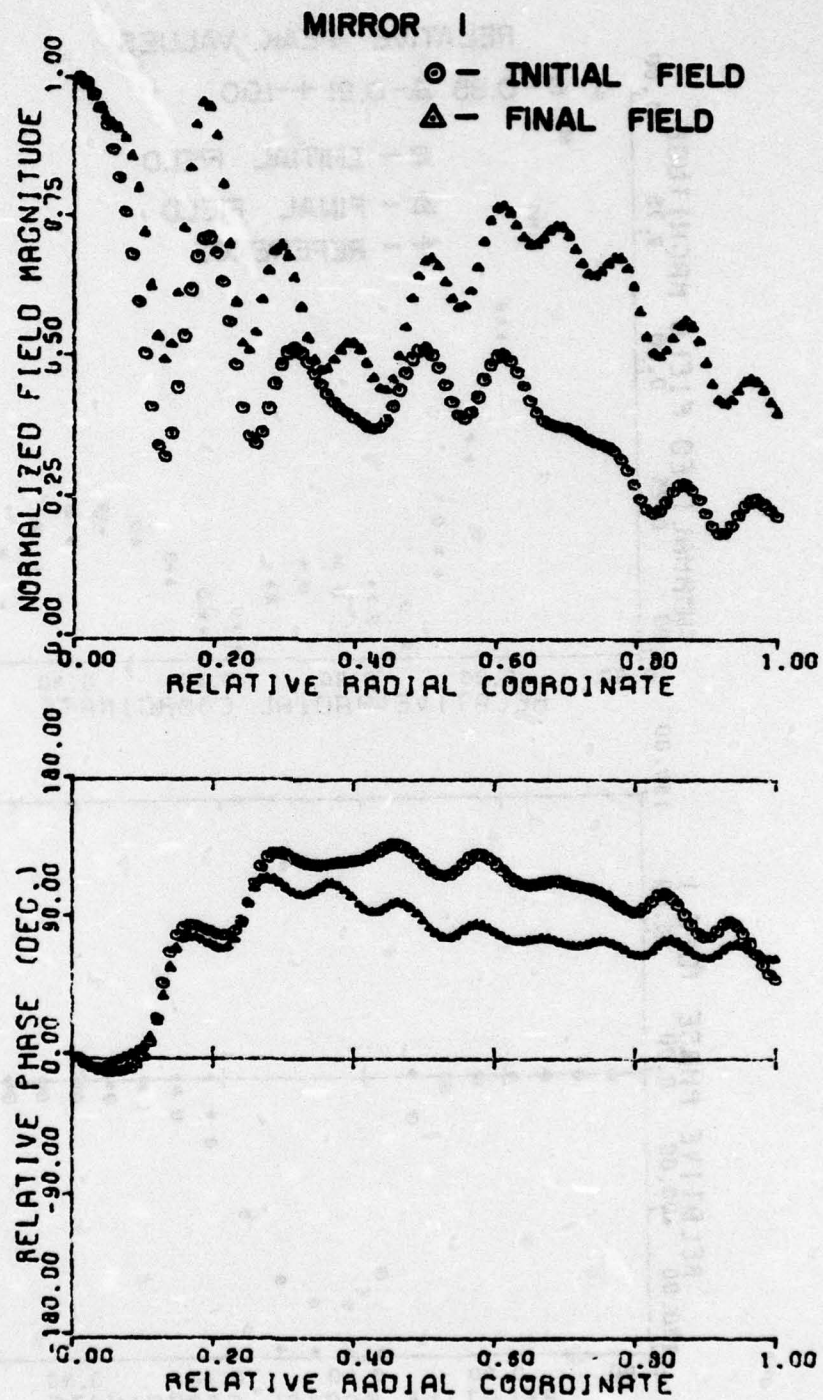
Figure 22c Field in a plane reflected from mirror 1
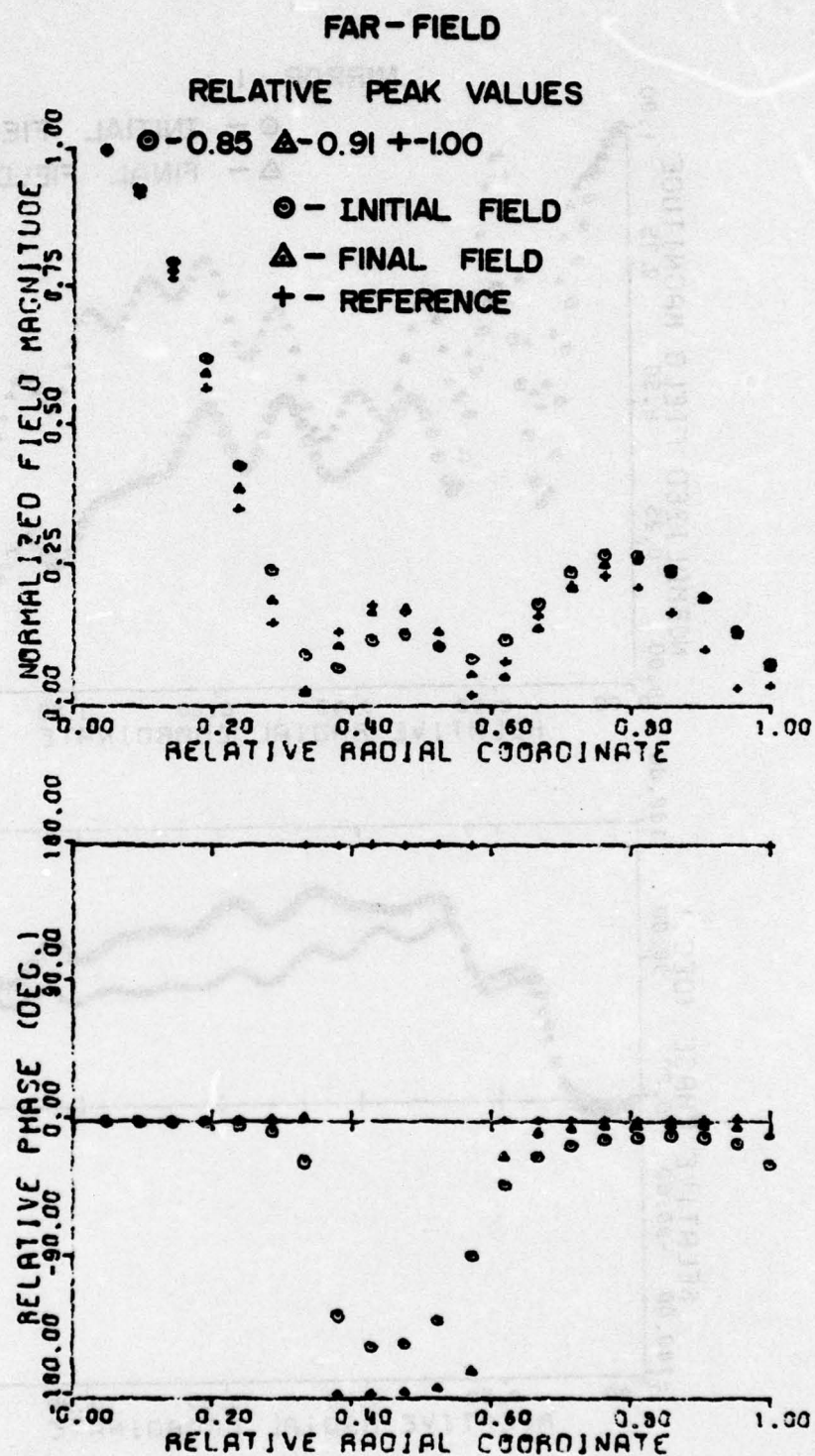
FAR‑FIELD

Figure 22d   Far-field patterns

96

is actually the ending configuration of a previous test where the desired field was specified as uniform phase in a plane incident on mirror 2 out to $r = A_1$ where A_1 is the radius of mirror 1. No restriction was placed on the field magnitude. In this case the requirement that the phase be uniform on the mirror was removed. Except near the edge of the hole where the field amplitude is relatively small, the phase of the final field is very close to the desired field phase. The mode discrimination ratio

$$|\frac{\gamma_{00}}{\gamma_{20}}| = \frac{0.515}{0.478} = 1.08$$

was the largest obtained for any hole-coupled resonator examined, except where the Fresnel number of the hole was trivially small. Even in this case the Fresnel number of the hole is only

$$NH1 = (1/3)^2 N = 1$$

and less than half of the total output is through the hole.

F. Rimmed Resonator Test

One additional test will be described to further illustrate the utility of the program. The program was given the task of adjusting the slope and curvature of t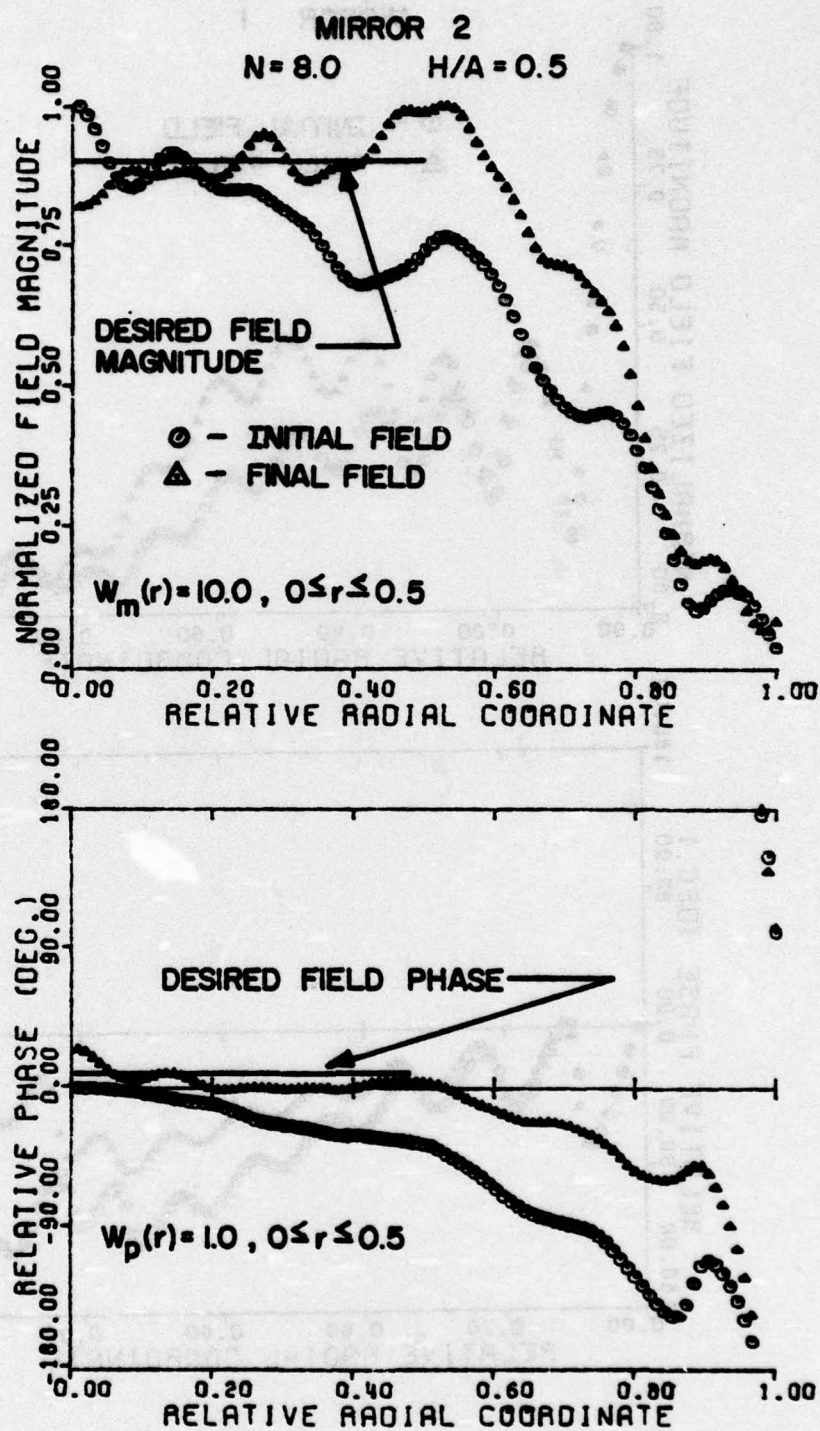he rim on one of the resonators described by Lax et al. [3]. They state that "...transverse mode can be suppressed at high power levels, provided the ratio of the fundamental-mode-irradiance spatial minimum to maximum exceeds a minimum value". Using the fitting program the fundamental mode irradiance can be tailored very easily. The beginning configuration (Figure 23a) was chosen without regard to their suggestion that the mirror and rim Fresnel numbers be non-integral or that $N_1 \approx N$. We note that there is little azimuthal discrimination since

$$|\frac{\gamma_{00}}{\gamma_{10}}| = \frac{0.985}{0.974} = 1.01$$

97

$N = 4.0$

$R_2 = 16B$
$D_2 = 0.05A$

$R_1 = -33.3B$
$D_1 = 0.0$

MIRROR 1   MIRROR 2

A   A/√2   B
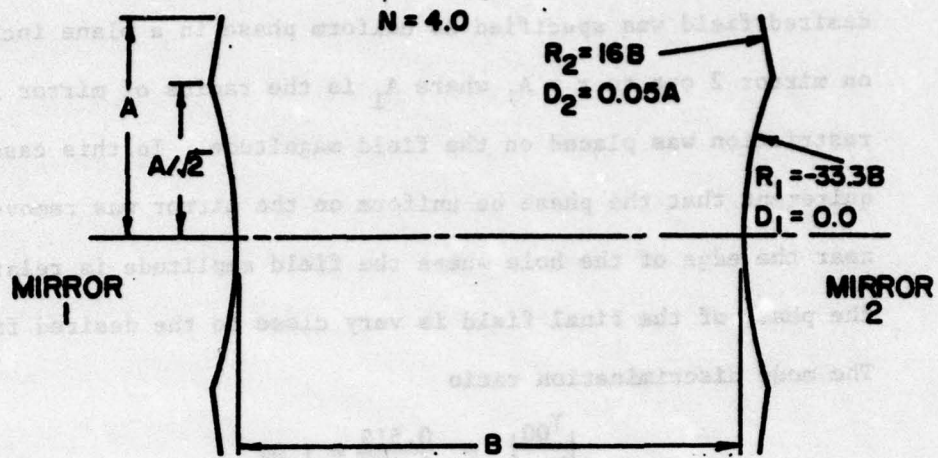
The Initial Cavity Eigenvalues, $\gamma_{\ell m}$

m\ℓ	0	1	2	3
0	0.985 −4°	0.974 2°	0.959 13°	0.939 27°
1	0.953 22°	0.916 41°	0.855 62°	0.801 85°

$N = 4.0$

$R_2 = 72.4B$
$D_2 = 1.84A$

$R_1 = -33.3B$
$D_1 = 0.0$

MIRROR 1   MIRROR 2

A   A/√2   B
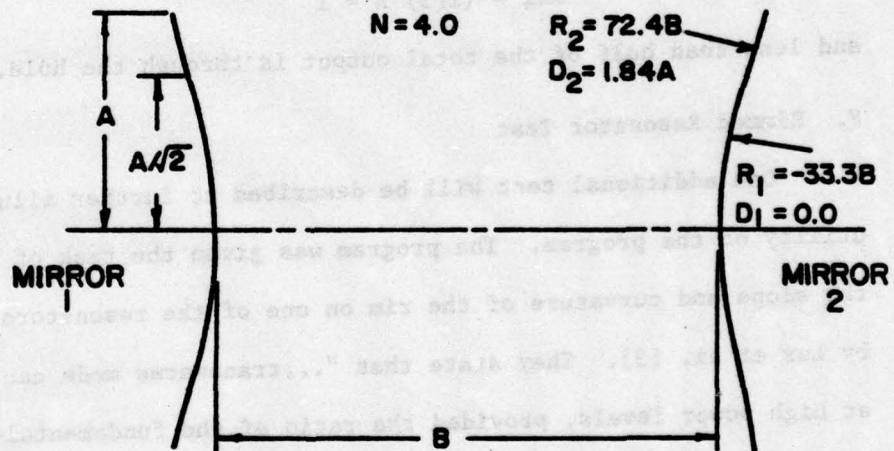
The Final Cavity Eigenvalues, $\gamma_{\ell m}$

m\ℓ	0	1	2	3
0	0.925 −9°	0.903 −5°	0.866 3°	0.845 14°
1	0.894 15°	0.849 31°	0.781 51°	0.718 71°

Figure 23a Rimmed resonator schematic (and eigenvalues) to achieve the desired field profile shown in Figure 23b, N = 4, ℓ = 0

98

for the starting resonator. The field profile (Figure 23b) of the $\ell=0$ mode for the beginning resonator is interesting in that the phase in the plane at the mirror(s) is almost perfectly flat. The desired magnitude was chosen to try to make the field amplitude more uniform over the mirror without increasing the losses too much, and the desired phase is that of a spherical wave coming from the virtual focus (see reference 4) of the geometric resonator mode with no rim. The final field magnitude profile is "flatter," and the azimuthal mode discrimination is somewhat improved in the ending resonator, but at the expense of higher losses over the mirror edges. It appears that the magnitude fit is not as good as might be expected, probably due to the non-uniform magnitude and phase weighting functions of W_m and W_p. The magnitude fit could be improved at the expense of the phase fit simply by increasing the W_m weights relative to the W_p weights. It is not understood, however, why the phase profile is not an even better fit than that shown. It is interesting that the rim was virtually straightened out to conform to the curvature of the central portion of the resonator. In any event, the ratio of the minimum to the maximum field values is 0.5 and hence satisfies the criteria stated in [3] for achieving good azimuthal mode discrimination.

G. Conclusions

In conclusion, the program is able to calculate mirror curvatures to fit a desired radial mode profile for no azimuthal variations. It has been found that requiring the field magnitude of the $\ell=0$ mode to be uniform in the output aperture virtually assures that the $\ell=0$ mode will not be the lowest loss mode (i.e. that higher order azimuthal modes will have lower losses in the same resonator). This suggests that possibly
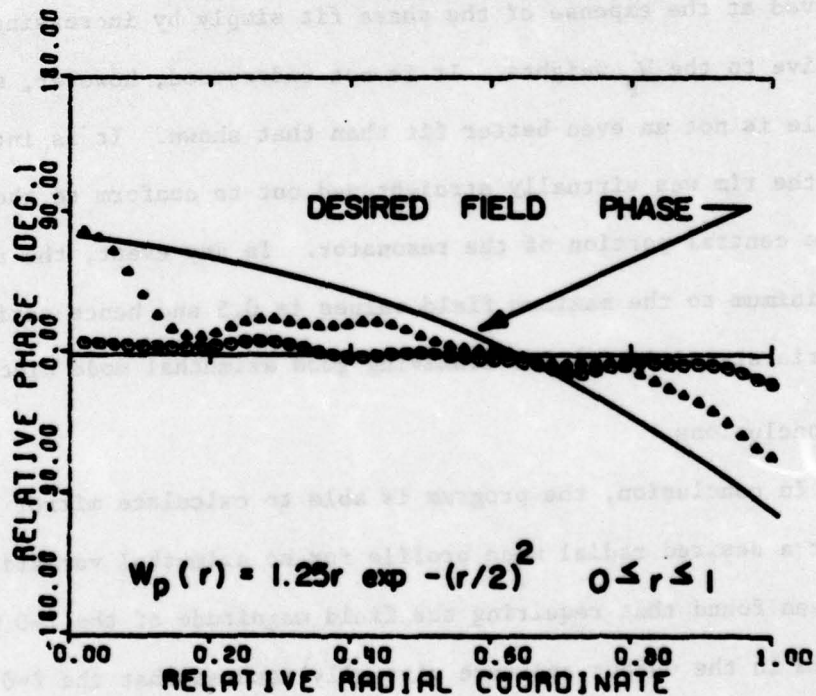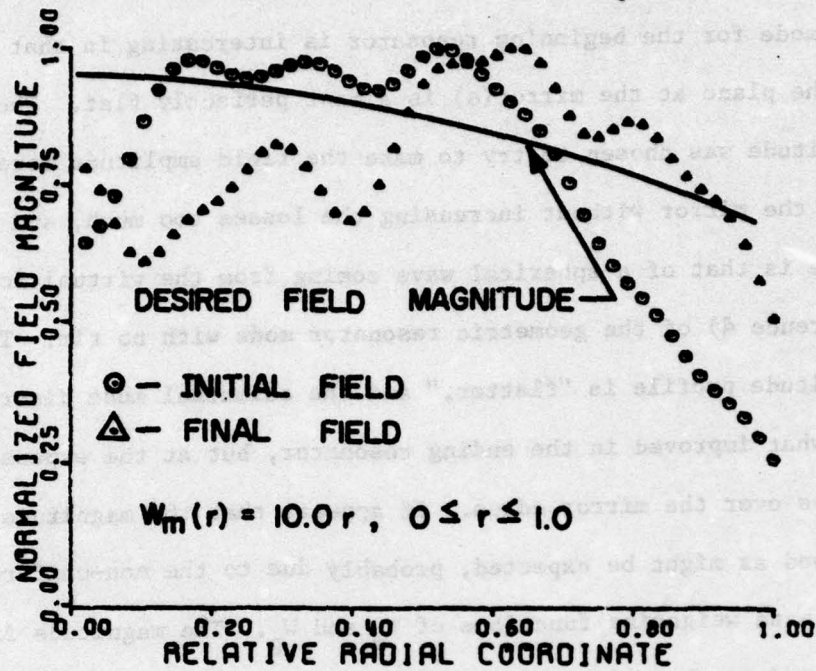
Figure 23b Fields in a plane at mirror 1 (or 2). Wm is the magnitude error weighting function and Wp is the phase error weighting function (weighting function described in Appendix B)

the program should be required to achieve uniform amplitude in
the hole for the lowest loss azimuthal mode to increase its losses
relative to the $\ell=0$ mode. The "brute force" way to obtain $\ell=0$
mode operation would be to have the program adjust the azimuthal mirror
profile in addition to the radial profile. This procedure, while straight-
forward with regard to generalizing the program to calculate the full
resonator field, would be more costly with regard to the computer time
required.

The objective of Task 3 was to determine the required ratio of annular to hole coupling such that the resonator of Figure 24 would have good azimuthal mode discrimination. To facilitate the discussion, we define the geometric ratio of the area of the annular output region $\pi A_2^2 - \pi A_1^2$ to the area of the hole πH_2^2

$$R = \frac{A_2^2 - A_1^2}{H_2^2}$$

In the limiting case where focal ring radius $D=0$ the resonator degenerates into a conventional unstable positive branch confocal resonator which is known to have good azimuthal mode discrimination. In this case $H_2=0$ and $R = \infty$. In another limiting case where $D=A_1$ the resonator degenerates into resonator 1 of Figure 1, which was investigated in Task 1 and found to have poor azimuthal mode discrimination. In this second case the area of the annulus is zero so that $R=0$. As the area of the hole increases and R decreases the azimuthal mode discrimination ratio (magnitude of the ratio of the largest $\ell=0$ eigenvalue to the next largest eigenvalue for any ℓ) will decrease. Somewhere within the range $0 < R < \infty$ the loss for the $\ell=0$ mode will equal the loss of one or more of the higher order azimuthal modes, and the mode discrimination ratio will be unity. It was hoped that a large fraction of the output could be hole coupled ($R \ll 1$) before this breakeven point was reached. To determine how much hole coupling could be allowed, while maintaining acceptable azimuthal mode discrimination the computer program developed under Task 1 was used to calculate the eigenvalues of the resonator for various values of D.
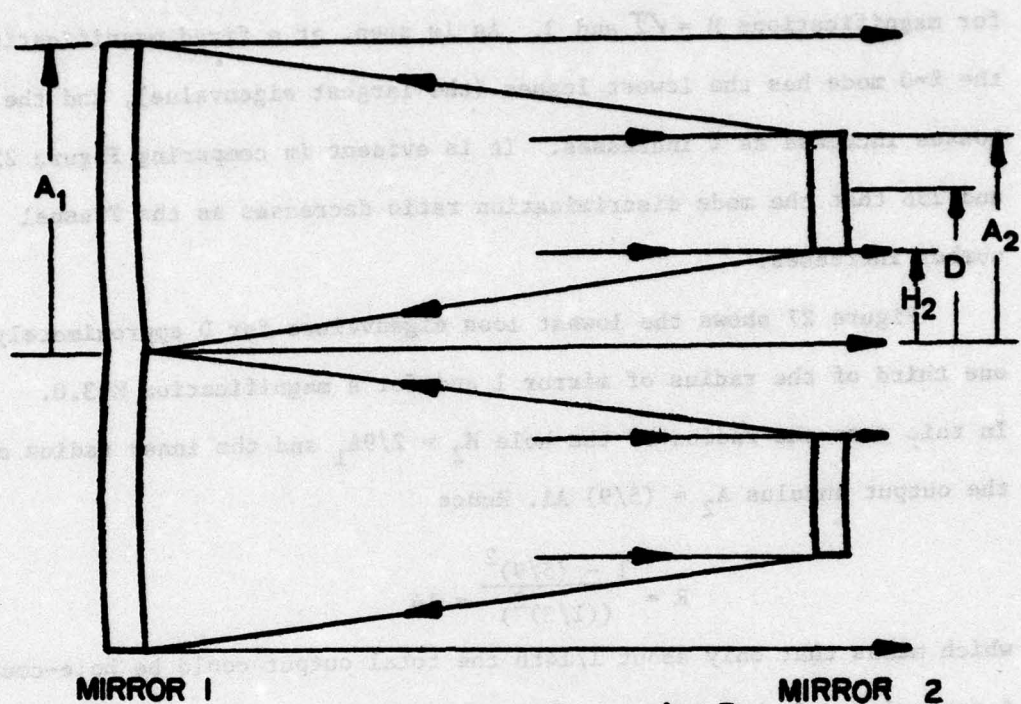
$$M = \frac{D}{D-H_2} = \frac{A_1 - D}{A_2 - D}$$

Figure 24   Resonator with hole and annular output coupling

Figures 25 and 26 show the eigenvalues for the case where D=0 for magnifications $M = \sqrt{2}$ and 3. As is seen, at a fixed magnification, the $\ell=0$ mode has the lowest losses (the largest eigenvalue), and the losses increase as ℓ increases. It is evident in comparing Figure 25a and 25b that the mode discrimination ratio decreases as the Fresnel number increases.

Figure 27 shows the lowest loss eigenvalues for D approximately one third of the radius of mirror 1 and for a magnification M=3.0. In this case the radius of the hole $H_2 = 2/9A_1$ and the inner radius of the output annulus $A_2 = (5/9)$ A1. Hence

$$R = \frac{1 - (5/9)^2}{((1/3)^2)} = 14$$

which means that only about 1/14th the total output could be hole-coupled. A comparison of the different azimuthal mode plots shows that the $\ell=0$ mode is dominant in the Fresnel number interval $0 < N < 4$, the $\ell=1$ mode is dominant for $4 < N < 15$, and the $\ell=2$ mode is dominant $15 < N <$ a higher fresnel number than is on the plot.

The eigenvalues were also calculated for D = A1/2 for magnifications $M = \sqrt{2}$ and 3, as shown in Figures 28 and 29. As in the previous case the azimuthal index of the dominant mode increases as the Fresnel number increases. Thus it is concluded that only for relatively small Fresnel numbers could any of the resonator output be hole-coupled in the $\ell=0$ mode. These Fresnel numbers are too small to be of interest for high power laser applications.
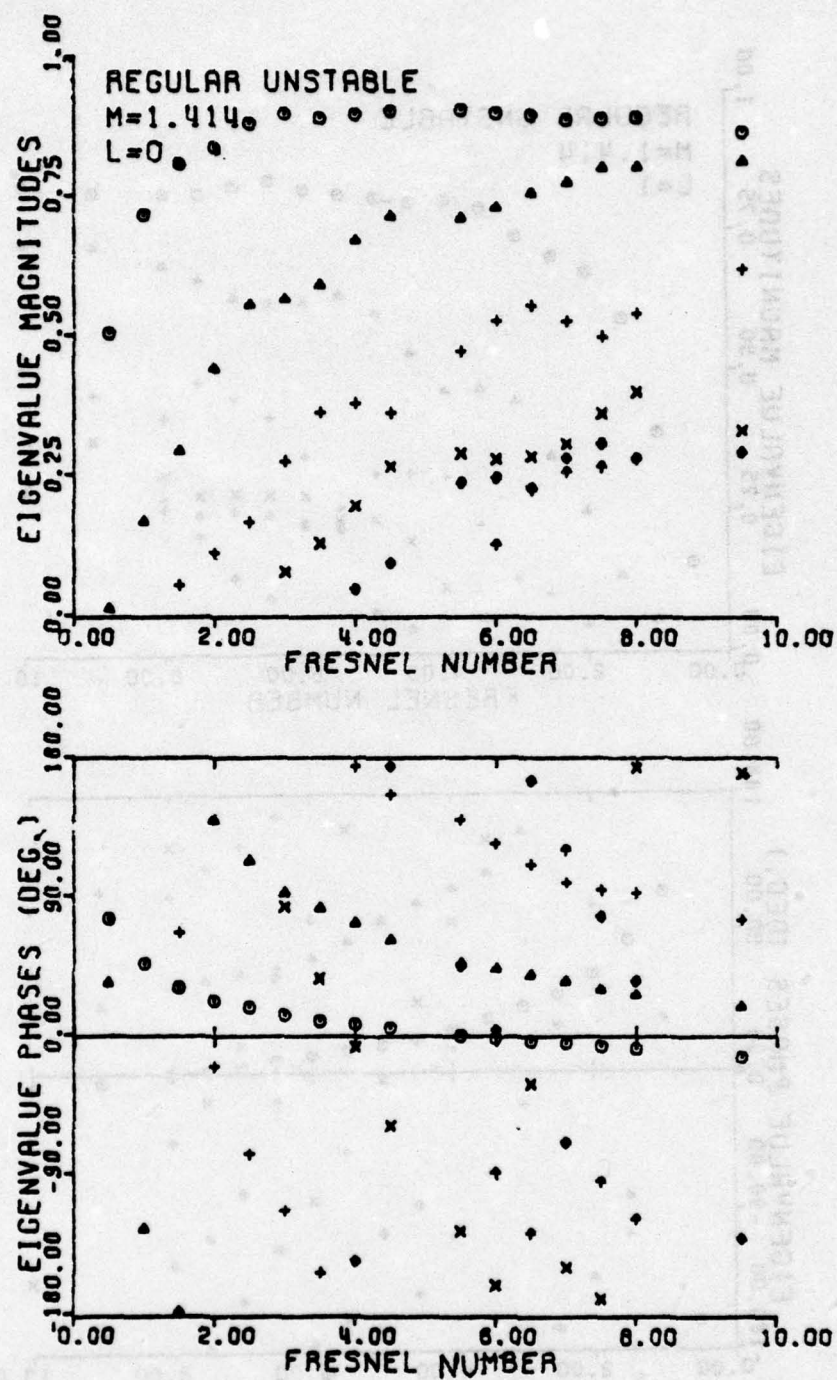
Figure 25a Eigenvalues of resonator of Figure 24 for D = H2 =0,
M = √2, ℓ = 0

REGULAR UNSTABLE
M=1.414
L=1

Figure 25b ℓ = 1

REGULAR UNSTABLE
M=1.414
L=2

Figure 25c ℓ = 2

REGULAR UNSTABLE
M=1.414
L=3

Figure 25d   ℓ = 3

108
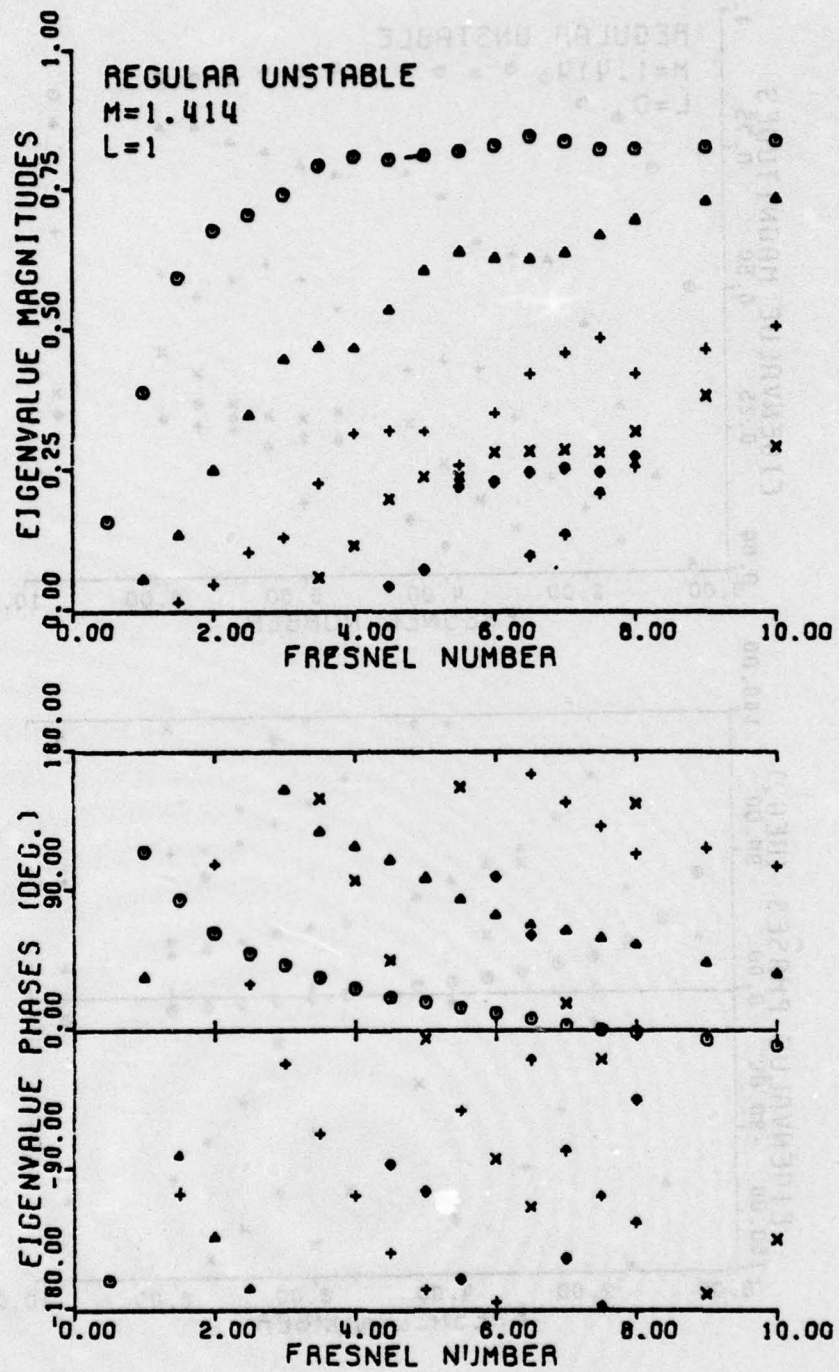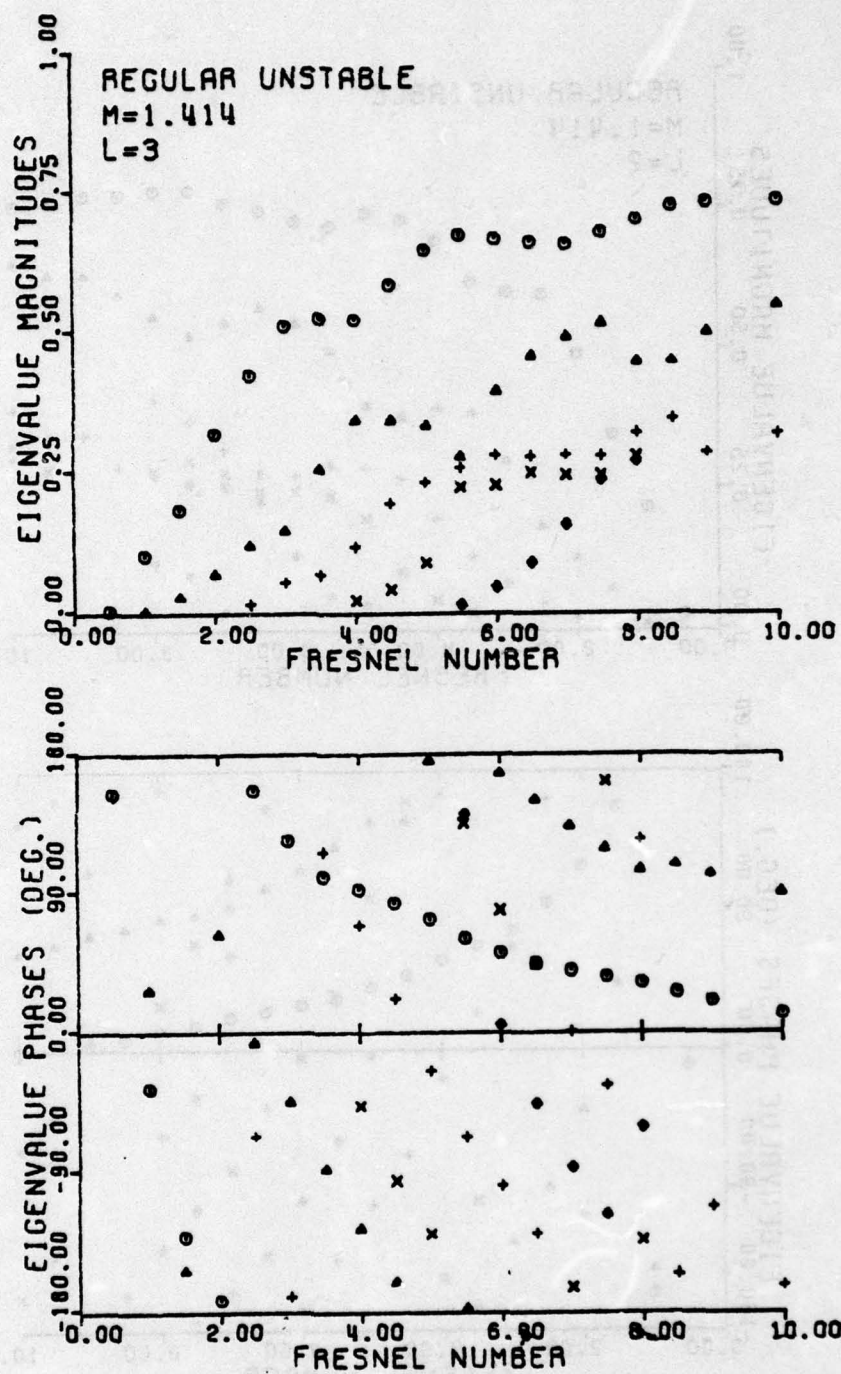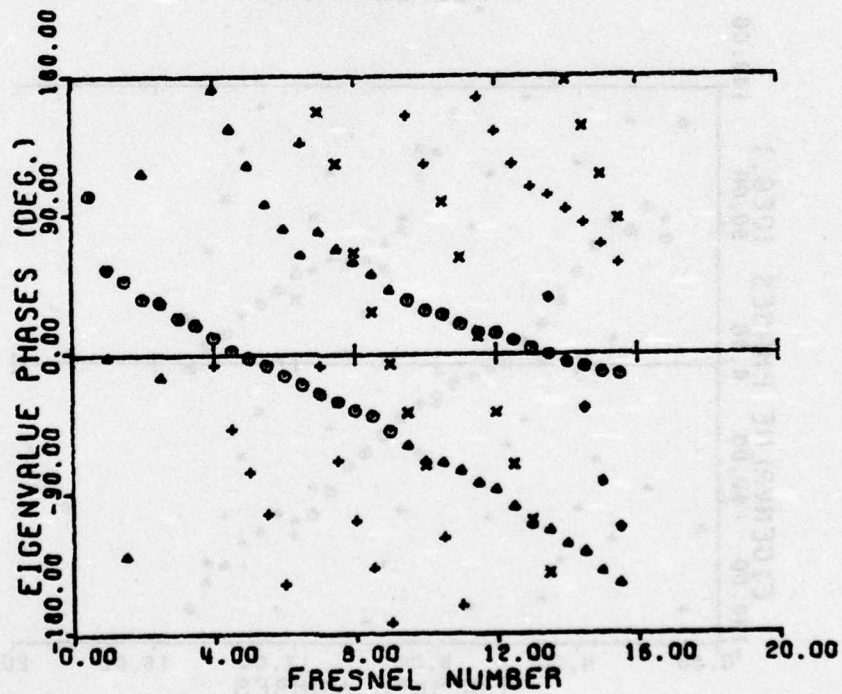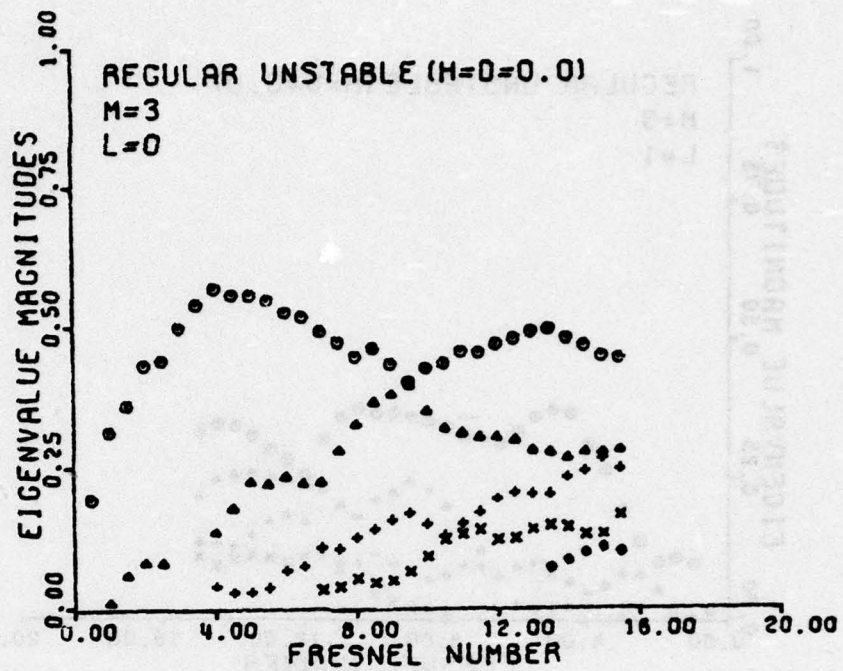
Figure 26a Eigenvalues of the resonator of Figure 25 for D=H2=0,
M = 3, ℓ = 0

109

REGULAR UNSTABLE (M=0=0.0)
M=3
L=1

Figure 26b ℓ = 1

110

Figure 26c ℓ = 2

111

Figure 26d $\ell = 3$

112
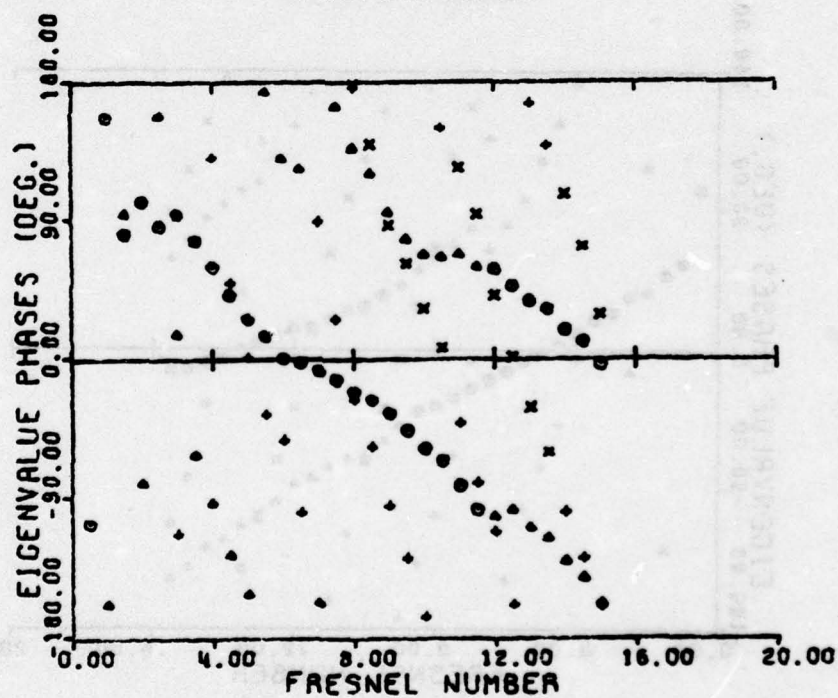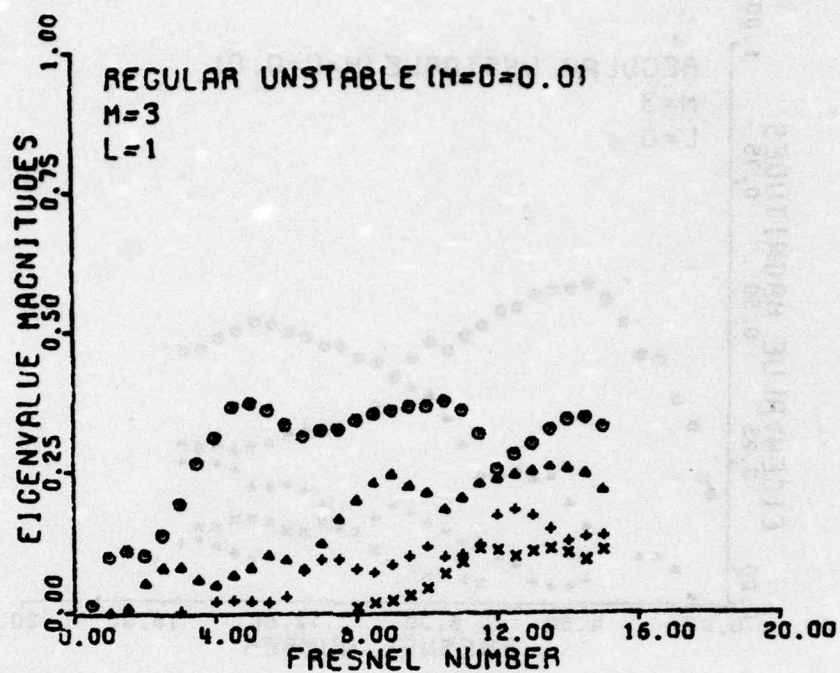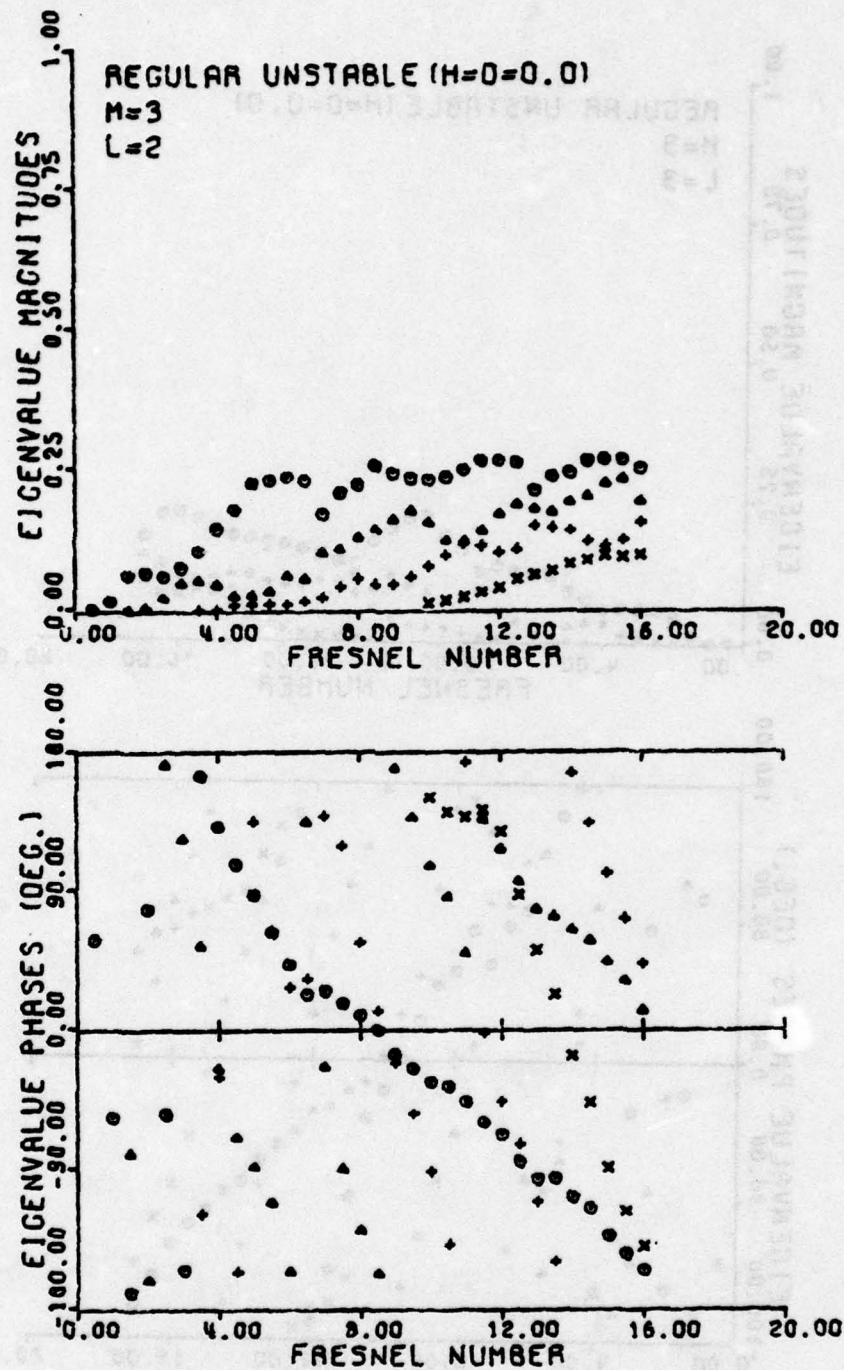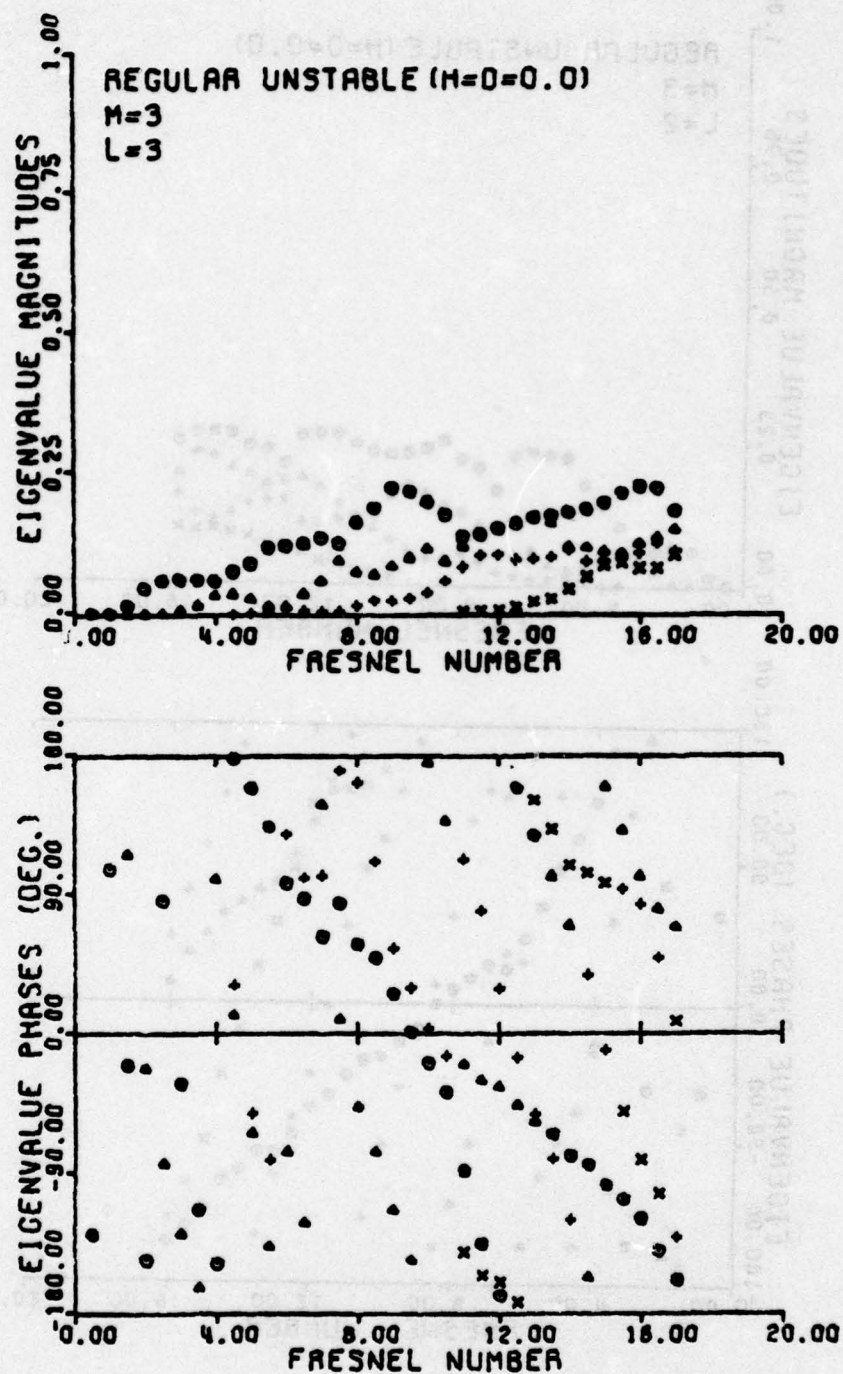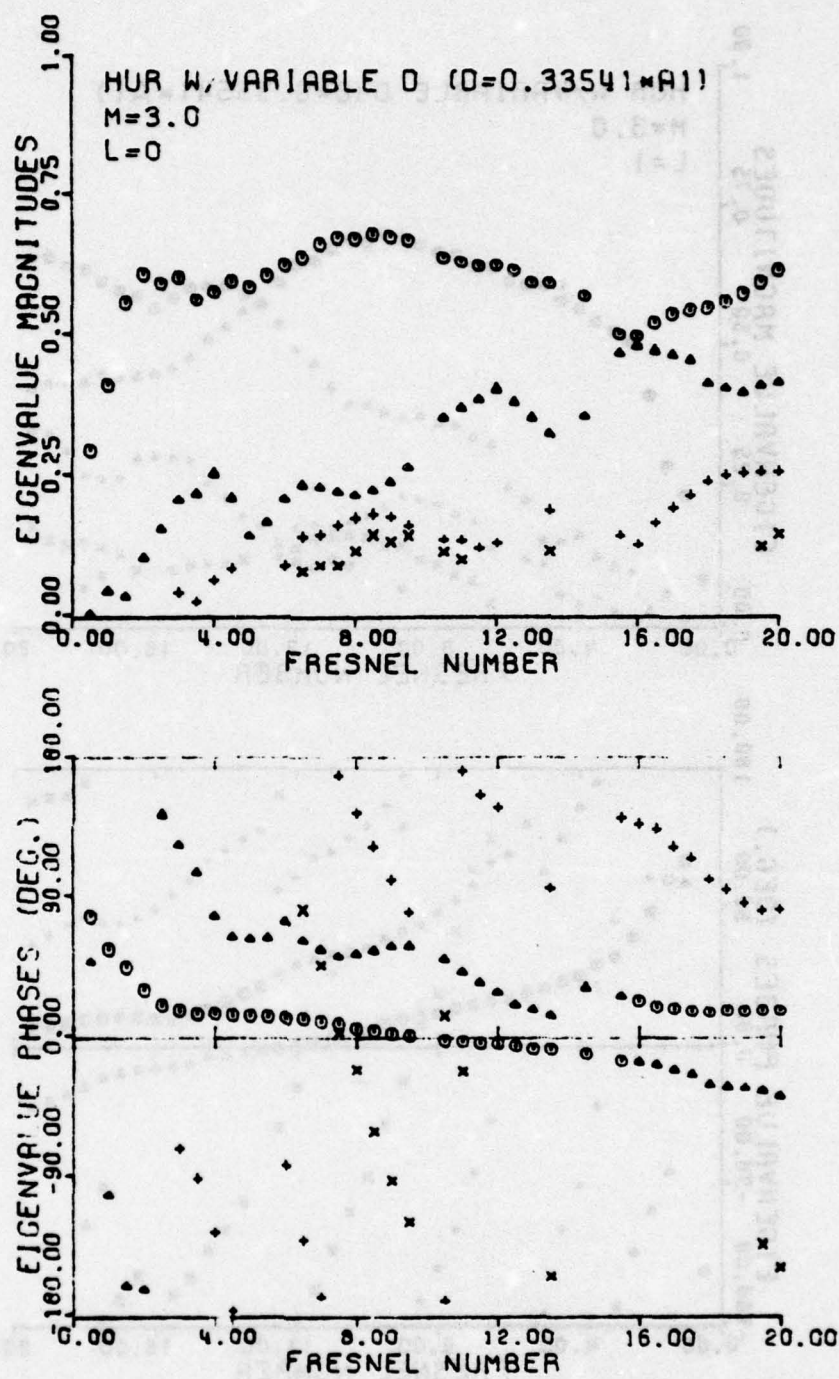
Figure 27a   Eigenvalues of the resonator of Figure 24 for
D = 0.355·A1, M = 3, ℓ = 0

113

HUR W/VARIABLE D(D=0.33541×A1)
M=3.0
L=1

Figure 27b ℓ = 1

114

Figure 27c $\ell = 2$

115

Figure 27d $\ell = 3$

116
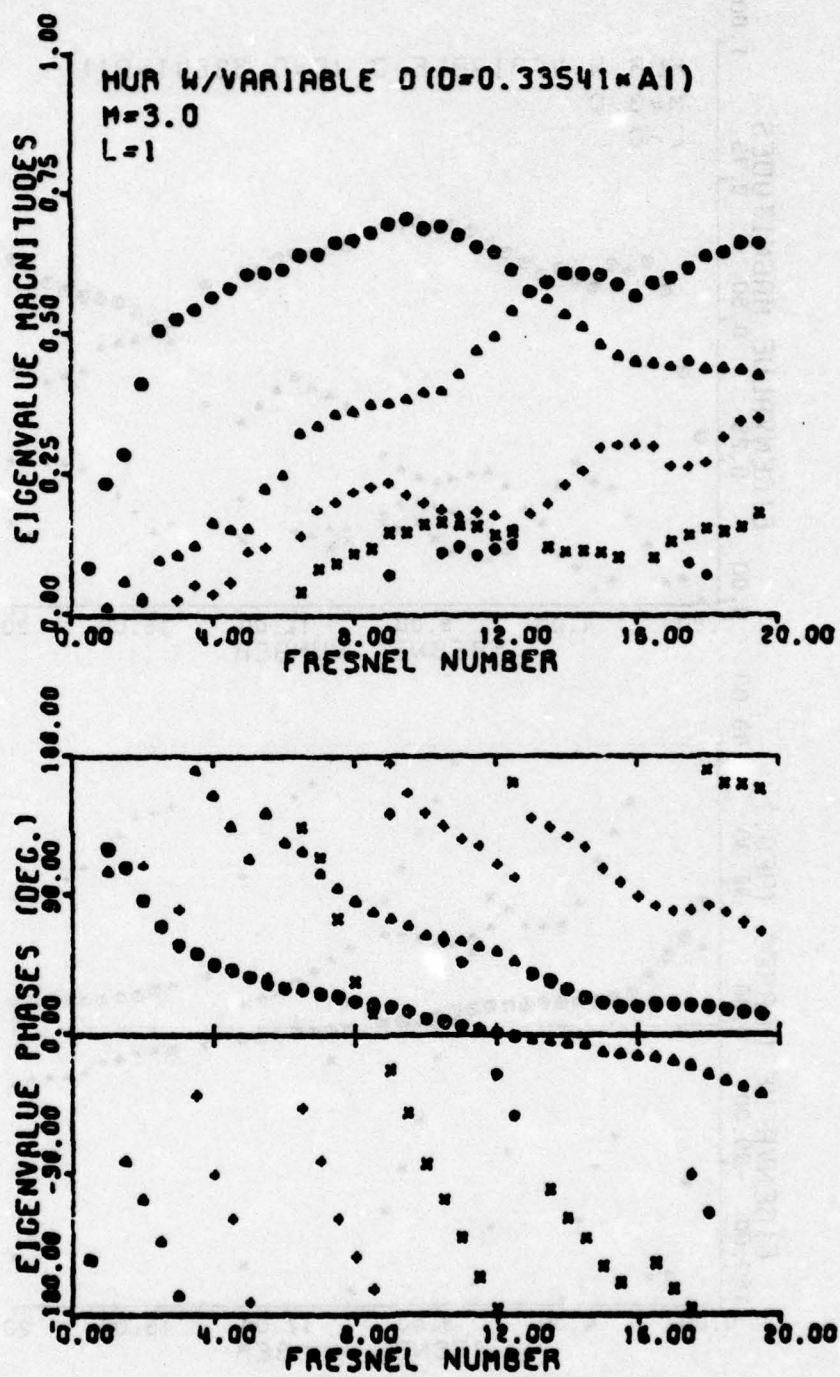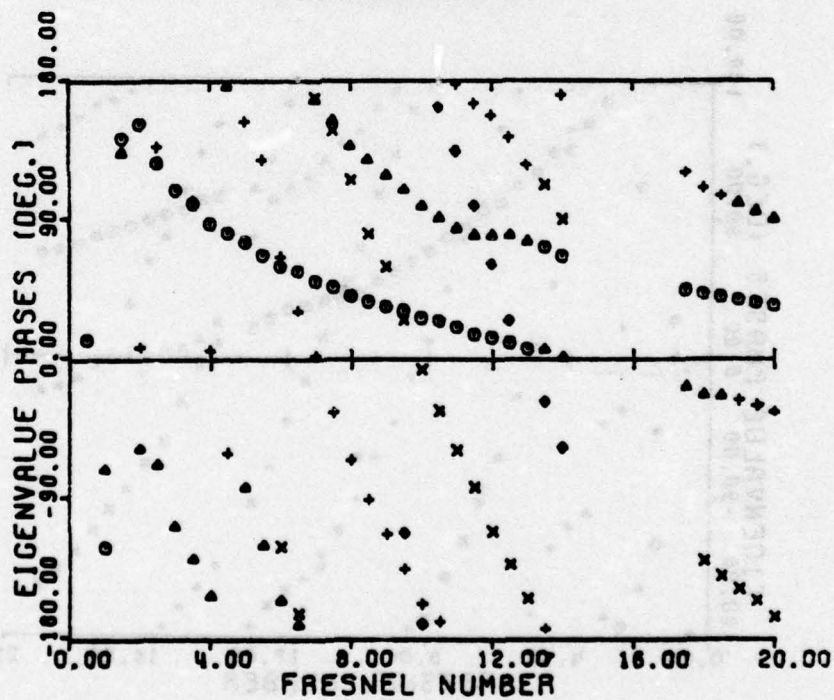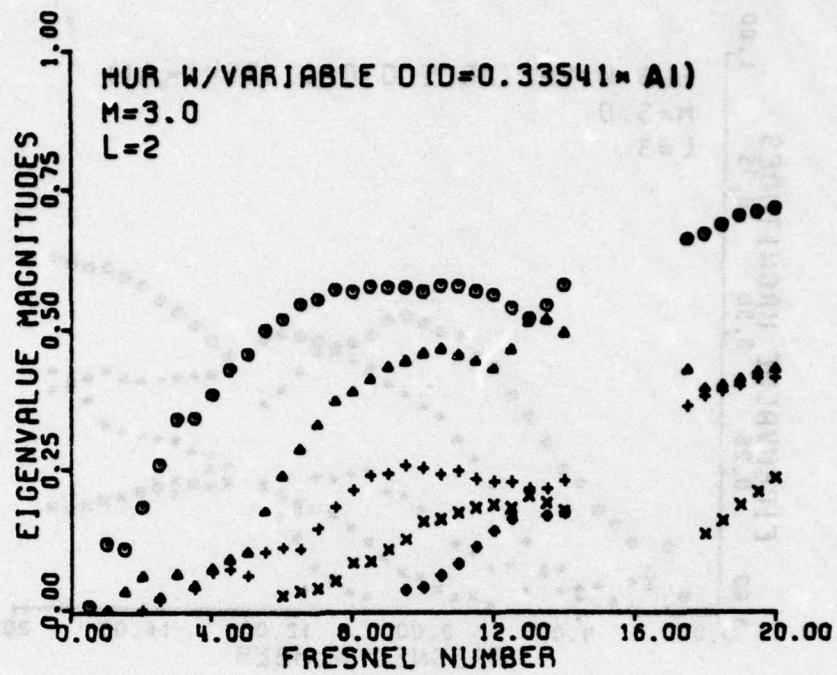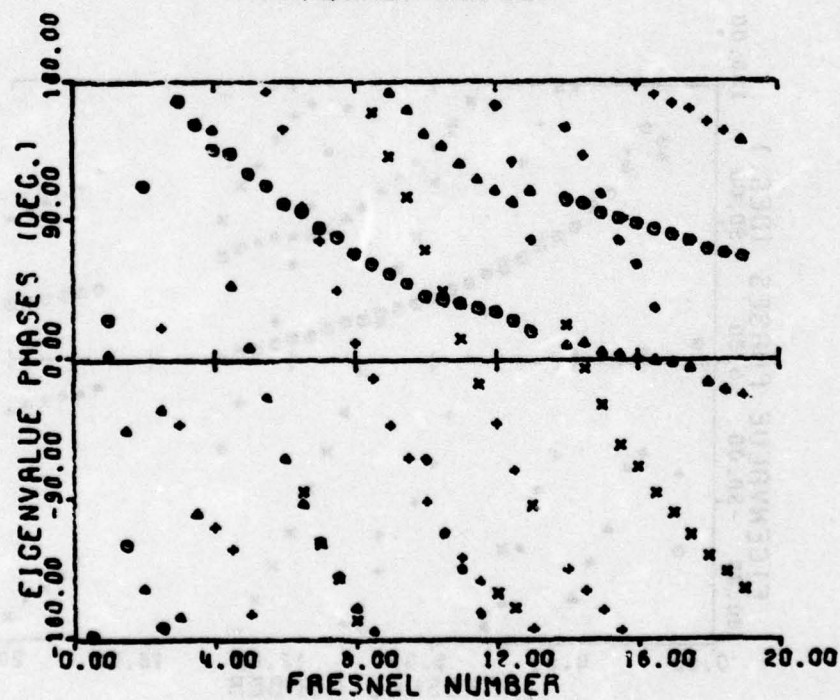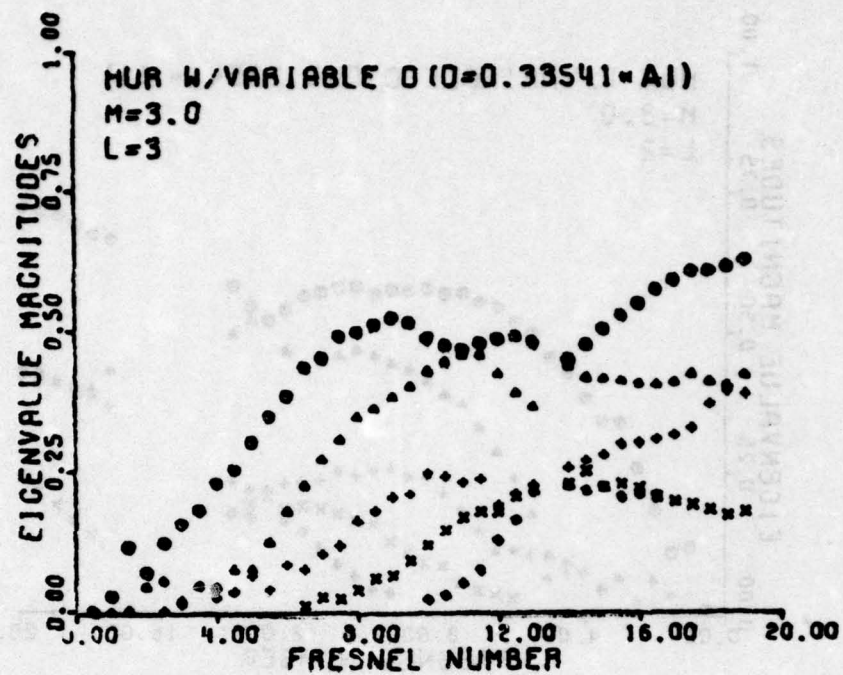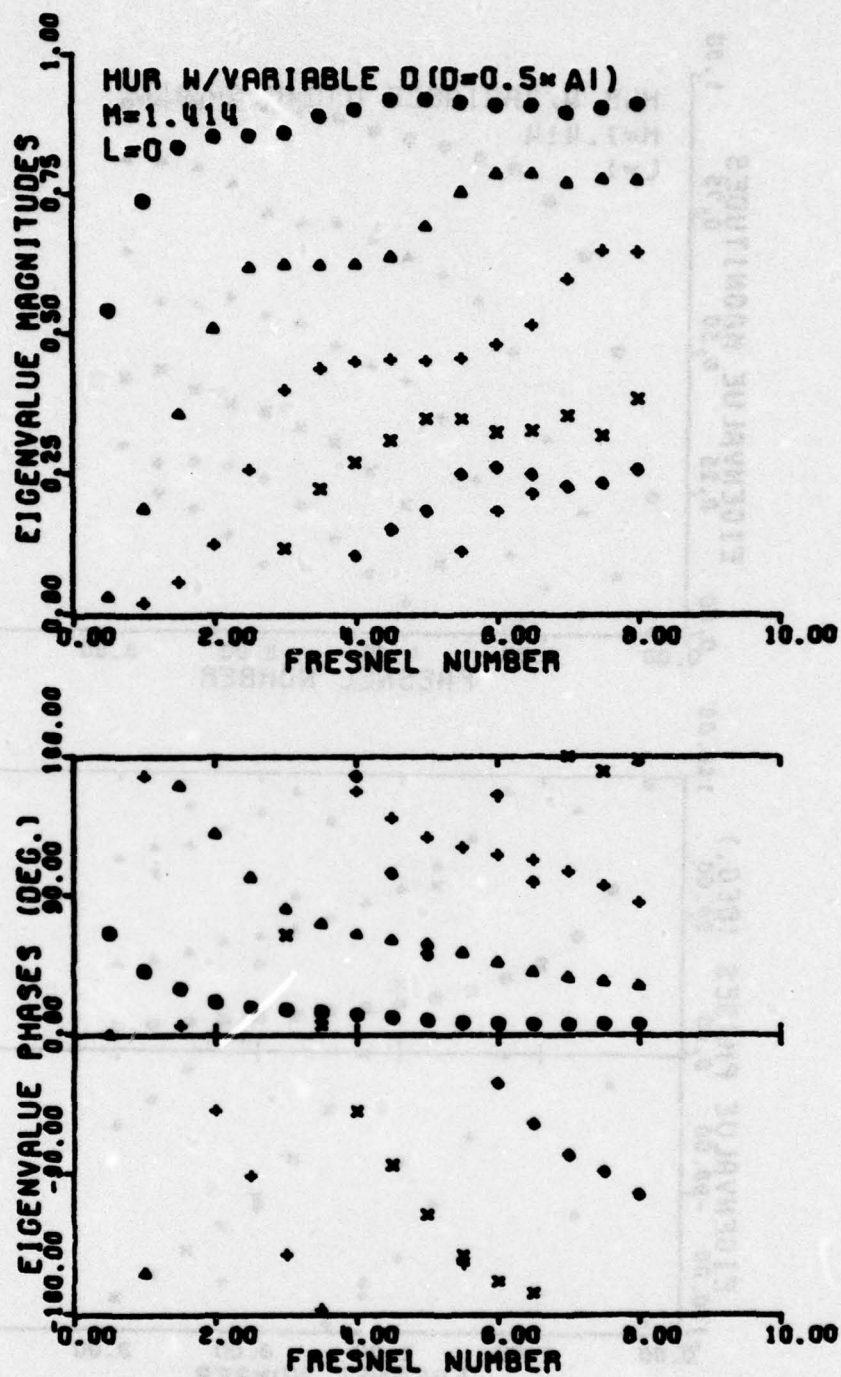
Figure 28a   Eigenvalues of the resonator of Figure 24 for D = A1/2,
M = √2, ℓ = 0

117

Figure 28b $\ell = 1$

118

Figure 28c $\ell = 2$

119

MUR W/VARIABLE D(O=0.5=AI)
M=1.414
L=3
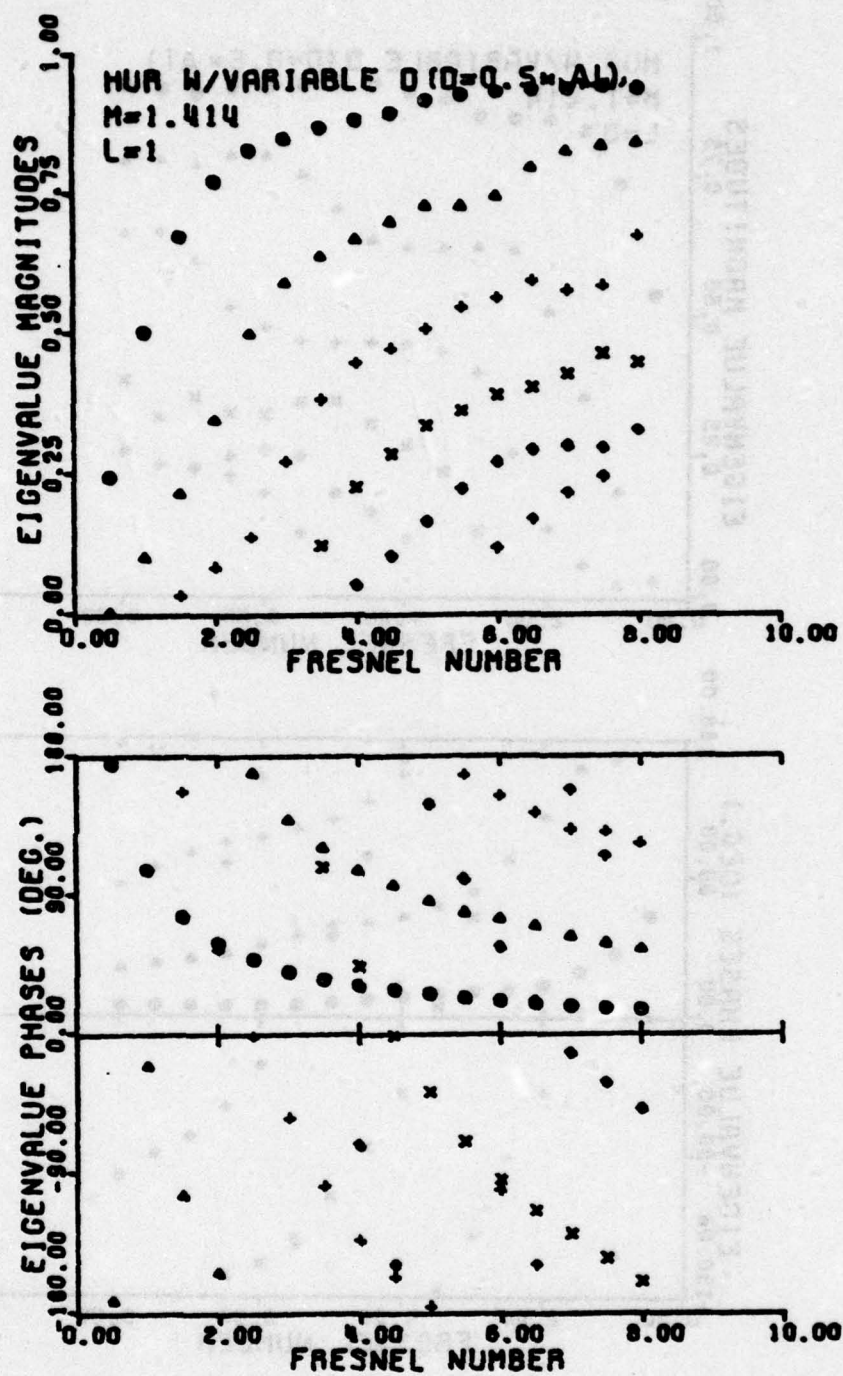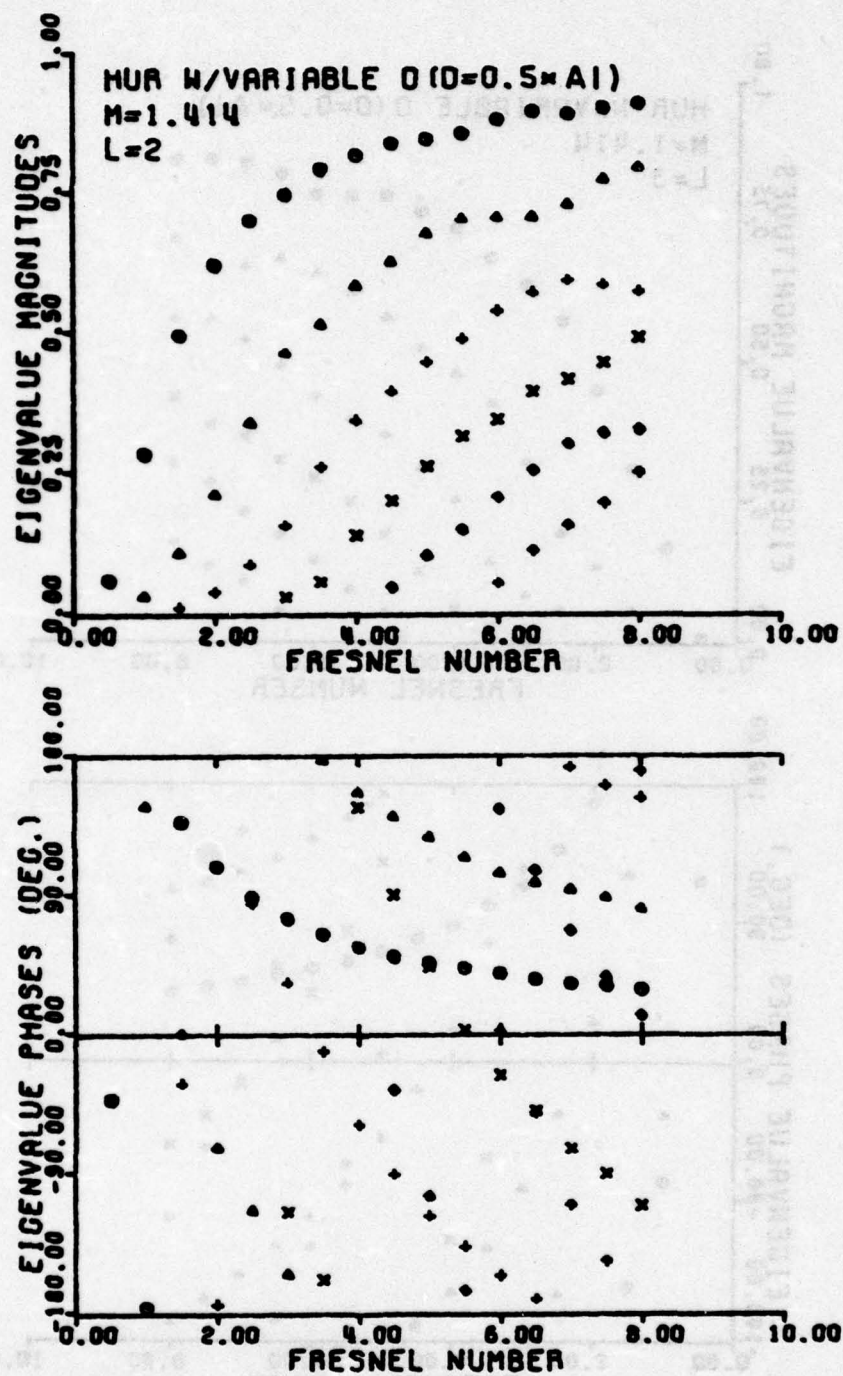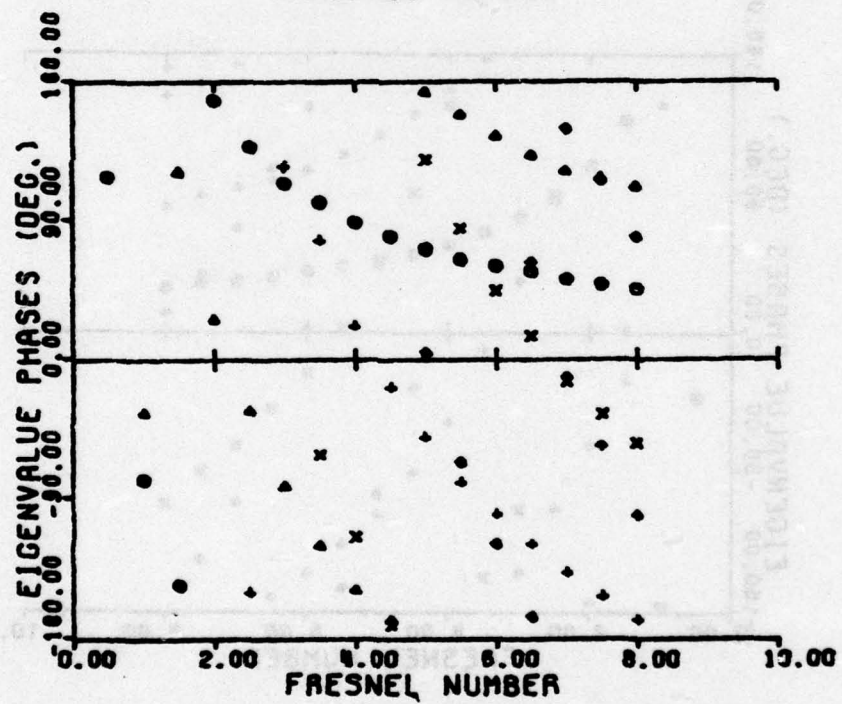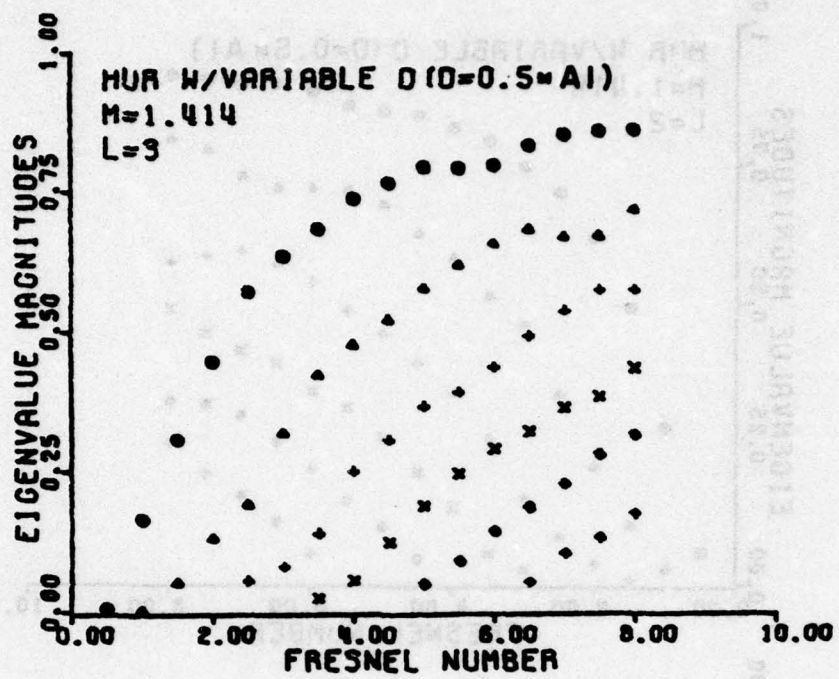
Figure 28d ℓ = 3
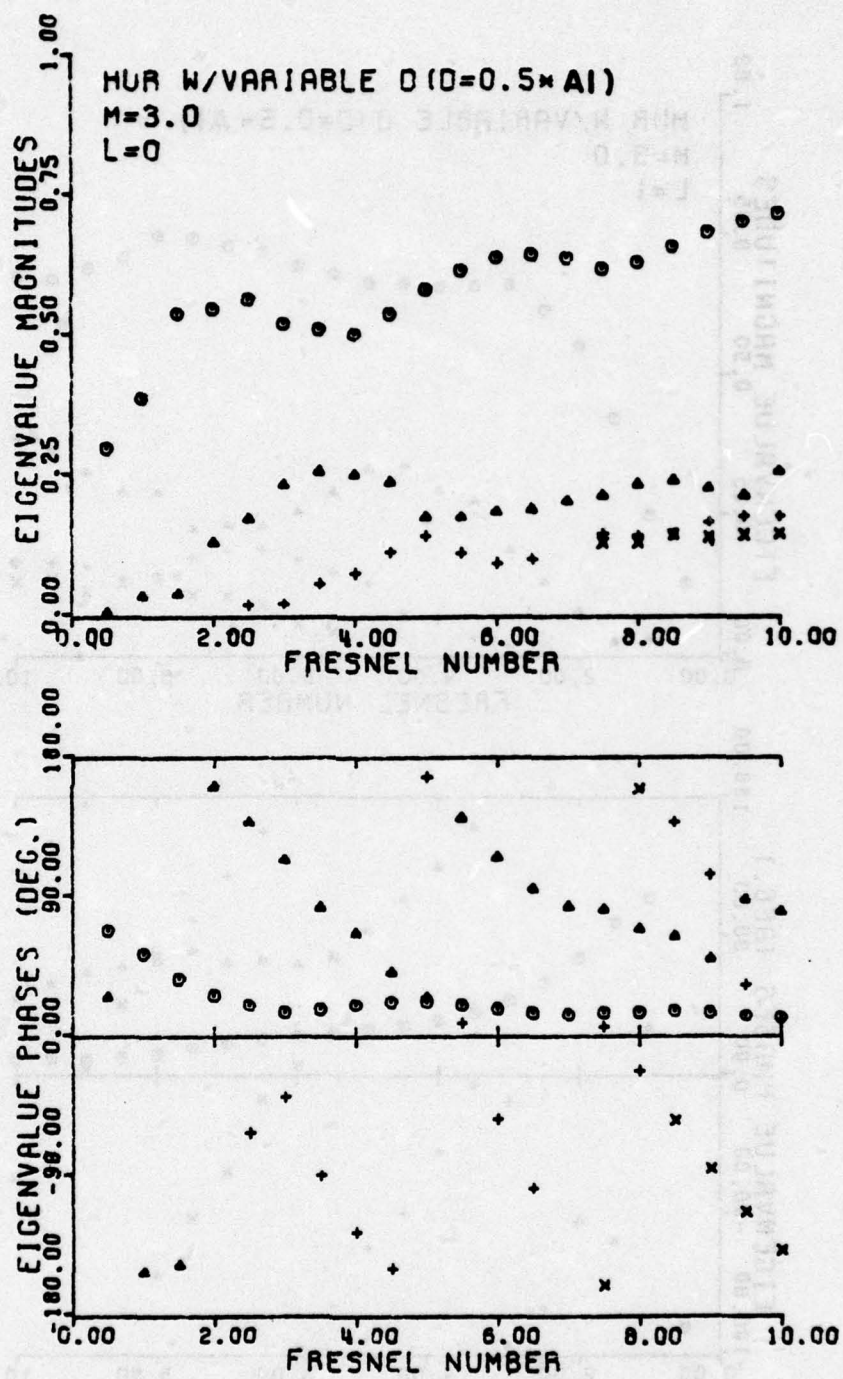
Figure 29a Eigenvalues of the resonator of Figure 24 for D= Al/2,
M = 3, ℓ = 0

121

HUR W/VARIABLE D(D=0.5*AI)
M=3.0
L=1
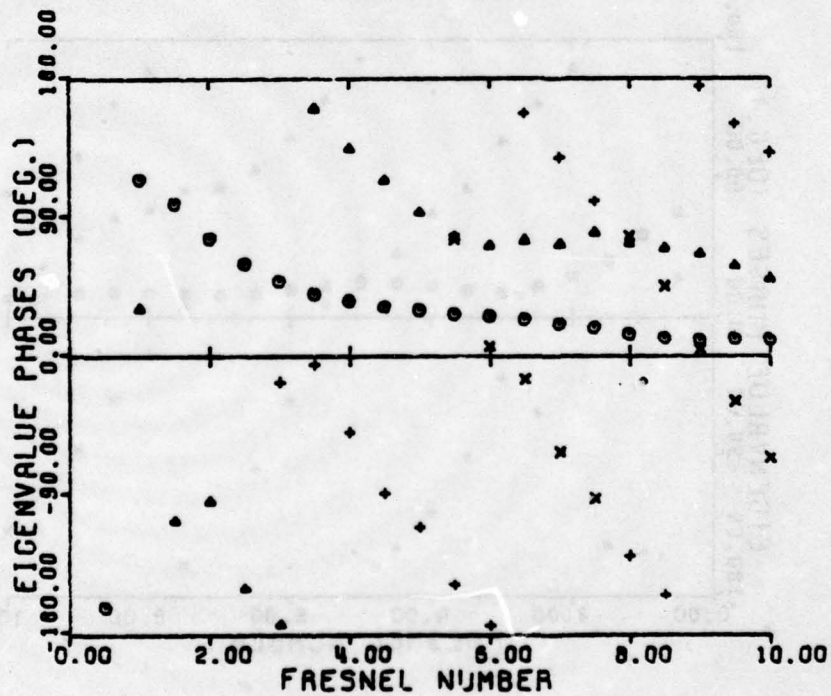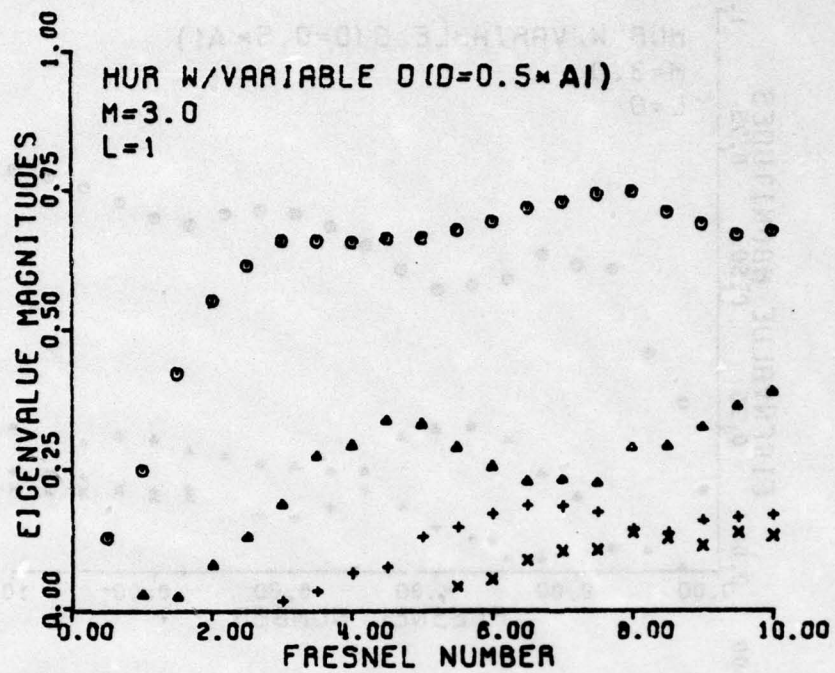
Figure 29b ℓ = 1

Figure 29c $\ell = 2$

123
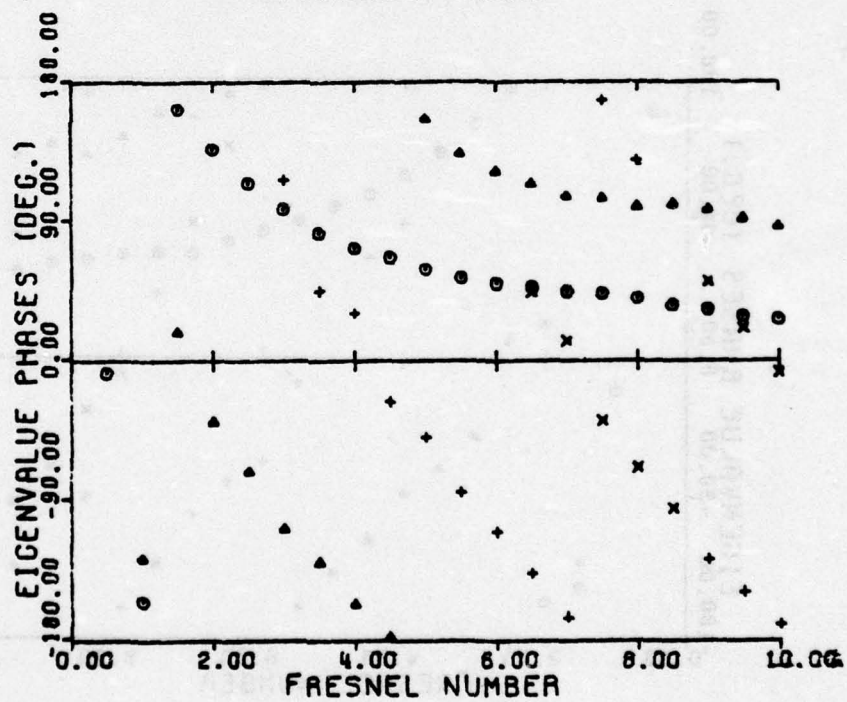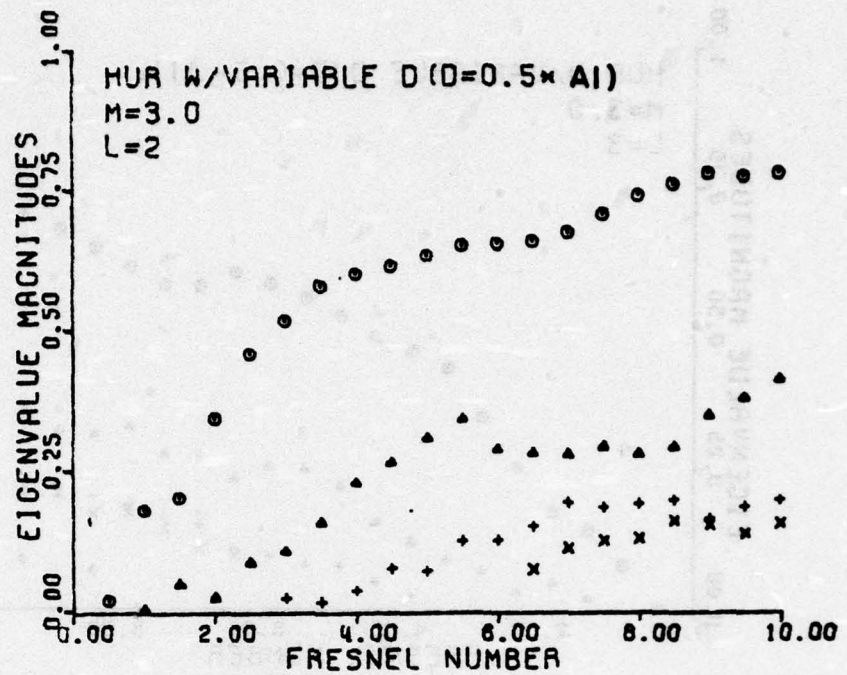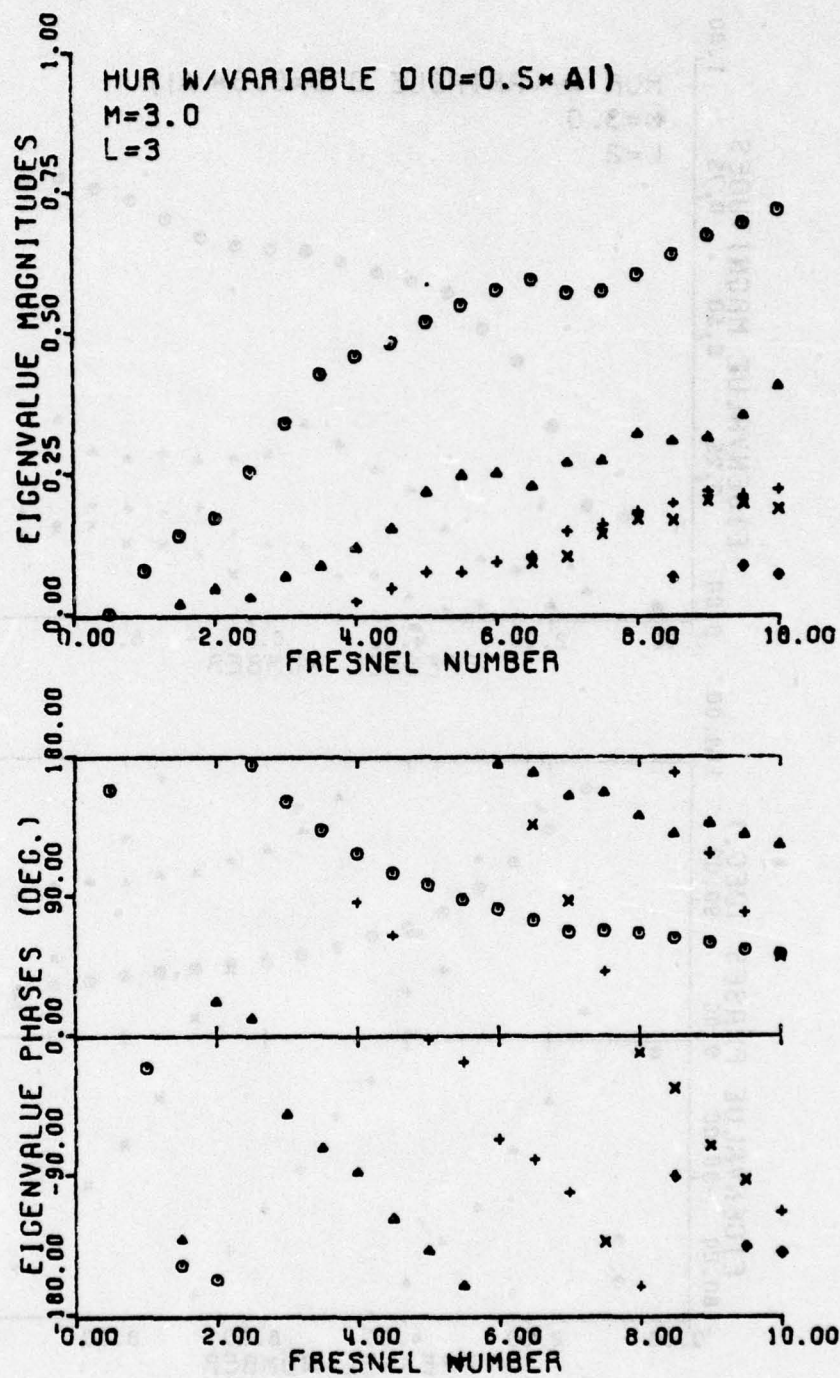
Figure 29d $\ell = 3$

SECTION V

TASK 4 RESULTS

The purpose of Task 4 was to study the behavior of the eigenmodes
of the resonator shown in Figure 30. This resonator is similar to the
one in Figure 24 which was analyzed in Task 3 except the centerline
has in effect been "blown up" into a circular cylinder of radius H1.
This resonator could be used when there is an on-axis obscuration
within the region $r \leq A1$ caused, for example, by the nozzle(s) of a
chemical laser. For parameterization purposes the Fresnel numbers
$NH1 = H1^2/(B\lambda)$ and $ND = D^2/(B\lambda)$ were defined. The behavior of the
eigenmodes was analyzed for various values of NH1 and ND as a function of
the outer resonator Fresnel number $N = A1^2/(B\lambda)$.

Figure 31 shows the resonator eigenvalues for ND = 1, NH = 1, and
M = 2. This choice of parameters results in a conventional unstable
confocal resonator whose centerline has been blown up from a radius
of zero to a radius of H1 which corresponds to a Fresnel number of 1.
As seen the dominant radial modes for $\ell=0$ and $\ell=1$ have essentially
identical eigenvalues over the range of Fresnel numbers considered
$2 < N < 10$. The losses of the $\ell=2$ and $\ell=3$ modes increase relative
to those of the $\ell=0$ mode for increasing N.

Figure 32 shows the resonator eigenvalues for ND and NH1 increased
to a value of 2 for M = 2. This increase in H1 results in less azimuthal
mode discrimination. It is apparent, that increasing the size of the
centerline (or H1) tends to make the azimuthal mode eigenvalues become
degenerate.

125

$$M = \frac{A_1 - H_1}{A_2 - H_2} = \frac{H_1 - D}{H_2 - D}$$
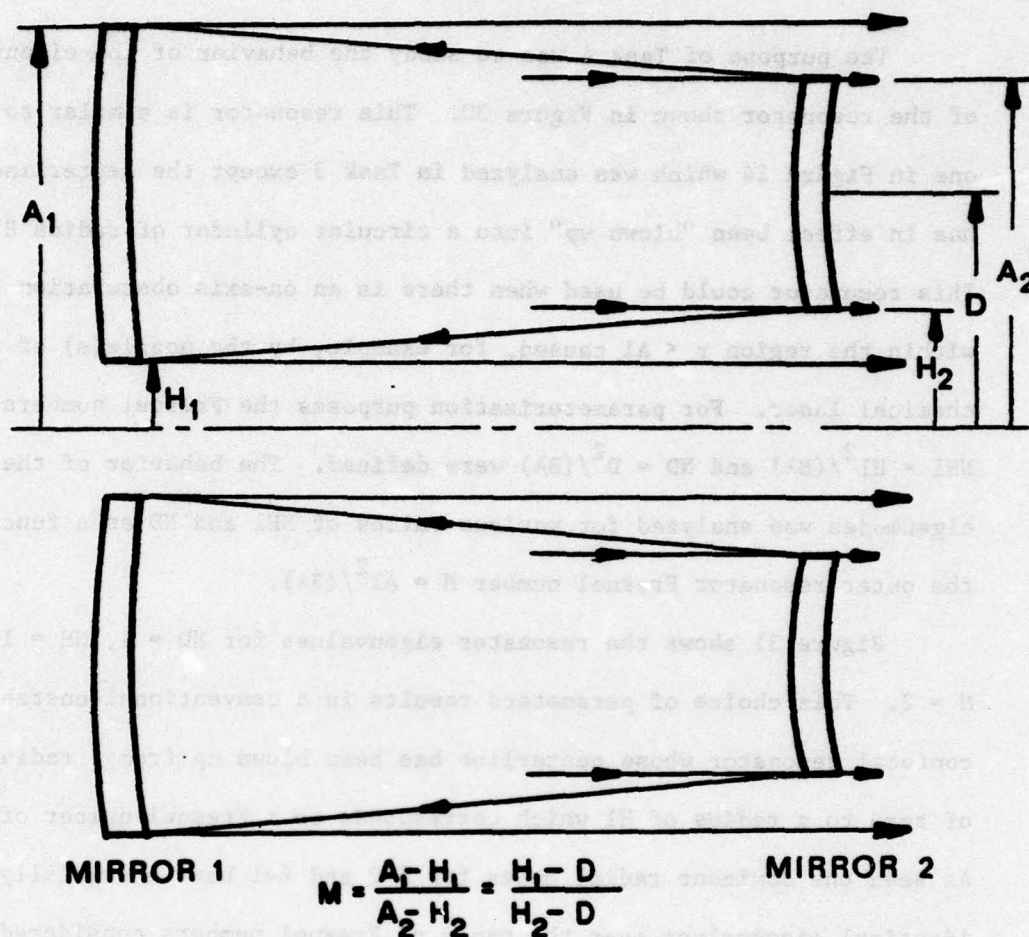
Figure 30   Resonator with a hole in both mirrors. The geometric output is through the annulus of area $\pi(H_2^2 - H_1^2)$ and through the annulus of area $\pi(A_1^2 - A_2^2)$
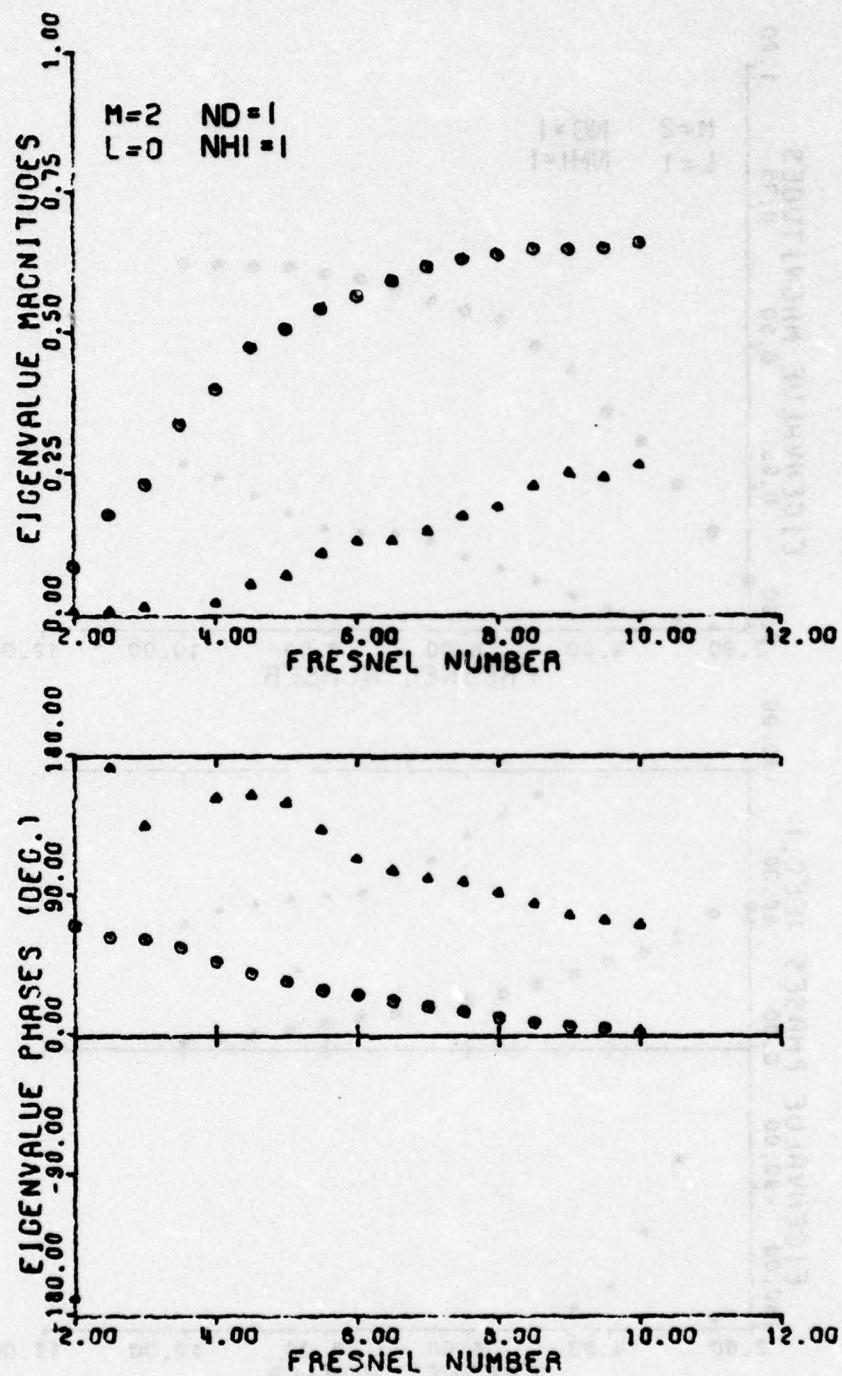
Figure 31a Eigenvalues of the resonator of Figure 30 for
ND = (D²/Bλ) = 1, NH1 = (H1²/Bλ) = 1, M = 2,
ℓ = 0

127
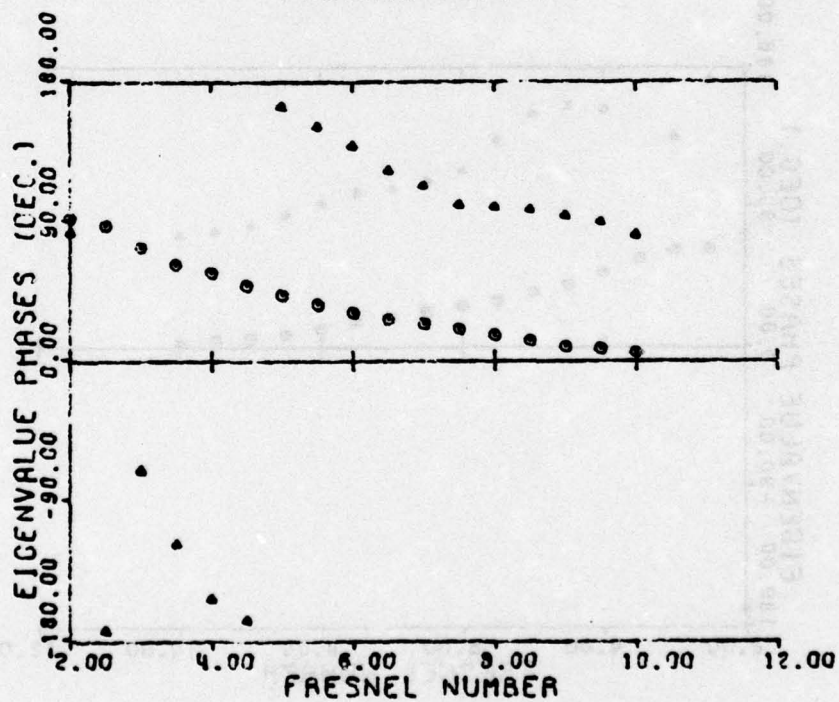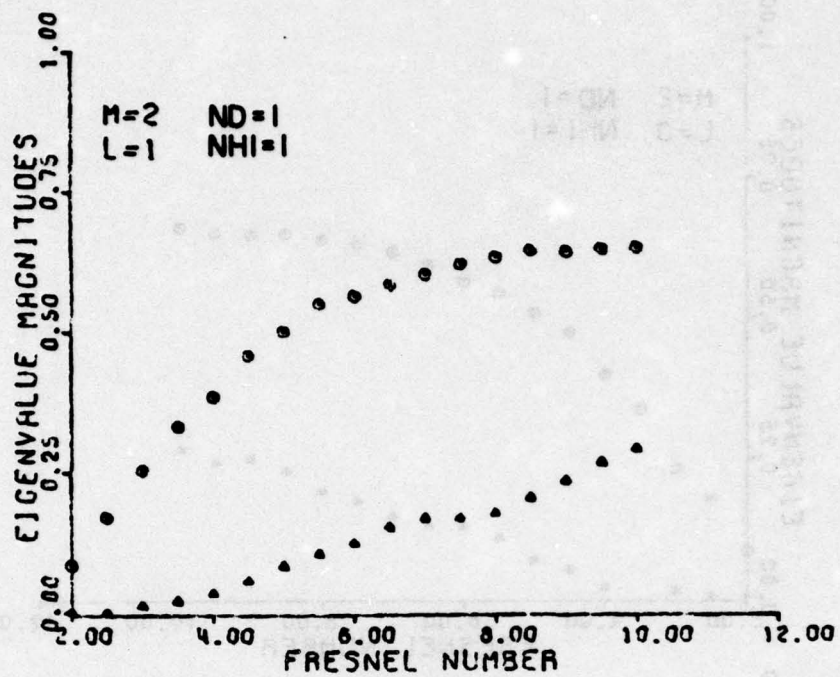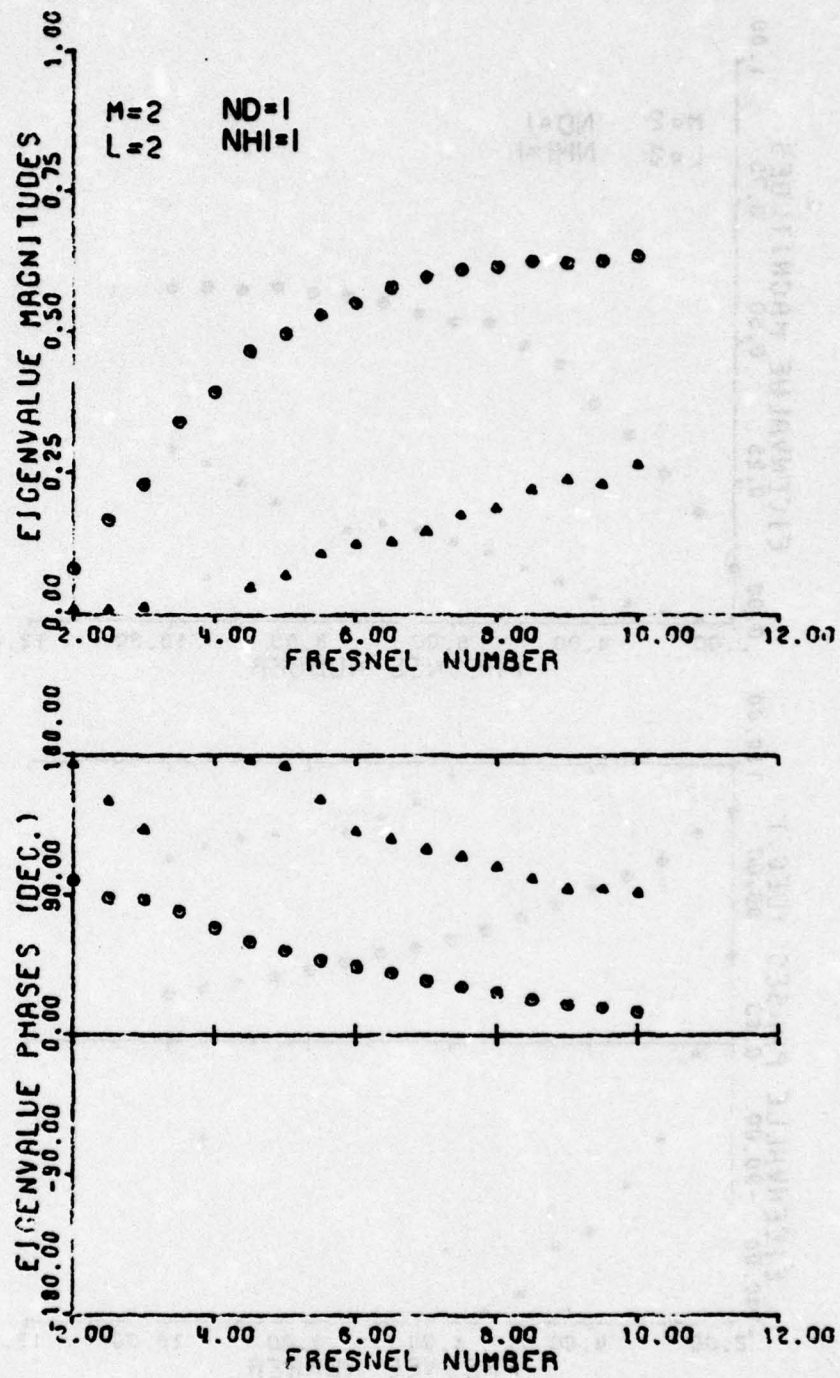
Figure 31b $\ell = 1$
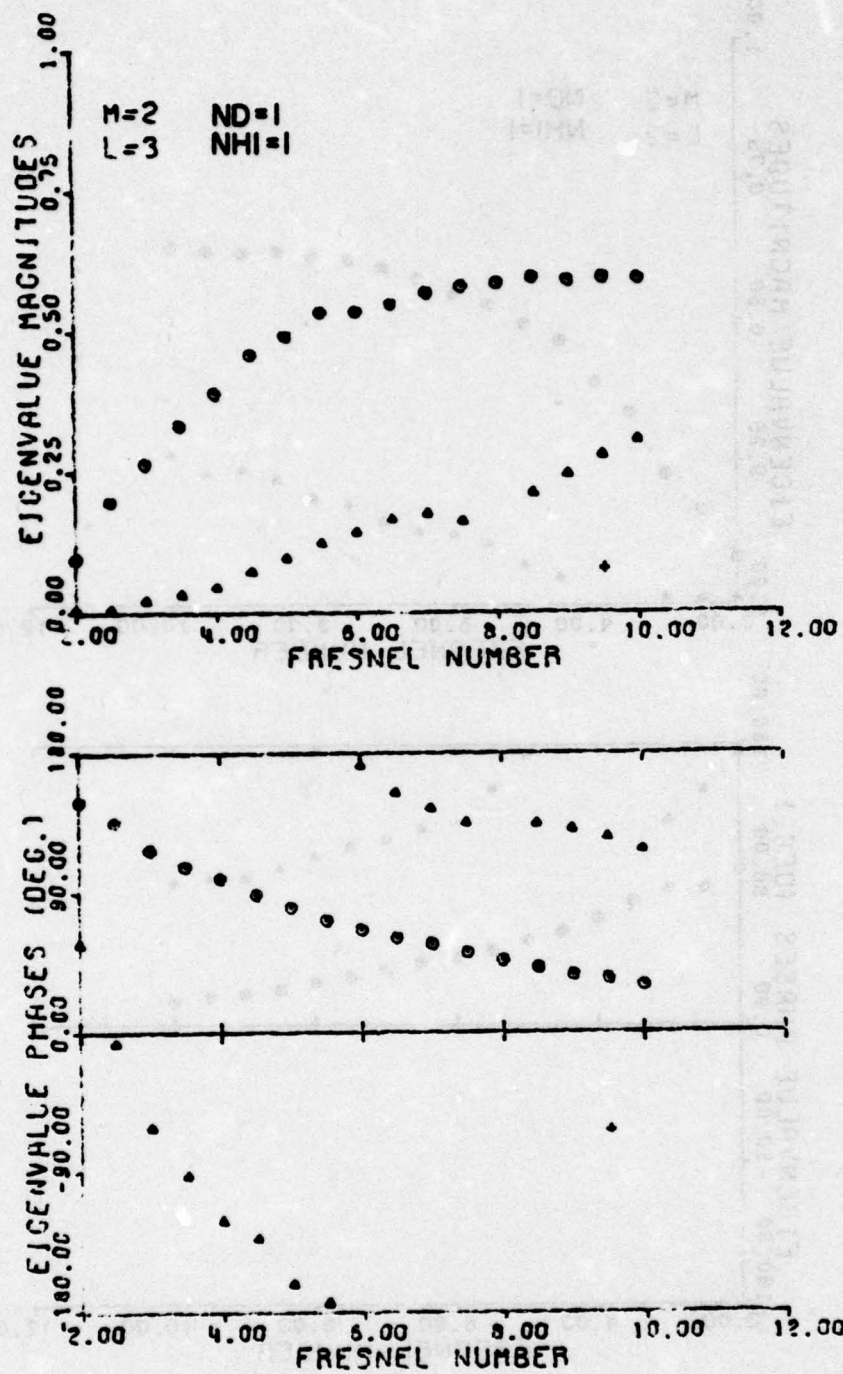
Figure 31c $\ell = 2$

Figure 31d $\ell = 3$
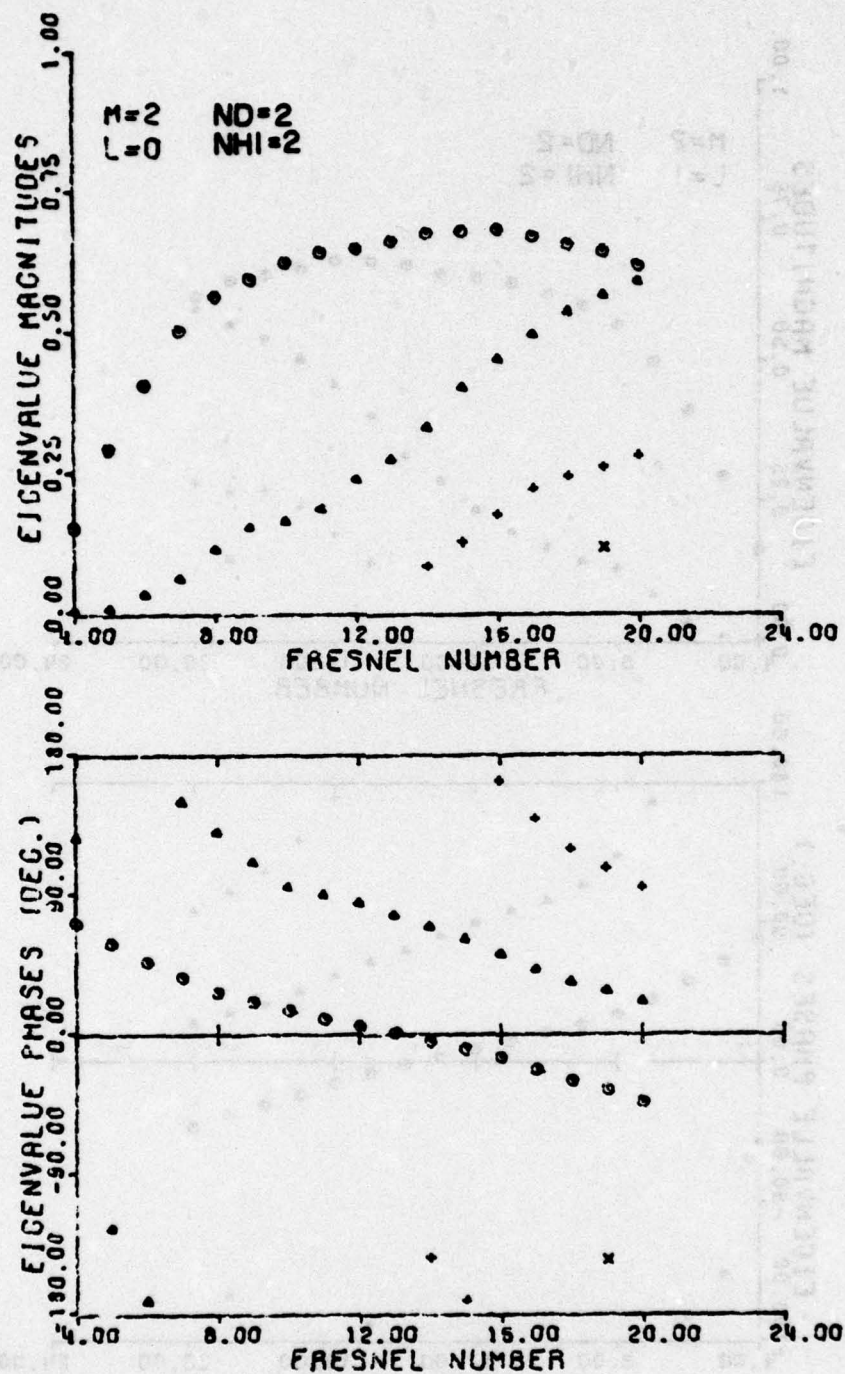
Figure 32a Eigenvalues of the resonator of Figure 30 for
ND = $(D^2/B\lambda)$ = 2, NH1 = $(H1^2/B\lambda)$ = 2, M = 2,
ℓ = 0

M=2   ND=2
L=1   NHI=2

EIGENVALUE MAGNITUDES

FRESNEL NUMBER

EIGENVALUE PHASES (DEG.)

FRESNEL NUMBER

Figure 32b $\ell = 1$

132

Figure 32c $\ell = 2$

133

Figure 32d $\ell = 3$

134
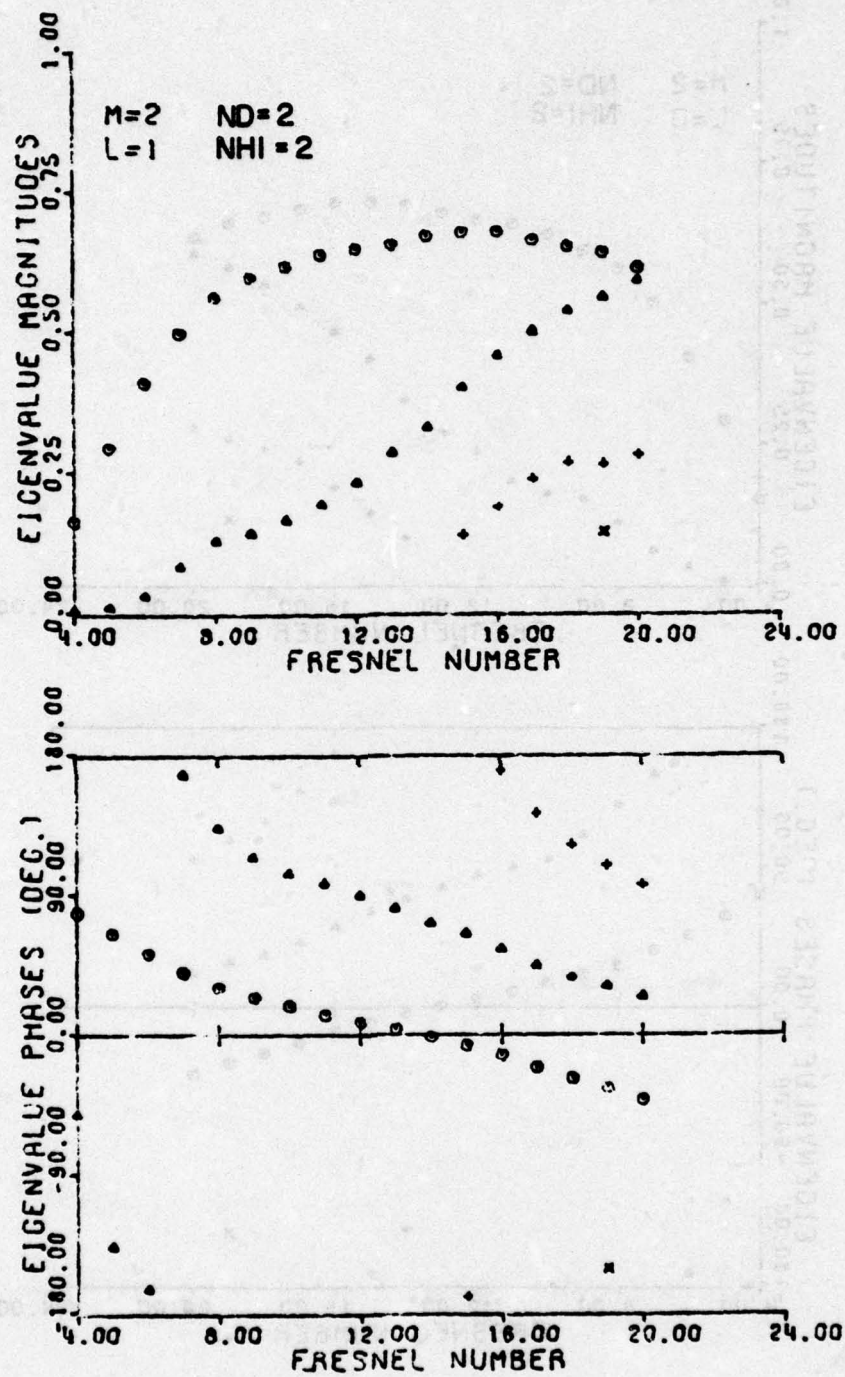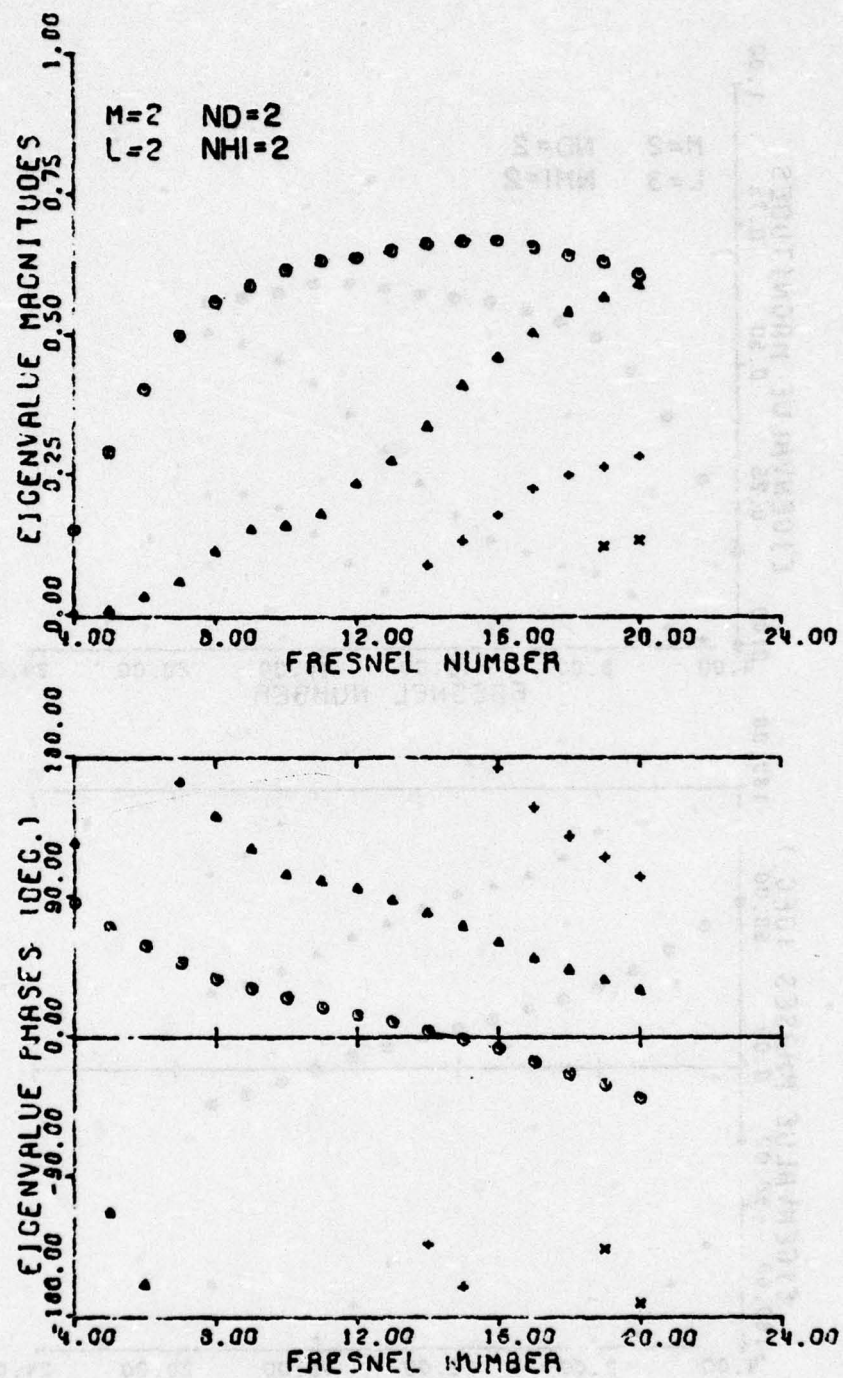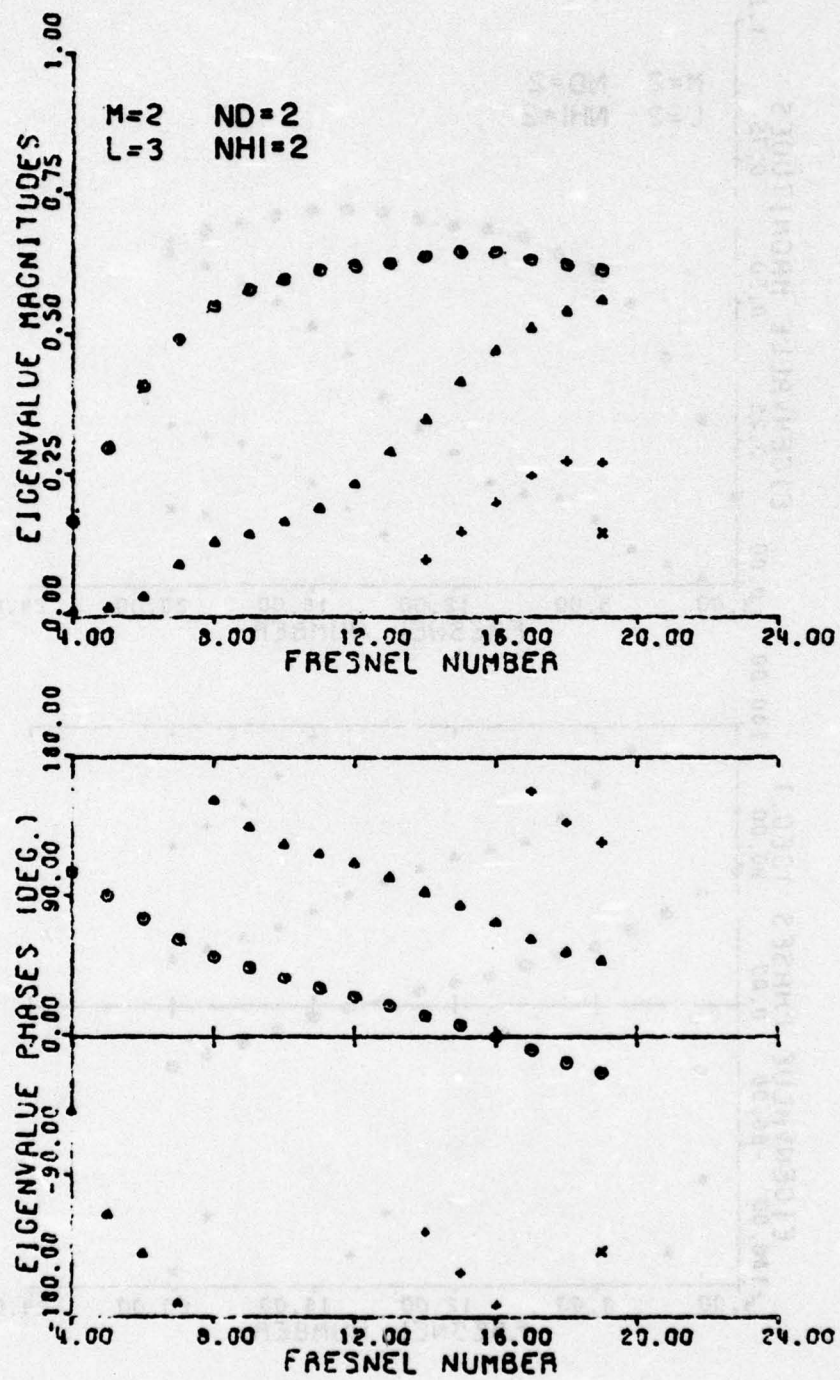
In an attempt to increase the azimuthal mode discrimination for NH1 = 2 and M = 2, the value of ND was decreased to 1. Geometrically, this decrease in D should increase the rate at which the fields are coupled over the outer edge of mirror 2. Since the higher order azimuthal mode fields tend to peak further out radially then the lower order azimuthal modes, the output coupling for the higher order modes should increase more rapidly than for the $\ell=0$ mode. The calculated eigenvalue magnitudes in Figure 33 for this case are smaller than those in Figure 32, indicating there is indeed more output coupling. However, there is no significant increase in the azimuthal mode discrimination.

The eigenvalues were also calculated for larger ratios of H1 and D to A1. For these cases the plots for the four lowest order azimuthal modes were very similar with the greatest differences being between the $\ell=0$ and $\ell=3$ plots. Since the $\ell=1$ and $\ell=2$ plots lie between the $\ell=0$ and $\ell=3$ plots, they are not shown.

Figure 34 shows the eigenvalues for H1 = A1/2 and D = A1/2 at a magnification M =3. Since D = H1 this resonator is like that of a conventional unstable resonator except the centerline has been expanded to a radius of H1.

Figure 35 shows the eigenvalues for H1 = A1/4, D= A1/2, and M = 2. Figure 36 shows the eigenvalues for the same conditions except D = 3A1/4 which increases the area of the smaller annulus relative to the outer annulus. There is very little difference in the eigenvalues for the two cases.

135
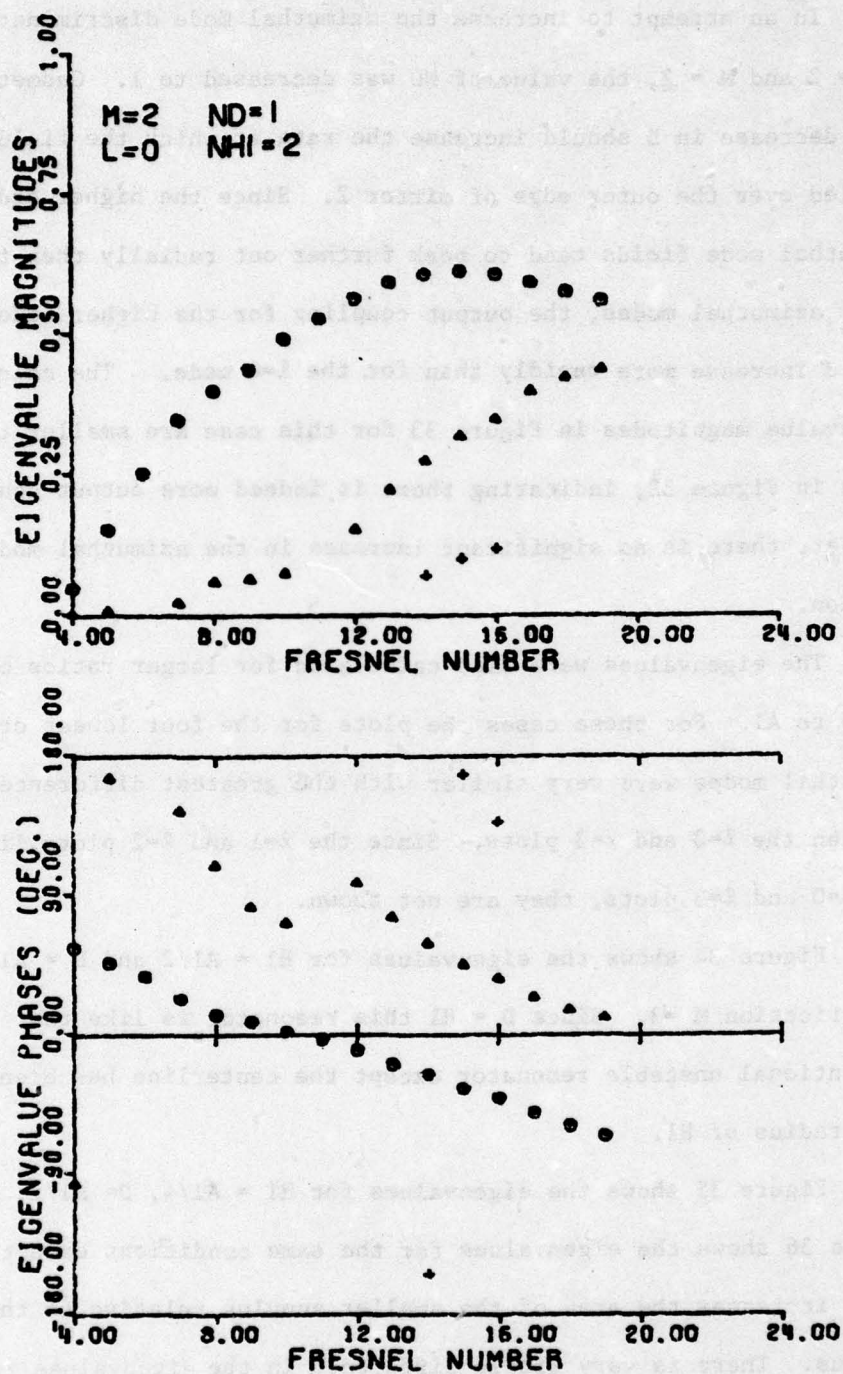
Figure 33a Eigenvalues of the resonator of Figure 30 for
ND = $(D^2/B\lambda)$ = 2, NH1 = $(H1^2/B\lambda)$ = 1, M = 2,
ℓ = 0

136

Figure 33b $\ell = 1$

137
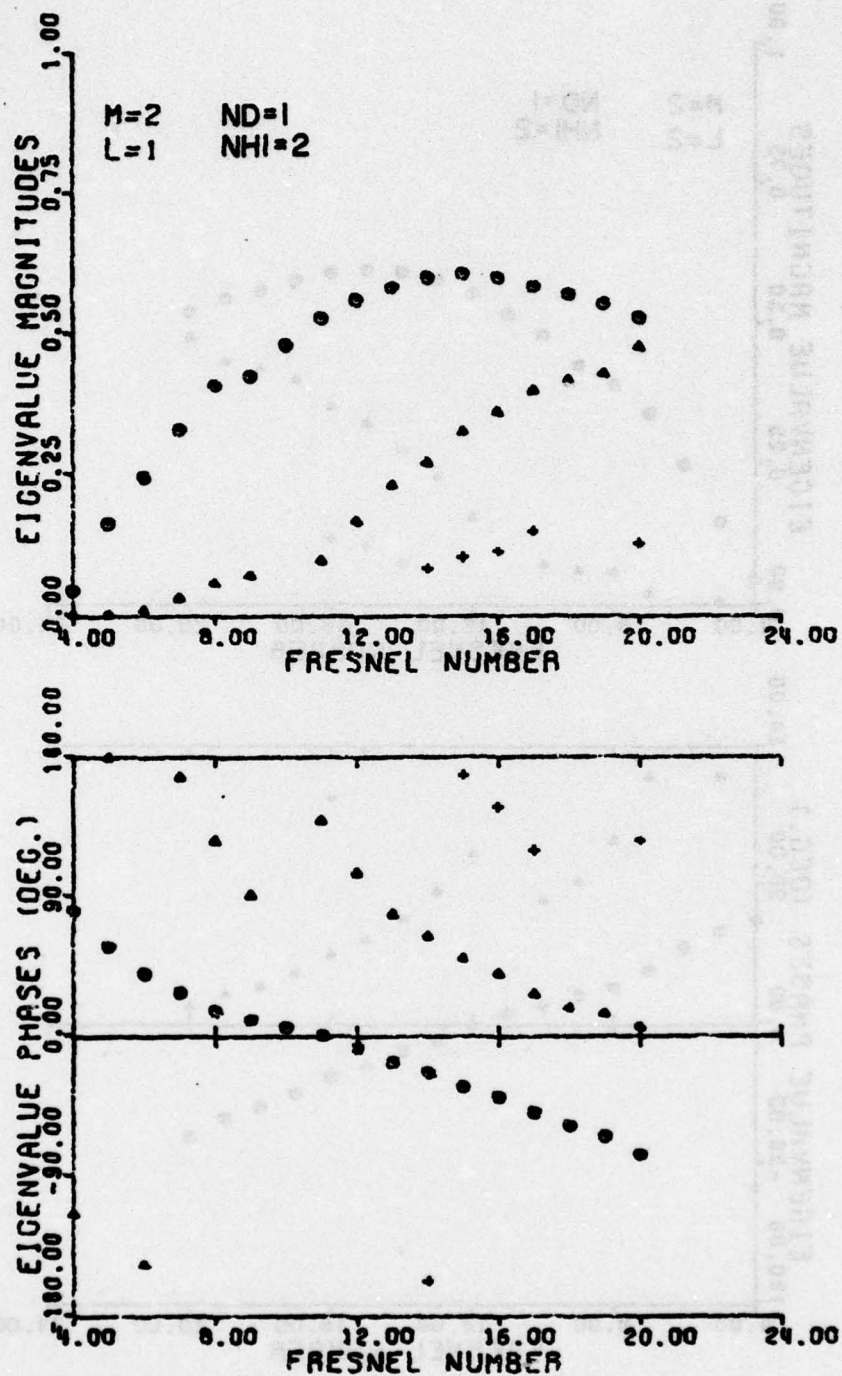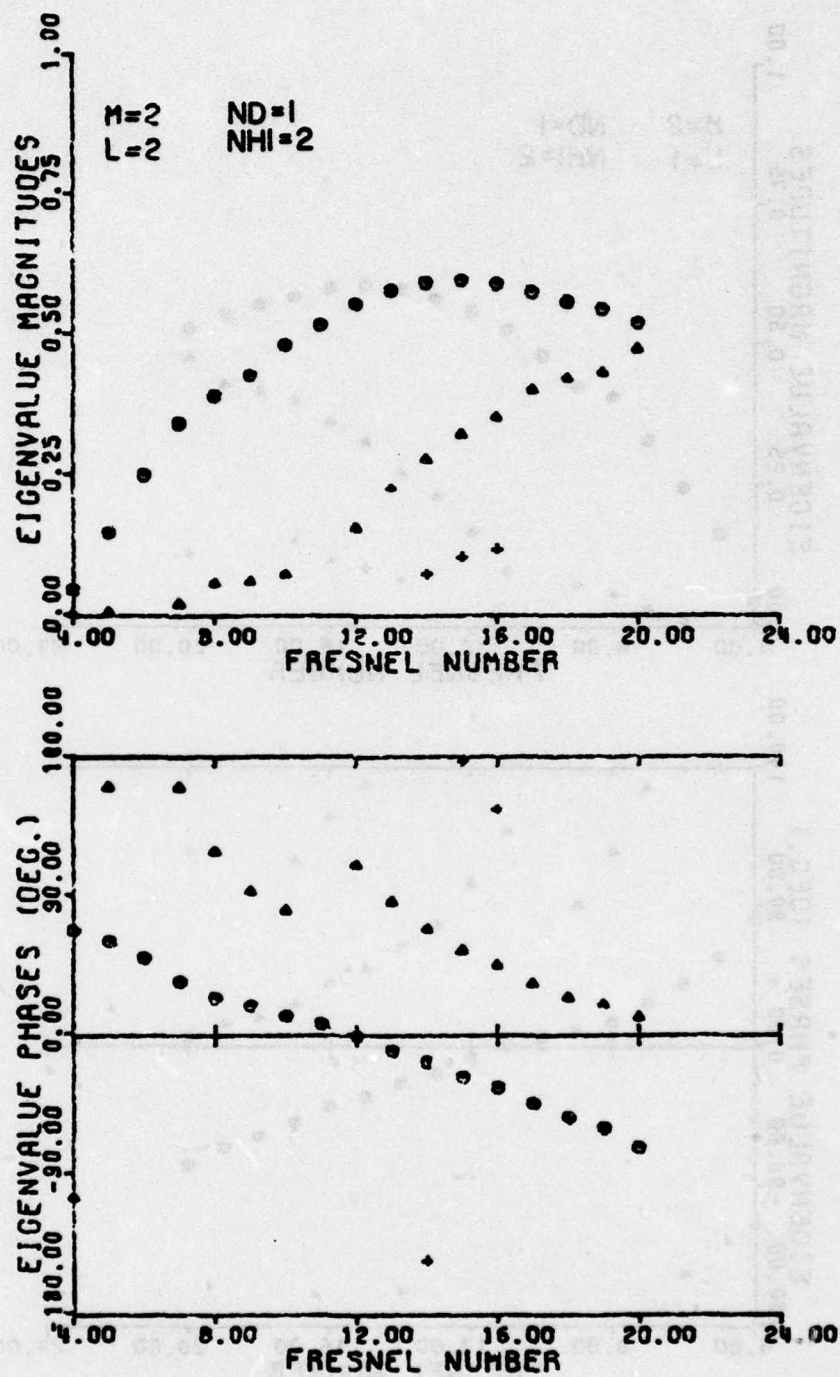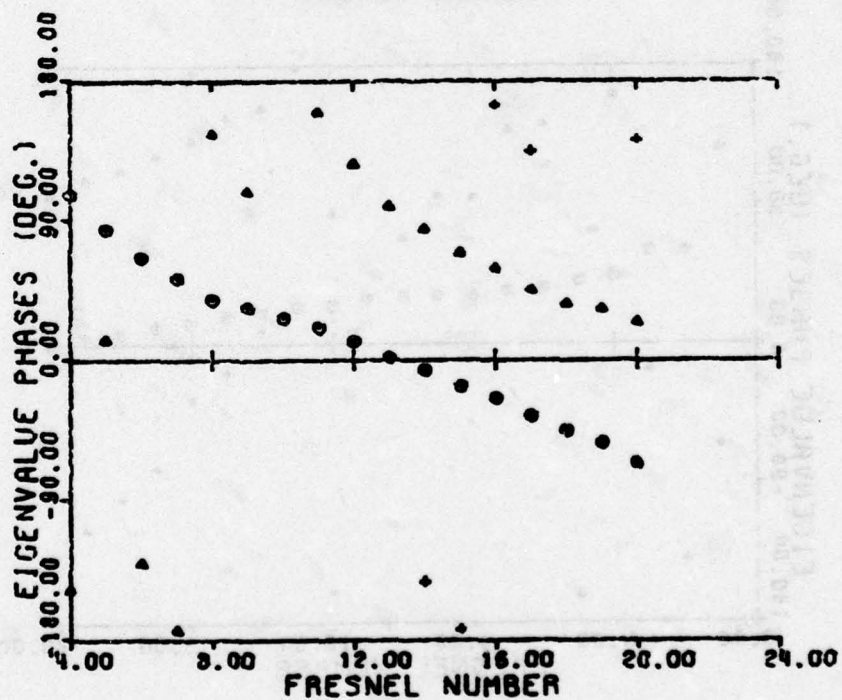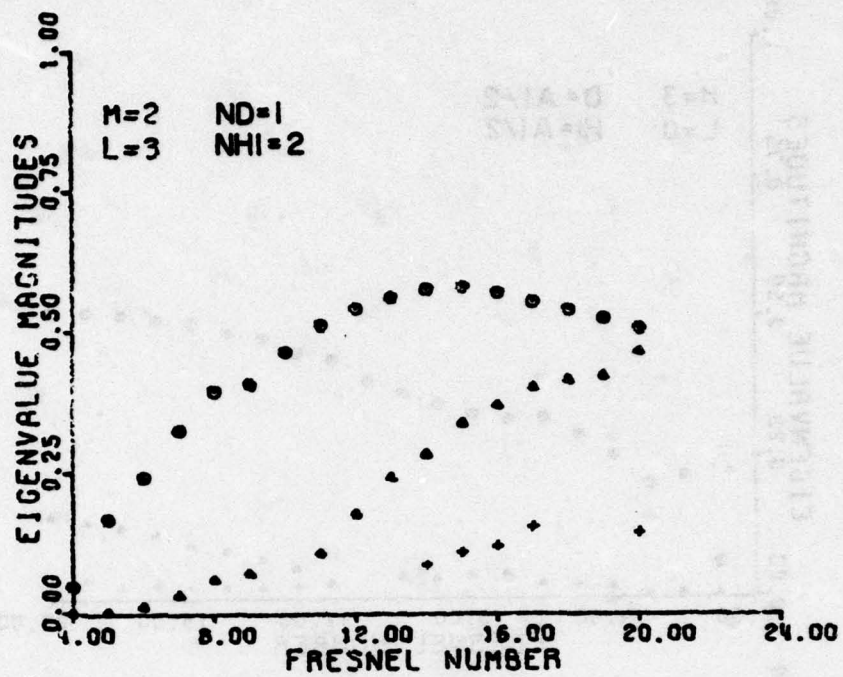
Figure 33c $\ell = 2$

Figure 33d $\ell = 3$
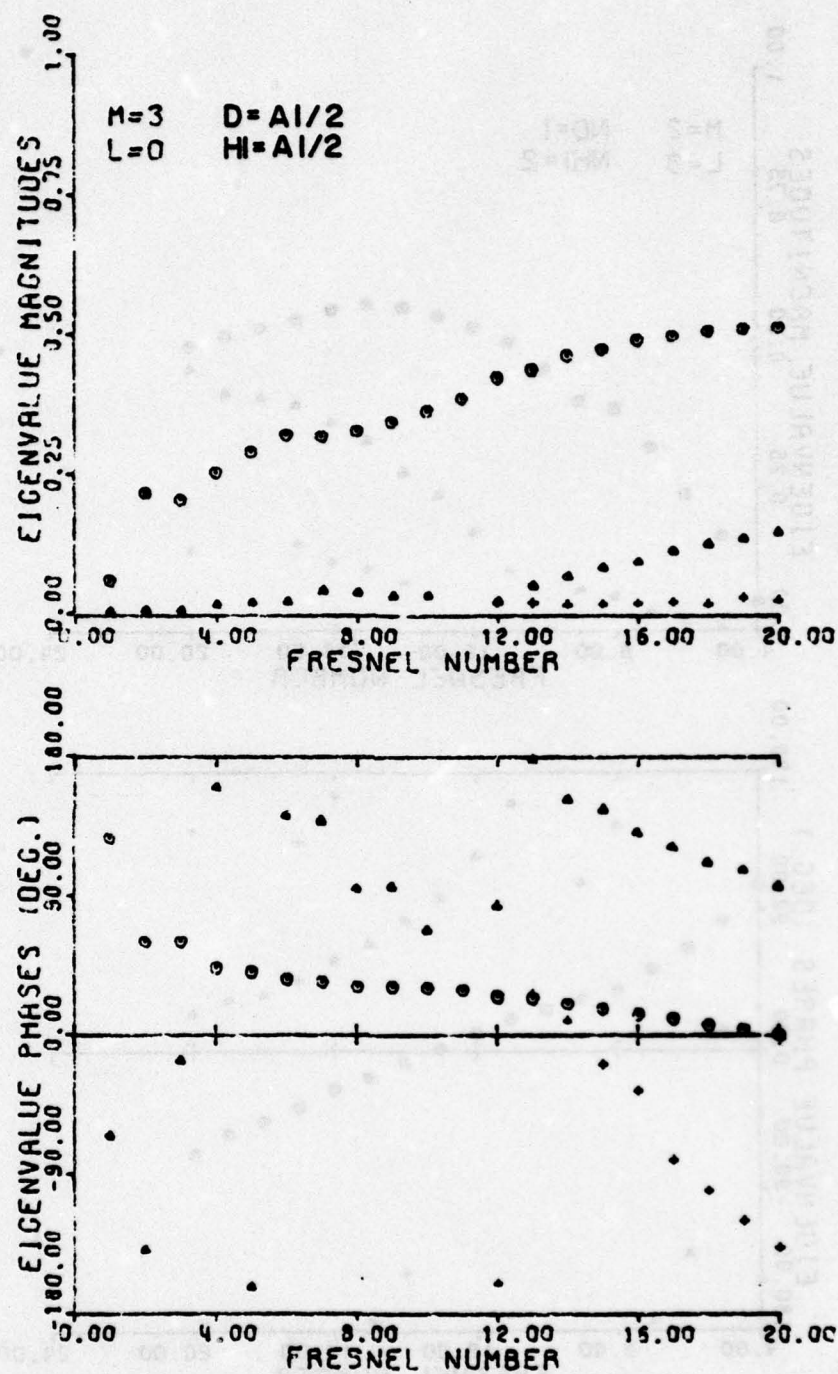
Figure 34a   Eigenvalues of the resonator of Figure 30 for H1 = A1/2,
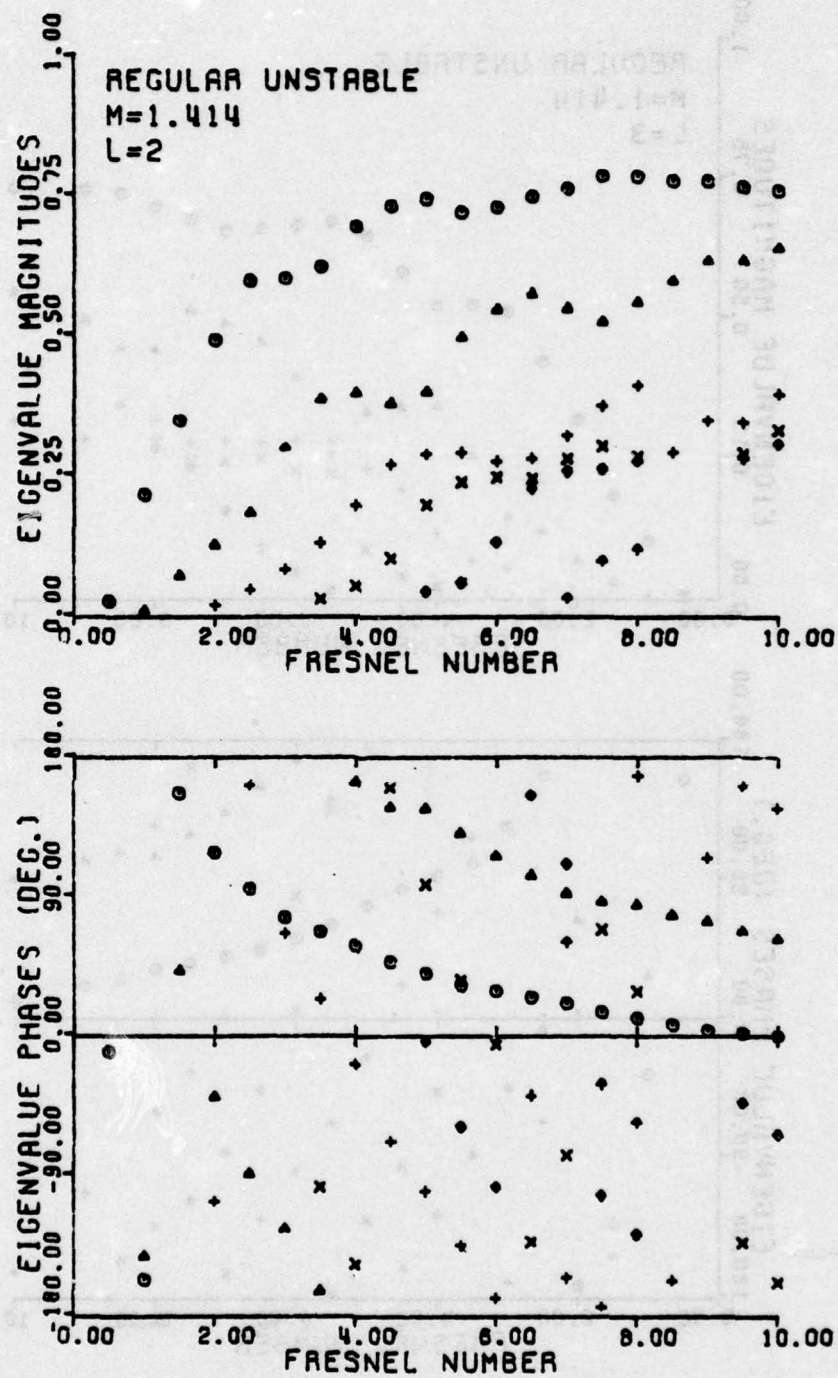D = A1/2, M = 3, ℓ = 0

140

Figure 34b ℓ = 3

141
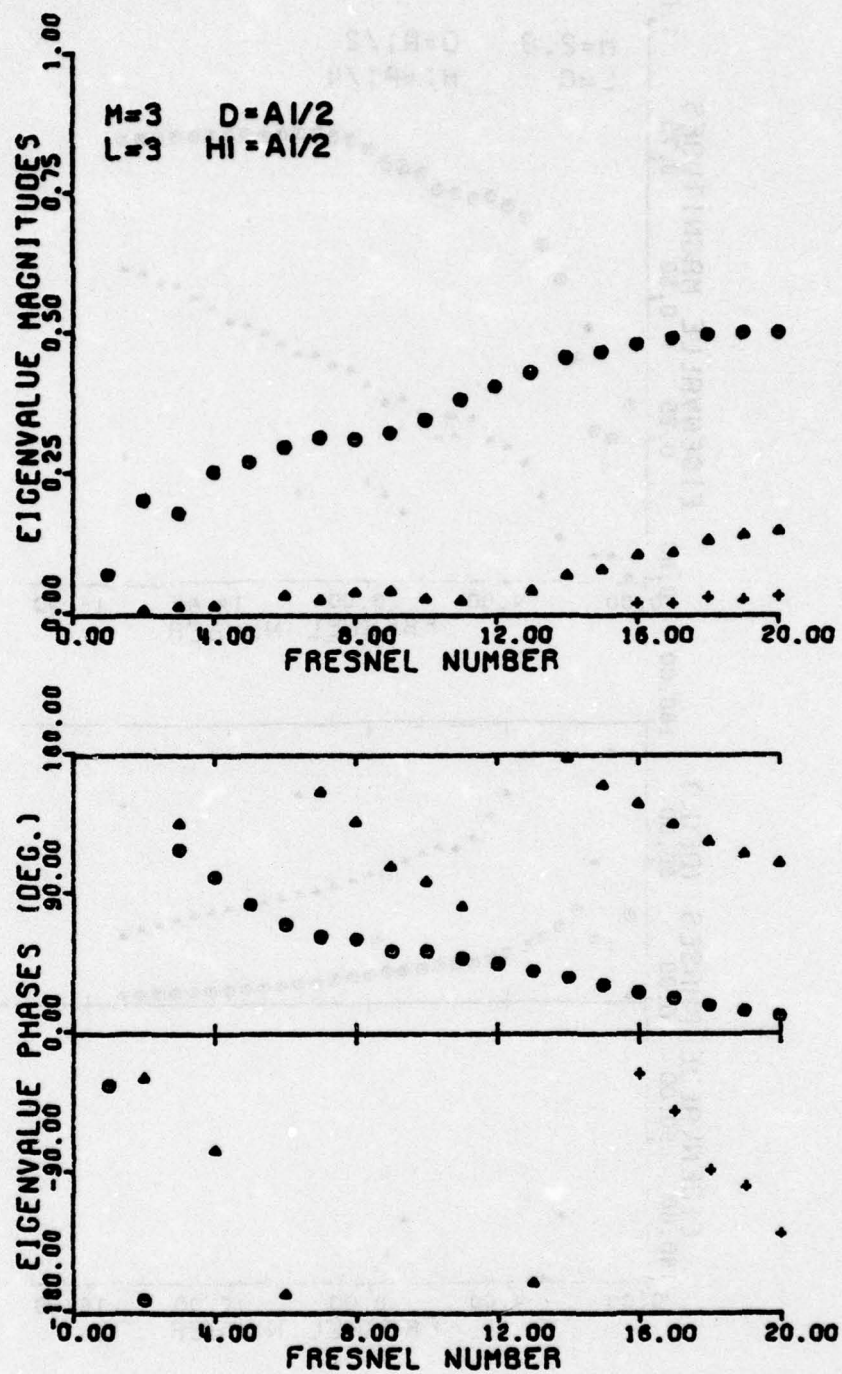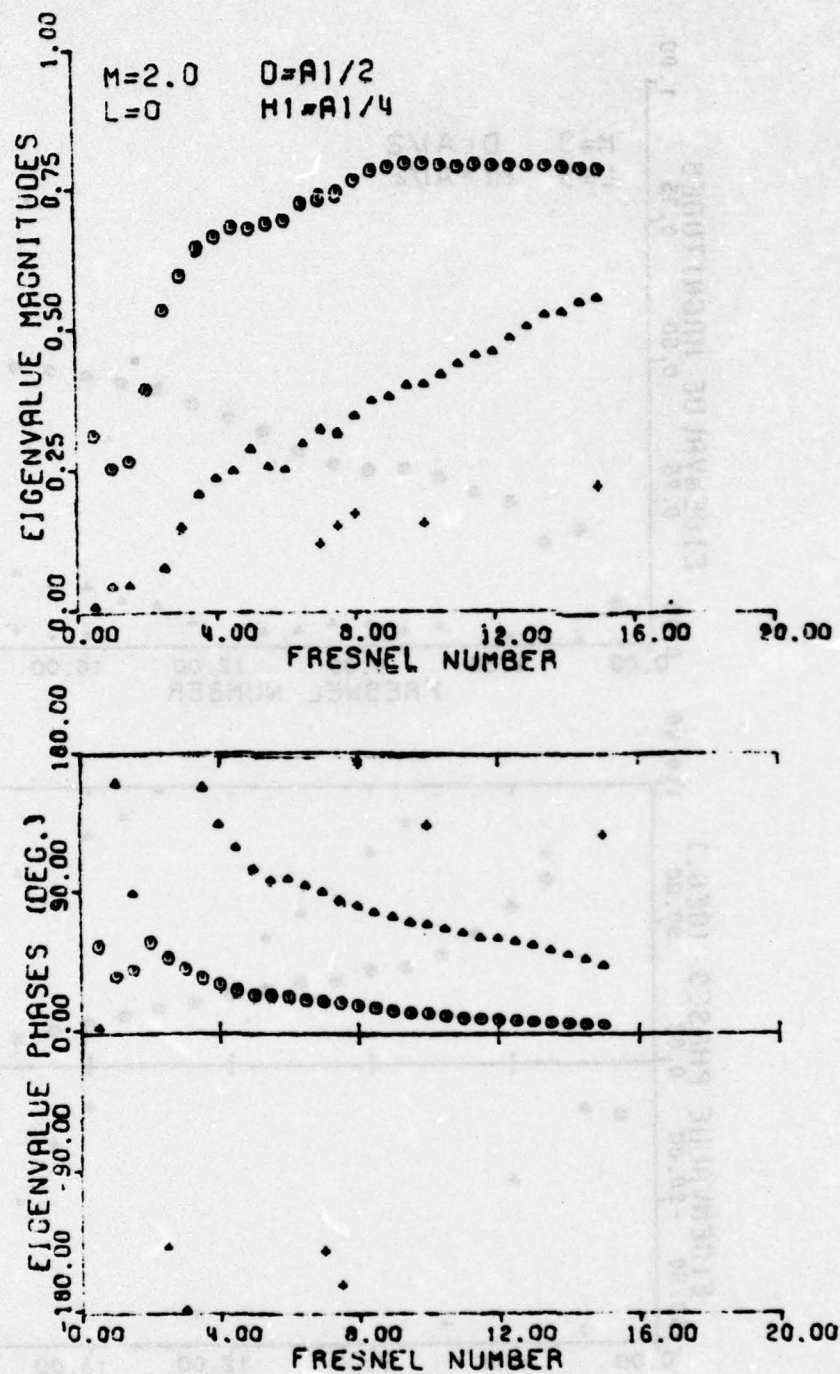
Figure 35a Eigenvalues of the resonator of Figure 30 for H1 = A1/4, D = A1/2, M = 2, ℓ = 0
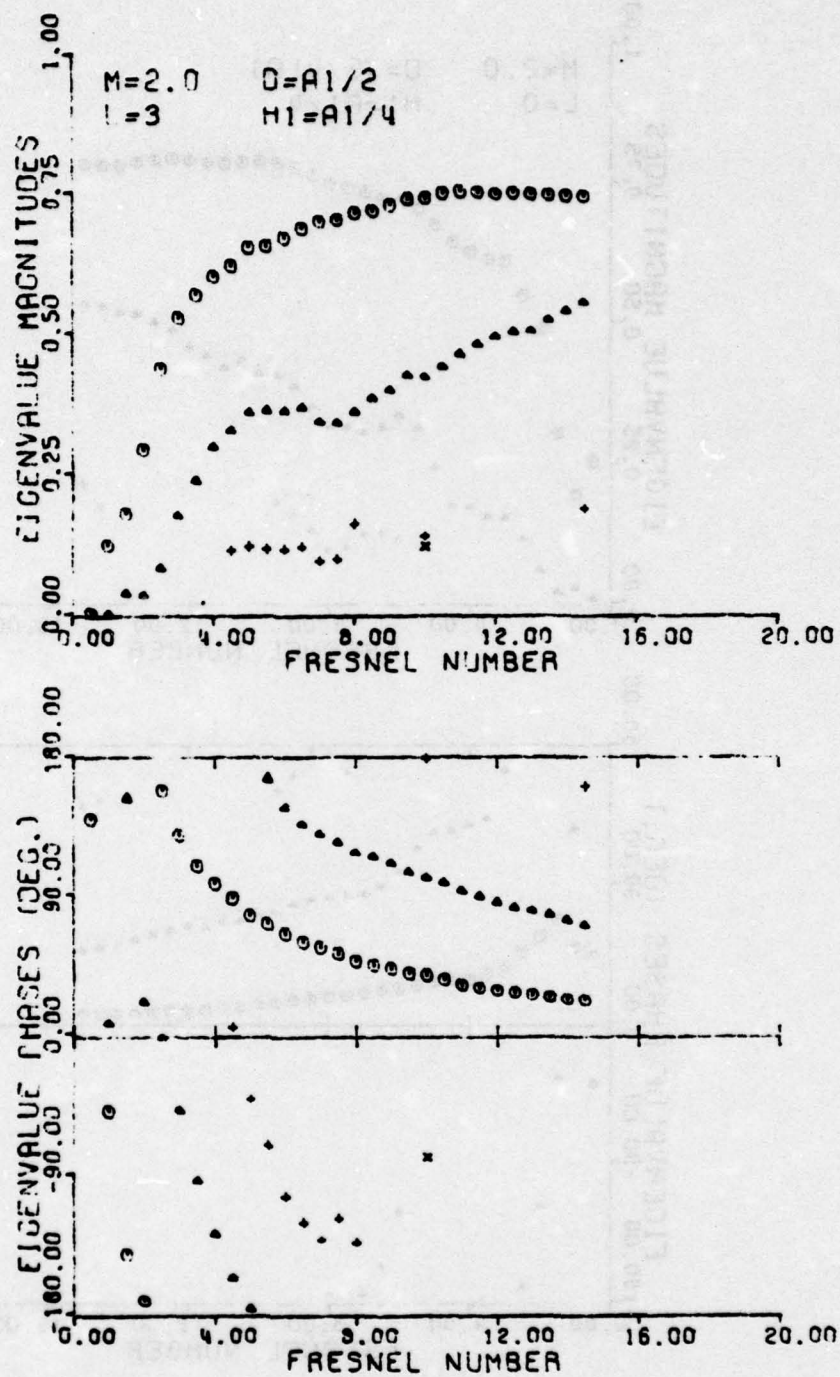
Figure 35b ℓ = 3
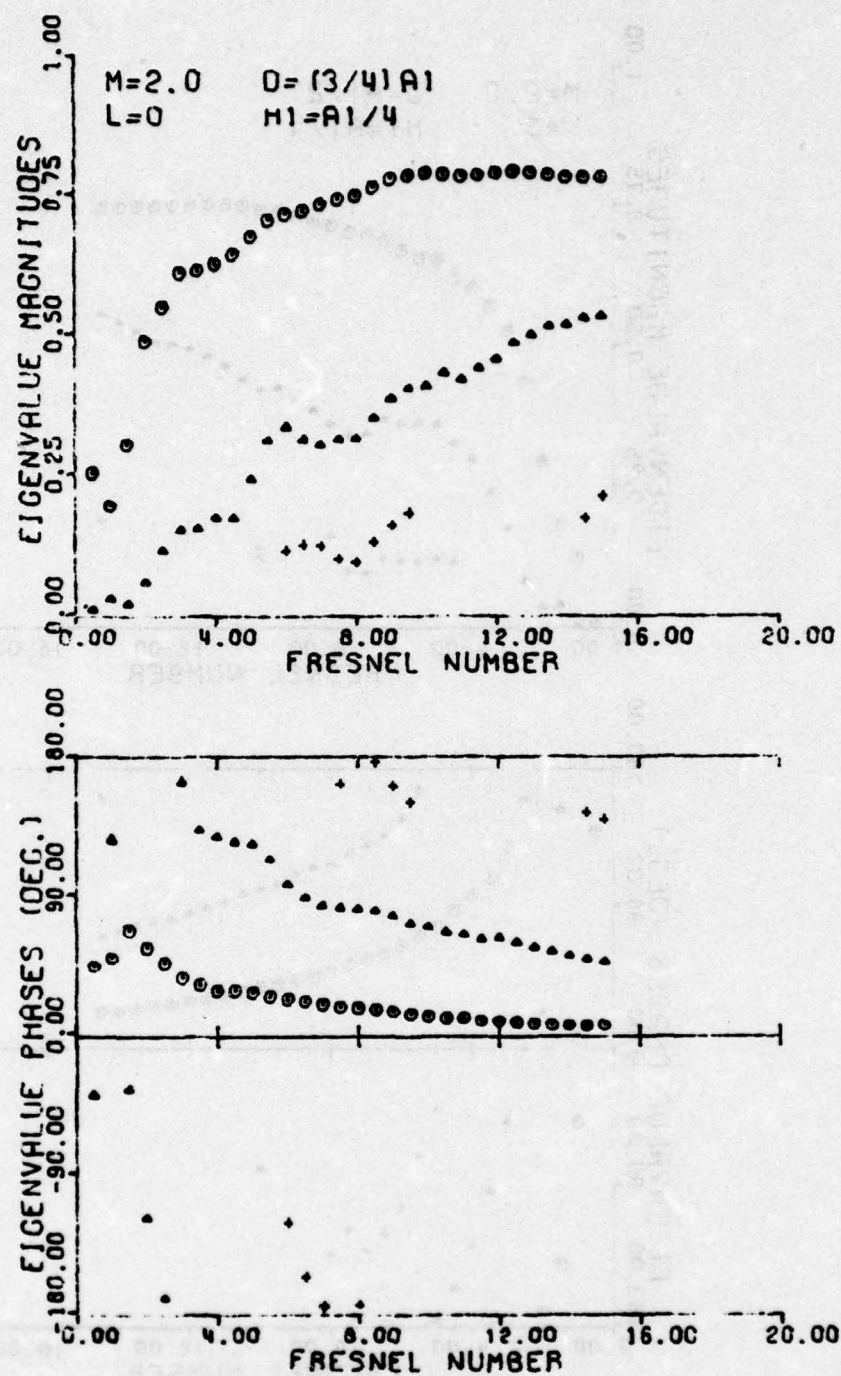
Figure 36a   Eigenvalues of the resonator of Figure 30 for H1 = A1/4,
D = 3A1/4, M = 2, ℓ = 0

144

M=2.0   D=(3/4)A1
L=3   H1=A1/4
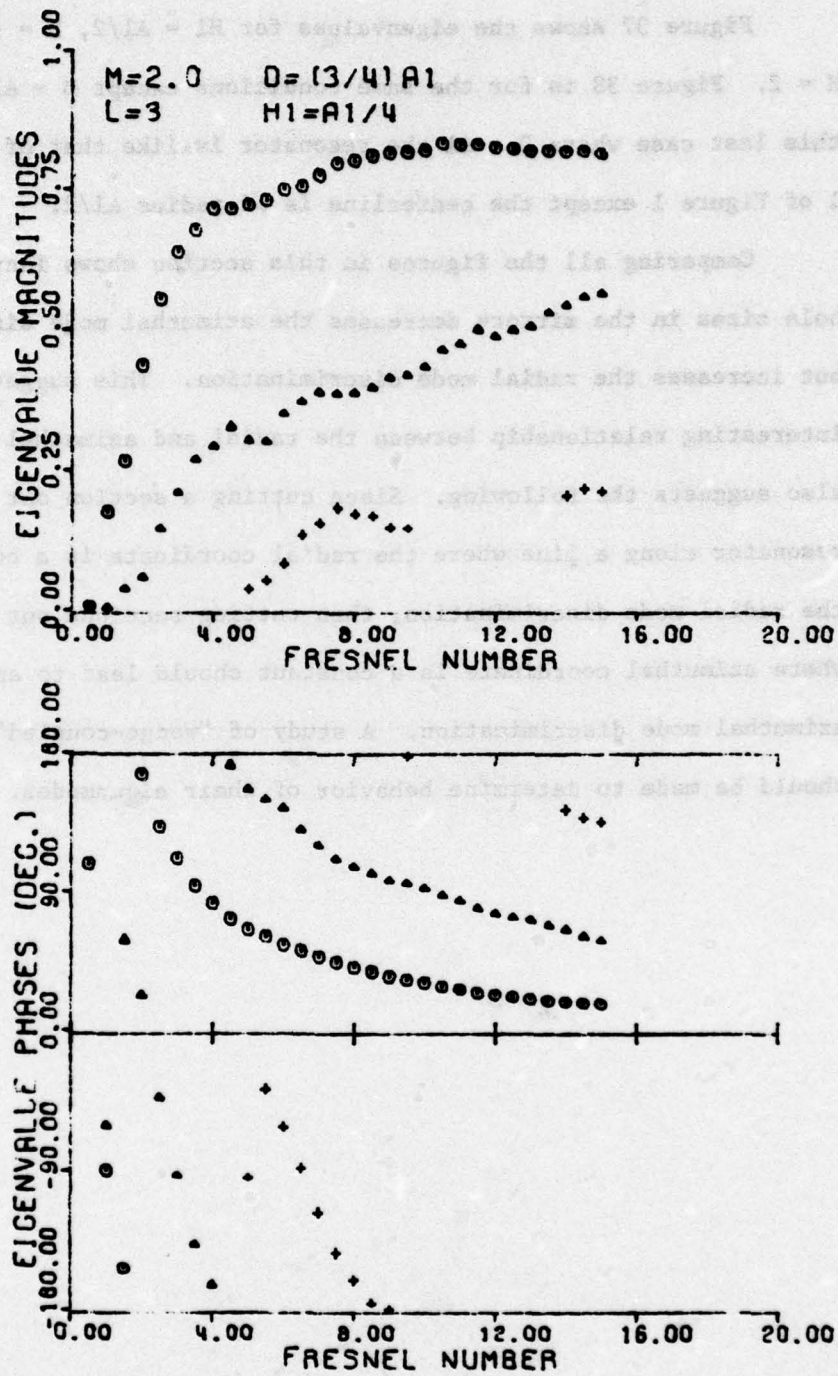
Figure 36b ℓ = 3

Figure 37 shows the eigenvalues for H1 = A1/2, D = 3/4A1 and
M = 2. Figure 38 is for the same conditions except D = A1. For
this last case where D = A1 the resonator is like that of resonator
1 of Figure 1 except the centerline is of radius A1/2.

Comparing all the figures in this section shows increasing the
hole sizes in the mirrors decreases the azimuthal mode discrimination,
but increases the radial mode discrimination. This suggests an
interesting relationship between the radial and azimuthal modes and
also suggests the following. Since cutting a section out of the
resonator along a line where the radial coordinate is a constant increases
the radial mode discrimination, then cutting sections out along lines
where azimuthal coordinate is a constant should lead to an increase in
azimuthal mode discrimination. A study of "wedge-coupled" resonators
should be made to determine behavior of their eigenmodes.
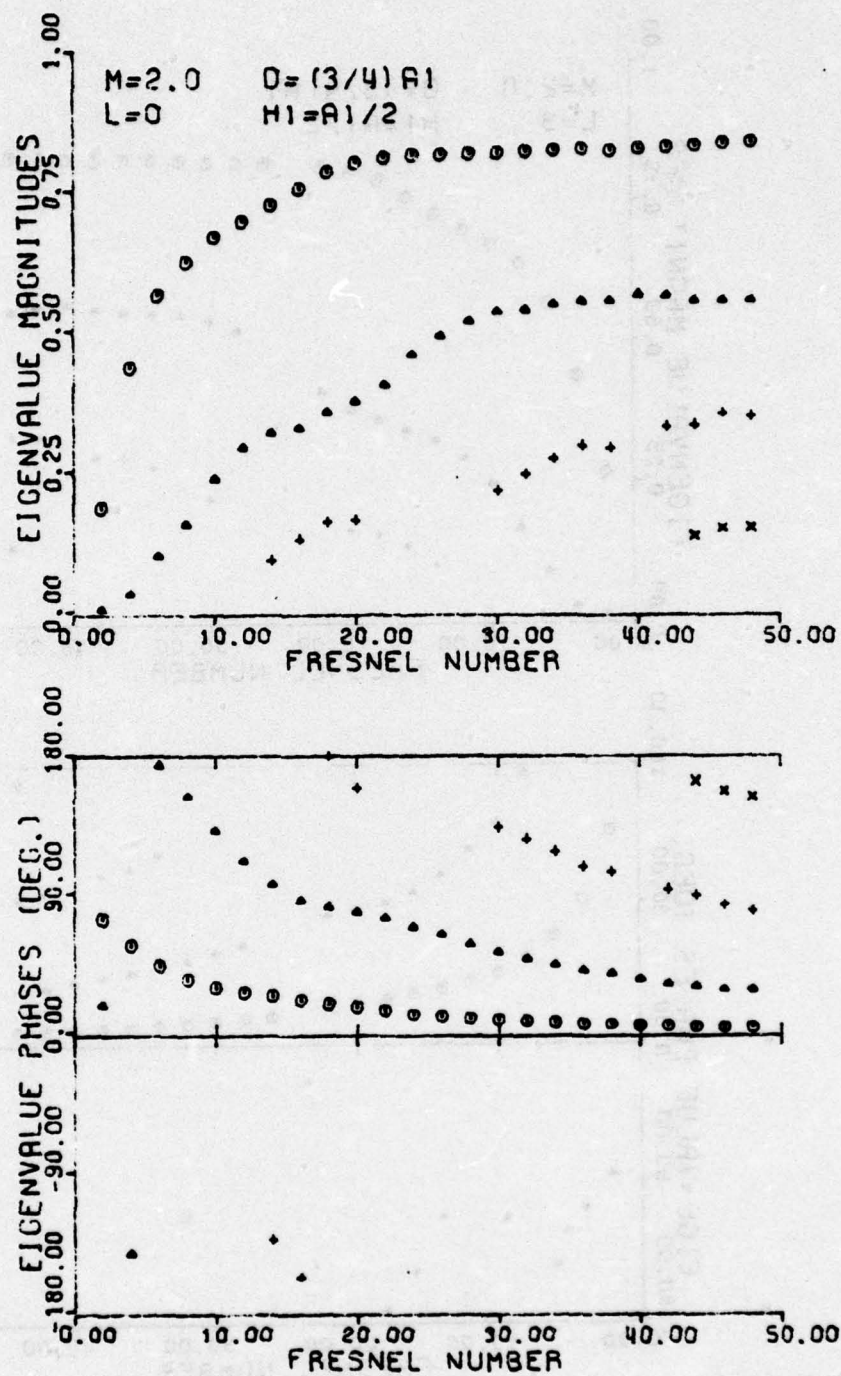
Figure 37a Eigenvalues of the resonator of Figure 30 for H1 = A1/2,
D = 3A1/4, M = 2, ℓ = 0

147
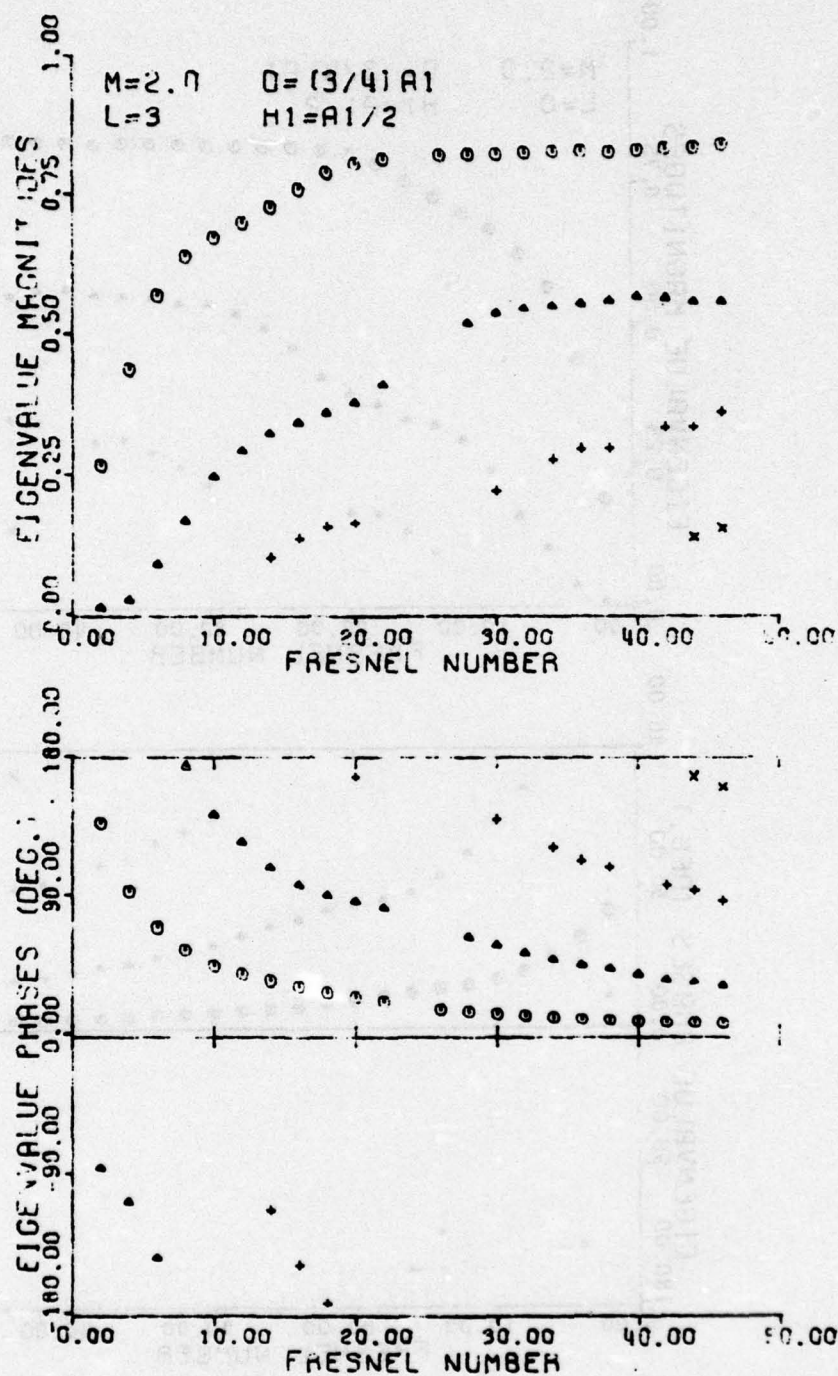
Figure 37b $\ell = 3$
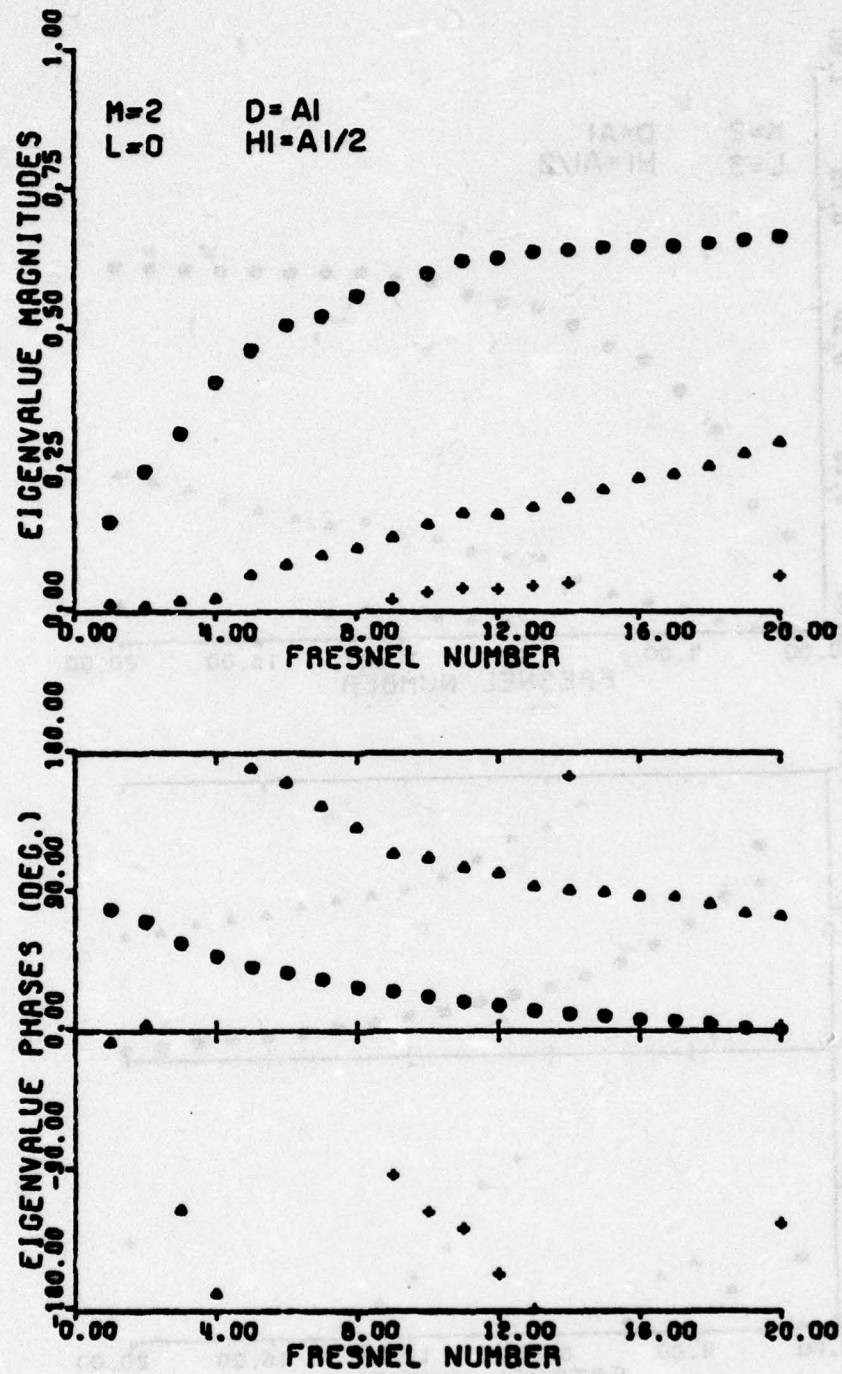
Figure 38a   Eigenvalues of the resonator of Figure 30 for H1 = 3A1/4,
D = A1, M = 2, ℓ = 0
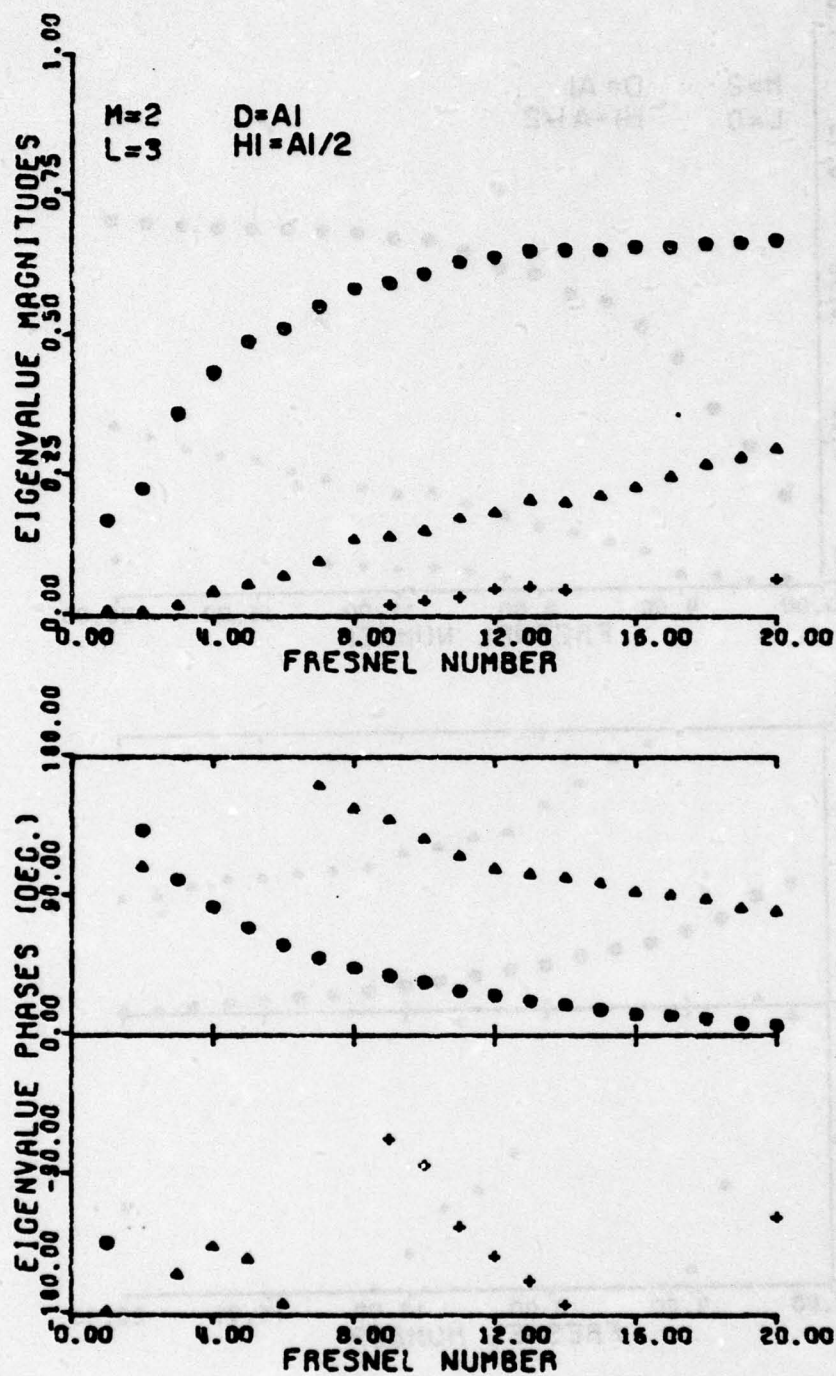
Figure 38b $\ell = 3$

SECTION VI

TASK 5 RESULTS

The purpose of Task 5 was to investigate the possibility of
using conformal mapping techniques to transform circular geometries
to rectangular geometries where the resonator eigenmode calculations
could be expedited using the fast Fourier transform. The conformal
transformation [5]

$$W = \exp (Z)$$

$$\text{where } W = u + iv = r \exp (j\phi)$$

$$\text{and } Z = x + iy$$

maps rings in the complex W plane into rectangles in the Z plane as
shown in Figure 39. It was hoped that the transform could be used to
link the eigenmodes of strip resonator calculations to the eigenmodes
of circular resonators. A problem arose which aborted the exercise.

The transform dictates

$$r = \exp(x)$$

In cylindrical coordinates the field on mirror 2 at r_2 for example
depends in a complex manner on the field at each source point r_1. In
Cartesian coordinates the field at x_2 depends on the field at each source
point x_1 but through a Kernel which is a function of the difference in
the coordinates x_2 and x_1. Therefore a strip calculation can be made for
a fixed width strip resonator anywhere in the Z plane. For example,
if the strip mirrors are translated a distance b in the x direction
relative to the origin, then the circular mirrors are scaled by a factor
$\exp(b)$ in the W plane. The eigenmode losses for the resonator whose
mirrors are scaled by a factor $\exp(b)$ in the W plane are not the same as
the losses for the unscaled calculation, assuming the distance between

151

iv

E

B

D   C   A   F   u
H   I

J

G

iy

π   C   D

B   E

A   F   x

J   G

-π I   H
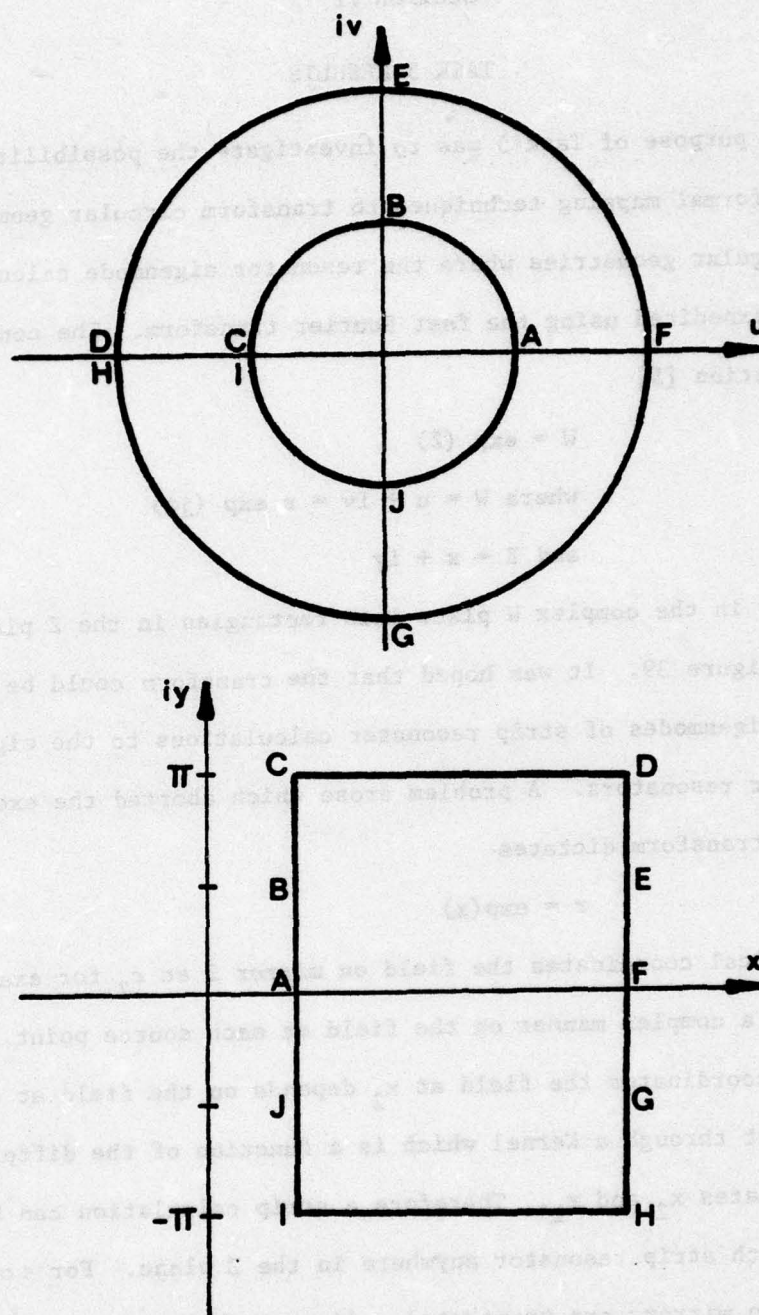
Figure 39   Transformation regions for the complex transform
W = exp Z where W = u + iv and Z = x + iy

the mirrors is not changed. A possible solution would be to scale the distance between the mirrors and the wavelength by the same factor exp(b) which would make the Fresnel number of the circular resonator invarient to transverse shifts of the strip resonator as should be the case. The point has not yet been resolved.

SECTION VII

SUMMARY, CONCLUSION, AND FUTURE WORK

A computer program was developed during Task 1 for calculating
the radial eigenmodes of circular cylindrical resonators where the
azimuthal variation is of the form $\exp(\pm j\ell\phi)$ where ℓ is any integer.
The program was used to analyze several confocal hole-coupled resonator
configurations to determine whether or not the $\ell=0$ mode would be the
dominant or lowest loss mode in the unload resonator. No purely hole-
coupled resonator was found in which the $\ell=0$ mode was clearly dominant
except for the uninteresting limit of small Fresnel numbers. One
resonator (Figure 1c) was found in which all azimuthal modes had
approximately equal losses (i.e., the modes were degenerate). Loaded
cavity analysis should be performed using a reasonable gain saturation
profile to determine the "saturated" mode profile. If these results
are promising, an experimental study of the resonator should be under-
taken.

Also, a computer program has been developed which demonstrates the
feasibility of a technique for calculating mirror figures to achieve
specified radial eigenmode profiles. The most serious limitation is
that the program considers only the radial mode profile, where in most
cases of interest, it is the azimuthal phase profile which is of
paramount interest. The program should be generalized to allow arbitrary
radial and azimuthal field variation so that the radial and azimuthal
mirror figure functions can be calculated to achieve hole-coupled output
with minimal azimuthal field phase variation.

Analysis of resonators with holes in both mirrors has shown that,
when both the holes are much larger than a Frensel number, there is

154

virtually no difference in the losses for the lowest order azimuthal eigenmodes, but that the radial mode discrimination is excellent. Since increased radial mode discrimination is achieved by cutting out sections of the resonator along line of constant radial coordinate (holes), it is likely that increased azimuthal mode discrimination can be achieved by cutting out sections of the resonator along lines of constant azimuthal coordinate (wedges). Therefore a study should be made of the eigenmodes of "wedge-coupled" resonators with higher order phase figures.

APPENDIX A

CALCULATION OF THE RESONATOR EIGENMODES

A computer program has been developed to calculate the bare cavity scalar radial eigenmodes for $\exp(j\ell\phi)$ azimuthal variation in circular cylindrical resonators. The resonator mirrors can have arbitrary radial curvature within the Fresnel approximation and arbitrary reflectivity. The eigenmodes are computed numerically via the Prony method as described previously by Siegman and Miller [1]. Their method is modified to allow for arbitrary mirror curvatures, and the procedure is iterated to assure convergence and accuracy of the computed eigenmodes and eigenvalues. The following three subsections extracted from the user's manual for the program discuss the relevant mathematical equations and some of the programming details.

1. WAVE PROPAGATION

The basic resonator integral equations for the radial field functions are [6]

$$\gamma_\ell^{(1)} R_\ell^{(1)}(r_1)\sqrt{r_1} = \int_o^{a_2} K(r_1,r_2) R_\ell^{(2)}(r_2)\sqrt{r_2}\, dr_2 \tag{A1}$$

$$\gamma_\ell^{(2)} R_\ell^{(2)}(r_2)\sqrt{r_2} = \int_o^{a_1} K(r_1,r_2) R_\ell^{(1)}(r_1)\sqrt{r_1}\, dr_1 \tag{A2}$$

where the kernel

$$K(r_1,r_2) = j^{\ell+1}\frac{k}{B}\exp[-j\frac{k}{2B}(g_1 r_1^2 + g_2 r_2^2)]\sqrt{r_1 r_2} \tag{A3}$$

and

·157

- the subscripts 1 and 2 refer to mirrors 1 and 2, respectively

$R_\ell^{(1)}$ - the phasor radial field on mirror 1, where the azimuthal

         field dependence is assumed to vary as $\exp(j\ell\phi)$

r   - radial coordinate

k   - wavenumber = $2\pi/\lambda$

λ - wavelength

B   - mirror separation

J_ℓ - Bessel function of order ℓ

a   - outer mirror radius

g   - resonator parameter = $1 - B/R$

R   - radius of curvature ·

$\gamma_\ell^{(1)}$ - single pass eigenvalue

The complete field is written as

$$E_{n\ell}(r) = R_{n\ell}(r) \, \exp(j\ell\phi) \tag{A4}$$

where n and ℓ are the radial and azimuthal mode indices, respectively. The fields (eigenmodes) are orthogonal on the mirror surfaces and can be normalized such that

$$\int_0^{2\pi} \int_0^a E_{mk}(r) E_{n\ell}(r) r \, dr d\phi = \delta_{mn}\delta_{k\ell} \tag{A5}$$

For computational convenience the integral equations will be written in a different form. Let us define a constant

$$C = j^{\ell+1} \frac{k}{B} \tag{A6}$$

a spherical phase factor,

$$t_i(r_i) = \exp\left(-j\frac{kr_i^2}{B}\right) \tag{A7}$$

158

and a "reflection coefficient"

$$\rho_1(r_1) = \exp\left(\frac{jkr_1^2}{R_1}\right) \qquad \text{(A8)}$$

The latter is interpreted as a reflection coefficient (or function) since $r_1^2/2R_1$ is the approximate distance the mirror surface is displaced from planar and thus kr_1^2/R_1 is the total phase shift the wave experiences at r_1 upon reflection. For higher order resonators the reflection coefficient can be generalized to

$$\rho_1(r_1) = \exp\left(j2kd_1(r_1)\right) \qquad \text{(A9)}$$

(arbitrary magnitude variations could also be included) where $d_1(r_1)$ is the distance the mirror is displaced from planar (the mirror figure function). In terms of the new variables, the kernel can be rewritten as

$$K(r_1,r_2) = CJ_\ell\left(\frac{kr_1r_2}{B}\right)\sqrt{\rho_1(r_1)\rho_2(r_2)t_1(r_1)t_2(r_2)r_1r_2} \qquad \text{(A10)}$$

Then with the additional definition

$$s_\ell^{(1)}(r_1) = \frac{R_\ell^{(1)}(r_1)}{\sqrt{\rho_1(r_1)}\,\sqrt{t_1(r_1)}} \qquad \text{(A11)}$$

and the grouping $T_1(r_1) = \rho_1(r_1)t_1(r_1)r_1$ the resonator integral equations may be written as

$$\gamma_\ell^{(1)}s_\ell^{(1)}(r_1) = \int_0^{a_2} J_\ell\left(\frac{kr_1r_2}{B}\right) t_2(r_2)s_\ell^{(2)}(r_2)dr_2 \qquad \text{(A12)}$$

$$\gamma_\ell^{(2)}s_\ell^{(2)}(r_2) = \int_0^{a_1} J_\ell\left(\frac{kr_1r_2}{B}\right) T_1(r_1)s_\ell^{(1)}(r_1)dr_1 \qquad \text{(A13)}$$

159

or correspondingly in matrix form as

$$\gamma_1 S_1 = J T_2 S_2 \tag{A14}$$

$$\gamma_2 S_2 = J T_1 S_1 \tag{A15}$$

where ℓ is understood. From (A11) it is seen that $s_\ell^{(1)}(r_1)$ is the field on a spherical surface of radius B just incident mirror i because multiplying by

$$\sqrt{t_1(r_1)} = \exp\left(\frac{jkr_1^2}{2B}\right) \tag{A16}$$

transforms the field to a plane in front of the mirror and multiplying by $\sqrt{\rho_1(r_1)}$ transforms the field to the mirror surface. Therefore, the product $\rho_1(r_1)t_1(r_1)$ transforms the field from the spherical surface, to the mirror surface, and back to the spherical surface but propagating in the opposite direction.

The radial fields on the spherical surfaces, can be normalized such that

$$\int s_{i\ell}^{(1)}(r) \, s_{j\ell}^{(1)}(r) \, T(r) \, dr = \delta_{ij} \tag{A17}$$

where the integral is over the mirror surface.

Finally the composite matrix equation for, say the fields on mirror 1, may be written

$$\gamma S_1 = J T_2 J T_1 S_1 \tag{A18}$$

where the round trip eigenvalue $\gamma = \gamma_1 \gamma_2$. For small number of points on both mirrors it is useful to form the round trip operator matrix

160

$M = JT_2 \, JT_1$. However, as the number of field grid points increases, two computational savings can be realized by not computing M. First, it takes one fourth the computer storage to store the the real symmetric matrix of Bessel functions J as opposed to the complex matrix M. Second, the number of multiplications required to form M can exceed the number of multiplications required to find the dominant eigenmodes by the iterated Prony method which will be described in the next section.

2. ITERATED PRONY METHOD

The basic Prony calculation used is exactly as described by Siegman and Miller [1] except the procedure is repeated until convergence is achieved and the number of eigenvalues is changed as required to facilitate convergence. The following discussion briefly describes the computational procedure.

Formally, we wish to find the first n dominant eigenvectors U_i and eigenvalues γ_i, i = 1 to n of the matrix equation

$$MU = U\gamma \qquad\qquad (A19)$$

where M is a complex symmetric matrix. In resonator terminolgy the eigenvectors are often referred to as "eigenmodes," "modes," or "fields." An initial vector, or field distribution, V_o is constructed and propagated n times through the resonator using the wave propagation procedure described in the previous section. The higher order modes, smaller eigenvalues, are attenuated more rapidly than the lower order modes, which have larger eigenvalues. The initial field and sequence of propagated fields may be written as:

161

$$V_o = k_1 U_1 + k_2 U_2 + k_3 U_3 + \ldots$$

$$V_1 = MV_o = k_1 \gamma_1 U_1 + k_2 \gamma_2 U_2 + k_3 \gamma_3 U_3 + \ldots$$

$$V_n = MV_{n-1} = k_1 \gamma_1^n U_1 + k_2 \gamma_2^n U_2 + k_3 \gamma_3^n U_3 + \ldots \qquad \text{(A20)}$$

where initially the k_i's and γ_i's are unknown. Two matrices of dot products are generated

$$F = \begin{bmatrix} F_{01} & F_{02} & \cdots & F_{0n} \\ F_{11} & F_{12} & \cdots & F_{1n} \\ & & \vdots & \\ F_{r1} & F_{r2} & \cdots & F_{rn} \end{bmatrix} \qquad \text{(A21)}$$

$$G = \begin{bmatrix} F_{1n} \\ F_{2n} \\ \vdots \\ F_{nn} \end{bmatrix} \qquad \text{(A22)}$$

where $r = n - 1$ and the dot products are

$$F_{ij} = \sum_k (V_i)_k (V_j)_k \qquad \text{(A23)}$$

The F matrix is inverted and the eigenvalues are computed as the roots of the polynomial

$$\gamma^n + Q_r \gamma^{n-1} + \ldots Q_1 \gamma + Q_o = 0 \qquad \text{(A24)}$$

162

where

$$Q = \begin{bmatrix} Q_o \\ Q_1 \\ . \\ . \\ . \\ Q_r \end{bmatrix} = F^{-1}G \qquad (A25)$$

Then a matrix

$$L = \begin{bmatrix} \gamma_1 & \gamma_2 \cdots \gamma_n \\ \gamma_1^2 & \gamma_2^2 \cdots \gamma_n^2 \\ . \\ . \\ . \\ \gamma_1^n & \gamma_2^n \cdots \gamma_n^n \end{bmatrix} \qquad (A26)$$

is constructed where the eigenvalues are ordered such that

$$|\gamma_{i+1}| < |\gamma_i| \quad 1 \le i \le r \qquad (A27)$$

Upon inversion of the L matrix the square of the k values can be computed

$$k^2 = \begin{bmatrix} k_1^2 \\ k_2^2 \\ . \\ . \\ . \\ k_n^2 \end{bmatrix} = L^{-1}F_o \qquad (A28)$$

where

163

$$F_o = \begin{bmatrix} F_{01} \\ F_{02} \\ . \\ . \\ . \\ F_{0n} \end{bmatrix} \qquad\qquad (A29)$$

Using the k_i's, γ_i's, and V_i's, $i = 1$ to n, estimates $\tilde{U}_i$'s of the U_i's are computed from (A20). Since there may have been components of higher order modes than n in the original vector V_o, we do not at this point know how accurate our computations of the eigenmodes are. Therefore a new initial vector is formed, using the just computed eigenmode estimates as

$$V_o = \tilde{U}_1 + \tilde{U}_2 + \ldots \tilde{U}_n \qquad\qquad (A30)$$

where the $\tilde{U}_i$ are normalized such that

$$\sum_k (\tilde{U}_i)_k (\tilde{U}_i)_k = 1 \qquad\qquad (A31)$$

The procedure is repeated until the calculated expansion coefficients k's are unity and the eigenvalues do not change from one calculation to the next. Ideally if

$$|\gamma_{n+1}| < |\gamma_n| \qquad\qquad (A32)$$

the procedure will always converge, but when

$$|\gamma_{n+1}| \simeq |\gamma_n| \qquad\qquad (A33)$$

convergence can take a large number of iterations. When this situation occurs, it is expedient to change n. If the eigenvalues tend to separate

164

as n increases, as is the case in resonator calculations, n should be increased. However n cannot always be increased since the finite word length of the computer will eventually truncate components of the higher order mode in V_n in equation (A20), i.e.,

$$\left(\frac{\gamma_n}{\gamma_1}\right)^n \tag{A34}$$

will become smaller than the resolution limit of the computer.

3. FAR-FIELD CALCULATIONS

By convention in the computer program, the output end of the resonator is at mirror 2. For display purposes, the field incident on mirror 2 is transformed to a plane via

$$u(r_2) = \sqrt{t(r_2)s(r_2)} \tag{A35}$$

The far-field pattern, $f(r)$, is computed by taking that part of $u(r_2)$ which exits the resonator, $u_t(r_2)$, and propagating it to the focus of a lense. For convenience the focus of the lense is B, the cavity length, so the previously computed Bessel function can be used. The field at the focus of the lens is computed from

$$f(r) = C \int J_\ell\left(\frac{krr_2}{B}\right) u_t(r_2)r_2dr_2 \tag{A36}$$

where the integration is over the output plane. The integrated far-field intensity, $p(r)$, can then be computed as

$$p(r) = \int_0^r |f(r')|^2 r'dr' \tag{A37}$$

165

APPENDIX B

LEASTS SQUARES METHOD FOR CALCULATING RESONATOR
PARAMETERS TO ACHIEVE A DESIRED EIGENMODE PROFILE

A non-linear regression algorithm has been utilized to calculate radial mirror figures of open resonators such that the radial profile of the lowest loss eigenmode (for a particular azimuthal symmetry) is the best fit in a least squares sense to a user specified, "desired", eigenmode profile. The method used is that of Marquardt [7] which is a maximum neighborhood method for least squares estimation of nonlinear parameters. It performs an interpolation between the Taylor series method and the gradient method in an attempt to combine the best features of the two methods while at the same time avoiding their most serious limitations. The algorithm described here for ease of reference is identical to that of reference [8] except for changes in nomenclature and the inclusion of point error weighting.

The model to be adjusted to the data can be written in the form

$$\hat{U} = f(r; \beta_1, \beta_2, \ldots \beta_k) \tag{B1}$$

where r is the independent variable(s) and β_1, β_2, $\ldots$ β_k are the population values of the k parameters to be estimated and $\hat{U}$ is the dependent variable. In the context of the resonator problem $\hat{U}$ is the lowest loss radial eigenmode profile (or intensity) for a particular aximuthal symmetry, r is the radial field coordinate, and the β's are the resonator parameters which one wishes to vary. The observed points will be designated as

$$U(r_i) \quad i = 1, 2, \ldots N \tag{B2}$$

166

which for the cases investigated to date are the desired radial field points in a plane adjacent to one of the resonator mirrors or desired radial points in the integrated far-field intensity profile. Standard techniques can be used to calculate the radial mode profile $\hat{U}$ at the specified coordinates for a given resonator geometry and radial mirror figures which are dependent on the β's. The problem could be structured even more generally so as to optimize azimuthal variation in the mirror figures provided the total field was calculated without restriction on the type of azimuthal symmetry.

The problem is to compute those estimates of the parameters which will minimize

$$\Phi = \sum_{i=1}^{n} W_i [u_i - \hat{u}_i]^2 \qquad (B3)$$

where $\hat{u}_i$ is the value of $u(r_i)$ predicted at the i-th data point and W_i is the associated weight for that point error. (u-magnitude and/or phase of U).

The Taylor series aspect of the combined Marquardt Method will now be described. Writing the perturbed model in a Taylor series through the linear terms gives

$$< u(r_i, \underline{b} + \underline{\delta}_t) > = f(r_i, \underline{b}) + \sum_{j=1}^{k} \frac{\partial f_i}{\partial b_j} (\partial_t)j \qquad (B4)$$

or

$$< u > = \underline{f}_o + P\underline{\delta}_t \qquad (B5)$$

In (B4), $\underline{\beta}$ is replaced by $\underline{b}$, the converged value of $\underline{b}$ being the least squares estimate of β and f_i is the value of the function evaluated at the i-th data point. The vector $\underline{\delta}_t$ is a small correction to $\underline{b}$, where

167

the subscript t is used to designate the $\underline{\delta}$ was calculated using the Taylor series method, and P is an [n x k] matrix whose elements are $\partial f_i/\partial b_j$. The brackets <> are used to distinguish predictions based on the linearized model from those based on the actual non-linear model. Therefore, the estimated sum of squares error (SSE) is designated as

$$<\phi> = \sum_{i=1}^{n} W_i[u_i - <u_i>]^2 \tag{B6}$$

In order to minimize $<\phi>$ the critical point(s) must be found, i.e.,

$$\frac{\partial <\phi>}{\partial \delta_j} = 0, j = 1, 2, \ldots, k \tag{B7}$$

which requires from (B4) and (B6) that

$$<\phi> = \sum_{i=1}^{n} W_i[u_i - f_i - \sum_{j=1}^{k} \frac{\partial f_i}{\partial b_j} (\delta_t)_j]^2 \tag{B8}$$

and

$$0 = \frac{\partial <\phi>}{\partial \delta_\ell} = 2 \sum_{i=1}^{n} W_i[u_i - f_i - \sum_{j=1}^{k} \frac{\partial f_i}{\partial b_j} (\delta_t)_j] \frac{\partial f_i}{\partial b_\ell} = 0 \tag{B9}$$

or

$$\sum_{i=1}^{n} W_i [u_i - f_i] \frac{\partial f_i}{\partial b_\ell} - \sum_{i=1}^{n} \sum_{j=1}^{k} W_i \frac{\partial f_i}{\partial b_j} \frac{\partial f_i}{\partial b_\ell} (\delta_t)_j = 0 \tag{B10}$$

or in matrix notation

$$A\underline{\delta}_t' = \underline{g} \tag{B11}$$

where

$$A^{[k \ x \ k]} = P^T DP \tag{B12}$$

168

$$P^{[n \times k]} = \left(\frac{\partial f_i}{\partial b_j}\right), \quad i = 1, 2, \ldots, n; \ j = 1, 2, \ldots, k \quad (B13)$$

$$g^{[k \times 1]} = \sum_{i=1}^{n} W_i [u_i - f_i] \frac{\partial f_i}{\partial b_j}, \quad j = 1, 2, \ldots, k \quad (B14)$$

$$= P^T D (\underline{u} - \underline{f}) \quad (B15)$$

and $\underline{\delta}'_t$ is the new perturbation as influenced by the weighting and $D^{[n \times n]}$ is a diagonal matrix of the weights. In practice $\underline{b}$ is only corrected by a factor of $\underline{\delta}'_t$ so that extrapolation does not go beyond the region where f is adequately described by (B4). Failure to do so would cause divergence of the iterates.

The steepest descent method takes a step in the direction of the negative gradient of Φ from the current trail value. Thus,

$$\underline{\delta}_g = -\left(\frac{\partial \Phi}{\partial b_1}, \frac{\partial \Phi}{\partial b_2}, \ldots, \frac{\partial \Phi}{\partial b_k}\right)^T \quad (B16)$$

Here again the step size requires careful control to insure convergence.

Having noted the inadequacies of both the Taylor and the steepest descent methods, note also that any proper method must result in a correction vector that is within 90° of the negative gradient or else Φ would increase with the iterate. Marquardt's Method is an interpolation between $\underline{\delta}_t$ and $\underline{\delta}_g$ for monotonic convergence of the procedure. This method has its foundation in three theorems which will be stated without proof. Proof of these theorems may be found in Marquardt [7] or Meeter [8]. Meeter states and proves a somewhat stronger version of Theorem 1.

Theorem 1: Let $\lambda \geq 0$ be arbitrary and let $\underline{\delta}_o$ satisfy the equation

$$(A + \lambda I)\underline{\delta}_o = \underline{g} \quad (B17)$$

169

then $\underline{\delta}_o$ minimizes $\langle\phi\rangle$ on the sphere whose radius $||\delta||$ satisfies

$$||\delta||^2 = ||\delta||^2 . \qquad (B18)$$

Theorem 2: Let $\underline{\delta}(\lambda)$ be the solution of (B17) for a given value of λ. Then $||\underline{\delta}(\lambda)||^2$ is a continuous decreasing function of λ, such that as $\lambda\to\infty$, $||\underline{\delta}(\lambda)||^2\to0$.

Theorem 3: Let γ be the angle between $\underline{\delta}_o$ and $\underline{\delta}_g$. Then γ is a continuous monotone decreasing function of λ such that as $\lambda\to\infty$, $\gamma\to0$. Since $\underline{\delta}_g$ is independent of λ, it follows that $\underline{\delta}_o$ rotates toward $\underline{\delta}_g$ as $\lambda\to\infty$.

Since the Marquardt Method combines both the Taylor series method and the steepest descent method, it is necessary to note one relevant property of these methods. The solution $\underline{\delta}_t'$ of (B11) is invariant under linear transformation of the $\underline{b}$-space. However, the steepest descent solution is not scale invariant. It becomes necessary to scale the $\underline{b}$-space in some convenient manner. Therefore, the $\underline{b}$-space is scaled in units of the standard deviations of the derivatives $\partial f_i/\partial b_j$, taken over the sample points $i = 1, 2, \ldots, n$. This choice of scale causes the A matrix to be transformed into the matrix of simple correlation coefficients among the $\partial f_i/\partial b_j$.

Thus, the scaled matrix A* and the scaled vector g* become

$$A^* = (a_{ij}^*) = \left(\frac{a_{ij}}{\sqrt{a_{ii}}\sqrt{a_{jj}}}\right) \qquad (B19)$$

$$\underline{g}^* = (g_j^*) = \left(\frac{g_j}{\sqrt{a_{jj}}}\right) \qquad (B20)$$

and the Taylor series solution leads to

$$A^* \underline{\delta}^*_t = g^*$$ (B21)

Then

$$\delta_j = \delta^*_j / \sqrt{a_{jj}}$$ (B22)

The algorithm is now clear. Specifically, at the r-th iteration the equation

$$(A^{*(r)} + \lambda^{(r)} I)\delta^{*(r)} = g^{*(r)}$$ (B23)

is constructed. This equation is solved for $\underline{\delta}^{*(r)}$ and (B22) is used to obtain $\underline{\delta}^{(r)}$. The new trial parameter vector

$$b^{(r+1)} = b^{(r)} + \underline{\delta}^{(r)}$$ (B24)

will lead to a new sum of squares error $\phi^{(r+1)}$. It is essential to select $\lambda^{(r)}$ such that

$$\phi^{(r+1)} < \phi^{(r)}$$ (B25)

It is clear from the foregoing theory that a sufficiently large $\lambda^{(r)}$ always can be found such that (B25) is satisfied, except when $\underline{b}^{(r)}$ is already a minimum of ϕ. Therefore, a trial and error procedure is required to find a value of $\lambda^{(r)}$ such that (B25) is satisfied and rapid convergence insured, i.e. minimize ϕ in the (approximately) maximum neighborhood over which the linearized function will give adequate representation of the non-linear function.

The strategy employed is as follows:

Let $\nu > 1$.

Let $\lambda^{(r-1)}$ denote the value of λ from the previous iteration Initially, let $\lambda^{(0)} = 10^{-2}$, for example.

Compute $\phi(\lambda^{(r-1)})$ and $\phi(\lambda^{(r-1)}/\nu)$ (see note below).

i. If $\Phi(\lambda^{(r-1)}/\nu) \leq \Phi^{(r)}$, let $\lambda^{(r)} = \lambda^{(r-1)}/\nu$

ii. If $\Phi(\lambda^{(r-1)}/\nu) > \Phi^{(r)}$, and $\Phi(\lambda^{(r-1)}) \leq \Phi^{(r)}$, let $\lambda^{(r)} = \lambda^{(r-1)}$.

iii. If $\Phi(\lambda^{(r-1)}/\nu) > \Phi^{(r)}$ and $\Phi(\lambda^{(r-1)}) > \Phi^{(r)}$, increase λ by successive multiplication by ν until for some smallest ω, $\Phi(\lambda^{(r-1)}\nu^{\omega}) \leq \Phi^{(r)}$. Let $\lambda^{(r)} = \lambda^{(r-1)}\nu^{\omega}$.

NOTE: If $\lambda^{(r-1)}$ is already negligible by comparison with 1.0 to the number of significant figures carried, then go to test ii or iii immediately without computing $\Phi(\lambda^{(r-1)}/\nu)$, and ignore comparisons involving $\Phi(\lambda^{(r-1)}/\nu)$.

On occasion in problems where the correlations among the parameter estimates are extremely high (> 0.99), it can happen that λ will increase to unreasonably large values. It has been found helpful for these instances to alter test iii. The revised test is:

$$\underline{b}^{(r+1)} = b^{(r)} + K^{(r)}\underline{\delta}^{(r)}, \quad K^{(r)} \leq 1 \tag{B26}$$

Noting that the angle $\gamma^{(r)}$ is a decreasing function of $\lambda^{(r)}$, select a criterion agnle $\gamma_0 < \frac{\pi}{2}$ and take

$$K^{(r)} = 1 \quad \text{if } \gamma^{(r)} \geq \gamma_0 \tag{B27}$$

However, if test iii is not passed even though $\lambda^{(r)}$ has been increased until $\gamma^{(r)} < \gamma_0$, then do not increase $\lambda^{(r)}$ further, but take $K^{(r)}$ sufficiently small so that $\Phi^{(r+1)} < \Phi^{(r)}$. This can always be done since $\gamma^{(r)} < \gamma_0 \leq \frac{\pi}{2}$ [7].

The procedure is considered converged when $(|\delta_j^{(r)}|/(\tau + |b_j^{(r)}|)) < \varepsilon$, for all $j = 1, 2, \ldots, k$ and suitable choices for ε and τ, for example 10^{-5} and 10^{-3}, respectively.

172

REFERENCES

1. Siegman, A. E. and Miller, H. Y., "Unstable Optical Resonator Loss Calculations Using the Prony Method", Appl. Opt., Vol. 9, No. 12, pp. 2729-2736, December, 1970.

2. Personal communication, J. A. Hanlon, Air Force Special Weapons Center, Kirtland Air Force Base, Albuquerque, New Mexico, June 1974.

3. Lax, M., C. E. Greninger, W. H. Louisell, W. B. McKnight, "Large Mode-Volume Stable Resonators," J. Opt. Soc. Am. 65, p. 642, June 10, 1975.

4. Siegman, A. E., "Unstable Optical Resonators for Laser Applications", IEEE Proc., 53, 277, (1965).

5. Churchill, R. V. Complex Variables and Applications, McGraw-Hill Book Company, New York, 1960.

6. Kogelnik, H. and Li, T., "Laser Beams and Resonators", Proc. of the IEEE, Vol. 54, No. 10, pp. 1312-1329, October 1966.

7. Marquardt, Donald W., "An Algorithm for Least-Squares Estimation of Nonlinear Parameters", J. Soc. Indust. Appl. Math., Vol. 11, No. 2, pp. 431-441, June 1963.

8. Meeter, Duane A., "Problems in the Analysis of Nonlinear Models by Least Squares", a Ph.D. thesis, The University of Wisconsin, 1964.